D Y N A M I C R A D I O T R A C E R S T U D I E S
O F S U R F A C E P R O C E S S E S

b y

S t e p h e n V y n n e N o r v a l, B.Sc.

A thesis submitted for the degree of Doctor of Philosophy

of the University of Glasgow

Department of Chemistry

December 1975

Summary

In the catalysis literature, the need has been recognised to study adsorption on the catalyst surface during catalytic reactions. The primary aim of this work was a determination of the size of the active pool of molecules on the catalyst surface, i.e. those adsorbed which may subsequently undergo reaction.

Chlorobenzene hydrogenolysis and ethylene hydrogenation were studied in catalytic flow systems by passing carbon-14 labelled tracer pulses over catalyst samples under both pulsed flow and constant reactant flow conditions. Adsorbed and gas phase radioactivity were monitored with time by Geiger-Muller counters viewing the catalyst sample and gas phase either directly or through thin plastic or mica windows. Catalyst and gas count rates were separable following experiments where either adsorption or gas phase count rate was reduced to negligible proportions. All experiments were conducted at ca. atmospheric pressure, the chlorobenzene experiments using irregularly shaped tracer pulses and those with ethylene, rectangular pulses. Adsorption of chlorobenzene-C14 was studied on 1.08 and 4.47% Pd/SiO_2, SiO_2 and Pd black under various flow conditions of hydrogen, nitrogen and hydrogen-chlorobenzene, mainly at room temperature but also up to 448 K. Ethylene-C14 pulses (typically with 75 torr partial pressure) were passed over Ir/SiO_2, Pt/SiO_2 and SiO_2 under various flow conditions of hydrogen, helium and hydrogen-ethylene at temperatures between 239 and 321 K. In the presence of hydrogen over metal bearing catalysts, conversions were typically 40% for chlorobenzene to benzene and 100% for ethylene to ethane. The adsorption of benzene-C14 and ethane-C14 pulses was also studied.

Results were analysed in terms of the theory of tracer dynamics. A model was chosen for this theory, initially with a constant flow of reactant molecules, part of which is a radioactively labelled pulse, passing over a catalyst bed. Adsorption was assumed to be a prerequisite for reaction. Equations were derived based on the mean lifetime or occupancy of a molecule in the system, by which the capacity, or number of exchangeable adsorbed molecules, could be

calculated from the total adsorbed counts or from adsorption and desorption curves if the tracer pulse was of rectangular shape. These analyses were later modified for experiments conducted under pulsed flow conditions.

With constant chlorobenzene-hydrogen flow conditions, chlorobenzene-Cl4 gave an adsorption of up to 4.6×10^{17} molecule $(mg\ catalyst)^{-1}$ on 1.07% Pd/SiO_2 and 5.8×10^{17} molecule mg^{-1} on SiO_2 under similar conditions, compared with ca. 4×10^{16} surface metal atoms per mg catalyst from CO chemisorption. Under pulsed flow conditions in H_2 carrier, the semi-log count rate versus time plots for chlorobenzene and benzene from Pd/SiO_2 showed fast and slow linear regions with an intersection at ca. 4×10^{15} and 1×10^{15} molecule mg^{-1} on 4.47 and 1.08% Pd/SiO_2 respectively, these figures being largely independent of the size of tracer pulse used. Under N_2 flow, similar but slower two-fold desorptions were observed with an intersection between 1.71×10^{16} and 4.1×10^{15} molecule mg^{-1} on 4.47% Pd/SiO_2. Less well defined curves were obtained with Pd black. In all experiments the fraction of tracer irreversibly adsorbed on the catalyst was negligible.

Ethylene-Cl4 pulses in hydrogen and hydrogen-ethylene flows resulted in a transient adsorption of ca. 1×10^{16} molecule mg^{-1} from 270 - 317 K on the 4.77% Ir/SiO_2 catalyst with ca. 4×10^{16} surface metal atoms per mg determined by CO chemisorption. This adsorption showed little variation with ethylene-Cl4 partial pressure but rose to 5.3×10^{16} molecule mg^{-1} at 239 K. Ethane-Cl4 gave an adsorption of 5×10^{15} molecule mg^{-1} at 294 K on the same catalyst. On silica, transient ethylene-Cl4 adsorption varied throughout the temperature range of 251 to 304 K from 1.0×10^{17} to 3.2×10^{16} molecule mg^{-1} with 75 torr ethylene-Cl4 and was dependent on the partial pressure. Analysis of the adsorption and desorption curves at lower temperatures gave values of capacity similar to the observed transient adsorption on Ir/SiO_2. Ethylene-Cl4 pulses also resulted in some longer lived species on silica, Ir/SiO_2 and Pt/SiO_2 (0.13 - 1.5%, 0.3 - 4.1% and 0.25 - 0.53% of the tracer pulse respectively), which depended on the previous catalyst treatment.

Acknowledgements

I wish to express my sincere gratitude to each of the following:

Professor S. J. Thomson, my supervisor, for suggesting the research topic, his help, encouragement and many stimulating discussions.

Dr. J. J. McCarroll of B. P. Ltd, my industrial supervisor, for discussions about the present work and providing an opportunity to gain experience in other fields.

Members of the surface chemistry group of Glasgow University, particularly Dr. G. Webb for supplying tritium exchange figures and Miss F. Green for technical assistance.

Mr. J. Connelly and the staff of the glass blowing workshop and Mr. A. Hislop and the staff of the mechanical workshop for their skillful workmanship.

Mr. J. Hardy and the staff of the electronics workshop for design and production of many essential pieces of apparatus.

Dr. T. Baird for providing electron micrographs.

Dr. Z. Paal for encouragement and advice during the early stages of the work.

Elizabeth, for help and encouragement in writing this thesis.

My parents, for their moral support.

Mrs. C. Norbury, my aunt, for her patience and endeavour in typing of the manuscript.

British Petroleum Ltd. and the Science Research Council for financing this work during the tenancy of a research studentship under the CAPS scheme.

Table of Contents

Summary

In the catalysis literature, the need has been recognised to study adsorption on the catalyst surface during catalytic reactions. The primary aim of this work was a determination of the size of the active pool of molecules on the catalyst surface, i.e. those adsorbed which may subsequently undergo reaction.

Chlorobenzene hydrogenolysis and ethylene hydrogenation were studied in catalytic flow systems by passing carbon-14 labelled tracer pulses over catalyst samples under both pulsed flow and constant reactant flow conditions. Adsorbed and gas phase radioactivity were monitored with time by Geiger-Muller counters viewing the catalyst sample and gas phase either directly or through thin plastic or mica windows. Catalyst and gas count rates were separable following experiments where either adsorption or gas phase count rate was reduced to negligible proportions. All experiments were conducted at ca. atmospheric pressure, the chlorobenzene experiments using irregularly shaped tracer pulses and those with ethylene, rectangular pulses. Adsorption of chlorobenzene-C14 was studied on 1.08 and 4.47% Pd/SiO_2, SiO_2 and Pd black under various flow conditions of hydrogen, nitrogen and hydrogen-chlorobenzene, mainly at room temperature but also up to 448 K. Ethylene-C14 pulses (typically with 75 torr partial pressure) were passed over Ir/SiO_2, Pt/SiO_2 and SiO_2 under various flow conditions of hydrogen, helium and hydrogen-ethylene at temperatures between 239 and 321 K. In the presence of hydrogen over metal bearing catalysts, conversions were typically 40% for chlorobenzene to benzene and 100% for ethylene to ethane. The adsorption of benzene-C14 and ethane-C14 pulses was also studied.

Results were analysed in terms of the theory of tracer dynamics. A model was chosen for this theory, initially with a constant flow of reactant molecules, part of which is a radioactively labelled pulse, passing over a catalyst bed. Adsorption was assumed to be a prerequisite for reaction. Equations were derived based on the mean lifetime or occupancy of a molecule in the system, by which the capacity, or number of exchangeable adsorbed molecules, could be

calculated from the total adsorbed counts or from adsorption and desorption curves if the tracer pulse was of rectangular shape. These analyses were later modified for experiments conducted under pulsed flow conditions.

With constant chlorobenzene-hydrogen flow conditions, chlorobenzene-Cl4 gave an adsorption of up to 4.6×10^{17} molecule $(mg\ catalyst)^{-1}$ on 1.07% Pd/SiO_2 and 5.8×10^{17} molecule mg^{-1} on SiO_2 under similar conditions, compared with ca. 4×10^{16} surface metal atoms per mg catalyst from CO chemisorption. Under pulsed flow conditions in H_2 carrier, the semi-log count rate versus time plots for chlorobenzene and benzene from Pd/SiO_2 showed fast and slow linear regions with an intersection at ca. 4×10^{15} and 1×10^{15} molecule mg^{-1} on 4.47 and 1.08% Pd/SiO_2 respectively, these figures being largely independent of the size of tracer pulse used. Under N_2 flow, similar but slower two-fold desorptions were observed with an intersection between 1.71×10^{16} and 4.1×10^{15} molecule mg^{-1} on 4.47% Pd/SiO_2. Less well defined curves were obtained with Pd black. In all experiments the fraction of tracer irreversibly adsorbed on the catalyst was negligible.

Ethylene-Cl4 pulses in hydrogen and hydrogen-ethylene flows resulted in a transient adsorption of ca. 1×10^{16} molecule mg^{-1} from 270 - 317 K on the 4.77% Ir/SiO_2 catalyst with ca. 4×10^{16} surface metal atoms per mg determined by CO chemisorption. This adsorption showed little variation with ethylene-Cl4 partial pressure but rose to 5.3×10^{16} molecule mg^{-1} at 239 K. Ethane-Cl4 gave an adsorption of 5×10^{15} molecule mg^{-1} at 294 K on the same catalyst. On silica, transient ethylene-Cl4 adsorption varied throughout the temperature range of 251 to 304 K from 1.0×10^{17} to 3.2×10^{16} molecule mg^{-1} with 75 torr ethylene-Cl4 and was dependent on the partial pressure. Analysis of the adsorption and desorption curves at lower temperatures gave values of capacity similar to the observed transient adsorption on Ir/SiO_2. Ethylene-Cl4 pulses also resulted in some longer lived species on silica, Ir/SiO_2 and Pt/SiO_2 (0.13 - 1.5%, 0.3 - 4.1% and 0.25 - 0.53% of the tracer pulse respectively), which depended on the previous catalyst treatment.

The chlorobenzene results were interpreted in terms of reaction occurring on ca. 30% of the total Pd surface, the remainder being hydrogen covered, product benzene adsorbed on this part of the surface giving rise to the slower part of the desorption observed in hydrogen flow. The faster parts of the desorptions were attributed to chlorobenzene removal from a support physisorbed state, either by desorption or reaction to benzene on the metal surface. A kinetic scheme was proposed for this desorption and rate constants determined by iterative curve fitting. Ethylene hydrogenation over Ir/SiO_2 was concluded to occur between one adsorbed ethylene molecule per four surface Ir atoms reacting with adsorbed hydrogen. At least ten types of hydrocarbon adsorption were thought to occur during the reaction, including adsorption on both metal and support. It was concluded that the tracer dynamics techniques employed yielded useful information on surface processes during catalysis, although more structural information on surface species was desirable.

C H A P T E R 1

Introduction

Chapter 1

Introduction

1.1. Preliminary remarks

In any study of chemical reactivity one of the most fundamental requirements is a knowledge of the concentrations of the reactants. For heterogenous catalytic systems this information is not normally available, due to the difficulties involved in measurements at an interface. One aspect of this problem concerns the relatively small number of molecules which comprise the interfacial layer relative to those present in the bulk phases, and the inapplicability of many physical techniques normally used for homogeneous systems in measurements across a solid/gas or solid/liquid boundary. The solid surface itself is rarely uniform resulting in a variety of possible adsorption modes for substrate molecules and a corresponding distribution of catalytic activity dependent on these irregularities. The implications of the concept of surface heterogenity in catalysis were first clearly recognised by Taylor in 1925 (1) when he suggested that catalytic reactionswould be found where the fraction of the surface which is active would range from a small number of "active centres" to every surface atom, depending on the catalyst and the reaction catalysed.

The aim of the present study was to obtain more information about the active surface of a heterogeneous catalyst, and more specifically, the number of reactant molecules adsorbed on the surface which subsequently undergo reaction. The remainder of this chapter will be devoted to a survey of studies relating to the extent of surface catalytic activity and the use of radiotracers for the direct observation of adsorption. In chapter 2, previous concomitant studies of adsorption and catalytic activity will be discussed, and the background theory of a new dynamic radiotracer approach described. Chapter 3 will deal with the choice of chemical systems for study and the present state of knowledge of these systems. The succeeding chapters will be devoted to description and discussion of the experimental techniques employed and the results obtained.

1.2. The active surface

While it is seldom possible to define exactly the nature and concentration of active sites on a catalytic surface, one physical characteristic, the surface area, may be obtained with relative ease. If it is assumed that the concentration of active sites, or "site density", will be constant for a particular type of surface, then a knowledge of the surface area enables a comparison to be made of reaction velocities over catalysts having a common active surface. The method most widely accepted for the determination of surface areas of finely divided materials is that developed by Brunauer, Emmett and Teller (2). This technique is based on the assumption of a constant area occupied by a physisorbed gas molecule at low temperatures and monolayer coverage. For a homogeneous material the surface area derived is perfectly adequate, but where one wishes to distinguish between different components in the solid more sophisticated methods must be used. The industrial importance of supported metal catalysts has led to a great deal of activity in the determination of the area of the metal component. Both physical and chemical methods have been used, and although all are subject to certain limitations, by 1969 Boudart was sufficiently confident in the progress made to suggest that all future investigations of catalysis on supported metals must include a determination of the metal surface area (3).

If it is assumed that a particular reaction takes place only on the metal surface of a supported metal catalyst, a "specific rate constant" can be calculated from a knowledge of the metal surface area (4). This rate constant may be defined as the number of molecules reacting per unit time per surface metal atom (5).

Selective chemisorption

In principle, for a supported metal catalyst, if an adsorbate can be found which will adsorb selectively on the metal surface with known stoichiometry then a value may be obtained for the surface area of the metal. In practice the three adsorbates most widely used have been carbon monoxide, hydrogen and oxygen, although none of these is ideal.

Some of the earliest work in this field was carried out by Brunauer and Emmett using carbon monoxide as adsorbate (6). They compared CO chemisorption with the low temperature adsorption of N_2 on iron powders, but interpretation of their results is difficult due to the likelihood of some nitrogen chemisorption having occurred. Similar work by Beeck, Smith and Wheeler (7) on evaporated nickel films suggested a single site chemisorption of CO, with formation of a surface complex NiCO, analagous to nickel carbonyl.

Lanyon and Trapnell (8) produced results for CO adsorption on platinum and palladium films similar to those found by Beeck et al. for nickel. The situation concerning molybdenum and rhodium films was somewhat different. Here the values of CO chemisorption were respectively 1.23 and 1.40 relative to hydrogen chemisorption. Values such as these indicate both single and double adsorption sites for CO. Infra-red studies by Eischens et al. (9, 10) confirmed the occurrence of both adsorption modes on various metals supported on silica and alumina. Supported platinum and palladium showed both single and double modes, the former being of greater importance at higher CO pressures. This phenomenon may be attributed either to a reorganisation of adsorbed species at higher pressures or to surface heterogeneity. A third possibility, that of two CO molecules covalently bound to a single metal atom was found by Yang and Garland (11) on a rhodium surface.

A further complication concerning the use of CO is due to direct adsorption on alumina (12). It is thus necessary to make a correction for adsorption on the support, especially when studying catalysts with low metal loadings.

The adsorption of CO on transition metals has been reviewed by Ford (13), who has comprehensively treated the work on individual metals. In spite of the difficulties encountered in defining the precise mode of adsorption for a particular catalyst, the technique is now widely used for surface area determination (14, 15, 16). By allowing for the greater incidence of linear bonding on smaller platinum crystallites, Dorling and Moss (17) achieved satisfactory agreement between CO adsorption and physical techniques for particle size determination.

Another application of carbon monoxide in the study of surface areas was developed by Wentrcek, Kimoto and Wise (18), who chemisorbed oxygen on platinum in the form of powders and supported on carbon and alumina. The adsorbed oxygen was then titrated with gaseous CO, the stoichiometry of the reaction following the equation:

$$O(\text{adsorbed}) + 2CO \rightarrow CO(\text{adsorbed}) + CO_2.$$

Quantitative determination of the chemisorbed oxygen was either by the CO consumed or the CO_2 formed.

Simple oxygen chemisorption has been used in surface area determinations (19), but more commonly oxygen adsorption is followed by hydrogen titration (20, 21, 22). The most important use of oxygen chemisorption is in cases where interaction of the adsorbate with the support is likely (23). The "spillover" of chemisorbed hydrogen from metal to support has been widely recognised (see later), and represents the chief disadvantage in the use of hydrogen chemisorption as a measure of surface metal atoms. The technique has, however, been widely used, particularly in studies of dispersion in the type of supported platinum catalyst employed industrially for reforming reactions (24). A further problem in the use of hydrogen in connection with palladium and platinum catalysts is the phenomenon of absorption. The ability of palladium to absorb hydrogen is well known, and recent studies suggest a similar, although less marked occurrence for platinum (25, 26).

Physical techniques

The chemisorption techniques discussed have as their aim a direct determination of the number of surface metal atoms of a catalyst. The object of many physical techniques is to measure the same quantity indirectly by a determination of the metal particle size distribution. Assuming a particular geometry for the particle, a value for surface area may be calculated from the size distribution and catalyst metal loading.

The most direct measure of particle size has been obtained by electron microscopy, in particular using transmission techniques. Resolutions better than.2nmhave been obtained (27), enabling crystallites of 1 nmto be measured. The metal particles, having considerably greater density than the support, are usually readily discernible in micrographs of about 100,000X magnification. A particle size distribution may be calculated from approximate measurements of a large number of metal particles (28).

A less direct approach to metal particle sizes utilises X-ray powder diffraction. For samples with crystallite sizes less than about 100 nm, the diffraction lines are broadened to an extent which depends on the particle size distribution. Below about 4 nm, the lines become too diffuse to measure. The technique is of greatest use in the size range 50 - 50 nm (4, 28, 29, 30). A more sophisticated treatment of X-ray line broading has been employed by Moss et al. (17, 31, 32). In these studies, the apparatus was calibrated with catalysts of known large particle size. By comparing the results obtained for particles over about 5 nm, useful information was obtained about the remaining, more finely divided, metal.

One further physical method worthy of mention is limited to ferromagnetic materials, principally nickel (4, 33, 34, 35). As the Curie temperature is dependent on particle size, analysis of the thermomagnetic curves of the catalysts studied may yield a particle size distribution.

Support reactivity

The use of a porous nonmetallic support material to obtain a finely divided metal catalyst has been common for many years. Apart from its effect in reducing metal sintering, the influence of the support may be threefold, viz:

1. The support may be active in catalysis.
2. It may affect the surface area of the metal and its determination.
3. An electronic interaction may exist between metal and support, modifying the catalytic activity of either or both.

The last mentioned effect, postulated by Herbo for the influence of support on metal (36), has not been given conclusive proof (37), but the reverse interaction is more probable (38).

It is 1. and 2. above which most concern us in dealing with the magnitude of the active surface.

The most obvious example of support reactivity is that of bi-functional catalysis (39). In the catalytic reforming of hydrocarbons on acidified alumina or silica-alumina supported platinum (40), neither support nor metal alone fulfils the function of the supported metal. For other catalytic systems, the function of the support is not so clearly defined. In fundamental studies on supported metal catalysts, the possibility of hydrogen spillover from metal to support has rendered many results inconclusive. This phenomenon, recently reviewed by Sermon and Bond (41), has been widely observed and should be taken into consideration in conjunction with the possible spillover of other adsorbents in most supported metal studies.

Khoobiar first detected hydrogen spillover from platinum to a tungsten oxide support (42), and subsequent studies indicate that the primary requirements are a metal which does not adsorb hydrogen too strongly combined with a support with hydrogen-acceptor sites.

Studies of the catalytic effect of "activated" hydrogen adsorbed on the support have been inconclusive. Enhanced catalytic activity for the hydrogenation of ethylene on certain supports (e.g. alumina) has been attributed to the phenomenon (e.g. 43). This interpretation

was subsequently questioned by Schlatter and Boudart (5), who attributed rate enhancement to the scavenging of carbonaceous residues by the support material. A direct demonstration of low temperature ethylene hydrogenation on alumina previously in contact with a nickel-alumina catalyst has been given by Gardes, Pajonk and Teichner (44), although a proper appreciation of their results must await the publication of further detail. The spillover of hydrocarbon species from metal to support (45, 46, 95, 96)further substantiates the possibility of a catalytic function of the support.

Conclusions on surface areas

Before discussing the usefulness of active surface areas, it should be noted that while precise determinations appear difficult, it seems probable that correct values can be obtained to within a factor of 2 (3, 47). No single method of surface area determination may be considered infallible, and it has been recommended that several techniques should be applied to each individual catalyst under study (28.) While it may often be impractical to apply several techniques it would seem wise to compare a selective chemisorption with results obtained from a physical technique.

If the assumption is made that the metal contribution to the total activity of a supported catalyst is paramount (it is normally safe to assume that the metal is active), can one consider the metal area to be an adequate measure for the comparison of activities of different catalysts? If investigations are carefully conducted it has been demonstrated that the specific activity of a given metal in the form of a film is comparable with that of the supported metal (4, 5). When comparing different metals, the differing extents of surface heterogeneity may have to be taken into account. The occurrence of irreversibly adsorbed species on a catalyst during reaction has been established e.g. by spectroscopic (48) and radiotracer (49) techniques. The extent of the corresponding inactive portion of the surface varies according to the metal, from 6.5% on platinum to 63.5% on palladium (49). While adjustment of the specific rate constants could be made in accordance with such figures, the remainder of the surface may not be equally active in catalysis (50). Although the metal surface area is an important physical characteristic of a catalytic system it may not be an adequate measure of the "concentration" of the catalytically active species.

1.3. Active sites

In the previous section, no attempt was made to identify the precise nature of the seat of a heterogeneously catalysed reaction. This must, however, be an eventual goal of researchers in the field. For a comparison of the activities of catalysts, the number rather than the nature of the active sites may be sufficient. Thus we have defined the two broad areas, sometimes overlapping, into which studies on active sites have been directed. The literature on the subject has been twice reviewed by Maatman (51, 52).

The nature of the active sites

On metallic catalysts, reactions may be usefully categorised according to Boudart's nomenclature (53). Those whose rates do not vary with particle size, and are therefore assumed to occur with equal facility on crystallite faces, edges and corners, are termed "facile" or "structure-insensitive." Boudart has also observed (54) that Temkin's theory of catalytic reactions on continuously non-uniform surfaces predicts that sites which differ by leV in binding energy give rise to reaction rates differing by less than one order of magnitude, which will be even closer to the mean rate for all sites. The mean rate would therefore be dependent on the shape of the site energy distribution function, which in turn appears to be insensitive to particle size.

A well known example of a structure-insensitive reaction is the hydrogenation of ethylene. The comparison made by Schuit and van Reijen of rates over supported metal catalysts and metal films has already been referred to (4). A confirmation of the results obtained was made by Schlatter and Boudart (5) who found that a rigorous cleaning of a platinum-silica catalyst during pretreatment enabled a specific rate constant to be derived for ethylene hydrogenation within 30% of that obtained over an evaporated platinum film.

Plateeuw et al. studied the effect of varying metal particle sizes (Ni, Pt, Pd) on various support materials (silica, alumina, silica-alumina, silica-magnesia) from less than 1 nm to greater than 10 nm (55,56). The specific rate constants calculated for various

reactions (hydrogenation of benzene, isomerisation of n-hexane, dehydrocyclisation of n-hexane) were found to be independent of the particle size. Similar results have been obtained by Ratnasamy for benzene hydrogenation over supported platinum (57).

Evidence for structure-sensitive reactions on metals has been less frequently encountered. Balandin has suggested that special sites with a certain number of nearest neighbour metal atoms constitute the active sites (58). Direct proof of this theory is as yet unavailable.

An interesting case of a structure sensitive reaction is that of the hydrogenolysis of neopentane to isobutane and methane over platinum catalysts, where a competitive reaction, isomerisation of neopentane to isopentane also occurs. In an investigation of the reaction over platinum supported on a porous graphitised carbon, Boudart, Aldag, Ptak and Benson examined the effect of catalyst pretreatment on the reaction rates and the ratio of isomerisation to hydrogenolysis, i.e. the "selectivity" of the catalyst (59). It was found that the removal of carbon residues from the metal by repeated doses of oxygen increased the reaction rate by two orders of magnitude without affecting the selectivity. A different result was obtained when the catalyst was first fired in vacuo at 1173K, a treatment designed to promote equilibration of crystallite shapes without affecting particle size. Following this treatment, the selectivity was increased by a factor of five in favour of isomerisation. This result agreed with the earlier experiments of Anderson and Avery (60), who interpreted their results in terms of 1,3 - diadsorbed and triadsorbed neopentane on different crystal faces. Geometrical considerations indicate that the triadsorbed species occur only on the (111) face, or at triplet sites with similar geometry. If the hydrogenolysis reaction is more favourable from the diadsorbed species, the optimisation of appropriate sites for the triadsorbed species would explain the observed increase in selectivity for isomerisation due to the fall in the rate for hydrogenolysis.

A little more success has been achieved in identifying the active sites of non-metallic catalysts, largely due to the greater chemical distinction between the site and the surrounding surface.

One of the most important phenomena in nonmetallic catalysts is co-ordinative unsaturation. If an oxide catalyst is heated, particularly under vacuum, then the dehydration of surface hydroxyls ($2OH^- \rightarrow O^{2-} + H_2O$) exposes co-ordinatively unsaturated cations which are then able to participate in adsorption and catalysis. Eley and Zammitt (61) studied the reactions $pH_2 \rightarrow oH_2$, $oD_2 \rightarrow pD_2$ and H_2/D_2 exchange over γ- Al_2O_3. They correlated reaction rate with the number of free spins on the catalyst surface, and suggested the following structure, proposed by Acres, Eley and Trillo (62) as the probable location of activity:

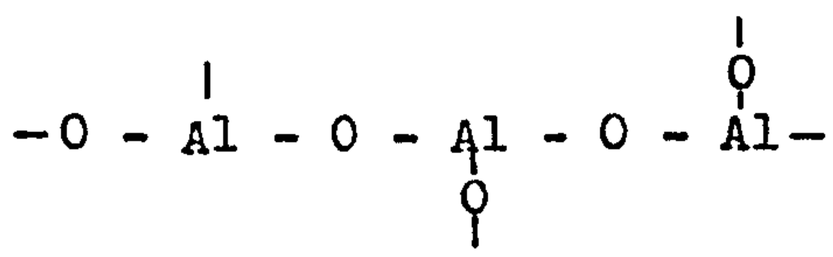

α- Al_2O_3 was found to be more active than γ- Al_2O_3 for the reactions. Since a higher impurity content and lower nonstoichiometry were associated with γ- Al_2O_3, it was concluded that the activity may be associated with the former.

The extensive studies on chromia catalysts by Burwell, Haller, Taylor and Read (63) showed that co-ordinatively unsaturated Cr^{3+} ions were involved in the hydrogenation of olefins, exchange of the toluene methyl group and olefin isomerisation. Sancier, Dozono and Wise (64) used electron spin resonance spectroscopy to identify Mo^{6+}/Mo^{5+} surface sites as the active centres for propylene oxidation over bismuth molybdate.

An interesting confirmation by experiment of the theoretically derived location of active sites is found in the case of the stereospecific polymerisation of propylene by $TiCl_3$ crystallites. Arlman (65) put forward the theory that the removal of chloride ions from the (1010) planes of α-$TiCl_3$ is more favourable for the maintenance of electrical neutrality than removal from the (0001) basal planes. This removal results in the exposure of Ti^{3+} ions, the activator for

propylene polymerisation. Electron micrographs subsequently located polymer nodules on a used catalyst only at the prismatic faces and the ledge of a screw dislocation on one of the basal planes which were otherwise free of nodules (66).

The catalytic activity of zeolites has attracted much attention in recent years (67). Due to their porous crystalline structure, they have perhaps the maximum possible ratio of surface area to bulk volume, the surface area being typically in the region of 1,000 $m^2 g^{-1}$. Y- zeolite contains large pores of about 1.2 nm diameter connected via 0.8 nm windows in a three dimensional network. The crystal framework consists of alternating silica and alumina tetrahedra sharing oxygens. Such a structure results in Al^{3+} ions which each require the presence of a positive charge, located at a counter ion in one of the pores, to maintain electrical neutrality. Rabo, Angell, Kasai and Schomaker (68) suggested that the divalent or trivalent charge compensating ions so introduced should result in large electrostatic fields in their vicinity, readily accessible to gaseous molecules small enough to negotiate the intercommunicating porous structure. The increased catalytic activity of zeolites over silica - alumina gels for reactions involving formation of carbonium ion intermediates from hydrocarbons, was initially ascribed to the polarising power of the large ionic fields to enhance the carbonium ion formation (68). It now seems more likely that the effect of the charge compensating ionic field is secondary, acting via the Brønsted acidity of hydroxyl protons (69). In studies of the Mössbauer spectra of Fe^{2+} and Fe^{3+} ions exchanged into Y- zeolites, this view was confirmed by spectroscopic perturbations due to molecules such as t-butyl alcohol and piperidine, which are too large to penetrate to the Fe^{2+} ions in the zeolite framework (70).

Active site densities

Maatman has given four basic approaches to the problem of determining site densities (52). These may be briefly listed as follows:

1. Theoretical methods.
2. 'Direct' measurement of some process directly connected with the site density.
3. Enumeration of the number of surface species known to be active in catalysis.
4. Indirect determination of the minimum and maximum values which are possible.

The theoretical approach to site densities relies entirely on the correct choice of reaction mechanism on which to base the calculations. One of the basic types of calculation makes the assumption that the adsorption step is rate limiting. For example, Ashmead, Eley and Rudham (71) calculated a value for ortho-para hydrogen conversion and hydrogen-deuterium equilibration over Nd_2O_3 at 588K. Constant values were used for the collision number, the sticking coefficient and the observed activation energy. The value taken for the active fraction of the surface was chosen to give a rate constant which agreed with that derived experimentally. It was found that a site density of approximately 10^{12} sites cm^{-2} gave best agreement with experiment.

The most widely used theoretical approach is based on the absolute rate theory of Glasstone, Laidler and Eyring (72). The most readily used equation is that for a zero order rate determining step:

$$\text{Rate} = c_a \frac{kT}{h} \exp(S/R) \exp(-E/RT),$$

where c_a = site density,
k = Boltzmann constant,
h = Planck's constant,
T = temperature,
S = entropy of activation,
and E = heat of activation.

If it is assumed that the entropy change on activation is approximately zero, i.e., the transition state entropy is little different from that of the adsorbed reactant, a value may normally be calculated for the site density using experimental values of reaction rate and activation energy (52). A recurrent feature of calculations based on this method is a tendency to very low site densities. Those reported by Maatman range from 6×10^{11} to 3×10^{3} sites cm^{-2}.

In certain cases a comparison may be made between experiment and theory. Misra (73) studied the dehydration of phenylpicryl-hydrazine adsorbed on TiO_2. Reactivity was due to F-centre electrons, 10^{11} of which were present per cm^2. Using this figure as a value for the site density, the above equation predicted a reaction rate within a factor of 20 of the experimental value. In contrast, the theoretical value of Maatman, Mahaffy, Hoekstra and Addink (74) for the dehydrogenation of cyclohexane over Pt - Al_2O_3 was 10^9 sites cm^{-2}, much lower than the value predicted by experiment. As mentioned previously, Aben, Platteeaw and Stouthamer (56) showed the reaction to be structure insensitive. If every surface platinum atom is active, then the site density should be of the order of 10^{14} cm^{-2}. Maatman et al. rejected the possibility of the very high decrease in entropy of activation (-23 eu) necessary to accommodate a facile reaction in their calculation, and concluded that for this reaction, as for that over Pd - Al_2O_3 (75), the reaction mechanism adopted was at fault. It was proposed that at least one intermediate took part in the reaction, and trace amounts of cyclohexene were detected (75).

Of the reactions discussed previously for which active sites have been identified, some values for concentration were also obtained. The electron spin resonance studies of Eley and Zammitt for "hydrogen" exchange over alumina (61) yielded a value of 1.9×10^{11} free spins cm^{-2}, this figure being equated with the site density. Sancier, Dozono and Wise found that the active sites of their bismuth molybdate catalyst for propylene oxidation constituted 1% of the total surface sites.

A further example of low site densities being obtained experimentally is found in the case of ethylene polymerisation over chromia supported on alumina and other carriers. Yermakov and Zakharov (76) determined the number of polymer chain ends by stopping the reaction with carbon - 14 labelled methanol, which combined with the chain ends. The number of incorporated labelled molecules led to values of site density between 10^{10} and 10^{12} cm^{-2}, depending on the oxide support.

Experimental results such as these tend to confirm the validity of some transition state theory calculations for nonmetallic catalysts. The fact that similar theory does not predict the values expected from experiment for metallic catalysts, generally assumed to have high densities, must leave some room for doubt in other cases.

Maatman has made a further point in favour of low site densities (52). Reactions catalysed by enzymes appear to be much more efficient than those of solid catalysts if high site densities are assumed. In general the efficiencies become comparable only when site densities as low as those predicted by transition state theory are adopted. It does not seem too unreasonable to assume, however, that enzymes developed by nature through millenia of evolution should be greatly superior in catalysis to the relatively simple systems used for heterogeneous catalysis.

1.4. Radiotracer studies

Since the introduction of the nuclear reactor, radioisotopes not found in nature have become readily available. In chemistry, few areas of mechanistic study have been unaffected by the possibility of following labelled atoms through chemical change of the molecules of which they are part. The field of heterogeneous catalysis, presenting as it does many mechanistic problems, has been no exception in finding uses for radioactively labelled compounds. A summary of some of these studies may be found elsewhere (77). In general, radiotracer applications in catalysis can be subdivided into two types, viz:

1. The more conventional type of mechanistic study using labelled reactant or suspected intermediate, and the distribution of the labelled species in the product.
2. The direct observation of labelled molecules adsorbed on the catalyst surface.

An example of the first type of study has been mentioned in relation to the polymerisation of ethylene over supported chromia catalysts (75). A further well known example is found in the studies of the Fischer - Tropsch synthesis by Emmett and coworkers (78 - 84), who investigated the incorporation of radioactively labelled intermediates into the product hydrocarbon chains. Both of these examples made use of carbon - 14 as the isotopic tracer, but tritium, ^{3}H., has also been used, e.g. in studies of hydrogen spillover (85, 86) and hydrogen retention by platinum blacks (26).

Our primary interest in this study is in applications of the second variety. Of particular importance in detecting adsorbed species by this method, is its sensitivity to small amounts of adsorbate. An argument based on that of Thomson and Webb (77) will illustrate this point.

If we consider a 1 cm^2 area of the (100) face of a nickel crystal, a value of 6.5×10^{15} surface nickel atoms may be calculated. Assuming a surface coverage of adsorbate in a ratio resulting in one carbon - 14 atom per surface nickel atom, the total activity

of carbon - 14 adsorbed would be $2.6 \times 10^{4} s^{-1}$. In the case of a C_2 compound, this corresponds to 5×10^{-9} moles of adsorbate. The figure given for adsorbed activity represents a maximum value, and would be expected to fall considerably if tracer of more normal specific activity were used. If a ratio of carbon atoms to surface metal atoms less than unity were encountered, taking into consideration the frequently low efficiency of detection of carbon - 14 β^- emission, one might reasonably expect an observed count rate in the region of $10 s^{-1}$ cm^{-2}, a perfectly acceptable activity level for determining surface coverage. In practice, this count rate may be considerably improved by the use of a highly dispersed adsorbent, such as a supported metal.

Much work in the field of direct observation of adsorption has been carried out by Thomson and coworkers (87 - 96). One of the main features of these studies has been an unambiguous demonstration of surface heterogeneity, and its importance in catalysis. Cranstoun and Thomson (91) showed by the displacement of tritiated hydrogen from a nickel film by ^{203}Hg, that desorption occurred on a "last on, first off" basis. The heterogeneity of metal surfaces in catalytic reactions was demonstrated for hydrocarbon adsorption. Ethylene-C14 preadsorbed on a nickel film and subsequent hydrogenation of ethylene over the film showed that more than half of the nickel surface was inactive during the reaction (90). Similar experiments with supported metal catalysts (93), gave varying fractions of the surface inactive in catalysis (Pd, 63.5%; Ni, 24%; Rh, 22.5%; Ir, 16%; Pt, 6.5%). More detailed studies by Reid, Thomson and Webb (95, 96) have recently been made of the adsorption of carbon - 14 labelled ethylene, acetylene, and carbon monoxide on rhodium catalysts supported on silica and alumina. Ethylene and acetylene adsorption was shown to exceed that of carbon monoxide "monolayer" coverage. The adsorption isotherms of ethylene and acetylene could be divided into two distinct regions, which were attributed to an initial metal adsorption, and support adsorption at higher pressures. Moss et al. have used similar direct monitoring techniques to find metal surface areas by monolayer adsorption of carbon - 14 labelled carbon monoxide (31, 32).

C H A P T E R 2

The Concomitant Study of Adsorption and Catalysis

Chapter 2

The Concomitant Study of Adsorption and Catalysis

2.1. Objectives

In the previous chapter, emphasis was placed on the nature and extent of the surfaces used as heterogeneous catalysts. The surface with which we will be primarily concerned in the present study is one on which reaction is taking place, with the appropriate reactant, intermediate and product molecules adsorbed.

Tamaru was one of the first investigators to recognise the importance of studying adsorption during catalysis (97). He pointed out that the coverage of the active area of surface during catalysis need not be that derived from the adsorption equilibrium with the ambient gases, but may depend on the mechanism or rate determining step of the reaction. In a later paper (98) Tamaru observed in more general terms, that a "clean" surface is not in itself a catalyst, which may better be defined as the surface bearing the active adsorbed species as present during the catalytic reaction. The properties associated with the catalyst should therefore be those pertaining under reaction conditions. Several techniques have been applied to the problem of determining adsorption during catalysis, and these, along with some of the results obtained, will be discussed in the following section.

In section 1.4., the technique of direct observation of radiotracer molecules adsorbed on a surface was noted as being of particular importance in demonstrating the heterogeneity of catalyst surfaces. Indeed, in certain of these studies, the conditions used have been related to those during reaction (e.g. 90, 93). One of the principal virtues of the method lies in the fact that no disturbance of the catalyst or ambient gas is necessary when carrying out adsorption studies, and a particular fraction of the reacting molecules may be observed without a change in the chemical nature of the system. This makes the radiotracer technique almost ideal for concomitant studies of adsorption and catalysis, the principal drawback, however, being the precise identification of the adsorbed species observed.

It was for these reasons that it was proposed to apply radiotracer techniques to observing adsorbed species during catalytic reactions. By the methods outlined in sections 3 and 4 of this chapter (see also appendix II), it was hoped to obtain the following information:

(1) The size of the active pool of molecules adsorbed on a catalyst surface which may be participating in catalysis. A distinction must be drawn between this value and the number of catalytically active sites; e.g., a large number of adsorbed reactant molecules may be adsorbed on sites of which only a few are active, most molecules migrating to these sites in order to react. The value obtained might be compared with the surface area available for reaction, and conclusions drawn about the proportion of metal (and for support) which is active for a supported metal catalyst.

(2) The mean lifetime of the adsorbed species. This value gives, in effect, an absolute value for the catalytic rate constant.

(3) A possible insight into the kinetics and mechanism of the reaction.

(4) The nature and extent of long lived species on the catalyst surface, and their role in catalyst poisoning.

The two related means of obtaining this information considered were based on the behaviour of labelled molecules in a flow system, which permits the use of steady state reaction conditions, and a simple and effective means of introducing reactant samples to the catalyst in a controlled manner.

2.2. Previous studies

One of the most obvious methods for the concomitant study of adsorption and catalysis is the gravimetric technique, although it is not necessarily straightforward in practice. Mars, Scholten and Zwietering (99) studied tne adsorption of nitrogen on iron catalysts during ammonia synthesis by means of a magnetically operated high vacuum balance. Of the problems encountered, perhaps the most important, experimentally, were the corrections for buoyancy and flow. Since only the net changes in catalyst weight could be determined, the effect of chemisorbed hydrogen was difficult to interpret, but the conclusion was made that under their reaction conditions the activated adsorption of nitrogen was rate determining. Gravimetric techniques have recently been adopted by Massoth and Scarpiello (100), who investigated the oxidative dehydrogenation of butene to butadiene on the Zn - Cr - Fe oxide system, and by Hsu and Kabel (101). In the last mentioned study, the vapour phase dehydration of ethyl alcohol to diethyl ether was observed over a hydrogen ion exchange resin. In addition to catalyst weight changes the vapour phase composition and total pressure were simultaneously measured. It was shown that the adsorption of ethyl alcohol was a much faster process than the subsequent surface reaction.

Volumetric techniques have also been used without simultaneous recording of other physical data. In the apparatus proposed by Tamaru (97, 102), the reactant was admitted into a closed circulating system, and the adsorption calculated from the pressure and composition of the gas phase. By this method, Tamaru studied the decomposition of ammonia on a tungsten catalyst (103), and Fukuda, Onishi and Tamaru the decomposition of formic acid on silver catalysts (104), which demonstrated an interesting case of surface heterogeneity. At 373 K, the reaction was found to be first order at low formic acid pressures and zero order in a medium pressure range, corresponding to an apparent "saturation" of active sites. On further increase of the pressure, however, it was found that adsorption once again increased and the reaction rate rose linearly with

the increased surface coverage. A second point, of equal interest, was the comparison made between the experimental value obtained for the number of active centres, and that calculated by the Transition State Theory of Glasstone, Laidler and Eyring (72), as discussed in Section 1.3. The calculated value of 1.8×10^{15} sites cm^{-2} compares remarkably well with the experimental value of 3.1×10^{14} sites cm^{-2} at 373 K.

Haering and Syverson have recently developed a rapid response pressure transducer technique for volumetric studies of adsorption under reaction conditions (105). They studied the dehydration of t-butyl alcohol over alumina at 195°C, and the adsorption of water, isobutylene and binary water/t-butyl alcohol mixtures. The results obtained were interpreted in terms of physi- and chemisorbed water on their catalyst, the water adsorption on active sites inhibiting the t-butyl alcohol adsorption. The method described is limited to cases where the rate of surface reaction is slower than the rate of adsorption, as the adsorption measurement relies on a slow pressure change due to reaction.

The retention time of a sample on a gas chromomatographic column represents a further means of measuring adsorption (see, e.g. 106). The technique can be further extended by studying reactions which are catalysed by the adsorbent, the reactant(s) being passed through the column either in an inert carrier flow (e.g. for a decomposition or isomerisation reaction) or in a flow of one of the reactants (e.g. hydrogen for a hydrogenation reaction). The retention time on the catalyst (column packing) can thus be measured during reaction, leading to a value for the reactant adsorption. The technique was first used by Tamaru who studied formic acid decomposition on a palladium catalyst (107), and Nakanishi and Tamaru (108) in their investigation into the mechanism of the water - gas - shift reaction on an iron catalyst. In this study it was shown that the properties of the catalyst surface in its working state undergo appreciable changes, depending upon the composition of the reacting gas (a mixture of oxidising and reducing agents).

Further applications of the chromatographic method include those of Bassett and Habgood (109), who derived the extent of adsorption under reaction conditions and the surface rate constant for the isomerisation of cyclopropane on a molecular sieve, and Owens and Amberg (110), who studied the hydrosulphurisation of thiophene over a chromia catalyst.

An interesting variation on the chromatographic technique has been introduced by Phillips et al. (111, 112, 113). For a reaction in which the reactants are more strongly adsorbed than the products, the product peak generally has a sharp front, but gradually tails into the reactant peak. If the flow of carrier gas is stopped for a short interval of time compared with the length of the product peak, while the reactant pulse is still in the catalyst column, peaks appear superimposed on the main product peak when the flow is resumed, one for each product present. From the duration of the pause and the size of the peaks so produced, a direct measure of the reaction rate may be obtained for the individual products.

The direct monitoring of adsorption during catalysis is possible by the use of radiotracer and infra-red techniques. In addition to the studies mentioned in section 1.4., Lawson has investigated the adsorption and decomposition of carbon-14 labelled formic acid on epitaxially grown silver films (114). In this case, a detailed tracer analysis did not show a direct relationship between adsorption and catalysis.

Fahrenfort, van Reijen and Sachtler used a kinetic infrared technique to study the decomposition of formic acid on nickel and gold catalysts (115). They were able to follow the decomposition kinetics by observation of the formate adsorption band at 1575 cm^{-1} on the nickel catalyst. Interpretation of the overall rate as measured from the gas composition was possible in terms of the directly observed surface species.

Sheppard, Avery, Morrow and Young (116), attempted to identify the active species adsorbed on silica supported platinum for the hydrogenation of ethylene under flowing reaction conditions by infrared spectroscopy. The results obtained were interpreted in

terms of diffusion limitation of the reaction rate due to the "pressed disc" form of the catalyst sample. In a study of this type, it is necessary that the rate be controlled by the surface reaction to maximise the number of possibly transient active species and so facilitate detection, apart from the desire to observe the catalyst working under optimum conditions.

Tétényi, Babernics, Guczi and Schachter used a kinetic analysis to determine the adsorption of hydrogen, cyclohexane, benzene, isopropanol and acetone on the catalytically active part of a nickel surface (50). It was suggested on the basis of bond strength value that the catalytic reactions studied "select" the most active part of the surface. Support for this theory was obtained by studies of ethylene hydrogenation in the presence of preadsorbed hydrogen.

The nature of a particular catalysed reaction may, on occasion, present a means of simultaneously studying adsorption. The decomposition of germane or germanium has been studied by Tamaru and Boudart (117) by a technique involving rapid cooling of the reaction system to "freeze" the state of the catalyst, and the subsequent analysis of the desorbed products at elevated temperatures. The method was applicable in this case due to the activated and reversible adsorption of hydrogen on the germanium surface. Apel'baum and Temkin (118) succeeded in measuring the fugacity of adsorbed hydrogen by the use of a very thin palladium film through which hydrogen was allowed to diffuse.

In conclusion, two general points may be made concerning the examples of the concomitant study of adsorption and catalysis discussed in this section. Firstly, the number of successful studies published to date is small, largely due to the difficulties surrounding such work on all but the simplest catalytic systems. Secondly, those studies which have proved successful have yielded useful information about the specific chemical systems investigated, and in some cases, heterogeneous catalysis in general. None of the techniques described appear to be of universal application, and therefore a greater range, or a technique of greater flexibility is necessary before this type of study can become a normal part of the investigation of a catalytic system.

2.3. The Occupancy Principle

The problem of finding a satisfactory mathematical description for the behaviour of radiotracers in a heterogeneous flow system has been of greater interest to biologists than chemists. Before proceeding to its possible applications to catalysis, it will, therefore, be appropriate to give a brief description of some biological work in this field. A more comprehensive discussion of the basic mathematical theory, derived initially from these studies, will be given in appendix II.

In 1961, Bergner formulated his theory of "Tracer Dynamics" (119, 120) in an attempt to provide a comprehensive treatment for studies of the movement of labelled molecules in biological systems. It was found that only rarely could this movement be regarded as representative of the "mother substance", or set of chemical species of which the tracer molecules are part. The model used by Bergner in his analyses was that of an organ of the body through which passes a flow of blood carrying metabolites with certain residence times in different parts of the organ. The result of greatest experimental importance was produced in a further paper (121), where a time statistical approach was adopted. It was shown that properties of the system such as flow rate and amount of "mother substance" in the organ could be related to time averaged behaviour of the tracer.

In 1968, Orr and Gillespie (122), published their "Occupancy Principle", derived from Bergner's time statistical approach, with a view to experimental use. A similar model was chosen, with a pulse of tracer metabolite being injected into the blood flow before the organ, and the activity of the organ and effluent blood flow monitored with time. The "Occupancy", θ , for any part of the system was defined as the total integral with respect to time of the fraction of the total tracer dose, f(t), present in that part of the system after time t:

$$\theta = \int_0^\infty f(t)dt \qquad \text{Equation 2.1.}$$

A more meaningful terminology for the symbol θ was used by Bergner (121,123), the "tracer time of sojourn" in that part of the system. The "Capacity" C, of the part of the system under study, is defined as the quantity of "mother substance" (not necessarily tracer) that is in that part at all times, the "mother substance" moving through the system with a constant flow rate, F.

The Occupancy Principle states that for a rheostatic (constant flow) system, the ratio of occupancy to capacity is the same for all parts of the system, and equals the reciprocal of the entry flow.

$$\text{i.e.} \quad \frac{\theta}{C} = \frac{1}{F} \qquad \text{Equation 2.2.}$$

(To avoid confusion with the accepted notation in catalysis literature, the occupancy will henceforth by designated $\bar{T}$).

A subsequent series of studies were carried out by Orr et al., in which the Occupancy Principle was applied to problems concerning the estimation of thyroid iodine (124), the prediction of a radioactive dose due to an internal radioisotope (125), estimation of individual drug-dosage regimens (126), and a model for thyroxine metabolism (127).

Let us now consider the Occupancy Principle in more detail, with respect to a flow of reactant gas over a catalyst bed, a system in certain respects analagous to a flow of blood through an organ. Such a system is illustrated schematically, in figure 2.1 where a constant flow of reactant gas passes over the catalyst in chamber A, and the radioactivity of the catalyst and gas is monitored by detector A. The gas flow then passes through a second chamber B, where the radioactivity of the effluent gas is monitored by detector B. If at time zero, a pulse of radiotracer is injected into the reactant flow at I as in figure 2.1,such that the quantity of tracer is negligible compared with that in the reactant flow, count rate versus time curves would be expected from the two detectors of the type shown in figure 2.2.

A number of important points may be made concerning the Occupancy Principle and its application to a system of this type, viz:

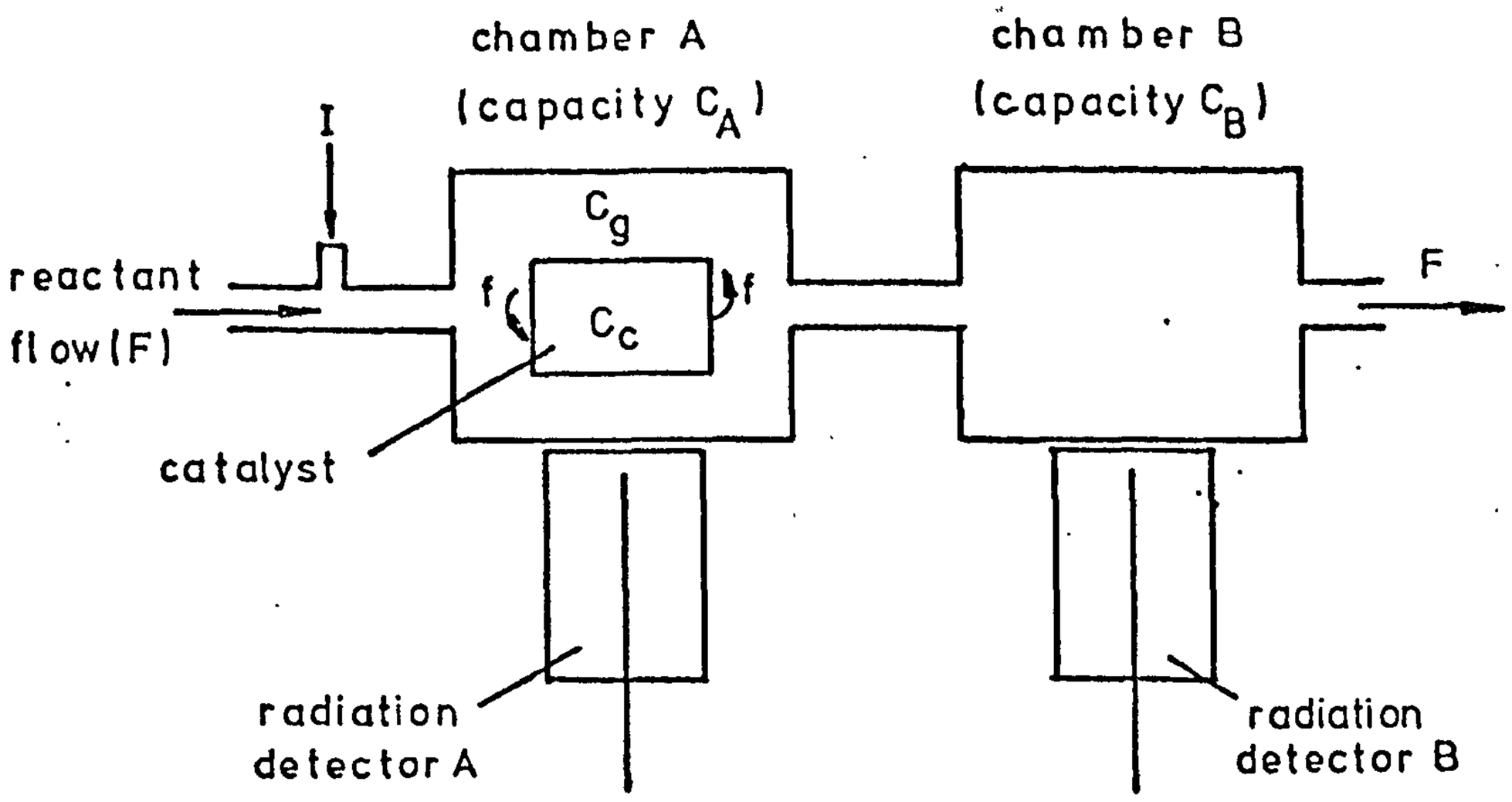

Figure 2.1. Model for the Occupancy Principle.

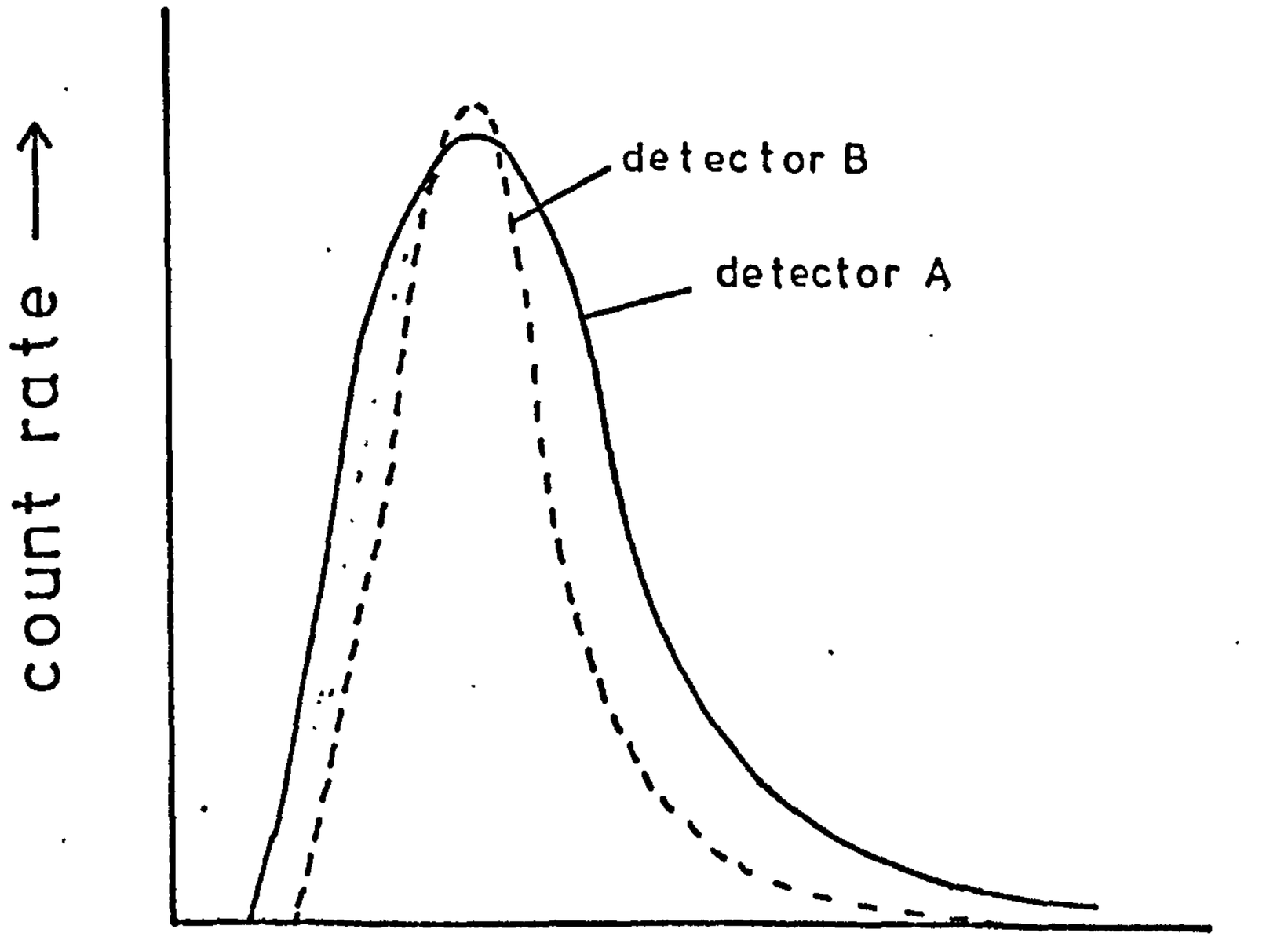

Figure 2.2. Expected count rate vs. time curve following injection of radiotracer pulse at I in figure 2.1, for detectors A (———) and B (- - - -).

(1) Equation 2.2 is independent of the number of phases present in each compartment, and the mean lifetime of a tracer molecule in each phase.

(2) The choice of a "chamber" is arbitrary, provided there exists a net through-flow of molecules equal to the total flow rate F.

(3) The net flow rate and capacity may be defined in any suitable units (normally molecule s^{-1} and molecule will be used respectively), but should be defined in terms of the "mother substance", which in this case includes reactant, product and surface intermediates. In general, the "mother substance" is that group of chemical species of which labelled molecules may at any time form a part.

(4) The count rates used in the application of equations 2.1 and 2.2 must be the total count rate for each chamber, i.e., the difference in counting efficiencies for different phases must be taken into account.

(5) A compartment may be subdivided, as for example Chamber A of figure 2, where the gas phase and adsorbed phase are divided, having respective capacities C_g and C_c. If it was assumed in this case that each adsorbed molecule reacted, desorbed and was not readsorbed, then the "flux" of molecules through the adsorbed phase, f (see appendix II), could be equated to the reaction rate. If the mean adsorbed lifetime is given a value, $\bar{\tau}_s$, then Equation 2.2 can be used to give:

$$\frac{\bar{\tau}_s}{C_c} = \frac{1}{f} \qquad \text{Equation 2.3}$$

(6) If the two chambers of capacities C_A and C_B have respective occupancies $\bar{\tau}_A$ and $\bar{\tau}_B$, we may write:

$$\frac{\bar{\tau}_A}{C_A} = \frac{1}{F} = \frac{\bar{\tau}_B}{C_B} \qquad \text{Equation 2.4}$$

since the total flow rate, F, is the same for both chambers. Thus, if values are known for the occupancies of chambers A and B, and the capacity of chamber B, a value may be calculated for the

capacity of chamber A. Equation 2.4 is of obvious importance in cases where a value of F is not readily available.

A practical difficulty arises when one considers how a value of $\bar{\tau}_A$ may be calculated. Detector A is required to monitor both adsorbed and gas phases, but the counting efficiencies for these phases will depend on the geometry of the system and the relative densities of gas and catalyst. Since, however, the relative mean gas phase lifetimes in chambers A and B will depend solely on their volumes, it should be possible to find a proportionality factor such that the number of disintegrations occurring in the gas phase of A can be determined from the number of counts collected by detector B. Once this value is obtained, the number of counts arising from the adsorbed phase may be calculated by difference. Using individual values for counting efficiencies from the gas and adsorbed phases, a total value for the number of disintegrations may be obtained, and hence a value of the capacity of chamber A by equations 2.2 or2.4. To obtain the capacity of the adsorbed phase, this must be separated from that of the gas phase of the chamber with a known capacity value for the latter.

In (4) above, we noted that the application of the Occupancy Principle equation must be to the chamber as a whole. As will be shown in appendix II, however, it is possible to use a modified version of the Occupancy Principle to apply to a specific section of the chamber. For the adsorbed phase:

$$C_c = F \frac{I_c}{D} \qquad \text{Equation 2.5,}$$

where I_c is the total number of disintegrations occurring on the catalyst during the experiment, and $D(s^{-1})$ is the total activity of the tracer dose used. Although this equation may superficially resemble that for the Occupancy Principle, F and D relate to the system as a whole, whereas I_c relates only to the adsorbed phase. the calculation of the capacity of the adsorbed phase is therefore considerably simplified.

What information then, of interest in catalysis, can be obtained from such a system as described above? A value of the capacity of the adsorbed phase will give the total number of exchangeable, reactant and product molecules adsorbed during the reaction. This measure of adsorbed species takes no account of their chemical nature, and without further evidence could not be equated to the number of molecules adsorbed on active sites.

The occupancy, or mean lifetime of the adsorbed species cannot be calculated directly. If the assumption is made, for example, that every reactant molecule adsorbs only once and then is desorbed as product, the required mean lifetime may then be calculated (see appendix II, equation II.7). This situation arises due to the applicability of the Occupancy Principle only to the complete chambers where these are heterogeneous. As will be shown in the following section, this difficulty may be overcome by the application of a time based approach, and analysis of the count rate versus time curve.

2.4. Time dependent tracer method

In the Occupancy Principle, we were concerned with the time averaged behaviour of molecules reacting in a catalytic flow system. We now wish to examine a technique based primarily on the desorption kinetics of a labelled molecule from a catalyst in a similar flow system.

Consider a constant flow system as illustrated in figure 2.1., where a constant flow of radiotracer reactant passes over the catalyst bed in chamber A. If the reactant flow is abruptly changed to an equal, but non-radioactive reactant flow, a desorption curve for the radioactive adsorbed species (or count rate versus time curve) would be anticipated as in figure 2.3. It should be noted that this change from radioactive to inactive reactant involves no change in the chemical nature of the system.

Assuming that only one type of labelled adsorbed species is present, or several rapidly interchangeable species, a probability may be assigned to the desorption of any individual tracer molecule in unit time, regardless of the order of the desorption reaction. This probability can be equated to the turnover number of the surface species, λ , and in the case of a facile reaction for which every adsorption/reaction site is equivalent, it may in turn be equated to the turnover number per site for the reaction. The rate of desorption of tracer will be given by the product of the turnover number and the number of adsorbed tracer molecules (n) at unit time t, i.e.:

$$\frac{-dn}{dt} = \lambda n \qquad \text{Equation 2.6}$$

Since the count rate observed from the catalyst at time t(x) is proportional to the number of tracer molecules adsorbed, we may write:

$$\frac{-dx}{dt} = \lambda x \qquad \text{Equation 2.7}$$

Integrating: $\ln x = -\lambda t + \ln x_o$ Equation 2.8

The turnover number obtained from a plot of lnx against time may be used to calculate a value for the number of adsorbed, exchangeable molecules, C_c, from the relation:

$$\lambda = \frac{r}{C_c} \qquad \text{Equation 2.9}$$

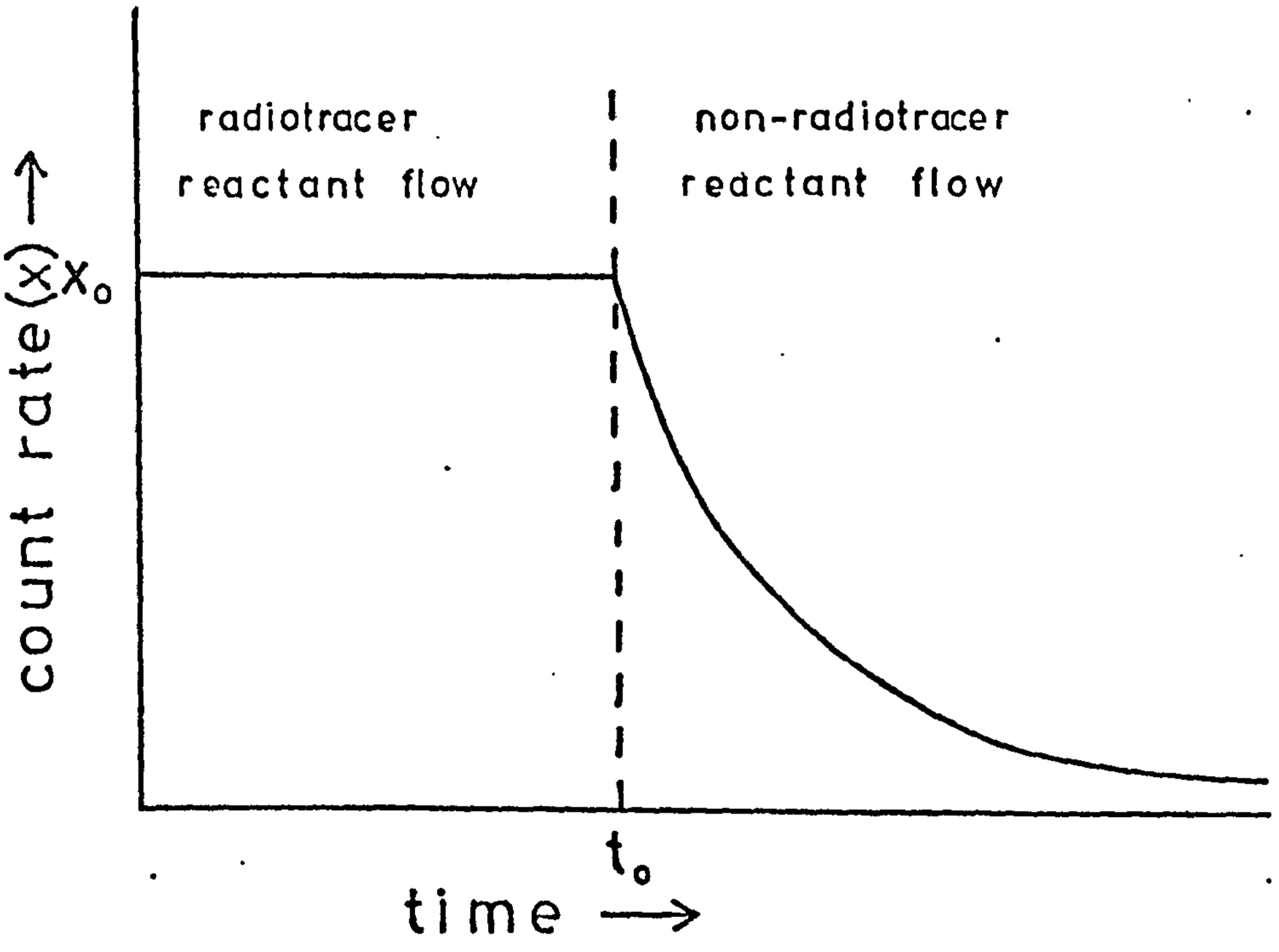

Figure 2.3. Expected curve type for radiotracer desorption experiment.

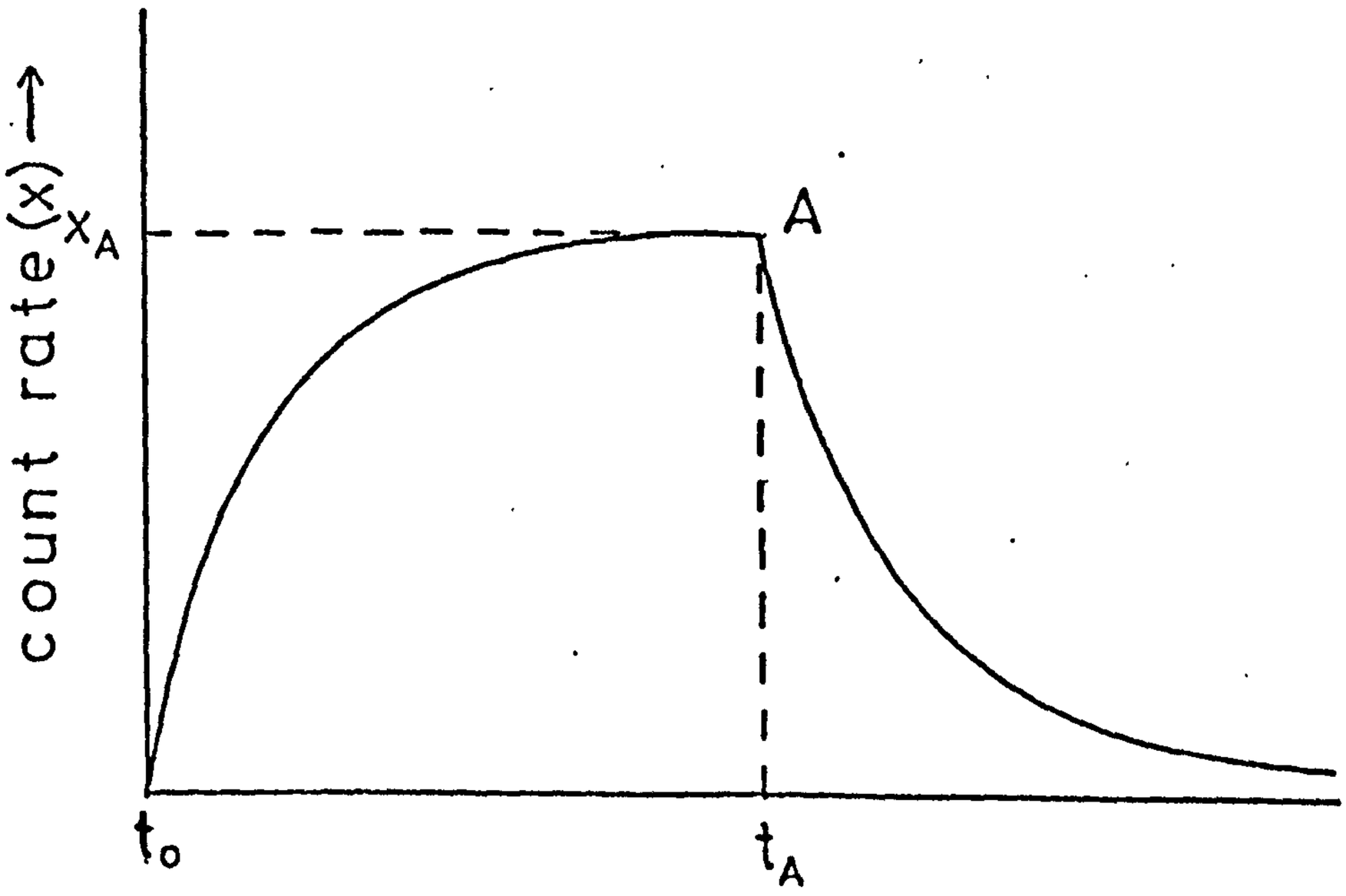

Figure 2.4. Expected curve type for passage of "rectangular" radiotracer pulse over a catalyst bed.

where r is the reaction rate. This relationship has been used in the calculation of specific rate constants where a number of active sites has been assumed (4, 5). Equation 2.9 can also be interpreted in terms of the Occupancy Principle, where λ is the reciprocal of the mean surface lifetime, and r corresponds to the flux of molecules through the adsorbed phase. Assuming that a value for the reaction rate is attainable, C_c may be calculated.

In principle, the number of adsorbed molecules might be calculated from the count rate before the introduction of the unlabelled reactant flow. In practice, this may be difficult if uncertainty exists as to the precise counting efficiency. Another difficulty which might arise in this type of experiment, is the detection of gas phase disintegrations concurrent with those from the adsorbed phase. As in the Occupancy Principle experiment, these counts may be compensated for by the use of a second, gas counting chamber, B.

Although the discussion has so far been concerned with desorption kinetics, the same principles may be applied to the adsorption process in the type of experiment for which a count rate versus time plot is illustrated in figure 2.4. Here a rectangular pulse of radiotracer reactant is inserted into the flow of inactive reactant, and the count rate rises to a maximum x_A at time t_A. Equation 2.6 may be modified to yield the adsorption equation:

$$-\frac{d(x_A - x)}{dt} = \lambda (x_A - x) \qquad \text{Equation 2.10}$$

The kinetic equations given so far can only strictly be applied to an ideal system, i.e. one in which only one type of adsorption/desorption process occurs. For a surface with adsorption sites of differing types or energies, a more complicated kinetic scheme may be expected. It should also be noted that for an experiment of the type shown in figure 2.4, the Occupancy Principle can also be applied, since the requirements regarding constant flow and chemical composition are satisfied. The analysis of tracer desorption should, however, yield more information if more than one type of process is found to occur.

Much of the foregoing treatment may be applied in certain circumstances to a non-constant flow experiment, i.e., one in which a pulse of tracer reactant is passed over the catalyst in a flow of carrier gas. Here, however, the order of the desorption process will be of primary importance, and one may find that the desorption kinetics vary with the fall in surface coverage. While the interpretation of such desorption curves might prove difficult, they may contain more information about detailed surface processes.

In the present study, it was decided to utilise both the Occupancy Principle and the time dependent methods in investigating catalytic systems. The chemical systems chosen for these studies will be discussed in the next chapter. At this point, it may be expected that constant flow conditions would be difficult to implement experimentally, due to the heat liberated in the catalyst bed and the consequent temperature instability, particularly in rapid reactions. The necessity might be envisaged to use pulsed flow conditions, in spite of the greater complexity in interpreting the results obtained.

C H A P T E R 3

Choice of Reaction Systems

Chapter 3.

Choice of Reaction Systems.

3.1. General remarks.

In the previous chapter, two new dynamic radiotracer methods were discussed for the concomitant study of adsorption and catalysis. In order to test these methods, it was first necessary to choose appropriate reaction systems. Some general principles governing this choice, mostly of a practical nature, may be laid down as follows:

(a) The catalyst for the reaction chosen should be a supported metal. The values of site densities collected by Maatman (52) indicate that higher concentrations of active species should be observed on such surfaces than for example on non-metallic catalysts. This consideration combined with the high surface area of a supported metal compared with an evaporated metal film or single crystal should optimise the detection of active species.

(b) The supported metal should be easily reduced under low temperature conditions. This limitation was imposed by the nature of the radiotracer counting systems employed (see chapter 4), and the difficulty of performing high temperature reductions in such a system. A noble metal catalyst is therefore indicated.

(c) The reaction rate should be convenient for study at, or near, room temperature to avoid the difficulties outlined in (b) above.

(d) The reactant chosen should be readily available commercially with carbon-14 labelling to avoid the problems of a necessarily small scale synthesis with radioactive materials.

The two systems chosen for study, the hydrogenolysis of chloro-benzene and the hydrogenation of ethylene, will be discussed in the remaining sections of this chapter.

3.2. The hydrogenolysis of chlorobenzene.

This reaction was initially chosen as a test system for the Occupancy Principle method, primarily because of the simplicity of the apparatus required.

The overall reaction may be written as

$$C_6H_5Cl + H_2 \rightarrow C_6H_6 + HCl$$

and is readily catalysed by palladium, platinum and rhodium. Hasbrouck (128) studied the liquid phase reaction (in ethanol solution) over palladium-, platinum- and rhodium-on-carbon catalysts, at room temperature and atmospheric pressure, with and without the addition of base. Palladium was found to be the most active metal under all conditions, the relative activities of platinum and rhodium varying according to the reaction conditions employed. In this type of reaction the halogen is normally removed without, or prior to, reduction of the aromatic ring (129).

Of the three metals used by Hasbrouck (128), palladium appears to be best suited to a study of the hydrogenolysis reaction. The activity of all three metals, supported on silica, was determined by Schuit and van Reijen for the hydrogenation of benzene (4), palladium having the lowest activity for this reaction. The combination of highest activity for hydrogenolysis and minimum activity for hydrogenation should result in fewer complications in the system due to secondary, possibly competitive, processes. Indeed, in studying the deuterium/chlorobenzene reaction over palladium films (273-323K, 1.23 torr chlorobenzene, 24.6 torr hydrogen), Harper and Kemball (130) found the hydrogenolysis reaction to predominate, although some evidence was observed for further decomposition of the product benzene in the latter stages of the reaction.

Kraus and Bazant (131) investigated the hydrogenolysis of various substituted halogeno-benzenes in a constant flow reactor at 473K over a palladium-on-charcoal catalyst. For the chlorobenzene hydrogenolysis high specificity was again observed and an empirical rate equation, thought to be a reduced form of a more complicated expression, was given:

$$r^{o} = \frac{k_1 k_2 p_A^{o} (p_H^{o})^{\frac{1}{2}}}{k_1 (p_H^{o})^{\frac{1}{2}} + k_2 (p_H^{o})^{\frac{1}{2}}}$$

where r^{o} = initial reaction rate

p_A^{o} = initial chlorobenzene partial pressure

p_H^{o} = initial hydrogen partial pressure

Rate determining steps with chlorobenzene reacting from the gas phase with adsorbed hydrogen, or reaction between the two adsorbed species were equally able to account for the observed kinetics.

By correlating the observed reaction rates for the different substituted halogeno-benzenes with the Hammett equation (132), the reaction was deduced to occur by a nucleophilic substitution. The relative activities of the halogeno-benzenes and analogy with the homogeneous hydride reaction supported this view. The mechanism was further deduced to be bimolecular, no halogen exchange being observed. The concept of a negatively polarised adsorbed hydrogen atom has been discussed by Horiuti and Toya (133), Parravano (134) and Bastl (135). The last mentioned author measured the Hall effect for hydrogen adsorbed on thin palladium films and interpreted his results in terms of positively and negatively charged adsorbed hydrogen.

The deuterium/p-chlorotoluene reaction was found to yield only one product, p-monodeuterotoluene, and no simultaneous deuterium exchange with the reactant. This result is in agreement with the deuterium/chlorobenzene studies of Harper and Kemball (130). Kraus and Bazant (131) suggested that the hydrogenolysis reaction involves only the Cl-C bond, adsorption occurring via a chlorine-metal charge-transfer chemisorptive bond, of the type proposed by Matsen, Makrides and Hackermann (136) and Garnett and Sollich-Baumgartner (137).

A preliminary study of the system in which pulses of chlorobenzene - Cl_4 were passed over a palladium-on-silica catalyst in hydrogen flow (138) had shown that adsorption was easily detectable in the type of system envisaged for the present study. An additional circumstance favouring this reaction for study was the production of hydrogen chloride during reaction. As H_2PtCl_6 was used in the catalyst preparation, traces of chlorine remaining after reduction might have less importance than in other reactions.

Taking all the above considerations into account, the hydrogenolysis of chlorobenzene over a palladium-on-silica catalyst appeared to be a suitable system for further preliminary investigation.

3.3. The hydrogenation of ethylene.

Since the discovery of the metal catalysed hydrogenation of ethylene to ethane by Sabatier and Sanderens in 1897 (139), many attempts have been made to ascertain the reaction mechanism. The summary of previous studies over nickel catalysts given by Koestenblatt and Ziegler (140) illustrates the extent of this work, but in spite of the vast quantity of frequently conflicting data available, definitive results have not been achieved. The three basic, alternative mechanisms for the reaction may be set out as follows:

L.H. An adsorbed ethylene molecule reacts with an adsorbed hydrogen molecule.

RI. An adsorbed ethylene molecule reacts with a hydrogen molecule from the gas phase.

RII. An adsorbed hydrogen molecule reacts with a gaseous ethylene molecule.

The designations of the above mechanisms, L.H., RI and RII are those of Laidler and Townshend (141). The L.H. type of mechanism was first postulated by Langmuir (142) and subsequently applied to a variety of reactions by Hinshelwood (143), and has since become known as the Langmuir-Hinshelwood mechanism. Mechanisms of the type RI and RII were also discussed by Langmuir (142) and later by Rideal (144), frequently being designated Rideal-Eley mechanisms.

Some of the previous studies on the hydrogenation of ethylene and the conclusions drawn will be described later in this section. It is however obvious from the mechanisms outlined above, that a knowledge of the extent of adsorption of ethylene during the reaction which is subsequently hydrogenated would be of value in elucidation of the mechanism. Following the studies of chlorobenzene hydrogenolysis, it was therefore decided to examine this reaction by the time dependent radiotracer method described in the last chapter.

Previous studies.

From the kinetic data available in the literature, there are few points of general agreement, excepting the order of the reaction with respect to hydrogen, normally found to be unity, and the energy of activation, usually found to be less than 60 kJ mol^{-1}.

The value obtained for the order with respect to ethylene are usually less than 0.4. The precise value of this order is of obvious importance since, particularly for the L.H. mechanism, the ethylene pressure should have some effect on the reaction rate over a wide range of pressures.

In the studies of Pease (145) with copper catalysts, Farkas and Farkas (146) on platinum wire and Toyama (147) on powdered nickel, increasing ethylene pressure was found to have an adverse effect on the reaction rate. Other investigators, such as zur Strassen (148) and Twigg and Rideal (149, 150) with nickel wire, Beeck (151), Jenkins and Rideal (152) and Kemball (153) with evaporated metal films, found that the reaction was zero order in ethylene. Laidler and Townshend (141) explained this inconsistency in terms of the precise experimental conditions. They found that over nickel and iron films the initial rate of reaction depended on the order of introduction of the reactants, being faster on prior introduction of hydrogen and a factor of three times slower with ethylene admitted first. When both reactants were admitted simultaneously, an intermediate initial rate was obtained, and at later times in the reaction, approximately equal rates were observed regardless of the order of introduction. These observations, taken in conjunction with the activation energies found under different methods of introduction of reactants (32.6 kJ mol^{-1} for simultaneous introduction and 41.8 kJ mol^{-1} for prior ethylene admission) and the analysis of the time courses of the reaction led to an interpretation in terms of two alternative mechanisms. It was postulated that with hydrogen admitted first and covering the metal surface, the RII mechanism predominated initially, but as ethylene was slowly adsorbed, an equilibrium was reached where the L.H. mechanism predominated. With prior admission of ethylene or simultaneous admission, the reaction was assumed to proceed primarily by the L.H. mechanism throughout its time course.

Jenkins and Rideal (152) had demonstrated the formation of "acetylenic" species on the surface of a nickel film during ethylene adsorption, and suggested that since these species were hydrogenated too slowly to take part in the normal ethylene hydrogenation, this

reaction occurred by the RII mechanism on isolated sites remaining after acetylenic complex formation. This complex formation was also suggested as the cause of the adverse effect of ethylene on the reaction rate observed in some studies. Kemball (153) found, however, that during the exchange reaction of deuterium with ethylene, there was an initial formation of C_2HD_3 and C_2D_4, showing that a transient, dissociative ethylene adsorption occurred during the hydrogenation. Laidler and Townshend (141) took this as further evidence to support a reaction involving adsorbed ethylene.

The more recent studies of ethylene hydrogenation have tended towards constant flow reaction systems with supported metal catalysts rather than the static systems of the earlier investigators. Wynkoop and Wilhelm (154) studied the reaction over a copper-magnesia catalyst, and Sussman and Potter (155) analysed their data along with their own results from propylene hydrogenation under similar conditions in terms of the Hougen and Watson rate equations (156). Using a systematic graphical method of analysis to find the equation best fitting their data, they concluded that the most likely mechanism involved atomically adsorbed hydrogen and adsorbed ethylene, i.e. a L.H. mechanism.

In their investigation of the reaction over nickel on alumina catalysts, Pauls, Comings and Smith (157) and Koestenblatt and Ziegler (140) were unable to differentiate between the RI and RII mechanisms on the basis of their rate equations. On the basis of the poisoning effect of ethylene on the reaction however, both sets of authors concluded that the RII mechanism was more probable. They essentially agreed with the earlier hypothesis of Jenkins and Rideal (152) that hydrogen is adsorbed dissociatively on a certain (probably small) fraction of the surface giving rise to reaction, the ethylene or acetylenic complex covered fraction being inactive.

In their more recent study of ethylene hydrogenation over a nickel-on-alumina catalyst under constant flow conditions, Koh and Hughes (158) used the graphical method of analysis and Sussman and Potter (155) to derive three possible mechanisms for the reaction. Of these the mechanism involving adsorbed hydrogen and adsorbed ethylene, with ethane desorption as the rate controlling step, was rejected on

the basis of reports of low hydrogen adsorption (149, 159). Reaction between adsorbed ethylene and gas phase hydrogen with ethane desorption controlling was rejected on the grounds that Rideal (152, 160) had shown the desorption of ethane to be almost instantaneous. The remaining mechanism, with reaction between adsorbed ethylene and gas phase hydrogen as the rate determining step (RI) was therefore adopted. Previous objection to this mechanism on the grounds of the poisoning effect of ethylene were discarded, as no change in catalyst activity was detected under their operating conditions. Earlier studies had shown unusual variations of the activation energy of the reaction, which tends to decrease with rising temperature, in some instances becoming negative above a certain "inversion temperature" (160, 161), depending on the pressure employed. Koh and Hughes (158) found that below 408K the activation energy was 50.2 kJ mol^{-1}, decreasing to 26.8 kJ mol^{-1} above this temperature. This result was explained in terms of low ethylene adsorption at high temperatures where the apparent activation energy would be lower than the true value by the heat of adsorption. With lower temperatures and higher surface coverage, due to the heterogeneous nature of the surface, it was argued that the most active part of this surface for the reaction would have a low heat of adsorption and hence the observed energy of activation would be the true value.

Infra-red studies of ethylene adsorbed on supported metal catalysts have yielded a considerable amount of information about the various possible modes of adsorption (162 - 166, 116). As mentioned briefly in chapter 1, Sheppard, Avery, Morrow and Yates (116) have recently attempted to give this type of study a more direct meaning for catalysis by studying the hydrogenation of ethylene under flowing reactant conditions over a platinum-on-silica catalyst. Absorption bands were observed which were attributed to $\underline{M}CH_2 - CH_2\underline{M}$ and $\underline{M}_2CH - CH\underline{M}_2$, similar bands being observed under static conditions of ethylene adsorption. On flushing the catalyst sample with hydrogen, both of these bands were found to disappear. The band attributed to $\underline{M}_2CH - CH\underline{M}_2$ was reduced in intensity first, presumably through hydrogenation to $\underline{M}CH_2 - CH_2\underline{M}$, and subsequently to gas phase ethylene. The

reaction kinetics observed, however, suggested that the rate was controlled by ethylene diffusion through the catalyst sample which was in the form of a "pressed-disc". Although the observed species appear to play some part in the ethylene hydrogenation, the diffusion controlled kinetics of the system and their apparently long surface lifetime may indicate that another mechanism is responsible for the greater part of the reaction.

In the course of this study, only the "classical" type of σ - bonded species, suggested by Horiuti and Polanyi (167) were observed. There was no indication of species of the π - bonded type suggested by analogy with hydrogenation reactions over homogeneous transition metal catalysts (168), although this may be simply a reflection of their short surface lifetime. More recent work (169) has shown an infra-red adsorption band at 1510 cm^{-1} with a shoulder at 1520 cm^{-1} to occur during ethylene adsorption on a palladium-on-silica catalyst. The surface species responsible for this band is labile to hydrogen and carbon monoxide, and is slowly removed by evacuation. By analogy with the remarkably similar bands observed by Atkins, MacKenzie, Timms and Turney (170) for tris-(ethylene) palladium, the surface species was identified as ethylene π - bonded to surface palladium. We may conclude, therefore, that this may well be the primary surface species involved in the hydrogenation reaction.

The contribution of deuterium as a tracer in the study of olefin hydrogenation mechanisms over metallic catalysts has been extensive and widely discussed (171 - 175). It has been concluded from these studies that the hydrogenation and deuterium exchange reactions are closely related, involving the same types of intermediates (173, 176). For the purposes of the present study, perhaps the most important conclusion was stated by Bond and Wells (173), when they said that it is clear beyond all doubt that adsorption of an olefin precedes its hydrogenation. While the π - adsorbed olefin was thought to be the active adsorbed intermediate responsible for many of the observed phenomena, greater difficulty was found in distinguishing between hydrogen reacting from the adsorbed phase or from the gas phase. The dissociation of the hydrogen molecule, necessary to explain the

observed results from exchange and deuteration, might equally well occur during reaction from the gas phase with the adsorbed π - bonded molecule to give a σ - bonded alkyl radical, or by a preliminary dissociative adsorption of hydrogen on the metal.

The poisoning effect of certain species formed by ethylene adsorption is a topic of interest in any investigation of the hydrogenation reaction, since allowance may have to be made for the variable catalyst activities so caused. One of the clearest demonstrations of the existence of a non-reactive fraction of the surface was by Cormack, Thomson and Webb (93). They found that a certain fraction of carbon-14 labelled ethylene, preadsorbed on various alumina supported metals was not removed by subsequent hydrogenation, molecular exchange with non-radioactive ethylene and evacuation. The proportion of initially adsorbed ethylene retained was the same for each of these treatments. In their study of the poisoning of a nickel-on-alumina catalyst during ethylene hydrogenation, Koestenblatt and Ziegler (140) monitored the catalyst activity over periods of days following various pretreatments. They found that the poisoning, assumed to be due to ethylene complex formation, depended on the precise reaction conditions. The proportion of the surface rendered inactive by such complexes therefore appears to vary with the reaction conditions rather than being restricted to the same fraction of the metal surface over a wide range of conditions. This conclusion is in keeping with the "structure-insensitive" or "facile" nature of the reaction mentioned in section 1.3.

In the case of a reaction over a supported metal catalyst, attention must be given to the possibility of reaction occurring on the support. The previously mentioned study of Gardes, Pajonk and Teichner (44) shows the likelihood of some ethylene hydrogenation occurring on an alumina support. However, Schlatter and Boudart's comparison of silica and alumina supported platinum (5) reveals no apparent difference in activity. If reaction does occur on the support, it may be concluded to be of a secondary nature, having little influence on the overall kinetics. The influence on the number of transiently adsorbed species present, however, may be considerable, depending on the relative turnover numbers for metal

and support active sites. The spillover of hydrocarbon to support was demonstrated by Reid, Thomson and Webb (95, 96) for adsorption of ethylene and acetylene on silica and alumina supported rhodium catalysts. Apart from the significance of such processes for the total observable surface coverage, the possibility of a further mechanism for reaction (probably secondary) should also be considered.

In conclusion, it appears from the above selective summary that conventional kinetic studies of ethylene hydrogenation have not, on their own, proved capable of elucidation of the reaction mechanism. Where conclusions have been reached, these frequently take into account other non-kinetic evidence. The mechanisms so derived are often as conflicting as the original kinetic measurements. Much of the confusion, so engendered, may be explained in terms of several different surface processes and adsorption modes occurring simultaneously or under different reaction conditions on similar catalyst surfaces. The study of the adsorption levels under catalytic conditions and the kinetics of the directly observed surface processes could well prove invaluable in the formulation of a definitive mechanism.

At this point, it seems worthwhile to list some of the possible situations on the catalyst surface which might be found by a study of ethylene adsorption during the hydrogenation reaction.

(a) The whole of the metal surface may be active - a facile reaction in Boudart's terminology (53).

(b) The active sites may be provided by the metal but amount to only a small fraction of the total metal area - as discussed by Taylor (1) and suggested by Maatman primarily for oxide catalysts (51, 52).

(c) No adsorbed ethylene may be found which takes part in the major catalytic processes as in the Rideal - Eley mechanism.

(d) Both metal and support may participate in the reaction through a spillover process, either of hydrogen or hydrocarbon.

Choice of catalysts.

Having decided to examine the hydrogenation of ethylene, the catalyst chosen in the first instance was platinum-on-silica, taking

into consideration the points made in (a) and (b) of section 3.1. This reaction system has been studied by various workers, some of whom are mentioned above, and was preferable to the even more widely studied reaction over a nickel catalyst due to the greater ease of reduction. The silica support was used as it is less prone to allegations of support activity than the common alternative, alumina (see e.g. 177).

On finding supported platinum too active a catalyst for convenient study of the reaction (see later), another less active noble metal catalyst was sought. From the comparative study of silica supported metals for ethylene hydrogenation of Schuit and van Reijen (4), the noble metals studied may be placed in the following order of decreasing reactivity:

$$Rh > Ru > Pd > Pt > Ir.$$

An iridium-on-silica catalyst was therefore employed in subsequent studies of the reaction.

CHAPTER 4

Experimental

Chapter 4

Experimental

Part A. Chlorobenzene Studies.

4.1. The flow system.

A schematic diagram of the system used is shown in figure 4.1. Flows of nitrogen and hydrogen controlled by needle valves and pressure regulators were passed over the catalyst via a liquid nitrogen cooled molecular sieve trap to remove water vapour.

A constant stream of chlorobenzene vapour could be injected into the carrier gas flow by the vapouriser described below. The gas flow then passed through the counting chambers, the first containing the catalyst bed. An injection port, sealed by a rubber serum cap was situated immediately before the counting chambers to facilitate injection of radiotracer samples.

The carrier gas flow rate was measured by a soap film "bubble meter", the passage of the soap film being timed with a stop-watch over a known volume. By bypassing the bubblemeter, the flow could be passed through two liquid nitrogen cooled traps to remove reactants and products from the gas stream. The products trapped over a known time interval were analysed in ethanol solution in an ultraviolet spectrophotometer to establish the flow and reaction rates.

The airtightness of the system was checked periodically by sealing the system between stopcocks A and D at an overpressure of about 100 torr. Leaks were detected by a fall in the pressure indicated by the mercury manometer.

The sections of the flow system indicated by single lines were of polyethylene tubing, other parts being of Pyrex glass. The stopcocks and glass joints were sealed with silicone high vacuum grease.

The radiotracer samples were injected into the gas flow using Hamilton precision microlitre syringes.

The vapour injector.

The apparatus used, illustrated in figure 4.2., was based on that of van den Brekel (178). The temperature of the heating coil was raised above the boiling point of chlorobenzene (405 K), normally

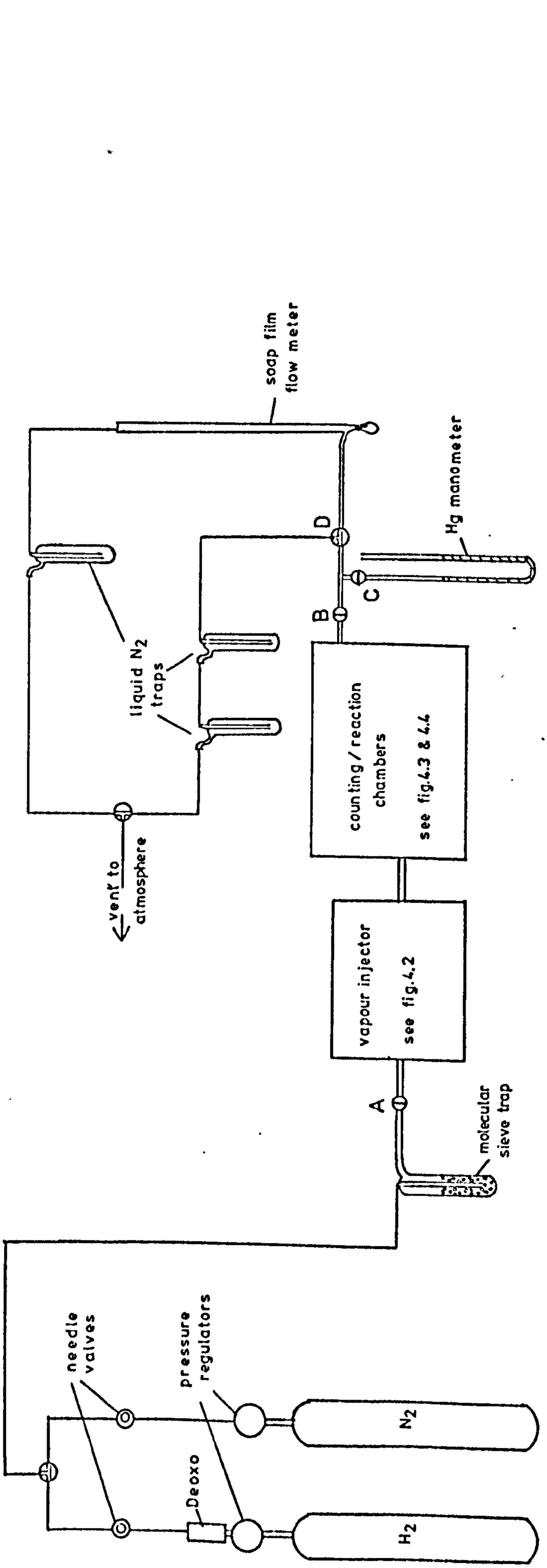

Figure 4.1. The flow system (chlorobenzene studies).

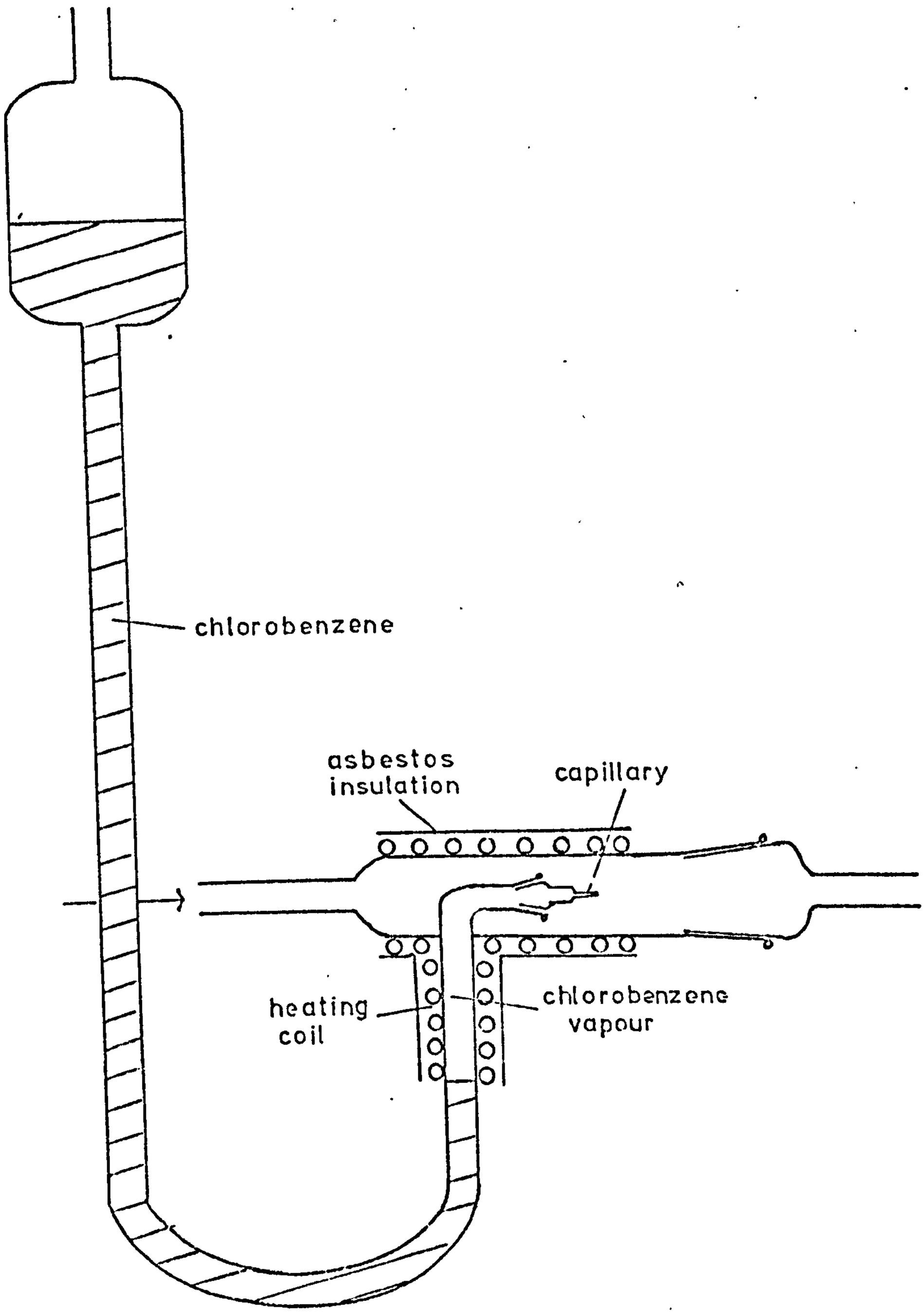

Figure 4.2. The vapour injector.

to about 423 K; control was by means of a Variac transformer. The chlorobenzene vapour so formed forced the liquid column below the heated region, creating a constant pressure head of chlorobenzene liquid. The vapour was passed into the gas flow via an interchangeable capillary. An appropriate capillary size was obtained by gradually shortening an initially too fine capillary until an appropriate vapour injection rate was established. (i.e. giving slightly less than saturated vapour pressure.)

The counting / reaction chambers.

Those used for the ambient temperature experiments are shown in figure 4.3. Thin window Geiger-Muller tubes sealed by rubber sleeves to glass flanges were clamped to the apparatus and sealed with silicone greased Teflon washers. The catalyst sample (about 150 mg) was placed in a boat sitting directly on top of the Geiger-Muller tube of the catalyst chamber. The catalyst boat consisted of a standard 10 mm inside diameter Teflon ring with a base of thin Melinex sheet, thickness 3.85 mg cm^{-2}. The pre-reduced catalyst sample (3 hours at 423 K in slow H_2 flow) was normally left overnight in a slow hydrogen flow (0.1 ml s^{-1}) prior to an experiment being performed.

The counting / reaction chamber used for high temperature studies is shown in figure 4.4. This chamber was inserted into the flow system immediately before the empty ambient temperature catalyst chamber. By means of the heating coil of Nichrome wire, and power supplied by a Variac variable transformer, the catalyst sample could be heated to 473 K. Experiments with a standard carbon-14 source showed that the counting efficiency of the Geiger-Muller tube remained unchanged for catalyst temperatures between 293 and 453 K. The temperature was monitored by a chromel/alumel thermocouple connected to a Comark Electronic Thermometer.

System volumes.

Volumes were measured by filling the apparatus with distilled water between stopcocks A and B of figure 4.1. The volume of water added with the apparatus in a vertical position was noted at various points to give the following values:

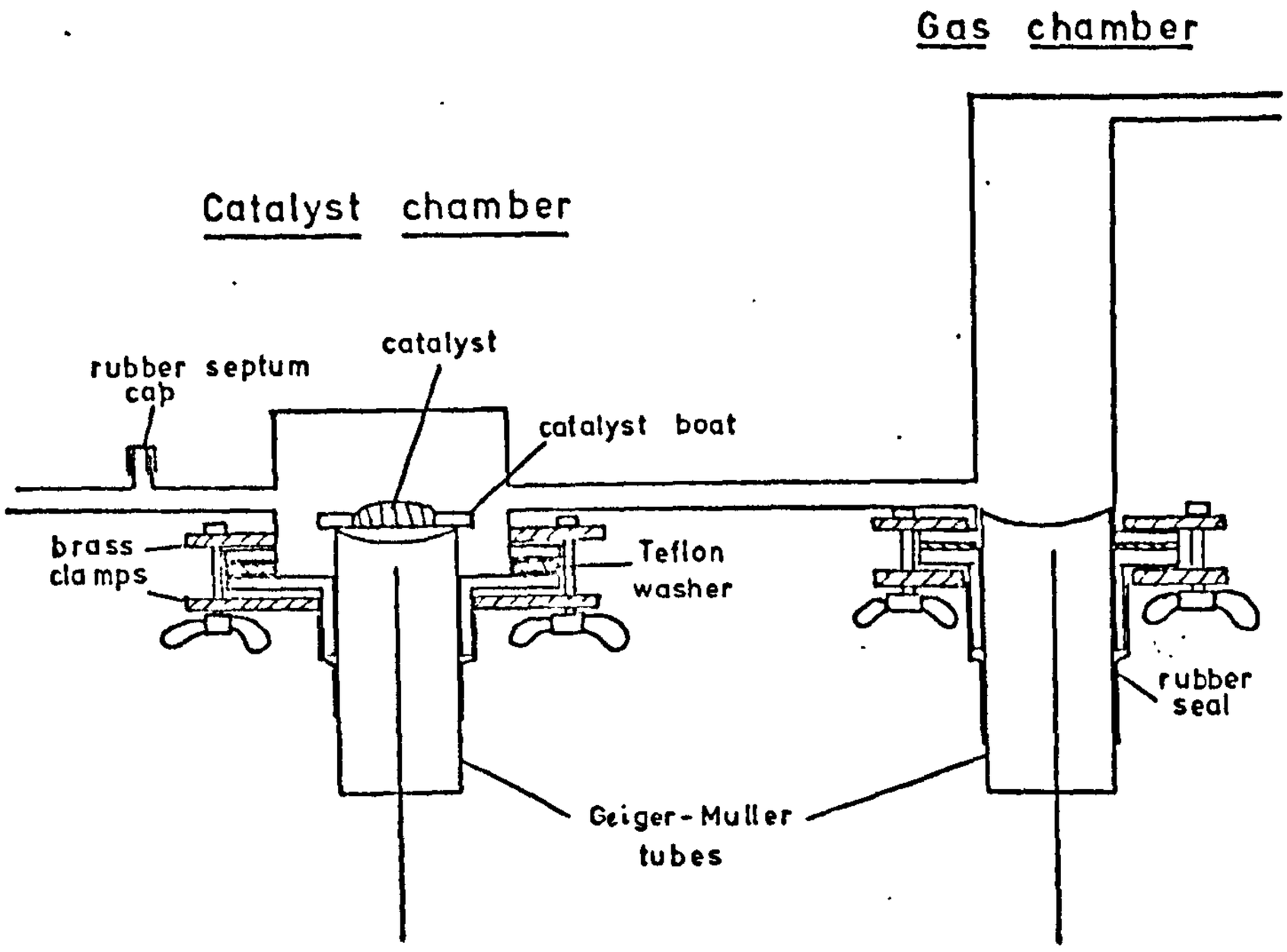

Figure 4.3. Ambient temperature counting/reaction chambers.

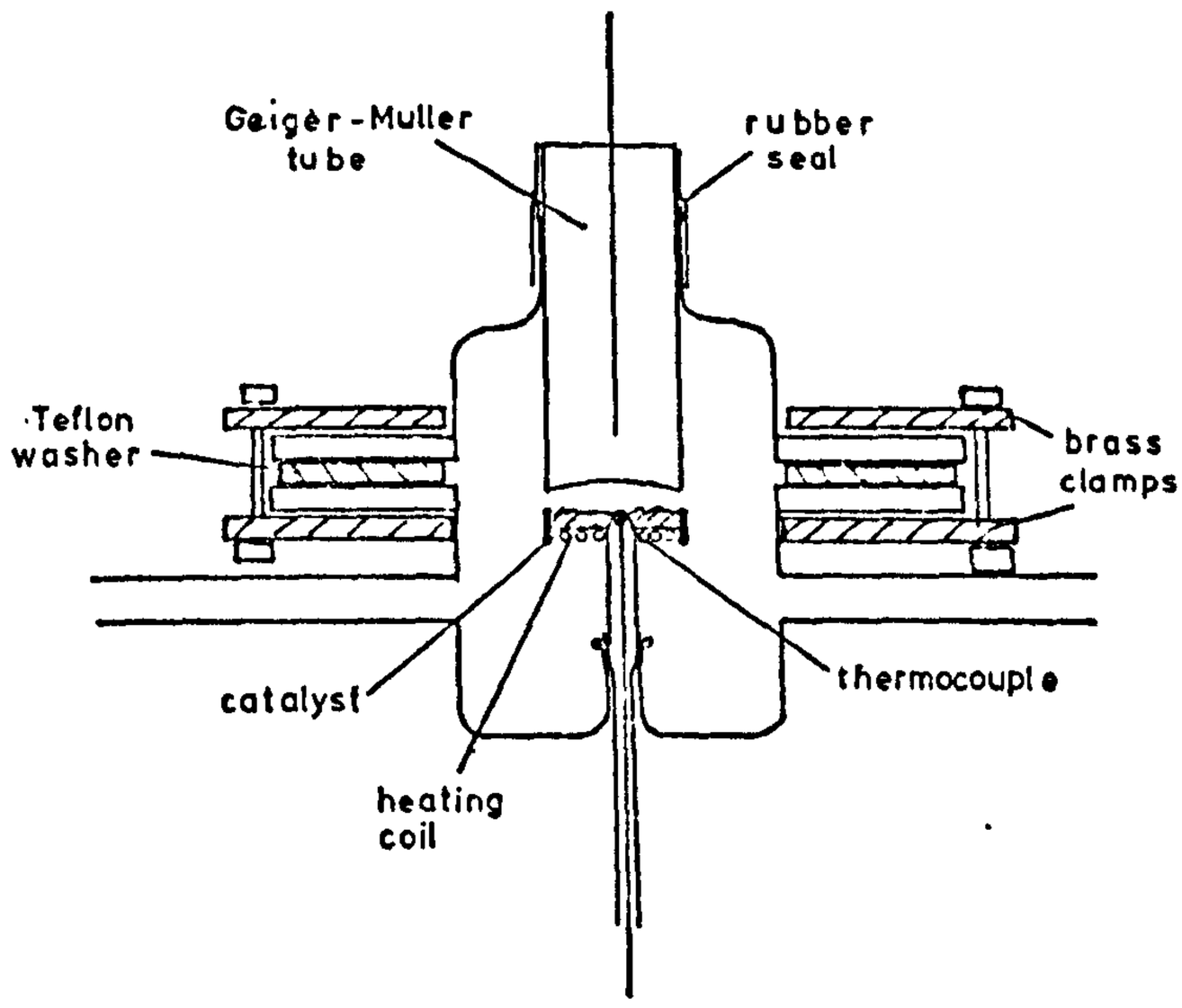

Figure 4.4. High temperature counting/reaction chamber.

Total volume of system from A to B = 183.0 ml.

Volume of catalyst chamber (ambient temperature) = 25.2 ml.

" " gas " = 87.0 ml.

Product analysis.

The products trapped over a timed interval (typically 30 minutes) after allowing the system to come to equilibrium for a period of about an hour, were collected from the appropriate trap by washing with ethanol and made up to 50 ml. This solution was analysed in a Pye Unicam SP800 ultraviolet spectrophotometer, and the concentrations of benzene and chlorobenzene estimated. From these values, the initial flow rate of chlorobenzene and its conversion to benzene could be calculated.

The system was calibrated by determining the appropriate extinction coefficients. Standard benzene and chlorobenzene solutions in ethanol were prepared, and the absorbances measured at 249.0 mμ and 271.7 mμ for each solution. The plots of absorbance versus concentration are shown in figure 4.5., with the exception of the absorbances for benzene at 271.7 mμ which were too low for meaningful measurement at lower concentrations. From the 0.01 M benzene solution, however, a value for the extinction coefficient at this wavelength was estimated to be 1.5 $1\ mol^{-1}\ cm^{-1}$. Extinction coefficients were calculated according to the Beer-Lambert relation:

$$A = \varepsilon cb,$$

where $A = \text{Absorbance} = \log_{10} \frac{(\text{Intensity of incident radiation})}{(\text{Intensity of transmitted radiation})}$

ε = molar extinction coefficient ($1\ mol^{-1}\ cm^{-1}$),

c = concentration ($mol\ l^{-1}$),

b = path length of the absorbing system (cm).

As the path length of the silica cells used was 1 cm, values of the extinction coefficient were equivalent to the slopes of the lines of figure 4.10. These were found to be: for chlorobenzene, 132.8 $1\ mol^{-1}\ cm^{-1}$ at 271.7 mμ and 62.7 $1\ mol^{-1}\ cm^{-1}$ at 249.0 mμ; for benzene, 190.3 $1\ mol^{-1}\ cm^{-1}$ at 249.0 mμ.

For a benzene/chlorobenzene mixture in ethanol, the total absorbances at 249.0 mμ and 271.7 mμ are given by the equations:

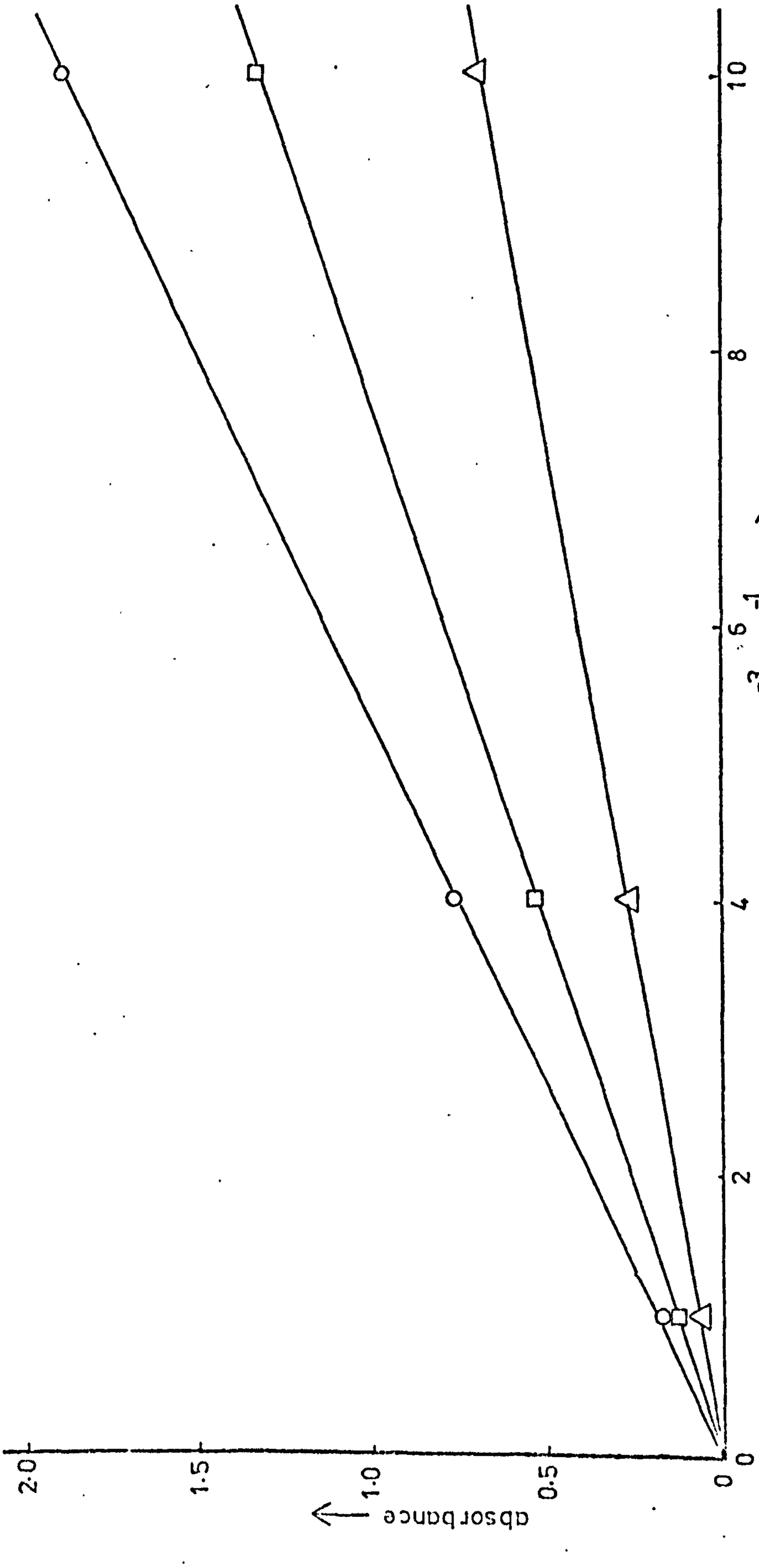

Figure 4.5. Absorbance versus concentration for :○ – benzene at 249.0nm; □ –chlorobenzene at 249.0nm; △– chlorobenzene at 271.7nm. All solutions in ethanol.

$$A_{249.0} = 68.5 \left[C_6H_5Cl\right] + 190.3 \left[C_6H_6\right]$$
$$A_{271.7} = 134.75 \left[C_6H_5Cl\right] + 1.5 \left[C_6H_6\right],$$

where square brackets denote concentrations.

Solving these equations, the concentrations may be calculated as follows:

$$\left.\begin{aligned} \left[\text{Benzene}\right] &= 5.277 \times 10^{-3}(A_{249.0} - 0.508\, A_{271.7}) \text{ mol } l^{-1}. \\ \left[\text{Chlorobenzene}\right] &= \frac{A_{271.7} - 1.5 \left[C_6H_6\right]}{134.75} \text{ mol } l^{-1} \end{aligned}\right\} \text{ Equations 4.1.}$$

4.2. The radiotracer counting system.

For the earlier chlorobenzene studies (up to experiment C2/3) the counting system consisted of two Geiger-Muller tube (Mullard MX 168) / head amplifier (Eko probe 558B) / scaler (Eko 529B) channels. This system was then expanded to include a counting ratemeter (Harwell type 1037C) and a Servoscribe chart recorder. The resulting system is shown schematically in figure 4.6. In the earlier experiments, count rates were determined by differences between readings of the counts accumulated by the scalers at regular intervals of time.

A typical plateau curve for one of the Geiger-Muller tubes is shown in figure 4.7. The plateau slope for this tube was 13% per 100 volts. The operating voltage was chosen just above the plateau shoulder at 410 volts. The head amplifiers were set to give a dead time of 500 μs.

Catalyst counting efficiency.

The estimation of counting efficiencies for carbon - 14 β^- emission from a solid source presents difficulties due partly to the lower energy of the radiation (E_{max} = 0.156 MeV). Self absorption, back-scattering, and geometric corrections are usually difficult to assess and extremely inaccurate. The best solution to these difficulties is the use of a constant counting geometry combined with a sample of effectively constant size (179). The method utilised here was that of an "infinitely thick layer" approximation for the self absorption correction which relies on the short

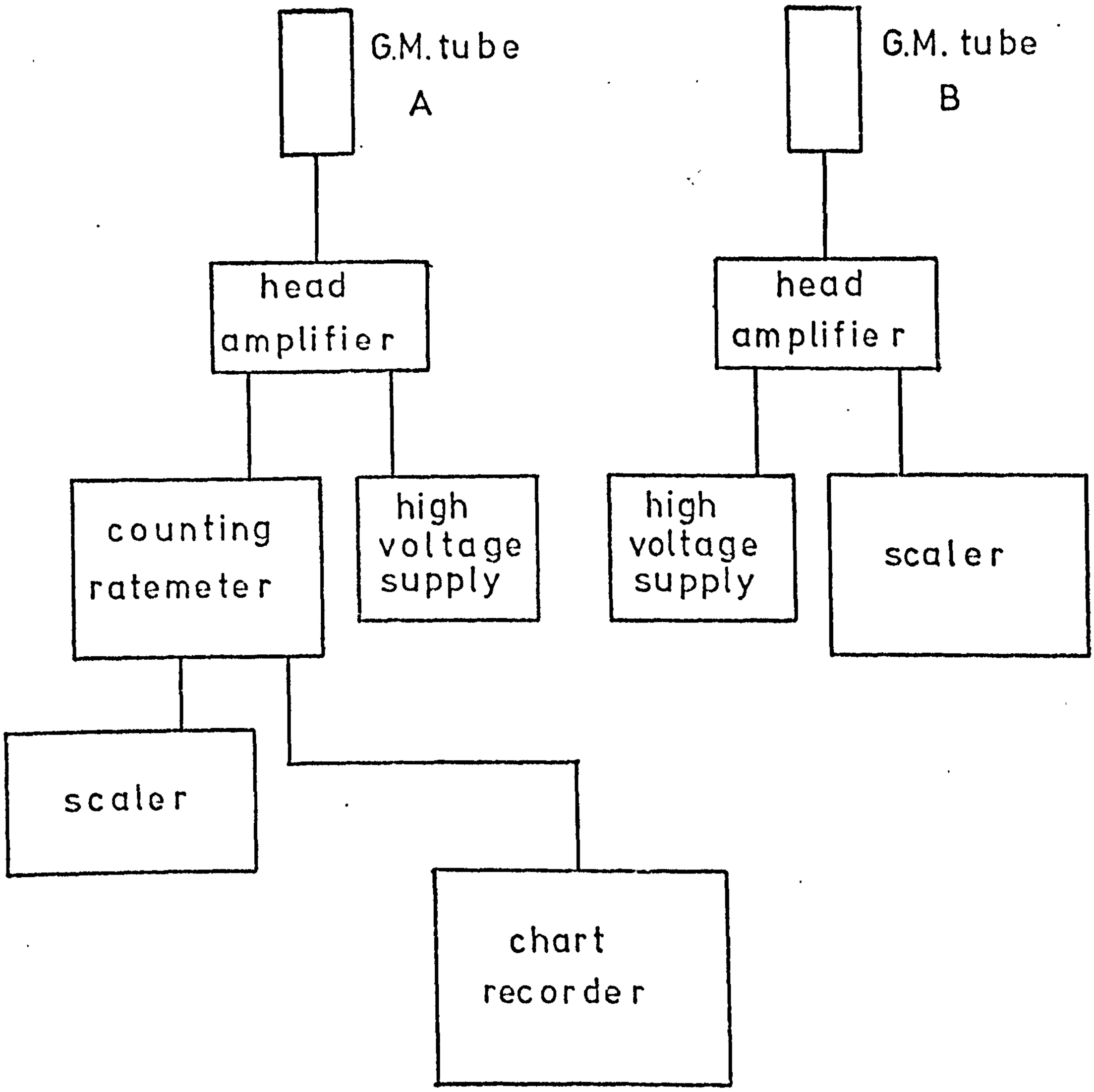

Figure 4.6. The radiotracer counting system (chlorobenzene studies).

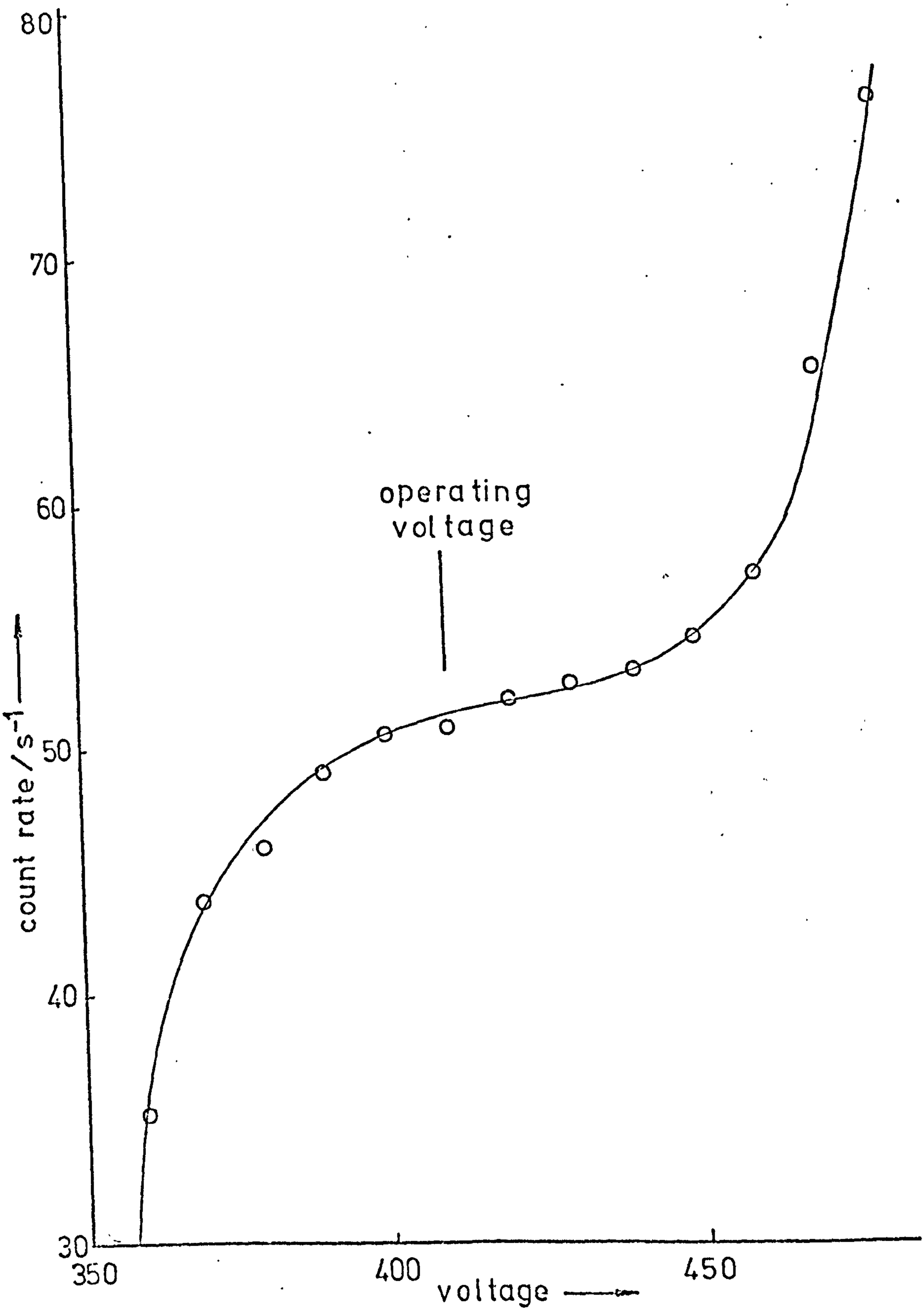

Figure 4.7. Count rate versus applied voltage for MX168 Geiger-Muller tube.

maximum range of the electrons ($\sim$28 mg cm^{-2} in Al). A sample of thickness greater than this maximum path length will give rise to a count rate approximately equal to that from an infinitely thick source of the same specific activity. Constant counting geometry was achieved in the ambient temperature experiments by use of a standard catalyst boat as described in section 4.1.

A standard source was prepared from a 5% by weight Pd-on-silica catalyst sample which was impregnated with a solution of anthracene-Cl4 in benzene. 1 ml of the anthracene solution (specific activity 2.61 x 10^4 s^{-1} ml^{-1}) was slowly added to 1.032 g of catalyst at a rate which allowed evaporation of the solvent before the next drop was added, ensuring complete uptake of the anthracene by the catalyst sample. The catalyst was then dried at 373 K and thoroughly mixed. The resulting standard source had a specific activity of 25.28 s^{-1} mg^{-1}.

Samples of up to 150 mg of the radioactive catalyst were placed in standard boats and the observed count rate plotted against the sample weight (figure 4.8.) The final point on this curve represents the mean value of the count rate obtained from 7 samples of approximately 150 mg, the standard deviation being 3.1%. From the curve, samples of 150 mg appeared to be suitable to establish an effectively infinite sample thickness.

The counting efficiency was calculated as follows:

$$\text{Catalyst counting efficiency} = \varepsilon_c = \frac{\text{observed count rate}}{\text{specific activity (mg}^{-1})} \quad \text{Equation 4.2.}$$

$$= \frac{4.37 \pm 0.14 \text{ mg}}{25.28}$$

$$\text{i.e.} \quad \varepsilon_c = 0.173 \pm 0.006 \text{ mg}$$

An observed count rate divided by ε_c will yield an activity value per mg of the catalyst.

Gas counting efficiencies.

Two calibrations were necessary for gas counting: the absolute counting efficiency for the gas counting chamber and the ratio of count rates from the gas phase of the catalyst counting chamber and the gas counting chamber. These determinations were carried out simultaneously using a hydrogen/carbon-dioxide-Cl4 gas mixture of known composition and specific activity.

$^{14}CO_2$ was produced by slowly dropping 5M HCl into a solution

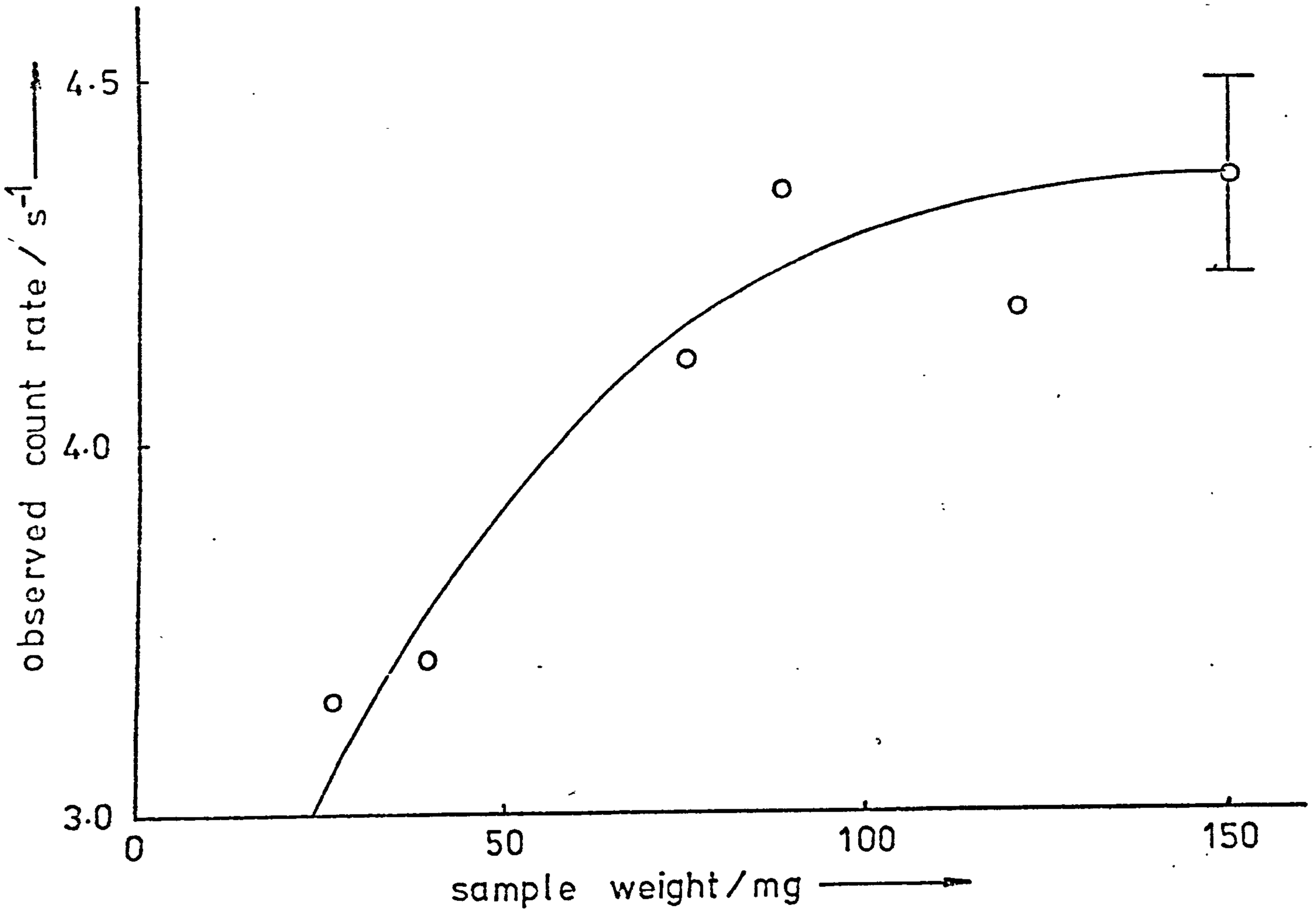

Figure 4.8. Observed count rate versus weight of sample in catalyst boat.
(anthracene-C14 / 5% Pd / SiO_2)

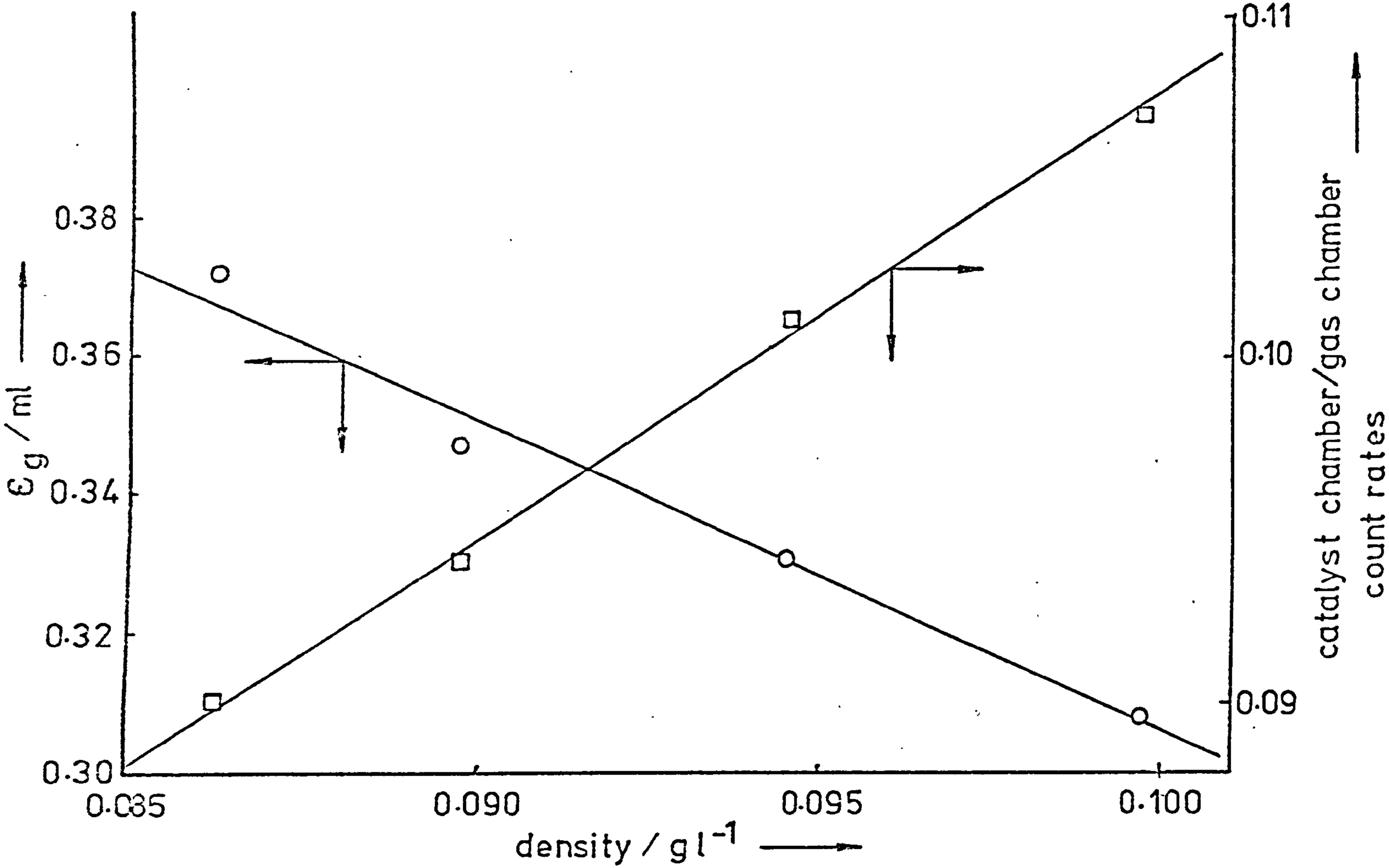

Figure 4.9. Variation of gas counting efficiency(ε_g) and gas count rate ratio for catalyst and gas chamber counters with gas density (H_2/CO_2 mixtures).

containing 0.1 mol of sodium carbonate-C14 of specific activity 4.25×10^7 s^{-1} mol^{-1}. Samples of the $^{14}CO_2$ produced were removed with a Hamilton gas tight syringe via a serum cap and injected through the serum cap of the flow system containing static hydrogen at 1 atmosphere pressure. Count rates were monitored with time for both detectors until stable values were obtained. This was achieved in about 2 hours. The counting efficiencies found for various gas densities produced by the use of different H_2:CO_2 ratios are shown in figure 4.9. The efficiency of the gas counter (ε_g) was calculated as the ratio of observed count rate to the activity of 1 ml of gas, and does not therefore depend on the volume of the gas counting chamber.

Part B. Ethylene Studies.

4.3. The flow system.

The layout of the system is illustrated schematically in figure 4.10. The various sections of the system will be described separately.

Flow controls. (figure 4.11.)

Hydrogen and ethylene gas flows were taken directly from cylinders, the hydrogen being passed through a catalytic purifier, and both flows through magnesium perchlorate tubes. In addition to the cylinder head pressure regulators, fine control was achieved using Negretti-Zambra precision pressure regulators, which gave stable gas flows over periods of days.

Pressures were measured at three points in the flow system by pressure transducers (see below), i.e. in the hydrogen flow immediately after the controlling needle valve, before the reactor and after the reactor in such a position that the gas sampling pressure could also be measured. The pressure in the ethylene line was monitored by a mercury manometer, the other arm of which was connected to the hydrogen flow line. Ethylene pressure was thus controlled relative to that of hydrogen, and normally set at an equal value. Although the pressure in this part of the apparatus was not of direct relevance to the reactor conditions, the rotameters used to measure flow rates required constant known pressure conditions for accurate operation.

The hydrogen and ethylene flow rotameters were calibrated against

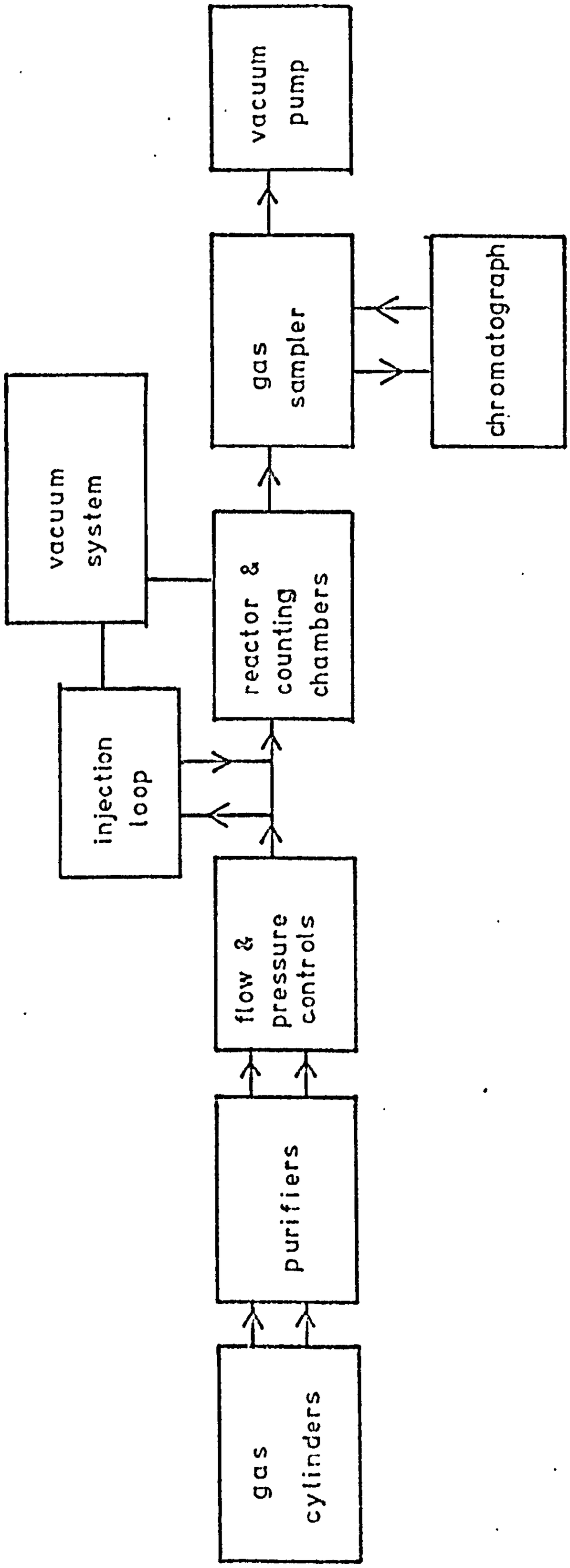

Figure 4.10. Schematic diagram of the flow system (ethylene studies).

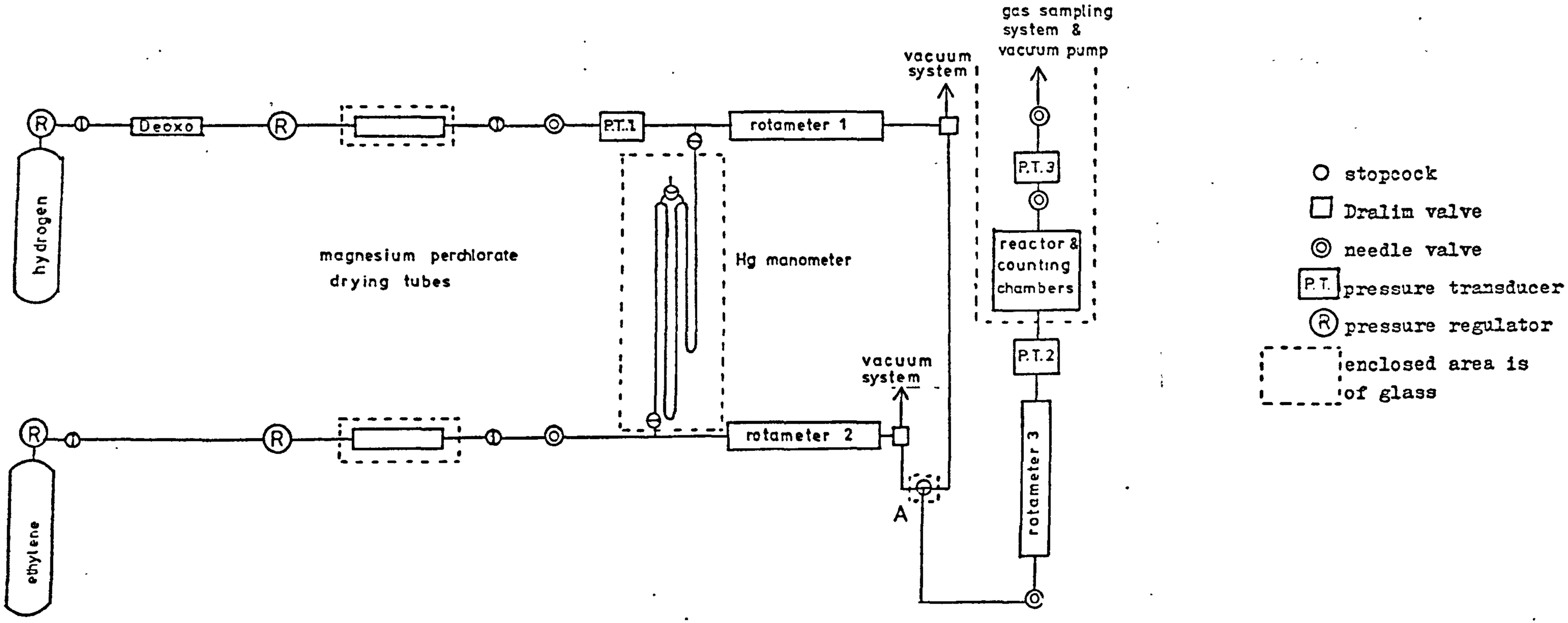

Figure 4.11. The flow system (ethylene studies).

a soap film meter which provided an absolute standard. The rotameter pressure chosen was 50 torr over atmospheric, and the curves shown in figure 4.12 obtained. For experiments involving a helium carrier flow, the flow rate was initially determined by a soap film meter and the rotameter reading then maintained at a constant value. A similar procedure was adopted for the hydrogen flow when the pressure of measurement was necessarily greater than the adopted standard.

The hydrogen and ethylene flows could be mixed or passed separately through the 3-way stopcock at A of figure 4.11., then through rotameter 3. The primary function of this rotameter was to monitor small changes in the ethylene/hydrogen ratio which were easily observable due to the relatively large fluctuations produced in the flow rate indication. Although this effect could not easily be used to measure the gas composition, it provided a check on the stability of the ratio. Having passed through the reactor, the gas flow was either vented to atmosphere or passed through the gas sampling system for analysis.

The flow controls were constructed primarily of copper or brass, connections being of copper tubing ($\frac{1}{4}$ inch or $\frac{1}{8}$ inch) joined by brass Swagelock seals. The parts of the apparatus constructed in Pyrex glass are shown enclosed by broken lines in figure 4.11. Metal to glass connections were made with $\frac{1}{4}$ inch Swagelock seals with brass ferrules for the metal seal and Teflon ferrules for the glass seals. The rotameters used had glass bodies, stainless steel bobs and nylon end blocks. The system was designed to take up to at least 1 atmosphere overpressure, glass stopcocks being spring loaded.

In experiments requiring a helium flow, the ethylene cylinder of figure 4.11. was exchanged for one of helium. Hydrogen and ethylene gases required for use in the vacuum system were diverted from the flow system via a Dralim valve immediately after the rotameter measuring the respective gas flow.

Tracer injection loop.

The difficulties involved in changing abruptly from one type of gas flow to another without seriously affecting the flow rate were

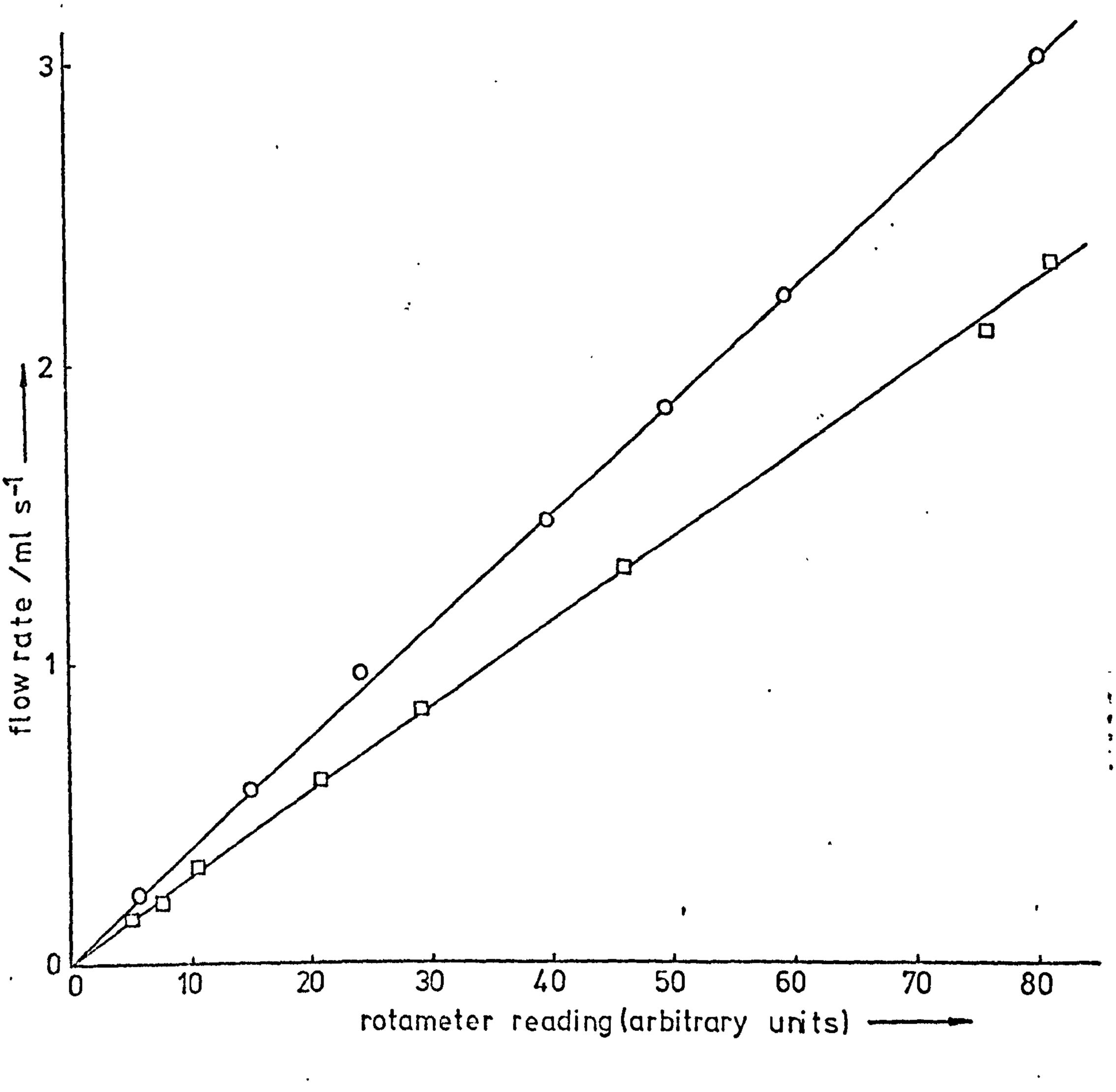

Figure 4.12. Rotameter calibration curves: ○ - hydrogen (rotameter 1); □ - ethylene (rotameter 2).

solved by use of the tracer injection loop shown in figure 4.13 Gas mixtures were made up in the loop by freezing a known amount of ethylene (normally carbon-14 labelled) from the vacuum system into the evacuated loop, allowing it to thaw, and then making up to the pressure of the gas flow with hydrogen via the vacuum line, The gas mixture was then allowed to mix for at least 2 hours, or shorter periods if the mixing was enhanced by heating the loop at B to improve circulation. The "rectangular" tracer pulse could then be injected into the gas flow by rotating the four-way stopcock, A, through 90° from the position shown in the diagram, causing only a minimal disturbance to the gas flow. The pulse was terminated by rotating stopcock A through a further 90° which gave a sharper boundary to the tail end of the pulse than simply allowing the complete sample to pass into the gas flow. The length of the pulse was timed to use approximately 2/3 of the original sample in the injection loop.

The volume of the loop could be varied by means of interchangeable glass sections connected by two spring-tensioned cone and socket joints. The volume determination of the loop with the section normally used is described below (see Vacuum system) and was found by weighing empty and filled with water, as was that of the standard section, giving a total volume of the loop with the larger section in place of 103.1 ml.

An alternative method used for rapidly filling the larger tracer loop with a non-radioactive ethylene/hydrogen mixture was from a 200 ml stainless steel gas-sampling cylinder. The requisite gas mixture was made up in this cylinder by adding the gases to pressures indicated by transducer 4 (see below.)

Reactors and counting chambers.

Two reaction/counting systems were used for the ethylene studies, the first of which (A) is illustrated in figure 4.14. The reactor is shown in the position required for counting and reaction. For reduction of the catalyst sample, the reactor was used in the inverted position, the sample being introduced via the 'O'-ring sealed cone and socket joint in the centre of the reactor. The sample was then reduced in a hydrogen flow while being heated by the surrounding furnace (4 hours at 473 K). On completion of the reduction, the reactor was sealed by the two 'O'-ring sealed stopcocks, detached

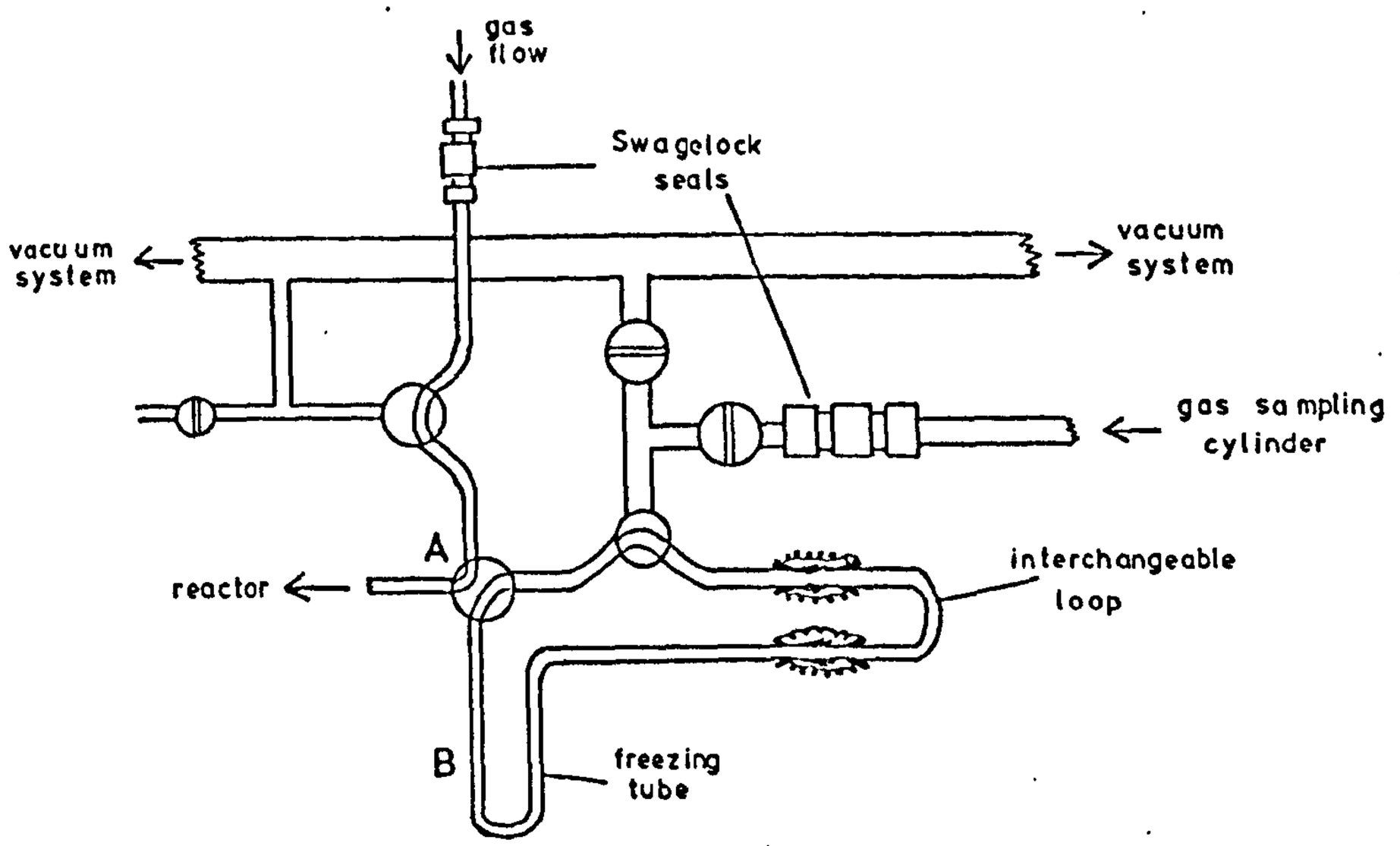

Figure 4.13. The tracer injection loop.

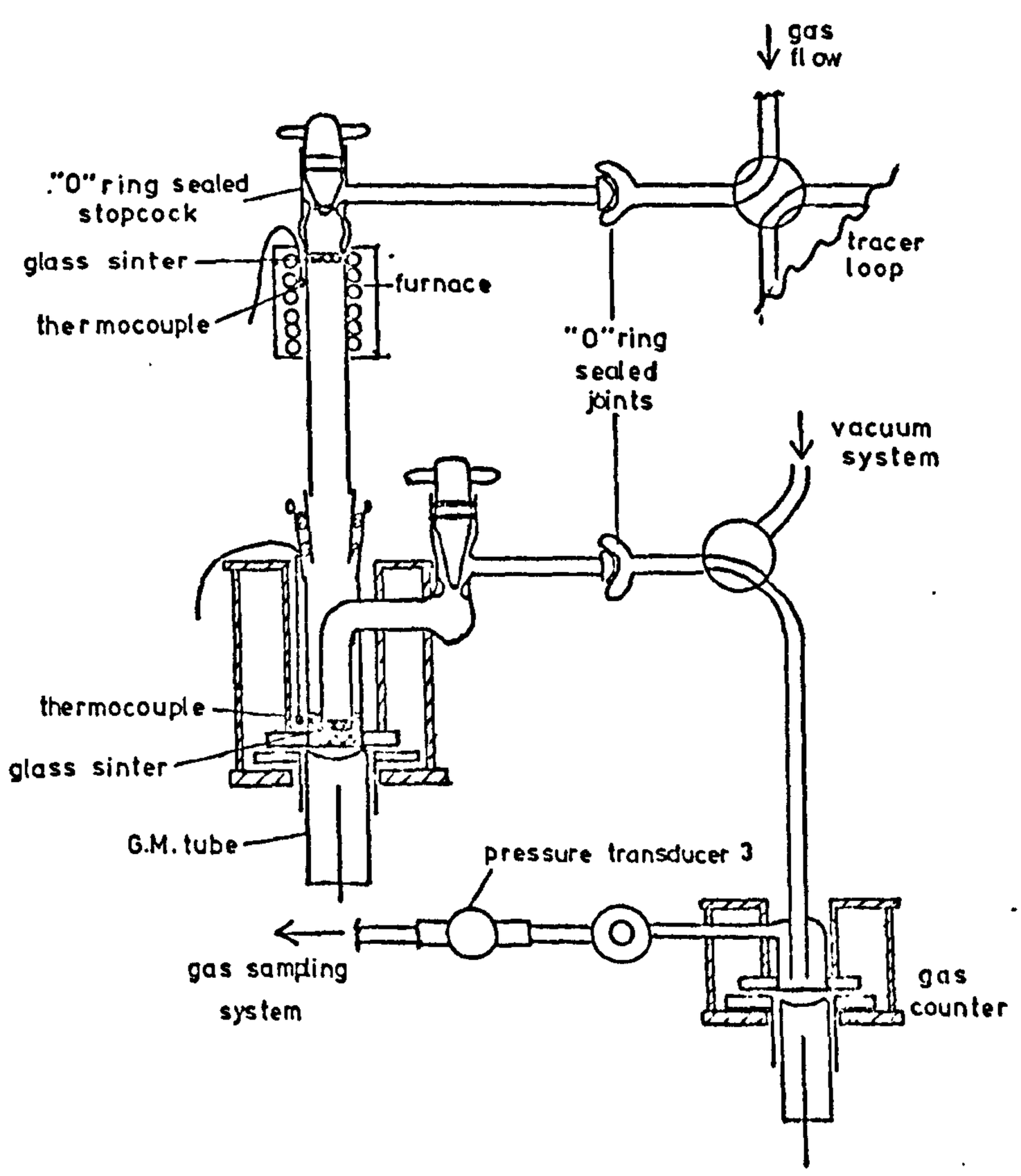

Figure 4.14. Reactor/ counting chamber and gas counting chamber A.

from the system at the ball and socket joints and inverted. The catalyst was manipulated until it lay in the position illustrated. The reactor was then reattached to the system in the upright position, the tubing sections at the joints evacuated, and the gas flow resumed.

The base of the reactor was sealed with a sheet of Melinex film (see section 4.1.) to facilitate counting from the catalyst, with the Geiger-Muller tube directly below. The film was held in position between two glass flanges, which in turn were clamped together by the aluminium framework illustrated. A vacuum tight seal was effected by Kel - F fluorocarbon wax, melting point 333K. The catalyst was retained within the reactor by the two porosity - 3 glass sinters shown.

For low temperature experiments, the section of reactor including the catalyst was enclosed in a polythene bag and insulated by an expanded polystyrene box. Cold nitrogen produced by the apparatus shown in figure 4.15. was passed through the polythene bag and the temperature monitored by a chromel/alumel thermocouple in the position shown connected to a Comark Electronic Thermometer. The gas counting chamber used in conjunction with this reactor was of a similar construction to the base of the reactor, with a Melinex film window for counting.

The second type of reactor, used for most of the ethylene studies (F5/1 onwards), was designed to abate some of the faults inherent in a glass construction such as reactor A. The principal fault in reactor A lay in its poor flow characteristics, which resulted in a rounding of the pulse shape. Secondly, temperature regulation was only possible for ambient and lower temperatures.

Reactor B as illustrated in figures 4.16. and 17. was constructed mainly of stainless steel with minimum dead-volume requirements as a prerequisite. The flat catalyst bed was held in position by a pair of porous Teflon plugs through which the gas flow passed. Radioactive counting was through a window either of Melinex film, or, in runs F 5/1 to G 1/7, of mica of similar thickness. Although

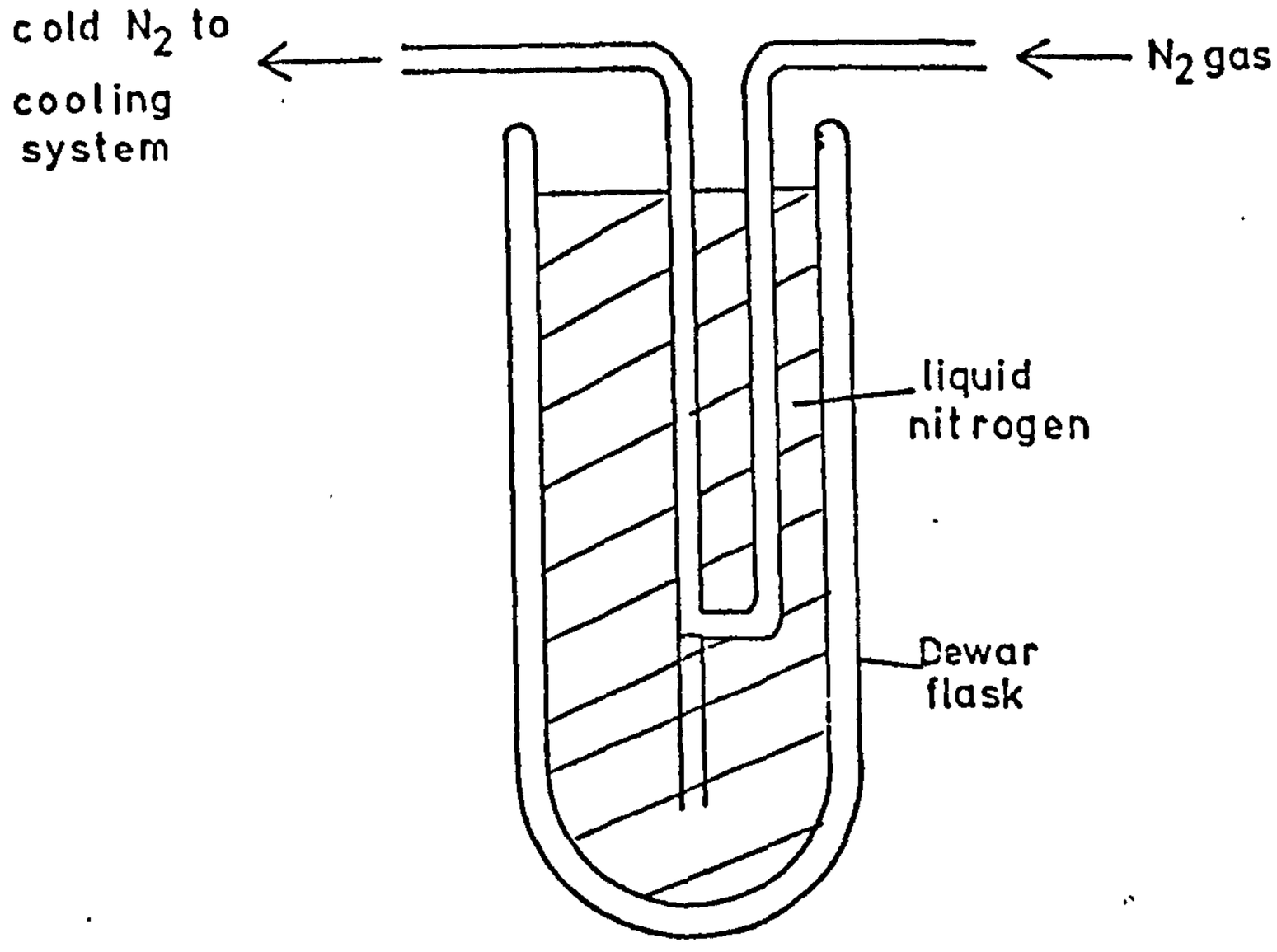

Figure 4.15. Apparatus for production of cold nitrogen flow.

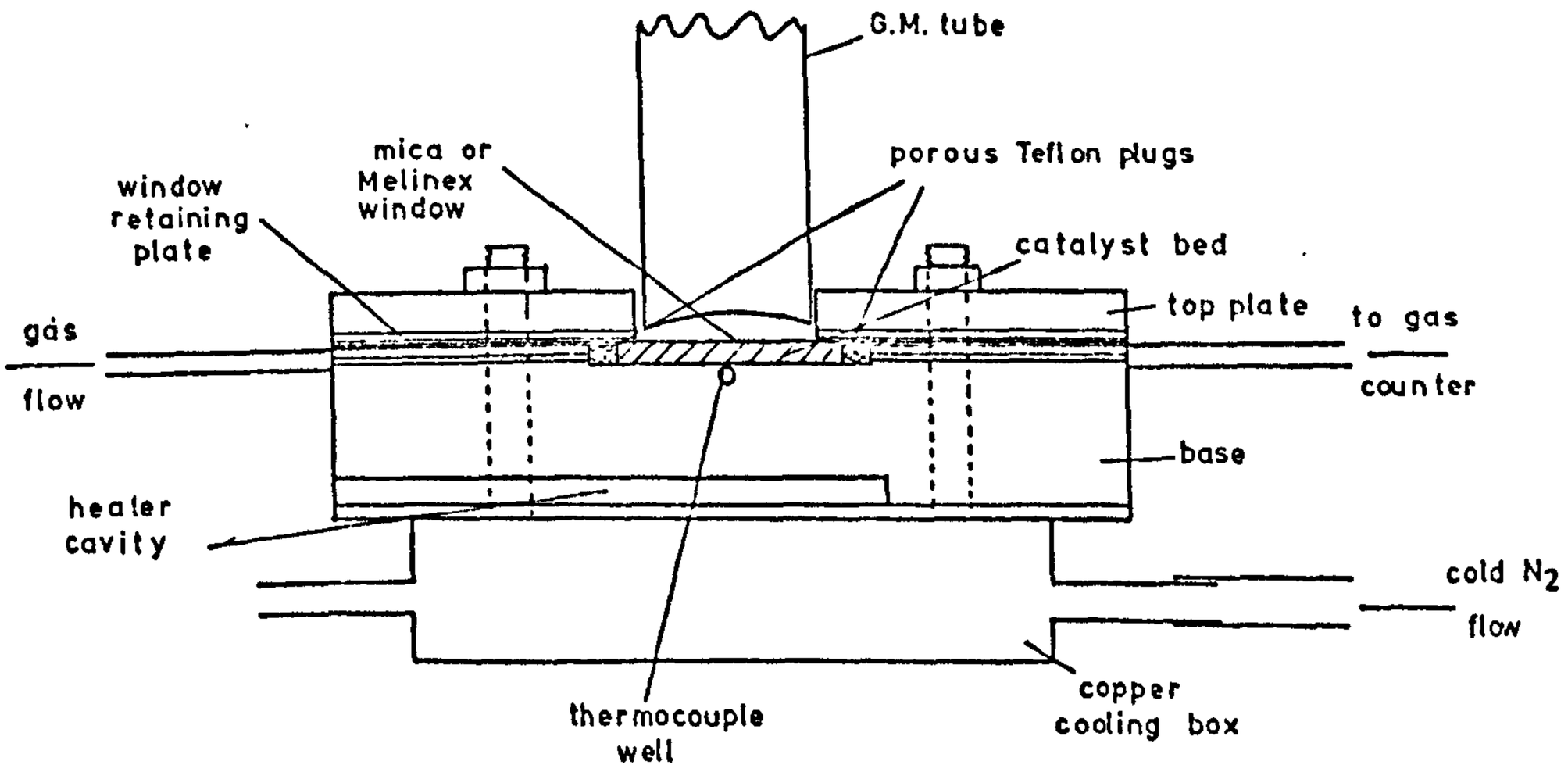

Figure 4.16. Section through reactor/ counting chamber B.

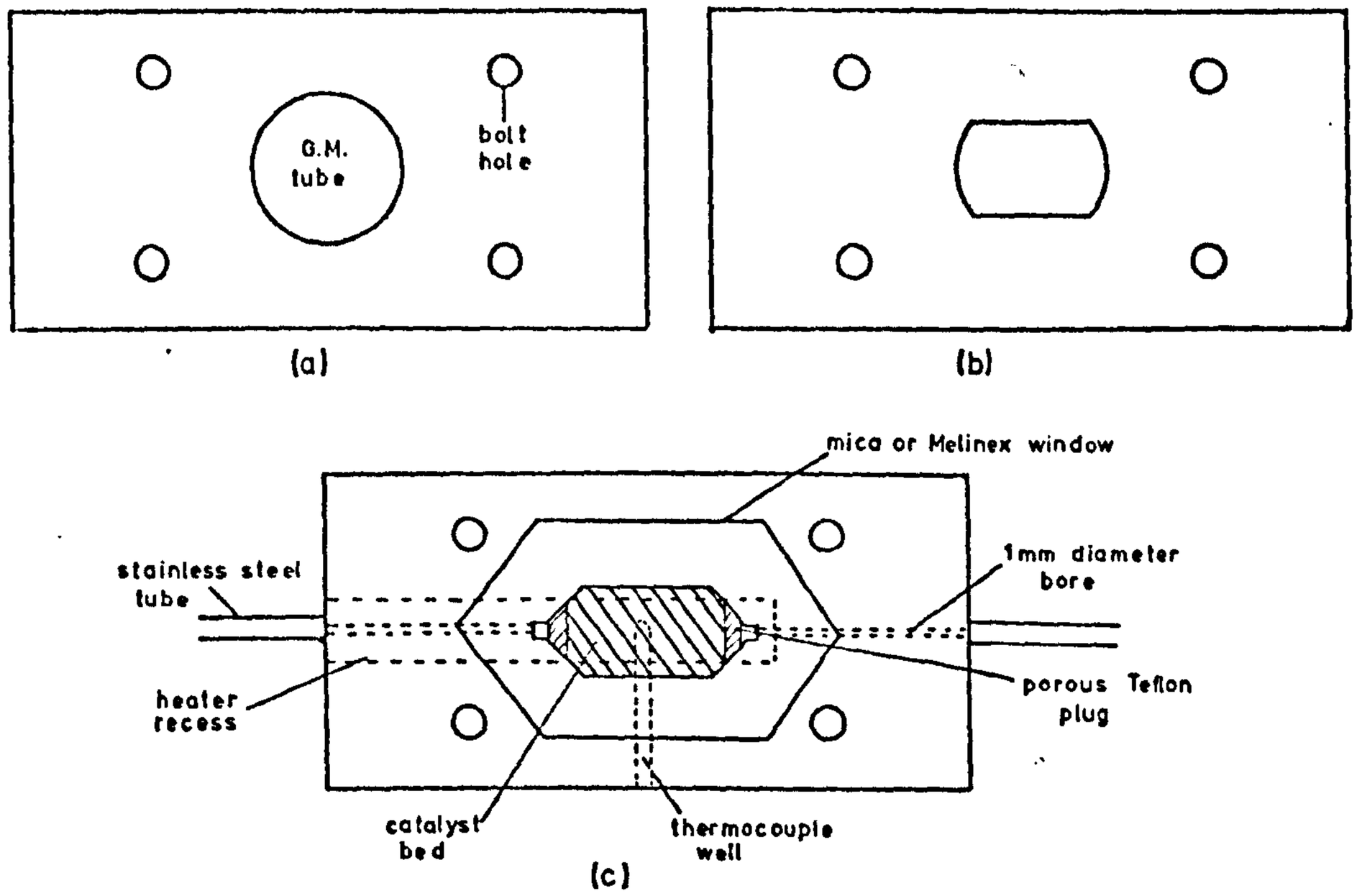

Figure 4.17. Plan view of reactor B component parts.

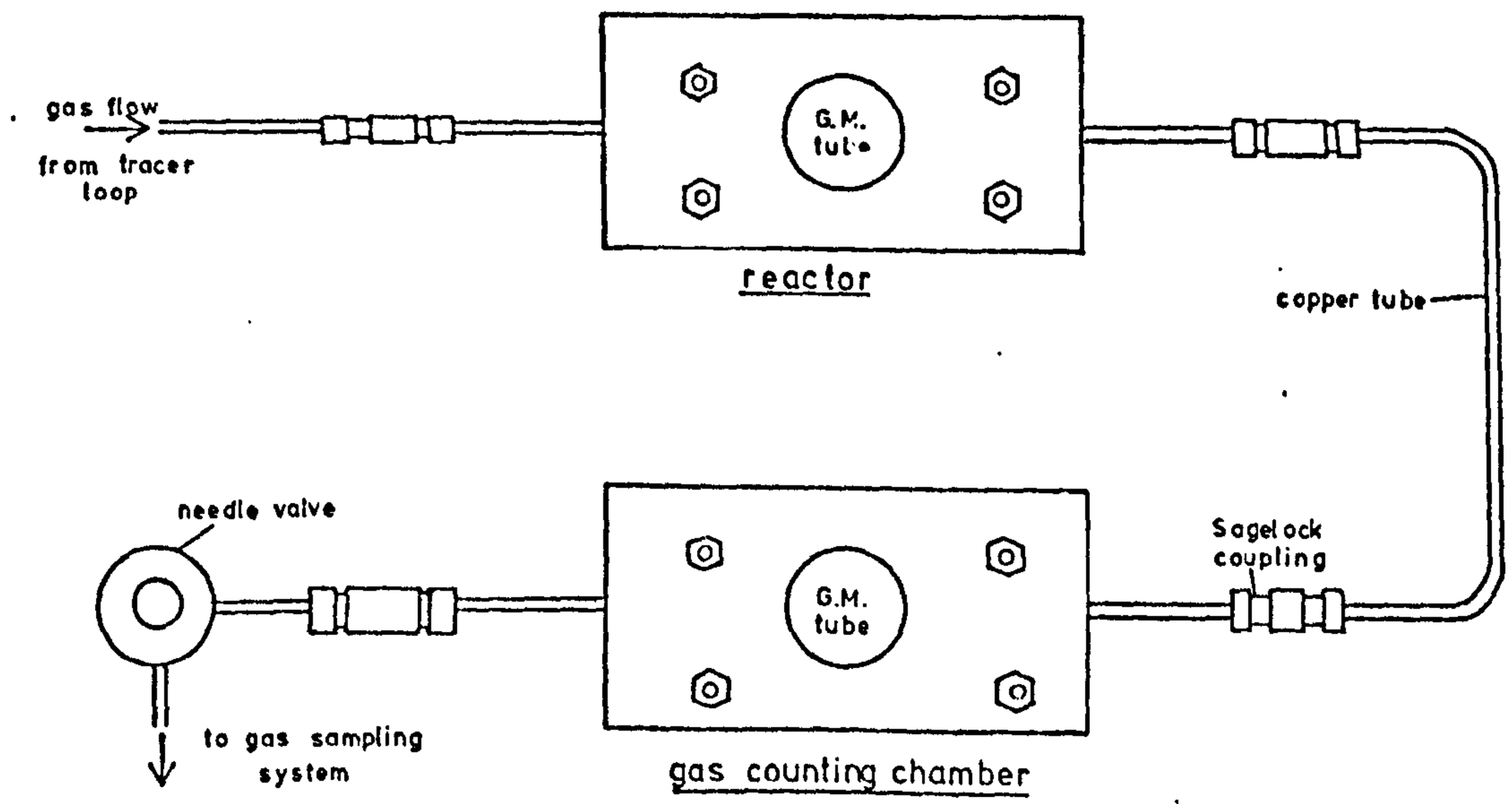

Figure 4.18. Layout of counting chambers B.

the mica windows were less sensitive to heat, they were difficult to prepare to the necessary thinness and prone to splitting, both while assembling the apparatus and while conducting experiments.

The counting window was held in position by a thin stainless steel template (figure 4.17(b)), surmounted by a thicker top plate (figure 4.17(a)), which also held the Geiger-Muller tube in a constant position for counting. These three sections were held together by four $\frac{1}{4}$ inch stainless steel bolts. A vacuum-tight seal was achieved between the reactor base and the counting window by applying a thin smear of silicone grease to the upper surface of the base.

Heating of the reactor was effected by a 40 watt flat soldering iron element inserted into the base, the reactor being surrounded by a shroud of several thicknesses of asbestos paper. Cooling was by a cold nitrogen flow from the apparatus described earlier, through a copper box attached to the base of the reactor. The temperature was measured by a chromel/alumel thermocouple, positioned in the well shown in figure 4.16., 0.5 mm below the centre of the catalyst bed.

Figure 4.18. shows the experimental layout of the reactor and gas counter. The gas counting chamber was of similar construction to the reactor, with the omission of heater cavity, cooling box, thermocouple well, and catalyst.

Connections between the tracer injection loop, reactor, gas counter and gas sampling system were of $\frac{1}{8}$ inch o.d. copper tubing coupled by Swagelock connectors. This arrangement helped to minimise the dead volume between the tracer loop and the reactor, and also to improve the flow characteristics.

Gas sampling system.

The sampling system was designed to take several samples of gas in rapid succession from the effluent gas flow of the reactor for subsequent chromatographic analysis. The apparatus (figure 4.19) was based on a series of loops which could be bypassed by double 'V' bore stopcocks.

The gas flow was led into the sampling system via stopcock A in the position shown, and with the other stopcocks in their illustrated

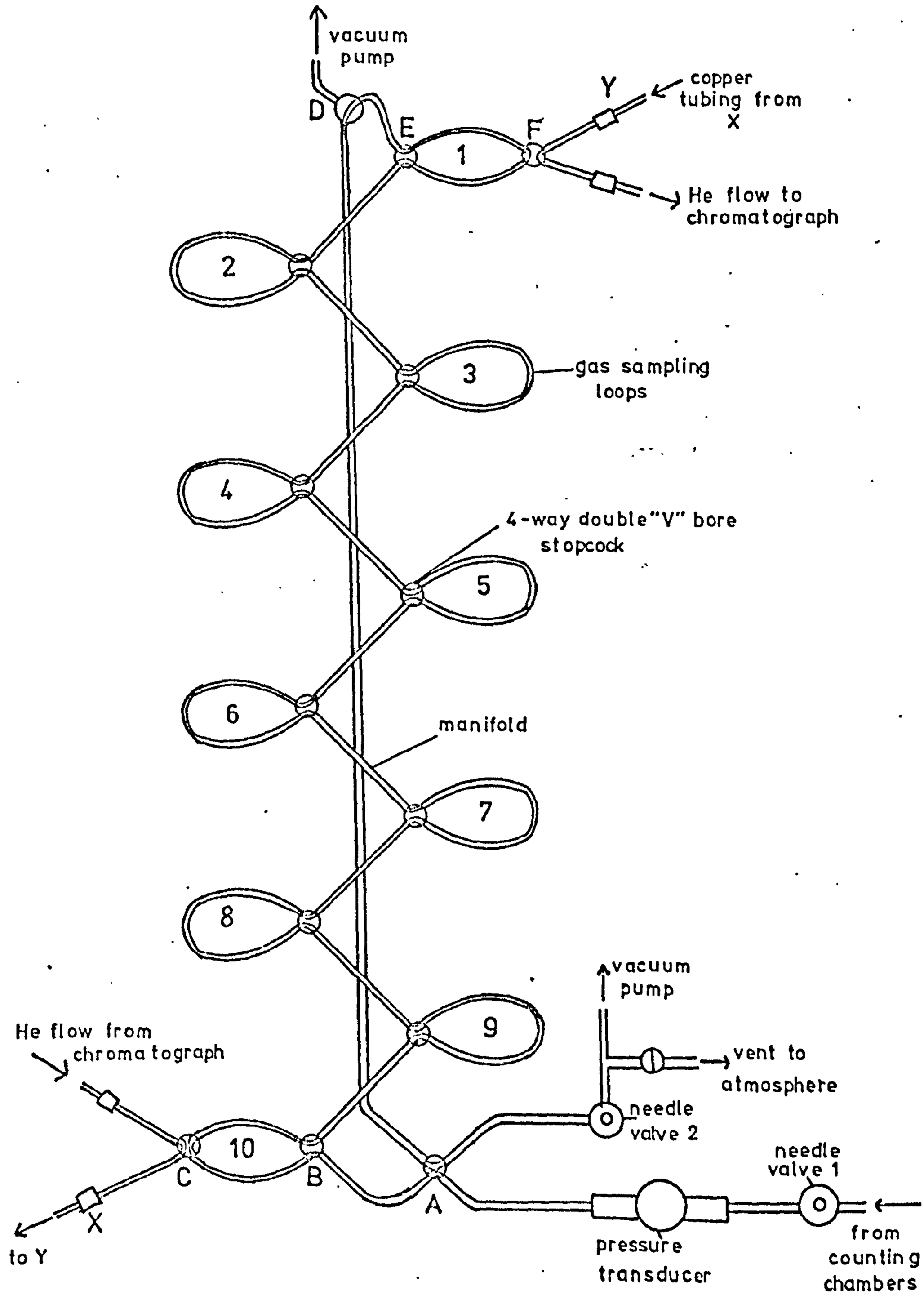

Figure 4.19. The gas sampling system.

positions was then passed through the sampling loops, leaving the system at A. By turning the stopcocks of loops 2 - 9 or stopcocks E and B for loops 1 and 10 respectively, a gas sample was removed from the flow. Alternatively, a set of samples could be taken by turning stopcock A through 90° to bypass the sampling system and subsequently sealing the individual loops.

With the loops sealed and the sampling system bypassed, the connections between the loops were evacuated via stopcock D. Samples from loops 1 or 10 could be injected into the helium flow of the gas chromatograph by turning stopcocks F or C respectively through 90°. The helium flow was then passed through the manifold of the system by rotating stopcocks E and B through 90° to the position shown in the diagram. Samples 2 to 9 were analysed by opening the appropriate loop to the helium flow. For regular monitoring of the gas flow over longer time intervals, loops 1 and 10 only were used, avoiding the necessity to pass the helium flow through the manifold.

The effective volume of the system was varied by adjusting the sampling pressure to a suitable value. The pressure was reduced by venting the system to a rotary vacuum pump and adjusting needle valves 1 and 2, while keeping the flow rate and hence the pressure in the reactor, constant.

The volumes of the sampling loops were determined by weighing the individual loops empty and filled with water, prior to being glass-blown into the system. The values obtained, numbered according to figure 4.19., are listed in table 4.1.

Table 4.1. Volumes of gas sampling loops.

Loop number.	1	2	3	4	5
Volume / ml.	7.71	6.69	6.28	5.96	7.09
Loop number.	6	7	8	9	10
Volume / ml.	3.12	3.04	3.08	3.05	3.45

The gas chromatograph. (figure 4.20)

The primary purpose of the chromatograph was for analysis of ethylene/ethane mixtures. The column used was 4 feet by $\frac{1}{4}$ inch outside diameter copper tubing packed with 40/60 mesh silica gel. The column was placed inside an oven consisting of a Pyrex tube wound with 33 m of Nichrome tape ($\sim 13\ \Omega\ m^{-1}$) insulated with asbestos paper. The space between furnace and column was packed with steel wool to aid heat conduction. The furnace was placed inside an asbestos tube filled with Vermiculite packing for thermal insulation. Power was supplied by a Variac variable transformer and the temperature measured by a thermometer embedded in the steel wool.

Prior to use, the column was baked in a slow helium flow overnight at 433 K to remove water. Normal operating conditions for good ethylene/ethane separation were at 353 K with a 1 ml s^{-1} helium carrier flow. The helium flow was controlled by a Nigretti - Zambra precision pressure regulator and measured by a rotameter.

The separated components of the sample eluted from the column were detected by a katharometer (Gow Mac Instrument Co.) operating on the basis of four Rh/W filaments connected as a Wheatstone bridge circuit (see figure 4.21.) The helium reference flow, passing over filaments R_1 and R_2 was taken before the point at which samples were introduced. The carrier flow containing samples was passed over filaments S_1 and S_2. Power was supplied from a constant current supply set at 200 mA. The bridge was connected to a Servoscribe potentiometric chart recorder.

Samples were admitted to the helium flow either from the gas sampling system as described above, or via the rubber injection septum of a bypass to the sampling system.

The chromatograph was calibrated by injection of samples of ethylene and ethane using a Hamilton gas-tight syringe and standard conditions. Figure 4.22. shows the calibration curves for both peak heights and peak areas measured by a triangular approximation. From the slopes of these curves, the peak height ratio for ethane:ethylene was 2.01 and the area ratio 1.09. Figure 4.23 shows a typical ethylene/ethane/hydrogen separation, the sample having been injected from the gas sampling system. Calibration of hydrogen peaks was not possible, due to the typical 'W' shaped peak.

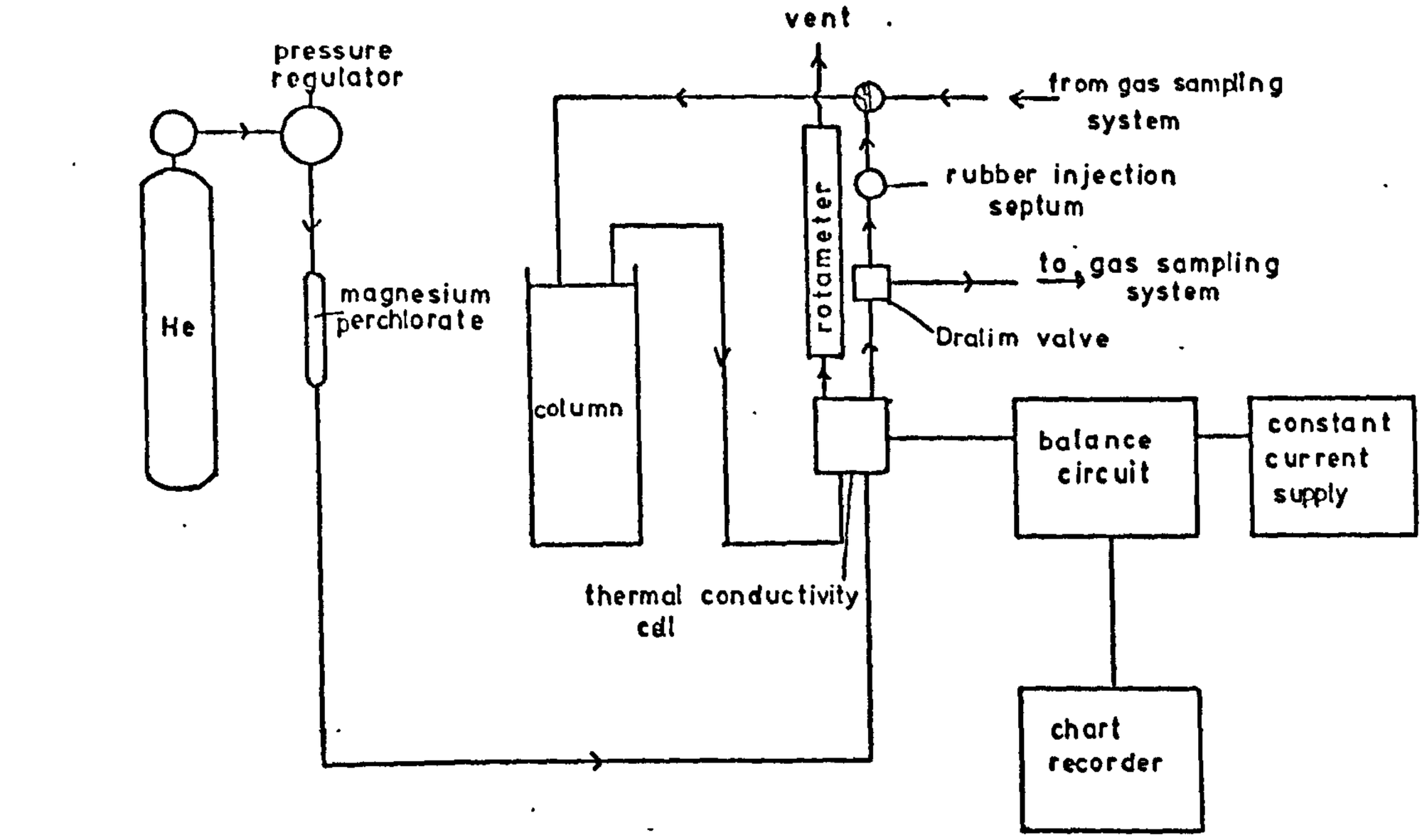

Figure 4.20. The gas chromatograph.

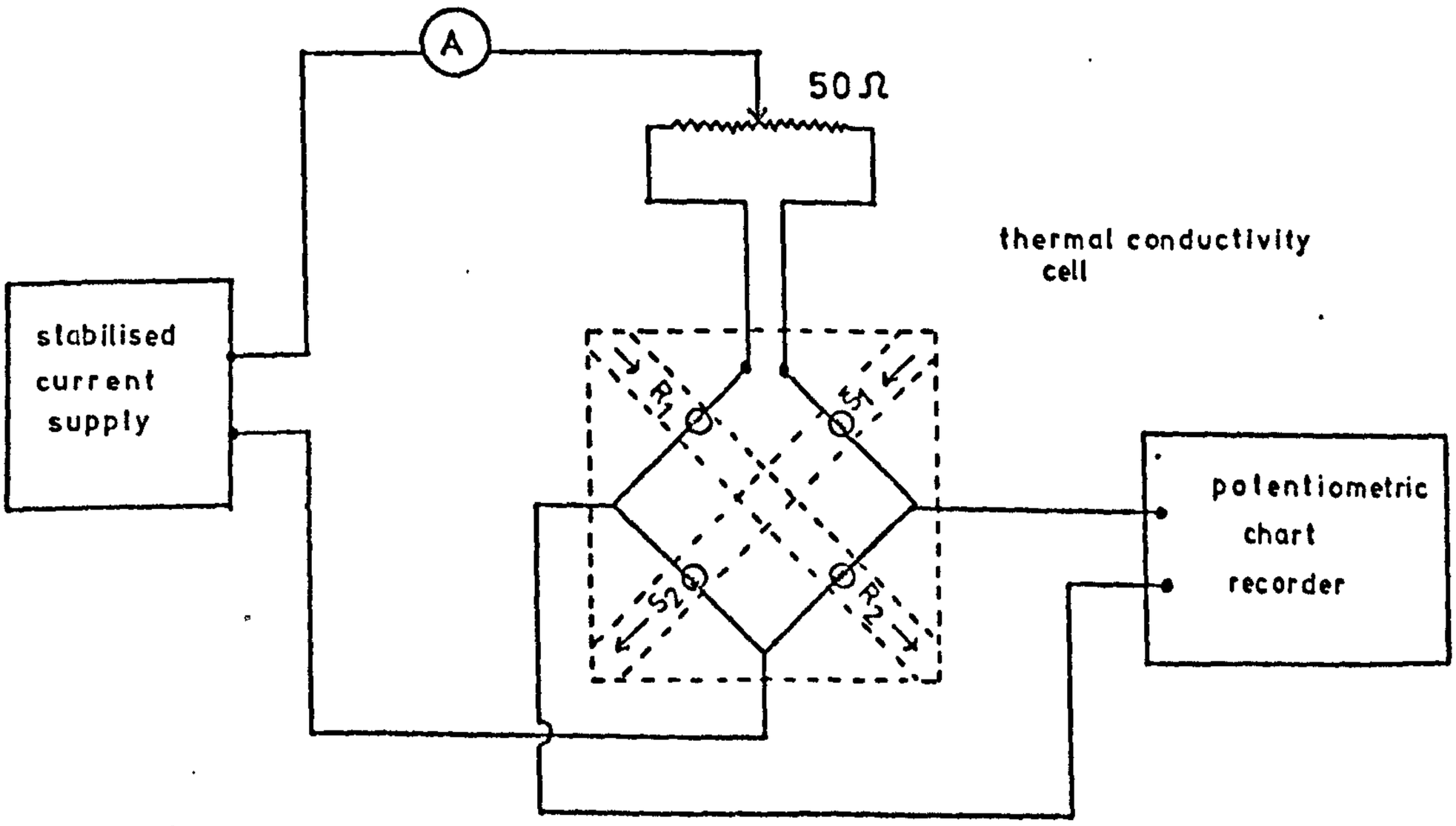

Figure 4.21. Electrical circuit for the gas chromatograph.

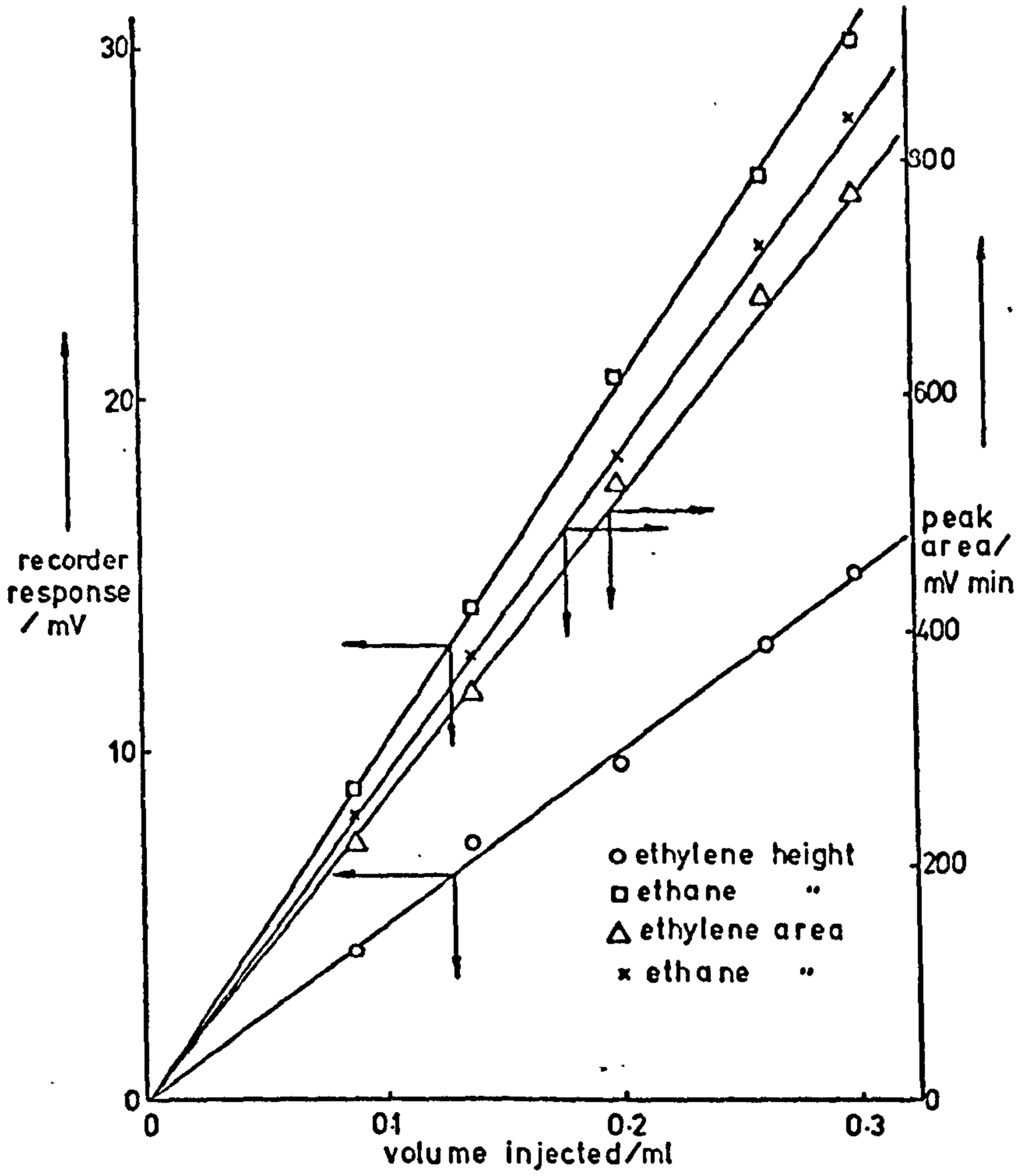

Figure 4.22. Chromatograph calibrations for ethane and ethylene peak heights and areas.

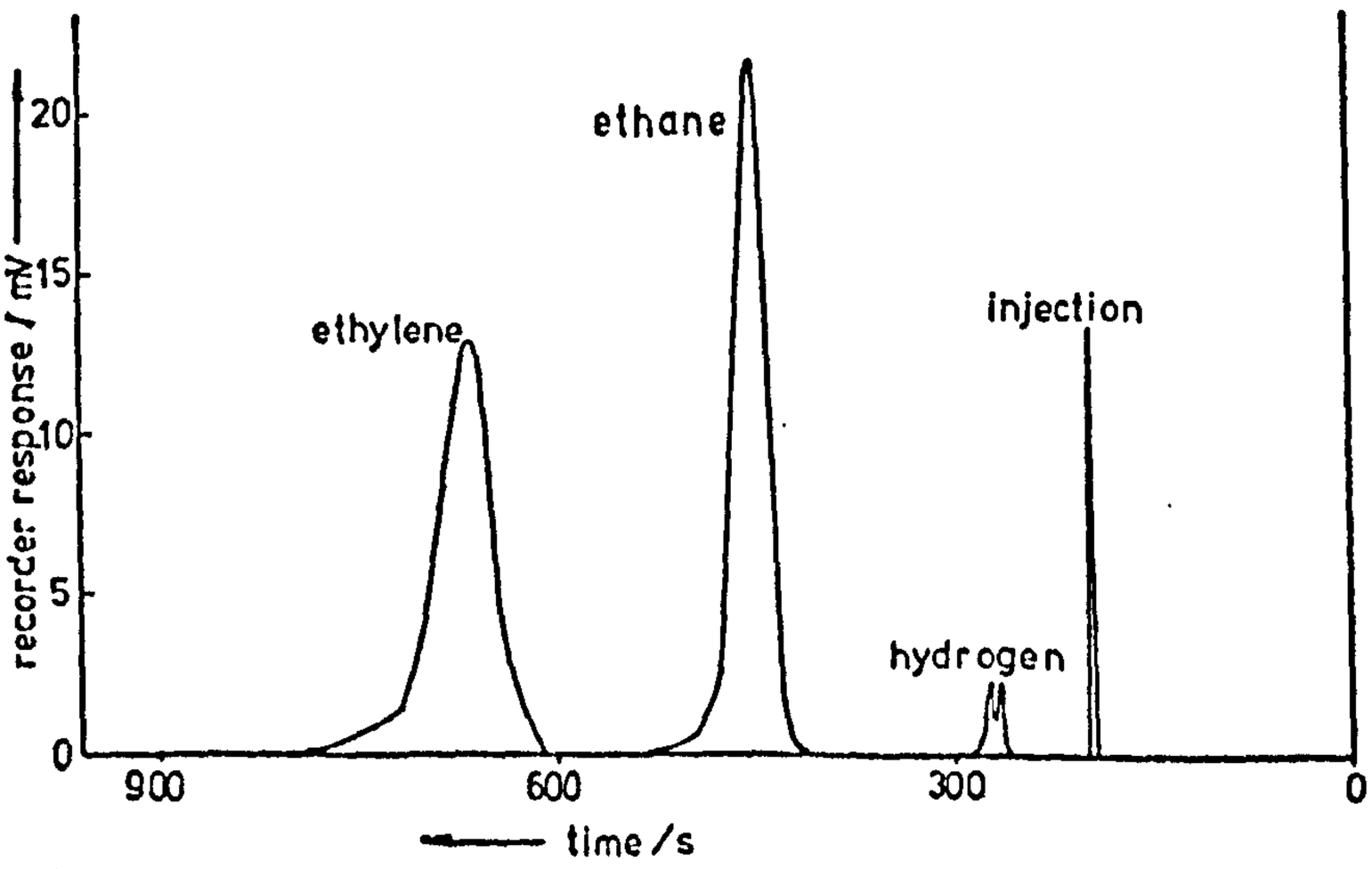

Figure 4.23. Typical chromatogram, showing ethylene-ethane-hydrogen separation.

The pressure transducers.

The differential pressure transducers, supplied by Ackers Electronics Ltd., comprised a piezo-resistive half bridge element mounted in a substantial brass housing (see figure 24(a)). The silicon beam on which the resistors were mounted was deflected by movement of a pressure sensitive membrane. The transducers were connected to the measuring electronics via a screened multi-core cable.

The input circuitry of the measuring electronics and the transducer formed a Wheatstone bridge configuration. The bridge output was a voltage proportional to the applied pressure differential. Amplification of the signal voltage (of the order of millivolts) was required to provide a meter indication and an output suitable for a pen recorder.

Balance and calibrating controls were provided, the former being used to zero the output for a given reference pressure, the latter being adjusted to give meter scale readings corresponding to pressure units (torr).

The electronic circuit (see figure 4.25.) consisted of a differential cross-coupled voltage follower pair feeding a differential amplifier. The voltage follower pair gave a high common-mode rejection and a high input resistance, thus minimising errors in subsequent amplification. The differential gain was set to a nominal value of twelve. The differential amplifier converted the differential input signal to a single ended output suitable for use with a moving-coil meter and a chart recorder. The gain of this amplifier was set to a nominal value of ten.

Monolithic integrated-circuit operational amplifiers type SN72747N (supplied by Texas Instruments) were used throughout the instrument.

The transducers used were of the following types (numbered as in figure 4.11.)

Nos. 2 and 3: Pressure range 0 - 760 torr (type AE831B).

No. 4: Pressure range 0 - 10 atmospheres (type AE831D). Used for making up gas mixtures in the gas sampling cylinder (see above).

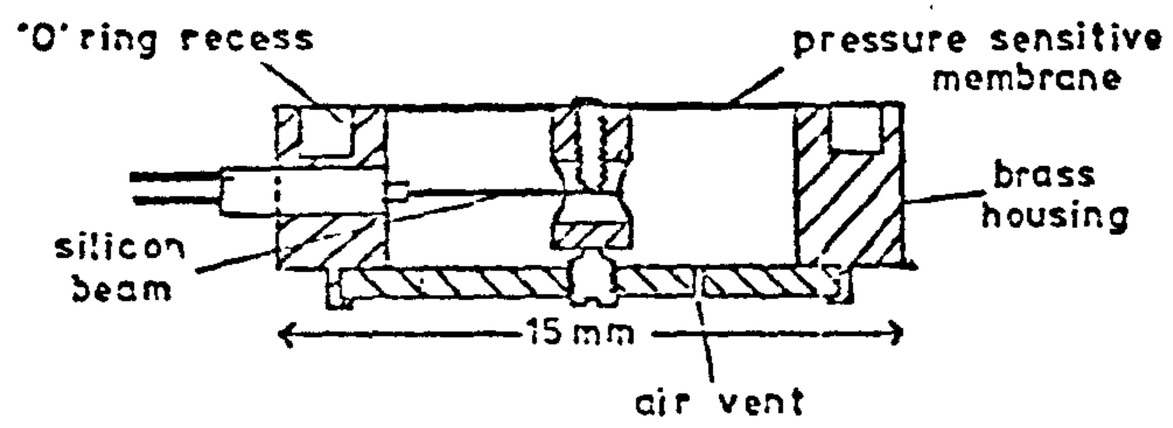

(a) section through AE831 transducer

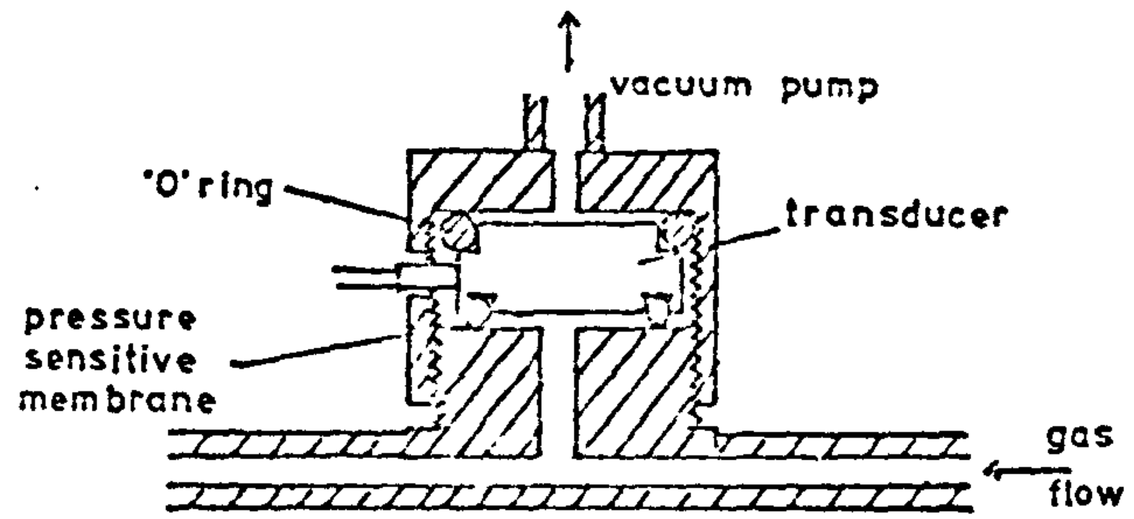

(b) housing A

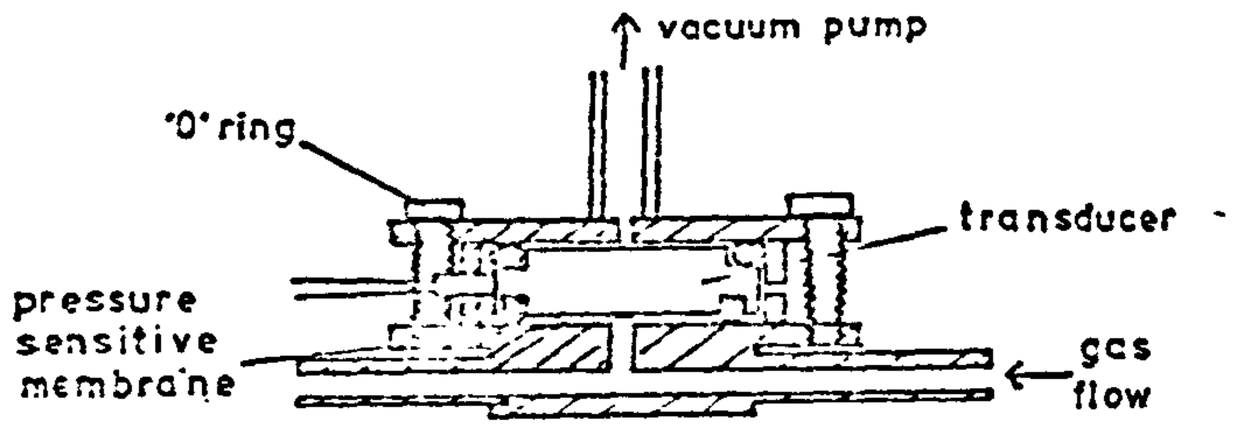

(c) housing B

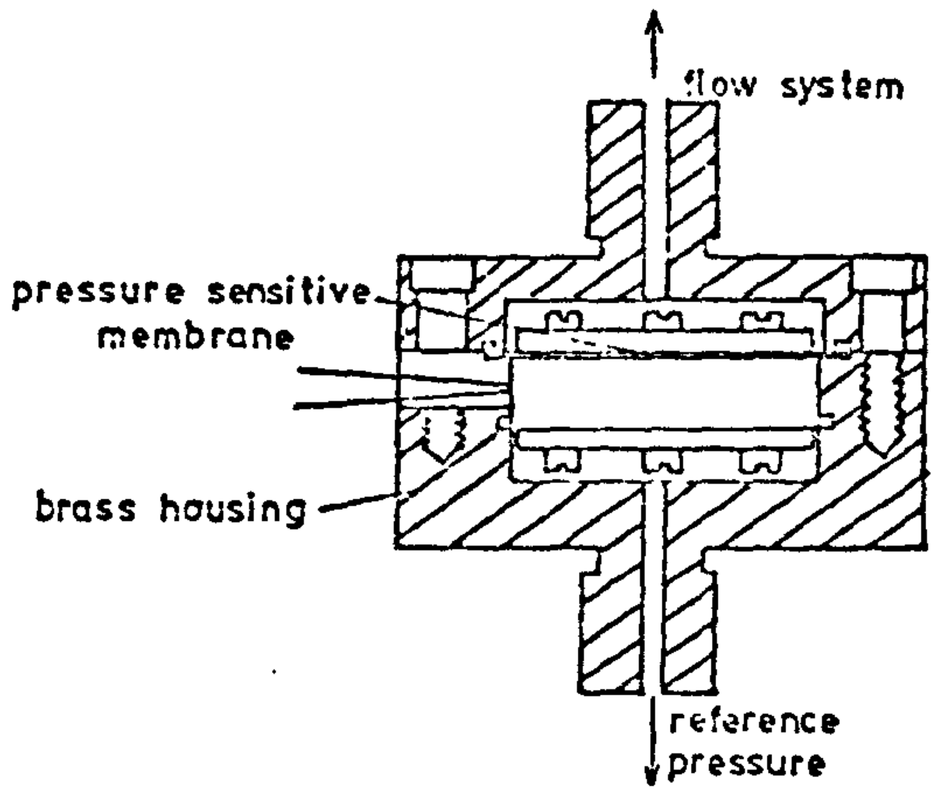

(d) housing for AE810 transducer

Figure 4.24. Pressure transducers and housings.

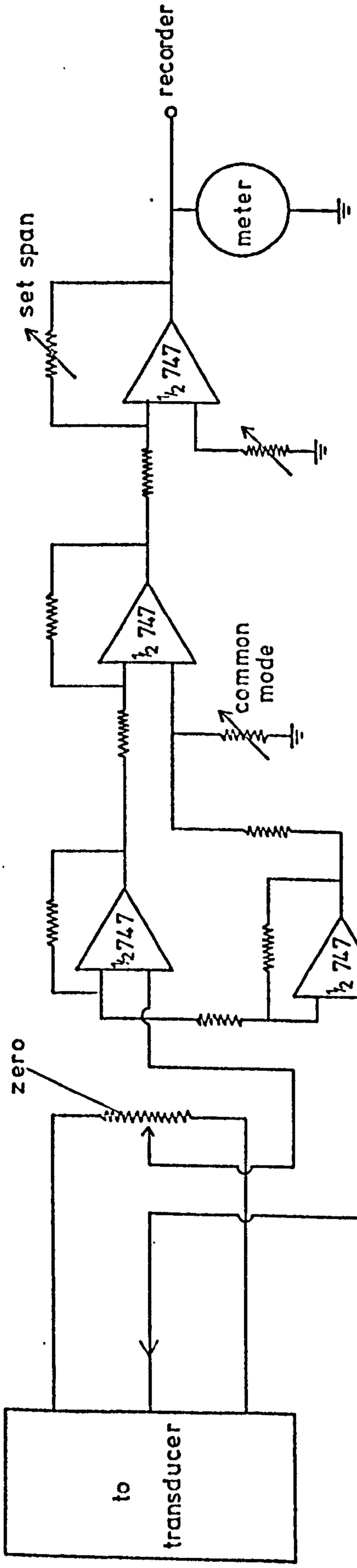

Figure 4.25. The pressure transducer measurement circuit.

No. 1: Pressure range -35 to +35 torr (Type AE 810).

Transducers 2, 3 and 4 were initially mounted in a housing of the types shown in figure 4.24 (b). This housing design had the disadvantage of causing damage to the electrical leads if frequently dismantled, and since this was the case with transducer 3, a housing of the type shown in figure 4.24 (c) was substituted. Transducer 1 was supplied with the housing illustrated in figure 4.24 (d). For measurement of pressures below atmospheric, housings for transducers 2, 3 and 4 were equipped with a vacuum connection to the low pressure side, enabling pressures to be measured relative to vacuum.

The transducers 2, 3 and 4 were calibrated by setting the amplifier to zero with both sides of the pressure sensitive membrane evacuated, admitting gas to atmospheric pressure on the high pressure side, and then adjusting the amplifier gain until a reading of 760 was obtained on the meter. Transducer 1 was calibrated against the mercury manometer of the flow system. The response of the transducers was assumed to be linear within the pressure ranges used - according to the manufacturers' specifications, linearity and hysteresis were within $\pm 1\%$ for transducers 2, 3 and 4.

4.4. The vacuum system. (figure 4.26.)

The apparatus was constructed of Pyrex glass, and all stopcocks, excepting those for storage bulbs 1 and 2, and all joints were sealed with Apiezon N high vacuum grease. The system was evacuated by a mercury diffusion pump backed by a rotary mechanical pump. Operating pressures were better than 10^{-5} torr. Three pressure measuring devices were incorporated in the system. For a rough indication of the vacuum achieved, a rotary Vacustat McLeod gauge was used (measuring down to 10^{-3} torr.) Accurate pressure measurements could be made down to 10^{-5} torr (approximately to 10^{-6} torr) using the McLeod gauge and a cathetometer to measure the heights of the mercury columns. Gas pressures in the region of 1 - 40 torr were measured by the deflection of a light beam by a spiral gauge. The pressure measured by the spiral gauge was relative to that on the side connected to the mercury manometer. When preparing gas mixtures

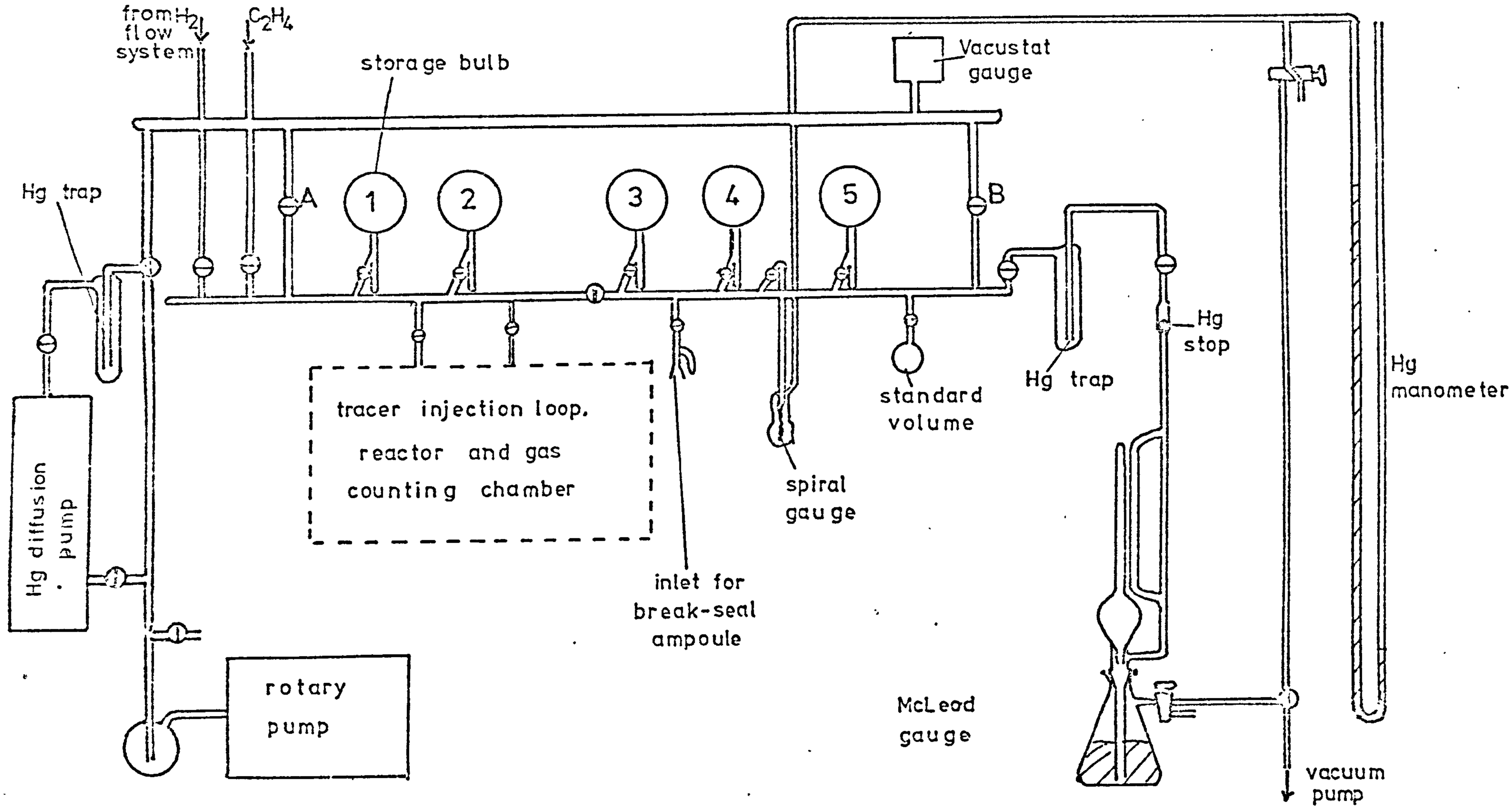

Figure 4.26. The vacuum system.

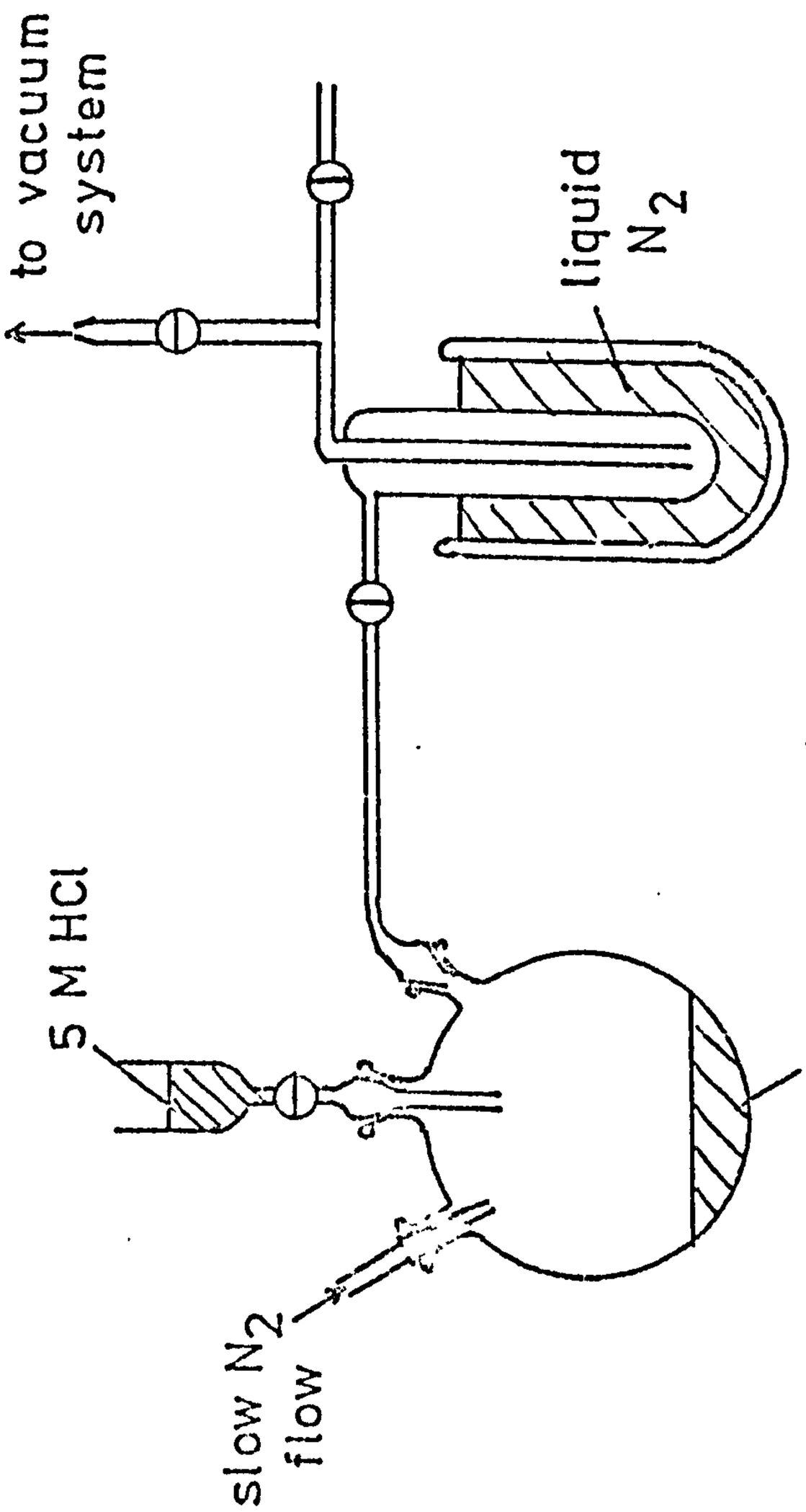

Figure 4.27. Apparatus for production of carbon dioxide-C14.

for the tracer injection loop, this pressure was set eitner to zero or to one atmosphere.

The primary purposes of the vacuum system were to dilute samples of radiotracer and to dispense them to the tracer injection loop. Carbon-14 labelled ethylene was admitted to the vacuum system from a break-seal ampoule via the inlet shown, and stored in bulbs 1 and 2. These bulbs were sealed by Westef 'O'-ring sealed stopcocks. Non-radioactive ethylene was taken from the flow system and stored in bulb 3. Samples of this ethylene were then used to dilute the radioactive ethylene to appropriate specific activities.

Carbon-14 labelled carbon dioxide was prepared in the apparatus shown in figure 4.27. The carbon dioxide was collected in the liquid nitrogen cooled trap and distilled into bulb 4 of the vacuum line, water vapour being retained by solid carbon dioxide cooling of the trap.

The sections of the vacuum system used in handling gases were maintained free of mercury from the diffusion pump and McLeod gauge by two liquid nitrogen cooled traps.

Calibrations.

The volume of the McLeod gauge bulb, found by weighing empty and filled with mercury, was 145.0 ml and the capillaries used were of 1 mm bore. Pressures were calculated according to the equation:

$$P_1V = P_2 \frac{Ad_1}{10} = \frac{Ad_1d_2}{10}$$

where P_1 = pressure in vacuum line (torr)

P_2 = pressure of gas trapped in capillary (torr)

V = volume of McLeod gauge bulb (ml)

A = cross sectional area of capillary (cm^2)

d_1 = height of gas column trapped in capillary (mm)

d_2 = difference in heights of mercury columns (mm)

We may substitute into this equation:

$$P_1 = \frac{Ad_1d_2}{10V} = \frac{3.142 \times 0.05^2 \, d_1d_2}{10 \times 145.0}$$

i.e. $P_1 = 5.42 \times 10^{-6} d_1d_2$ torr. Equation 4.3.

Volumes of various parts of the vacuum system were found by gas expansion, based on a bulb of previously determined volume (58.84 ml). Table 4.2. lists these sections of the vacuum line and the mean volumes determined over 5 expansions. The manifold + McLeod gauge volume was determined by expansion direct from the standard volume, and the spiral gauge, tracer loop and McLeod gauge volumes by expansion into the manifold. (The "manifold" here refers to the section between stopcocks A and B of figure 4.26.)

The spiral gauge was calibrated by plotting the deflection of the light beam on the translucent scale against the pressure measured on the mercury manometer by subsequently adjusting the pressure in the manometer until a zero deflection was produced (see figure 4.28.) From this plot, 1 mm deflection on the spiral gauge scale was calculated as being equivalent to 0.469 torr.

Table 4.2. Volumes of vacuum line sections by gas expansion.

Vacuum line section	Volume / ml
Manifold	146.1 ± 1.2
McLeod gauge	232.0 ± 0.9
Tracer loop	31.4 ± 0.5
Spiral gauge	12.6 ± 0.4

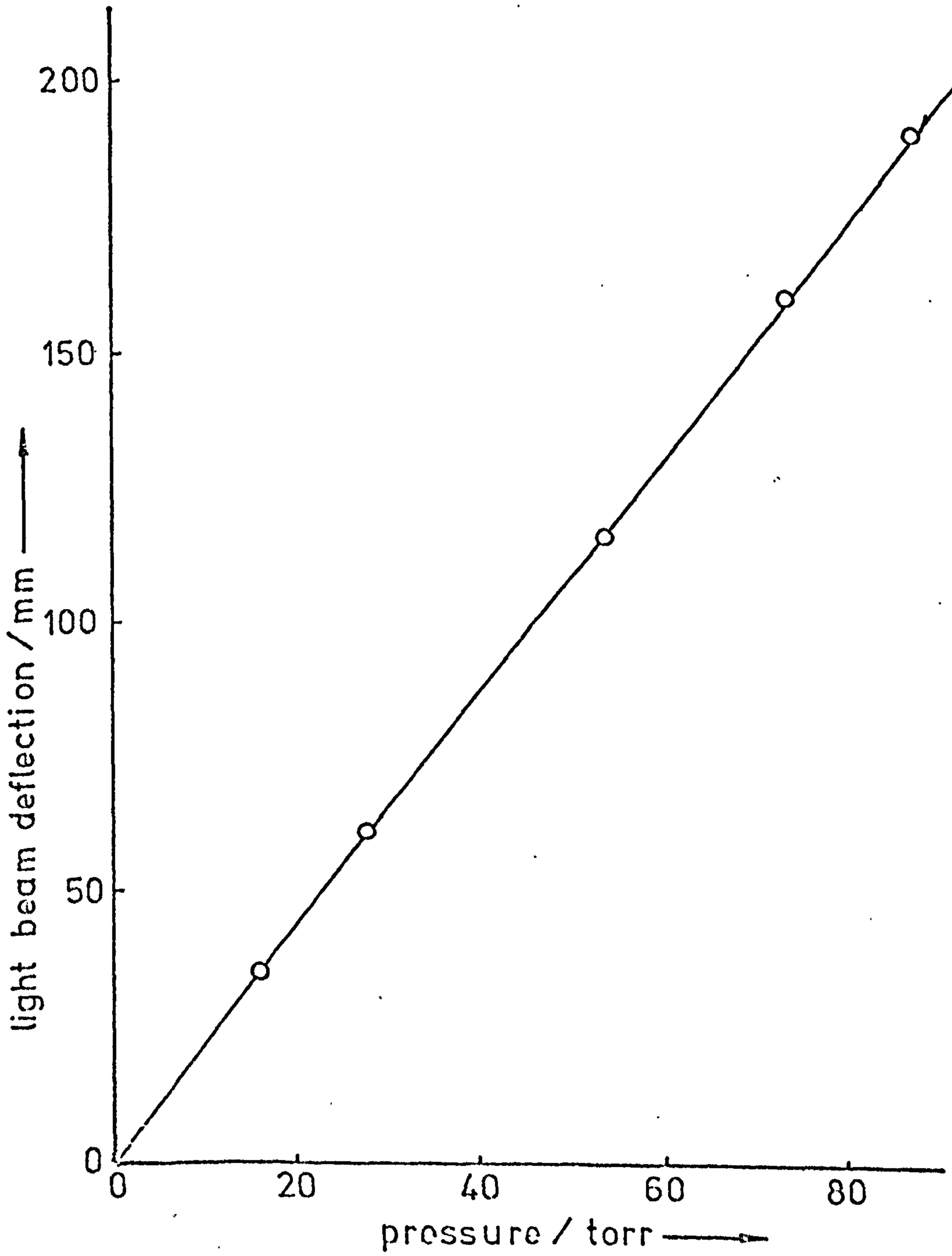

Figure 4.28. Spiral gauge calibration curve.

4.5. The radiotracer counting system.

The counting system, shown schematically in figure 4.29. was similar to that employed in the chlorobenzene studies. Additionally, a second counting ratemeter was added to the gas counting channel and a double pen Servoscribe potentiometric recorder gave simultaneous traces from the outputs of both counting ratemeters. The electronic pulses corresponding to the detected β^- particles were also recorded on magnetic tape for subsequent analysis as below.

The fast counting system.

In the initial experiments with reactor B, it was found that the counting ratemeters used to record a trace of count rate versus time were inadequate when measuring rapid changes ($t_{\frac{1}{2}} < 1s$). To obtain a curve suitable for analysis, the minimum time constant which gave a reasonably smooth curve was normally 1s. Count rate changes occurring with a similar or smaller half-life were masked by the instrument. An additional problem preventing a straightforward analysis of curves comprising a real change in count rate and also instrument time lag, was the lack of uniformity of time constant throughout the range of the ratemeters. To avoid these difficulties, it was decided to adopt a digital approach to recording and analysis of rapid count rate changes. Digital handling of the count rate data had the additional advantage of optimising the amount of information available from the number of radioactive disintegrations observed.

A 2-channel magnetic tape recording system was used for storage of the pulses derived from the radioactive disintegrations, enabling both the catalyst and the gas counting chambers to be monitored simultaneously. The magnetic tape recording could subsequently be played back into a multichannel analyser (Laben Spectroscope Model 400) operating on a multiscaler mode. In this mode, the instrument would count and store pulses over a maximum of 400 equal, predetermined time intervals (from 10^{-4} to 9×10^{4}s). Between each counting interval the instrument paused for a pre-set period (from 10^{-4} to 9×10^{4}s). This pause was normally set to the minimum

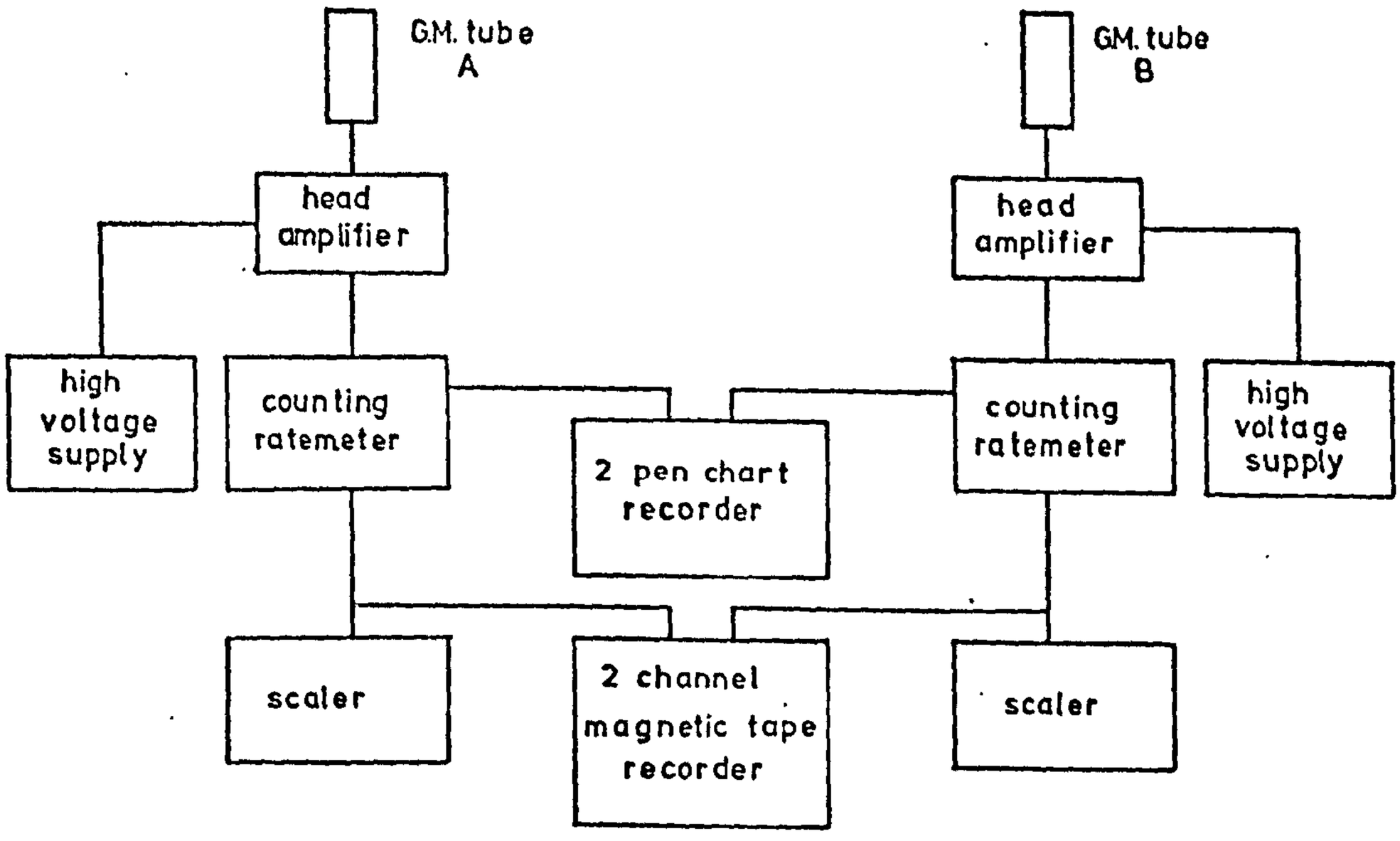

Figure 4.29. The radiotracer counting system (ethylene studies).

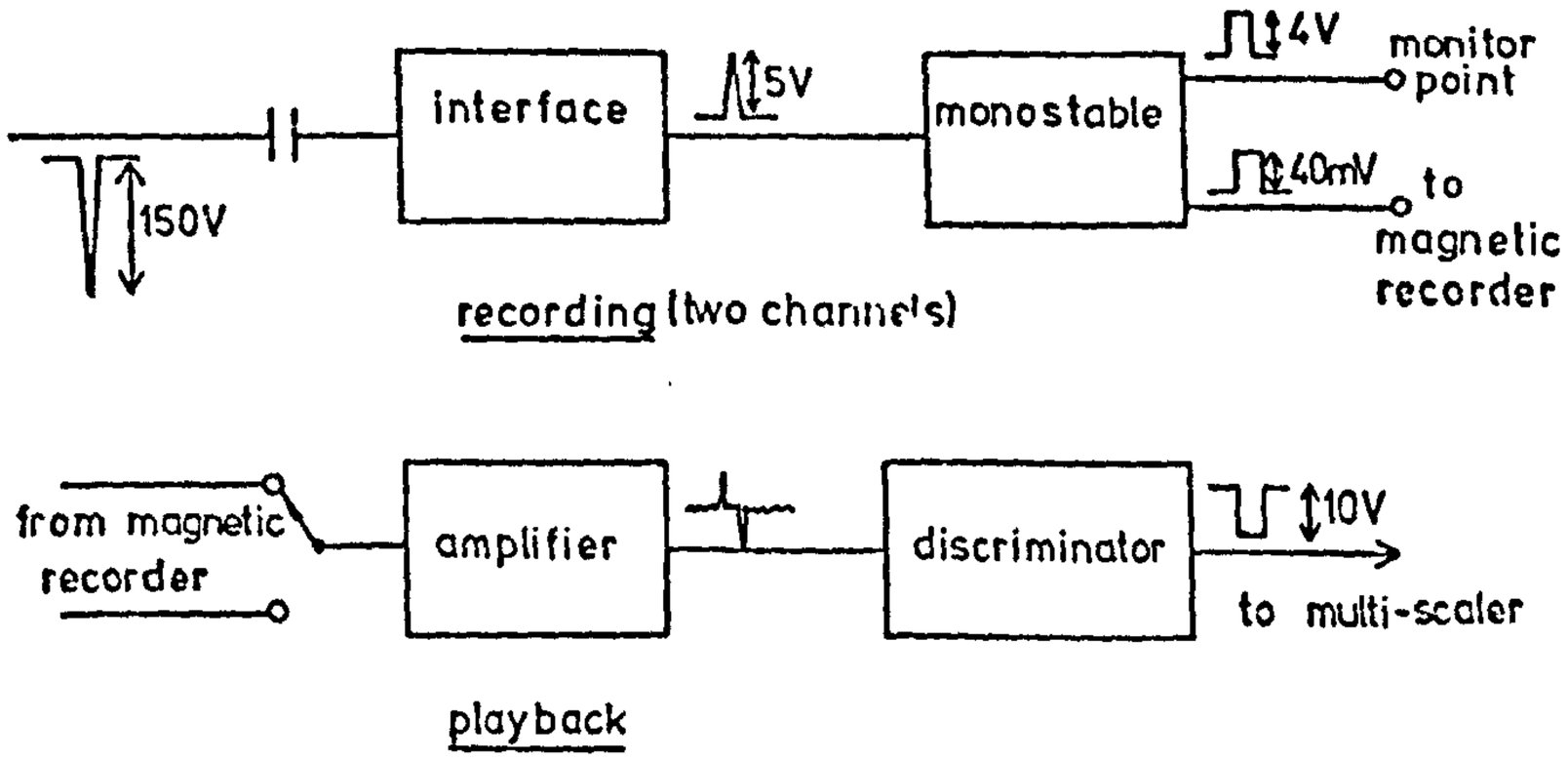

Figure 4.30. Schematic representation of recording and playback with the fast counting system.

value of 10^{-4}s, which, with the time intervals normally used for counting (minimum 0.2s) could be neglected.

Having collected the required data from a tape recording, this could be retrieved via an automatic printer.

In addition to the short counting intervals (resolution) which the system made possible, a secondary advantage was found in the ability to re-analyse a magnetic tape recording of a single experiment until a suitable value of resolution was obtained for the process under examination.

The recording/playback system is shown schematically in figure 4.30. A negative going pulse of 150 volt amplitude was available at the output of the discriminator in the ratemeter. This pulse was brought out and capacitatively coupled to an interfacing transistor, biased to give a positive going pulse of 5 volt amplitude. This pulse was coupled to a 74121 integrated circuit monostable which was then capacitatively coupled to a cassette tape recorder. The poor low frequency response of the recorder differentiated the input (square) pulse giving on playback a positive and negative excursion.

On playback the output of the tape recorder was first amplified, then the amplified signal was fed to a discriminator to discriminate against tape noise. The output of the discriminator was made compatible with the input of the Laben multiscaler.

As two points were to be monitored, a stereo recorder was used through two interface channels. Each channel was then replayed individually.

The circuit was tested using a pulse generator and an I.T.T. type 82 stereo cassette recorder. It was found that over 20 replays a deviation of $\pm$ 1% from the nominal count rate could be expected. The recorder was then replaced by a Thermionic Products type T 3000 recorder capable of reproducing square pulses. As expected, this recorder showed no improvement over the simpler instrument, showing that the derivative of the pulse only was required to reproduce the counts.

Calibrations.

The catalyst counting efficiencies were measured by the infinitely thick layer approximation described in section 4.2. Using the same anthracene - C14 labelled catalyst, the counting chambers were filled and the efficiencies determined for the various reactors and counting windows, a new calibration being necessary for each mica window used. The number of molecules adsorbed on the catalyst may be calculated from the counting efficiency and the specific activity of the tracer sample used according to the equation:

$$\text{Amount adsorbed(molecule mg}^{-1}) = \frac{\text{observed count rate (s}^{-1})}{\varepsilon_c(mg) \times \text{specific activity(s}^{-1}\text{molecule}^{-1})}$$

Equation 4.4.

where ε_c = catalyst counting efficiency.

To simplify the calculations involved in the estimation of adsorption levels from count rate data, table 4.3. lists the specific activities and adsorption levels equivalent to an observed count rate of $1s^{-1}$ for the experiments performed with reactor B, and the counting efficiencies for the windows used.

During the passage of a pulse of radioactive gas through the catalyst chamber, a contribution to the observed count rate was expected from both gas phase and adsorbed phase. With a catalyst sample in place in reactor B it was found that a considerable gas space was formed between the catalyst and the counting window. It was estimated that the contribution to the observed count rate from the interstitial gas of the catalyst bed would amount to less than 5% of that from the gas space above the bed. The interstitial gas contribution was therefore neglected.

The counts observed from the gas phase in reactor B were estimated as a fraction of those observed for a given radiotracer pulse in the gas counting chamber. Two equal pulses of ethylene - C14 were passed over the same catalyst sample under similar conditions. (For further detail see chapter 5, experiments G6/2 and 4.) The first pulse was passed over the catalyst bed in the normal position, i.e., with the counting window uppermost. The ratio of the total counts observed from the catalyst chamber to those of the gas chamber

Table 4.3. Catalyst counting efficiencies, specific activities of ethylene-C14, and conversion factor for count rate to surface coverage (ethylene studies).

Experiment numbers	ε_c /mg	Specific activity / Ci mmol^{-1}	Surface coverage = 1 count s^{-1} / molecule (mg catalyst)$^{-1}$
F5	0.423	84.1	4.85 x10^{14}
G1/1&2	0.442	84.1	4.86 x10^{14}
G1/3-5	0.442	542	7.20 x10^{13}
G1/6&7	0.431	526	7.43 x10^{13}
G2/1-4	"	105	3.71 x10^{14}
G2/5-8,BS3/1	"	558	6.97 x10^{13}
BS3/2-7	"	532	7.34 x10^{13}
G3/1&2,G4/1-3	"	550	7.12 x10^{13}
G5/1,G6/1-4	"	550	7.12 x10^{13}
G6/6&7,G7/1	"	550	7.12 x10^{13}

included a contribution from the gas space over the catalyst bed. In the second experiment, the reactor was inverted, allowing the catalyst sample to cover the counting window. The ratio of the counts observed from catalyst to gas chambers in this case did not include the same gas phase contribution. By taking the difference between the ratios from the two experiments, a ratio was obtained for the counts arising from the gas space in the catalyst chamber to those from the gas chamber. This ratio was found to be:

$$\frac{\text{Gas counts observed in catalyst chamber}}{\text{Counts observed in gas chamber}} = 0.47.$$

Since the catalyst weight and other conditions employed were similar to those of the other experiments with this reactor, this ratio could be used in calculating the gas phase contribution to the catalyst chamber counts.

The estimation of this figure was also attempted for reactors A and B by passing a pulse of carbon dioxide - C14 over the catalyst in a hydrogen carrier flow. The count rate versus time curves for the catalyst chambers are shown in figure 4.31. These may be compared with the curves obtained under similar conditions with Reactor B, but in the absence of a catalyst sample, shown in figure 4.32. Comparing the curves for reactor B, it appeared that a significant amount of adsorption of carbon dioxide was occurring on the catalyst sample. The ratio, total catalyst chamber counts : total gas chamber counts was found to be 1.81, which may be compared with the value 0.47 above, when no adsorption occurs. These results may be compared with those of Schay and Szekely (106) for carbon dioxide adsorption on a silica chromatographic column. It was concluded that carbon dioxide was unsuitable for this type of calibration.

The plots shown in figure 4.31. serve as an illustration of the greatly superior flow characteristics of reactor B. Analysis of desorption kinetics in reactor A would require a half-life for the desorption of approximately the length of the pulse (i.e. about 10s).

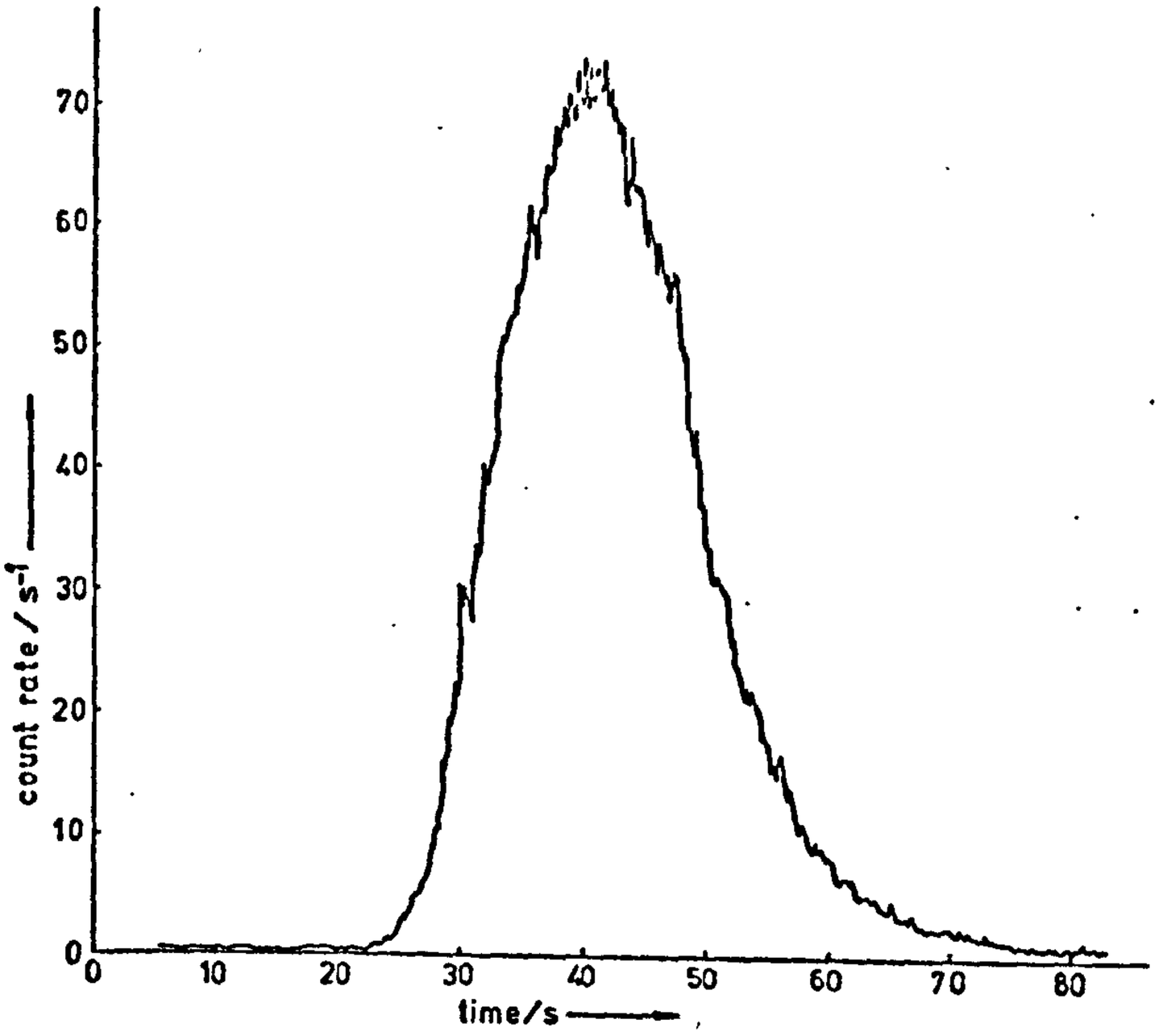

(a) reactor A

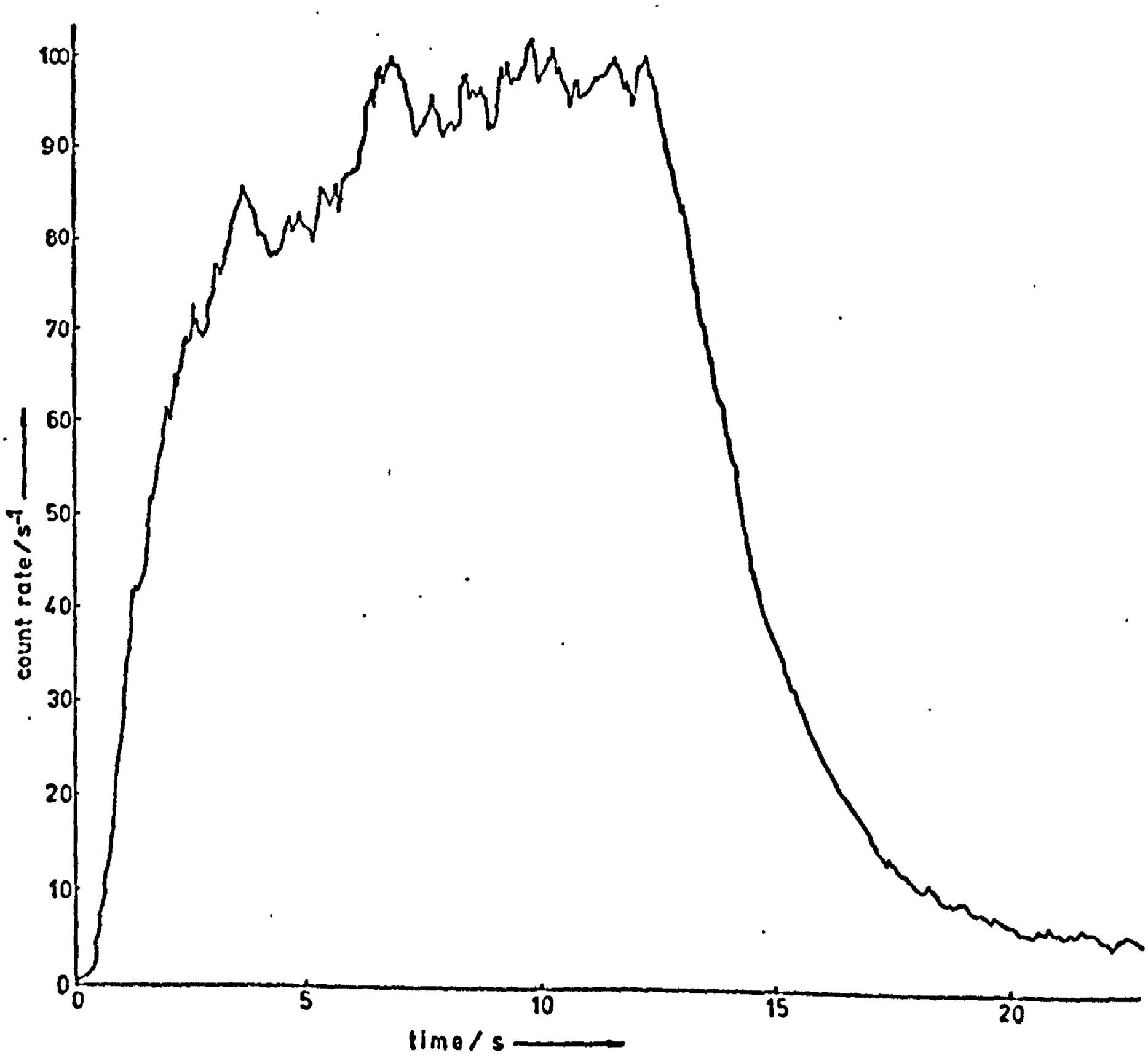

(b) reactor B

Figure 4.31. Passage of carbon dioxide-C14 pulses over Pt/SiO$_2$ samples in reactors A and B

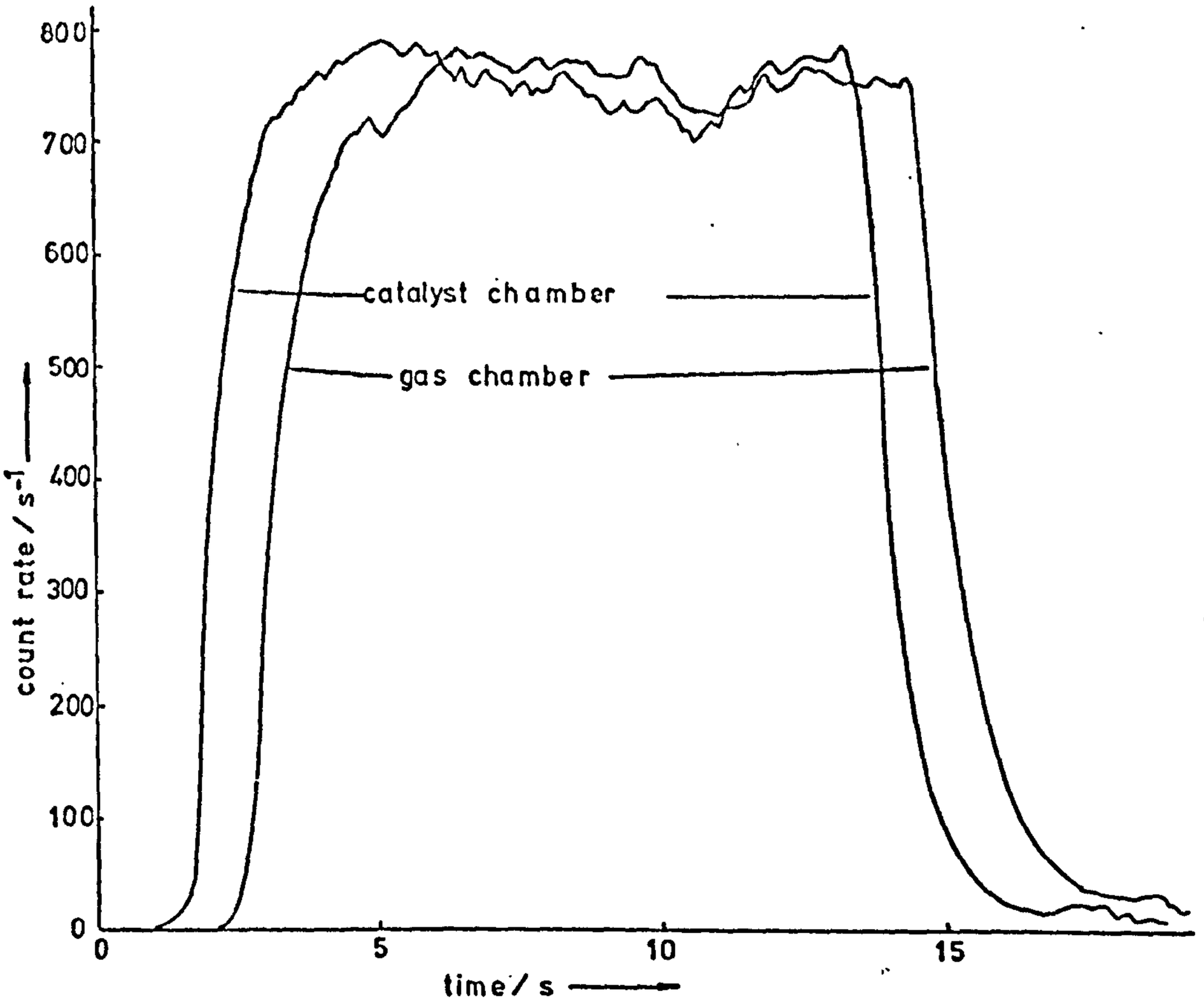

(a) ratemeter plot

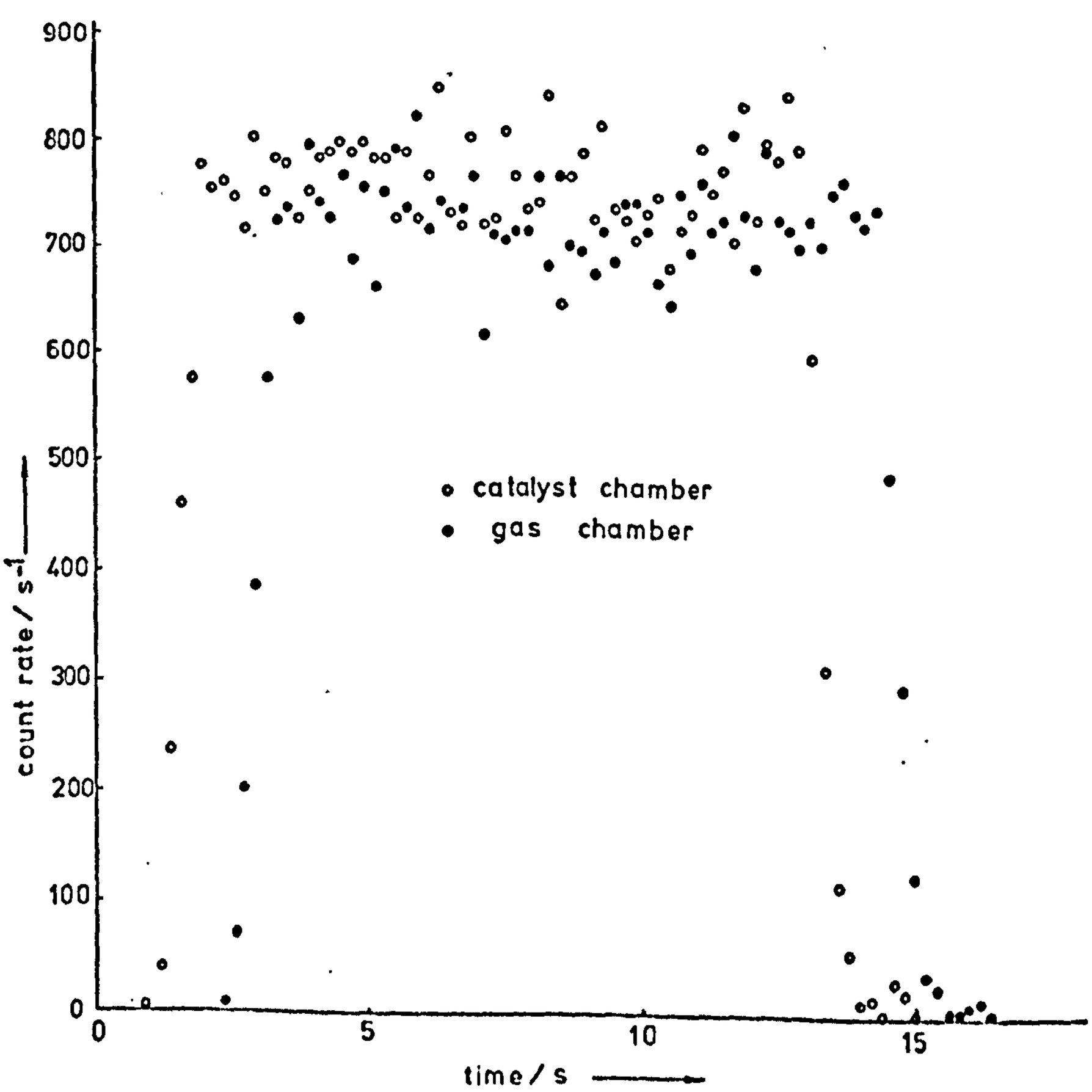

(b) fast counting system plot

Figure 4.32 Passage of CO_2-C14 pulses through empty reactor and counting chamber P. Pata

With a "rectangular" pulse shape such as that shown in figure 4.32 (a) for the empty reactor, however, the desorption half-life required for a significant analysis to be made would have to be little greater than that of the tailing process found for the empty reactor (~0.2s). To facilitate a more direct comparison with later results, the multiscaler analysis of the same pulse through the empty reactor is shown in figure 4.32 (b).

Part C. General.

4.6. Materials.

The radiochemicals were obtained from the Radiochemical Centre, Amersham. The chemical purity of all samples was quoted as 98%, and the radiochemical purity 99% for chlorobenzene - Cl4, benzene - Cl4 and sodium carbonate - Cl4, and 98% for ethylene - Cl4.

The non-radioactive chlorobenzene, benzene and sodium carbonate were Analar grade reagents supplied by B.D.H. Ltd. The ethanol used for the spectrophotometric analyses of benzene / chlorobenzene mixtures was Burroughs 99.8% grade.

Cylinders of nitrogen, hydrogen, helium and ethylene gases were obtained from Air Products Ltd. The hydrogen was purified by passage through a Deoxo catalytic hydrogenator (Engelhard Industries Ltd.) to reduce traces of oxygen to water. For the chlorobenzene studies water vapour was removed from the nitrogen and hydrogen flows by a liquid nitrogen cooled molecular sieve trap. During the ethylene studies, water was removed by passage through tubes (10 mm by 150 mm) packed with magnesium perchlorate granules. These tubes also served as dust filters. The ethylene was quoted by the manufacturers as being 99.8% pure, with methane (0.15%), ethane (0.005%) and carbon dioxide (0.003%) as the major impurities.

Catalysts were prepared by impregnation of the silica support with solutions of the metal salts. The metal salts used for the catalysts were $PdCl_2$, $H_2PtCl_6.xH_2O$, and $IrCl_3$, supplied by Johnson Matthey Chemicals Ltd. The required amount of metal salt was dissolved in a minimum amount of distilled water (dilute HCl for $PdCl_2$) and added to a slurry of Aerosil silica in an evaporating

basin. After partially evaporating to dryness over a steam bath with constant stirring, the catalyst was dried overnight at 393 K. The Aerosil silica used was quoted as having a surface area of 175 $m^2 g^{-1}$, measured by the Brunauer, Emmett and Teller method (6).

The catalysts used in the present study were as follows: Catalyst B, 1% w/w Pd-on-silica; Catalyst C, 5% w/w Pd-on-silica; Catalyst E, Pd black (supplied by Johnson Matthey Chemicals Ltd); Catalyst F, 5% w/w Pt-on-silica; Catalyst G, 5% w/w Ir-on-silica. The percentage metal components given are nominal values. More precise values will be given in section 5.16.

C H A P T E R 5

Results

Chapter 5. Results.

Part A. Chlorobenzene Studies.

5.1. Occupancy Principle experiments.

Experiments B1/1 and 2.

These experiments were designed to test the Occupancy Principle method in the calculation of the size of the active pool of molecules adsorbed on the Pd-on-silica catalyst used.

The catalyst sample B1 (see table 5.20) was pre-reduced for 3 hours at 393 K in H_2 flow at atmospheric pressure, and subsequently transferred in air to the ambient temperature counting chamber where it was left overnight in a slow H_2 flow. These catalyst reduction conditions will be referred to as "standard" throughout part A of this chapter. The experiment numbers are explained in appendix I.

The experimental results and calculations will be presented in full for B1/1. Those for B1/2 and subsequent experiments will be given in more concise form.

A summary of the experimental conditions and results are given in tables 5.1 and 5.2. Similar conditions were chosen for these experiments to check reproducibility. The count rate versus time plots recorded from the catalyst and gas chambers following the injection of the chlorobenzene-C14 sample into the carrier gas flow are shown in figure 5.1.

The Occupancy Principle calculation was performed as follows:

Total counts observed from catalyst chamber = 26559 ± 163 in 5160 s.

Background count-rate from catalyst chamber = $0.596 \pm 0.008\ s^{-1}$

Net counts observed from catalyst chamber = $26559 - 0.596 \times 5160$

= $(2.35 \pm 0.02) \times 10^4$

Total counts observed from gas chamber = 24212 ± 156 in 5100 s.

Background count-rate from gas chamber = $0.752 \pm 0.011\ s^{-1}$.

Net counts observed from gas chamber = $24212 - 5100 \times 0.752$

= $(2.04 \pm 0.02) \times 10^4$

Table 5.1. Occupancy Principle experiments. Conditions.

Experiment number	B1/1	B1/2	B1/3	BS1/1
Temperature / K	295	295	296	295
Total pressure / torr	755	755	755	752
Catalyst weight / mg	250	250	250	385
H_2 carrier flow rate / ml s^{-1}	1.23	1.15	2.60	2.66
Chlorobenzene flow rate /x10^{16} molecule s^{-1}	6.5	6.5	22.0	15.1
Chlorobenzene partial pressure / torr	1.48	1.58	2.33	1.62
Conversion to benzene / %	33	33	15	0
Gas density / g l^{-1}	0.0926	0.0927	0.0973	0.100
R	0.098	0.098	0.106	0.108
Chlorobenzene-C14 injected /x 10^{-5} l	1.00	1.00	1.00	1.00
Activity used /x 10^{4} s^{-1}	3.7	3.7	3.7	3.7

Table 5.2. Occupancy Principle experiments. Results.

Experiment number	B1/1	B1/2	B1/3	BS1/1
Background count rate (A)	0.596 ± .008	0.596 ± .008	0.715 ± .011	0.550 ± .007
Background count rate (B)	0.752 ± .011	0.752 ± .011	0.686 ± .010	0.658 ± .008
Net counts observed (A)/$x10^4$	2.35 ± .02	2.46 ± .02	1.50 ± .02	2.60 ± .02
Net counts observed (B)/$x10^4$	2.04 ± .02	2.38 ± .02	1.22 ± .01	1.20 ± .01
Total capacity calculated / $x10^{19}$ molecule	5.49	5.68	11.6	22.4
Capacity per mg catalyst / $x10^{17}$ molecule mg^{-1}	2.20	2.27	4.64	5.83
λ_s / $x10^3$ s	1.10 ± .02	1.27 ± .03	0.81 ± .02	3.04 ± .05
f / $x10^{16}$ molecule s^{-1}	5.0	4.5	14.3	7.4

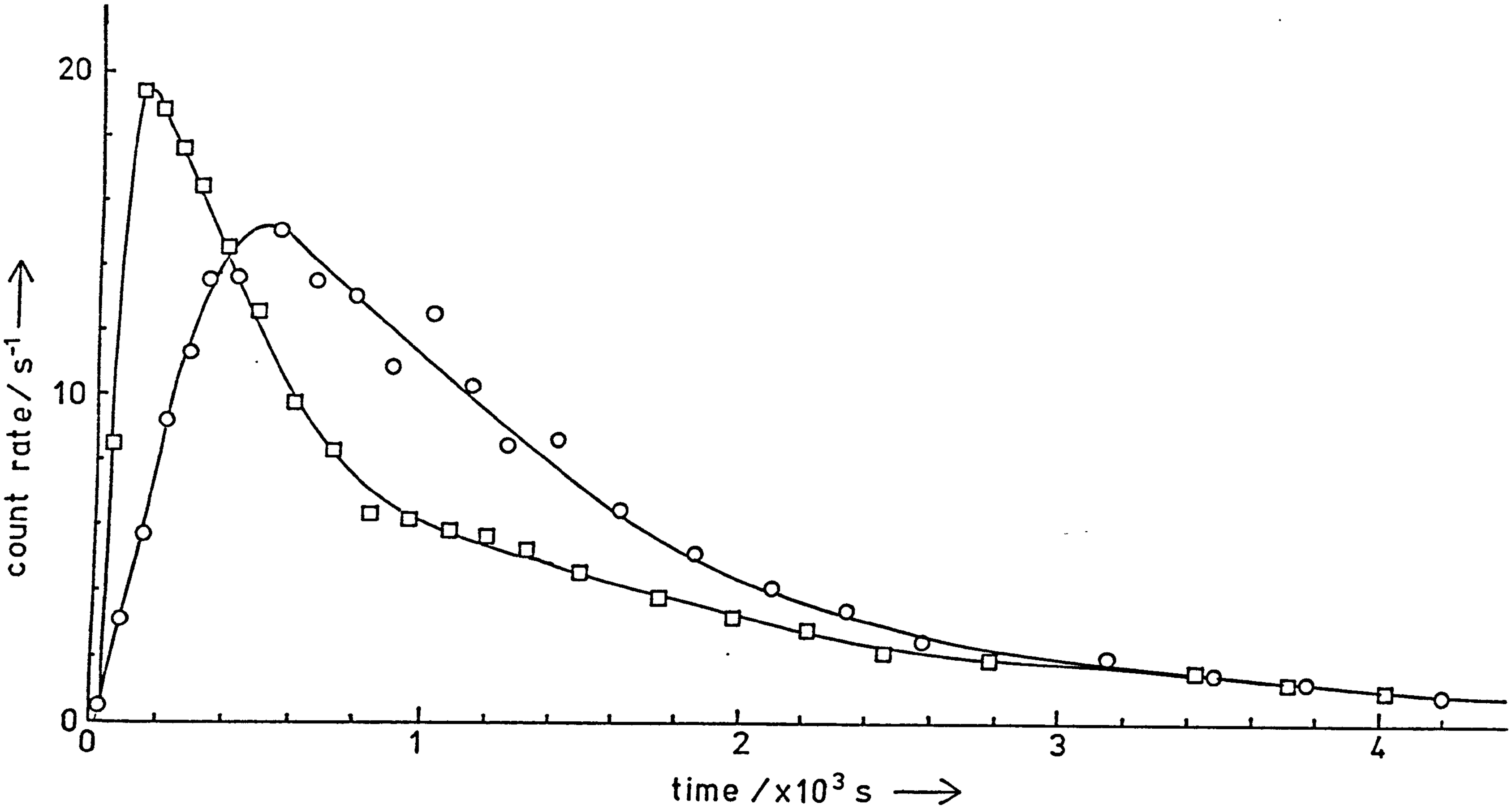

Figure 5.1. Count rate versus time for Occupancy Principle experiment , B1/1.
o- catalyst count rate; □ - gas count rate.

From equation 2.5 we may write:

$$\text{Capacity of Adsorbed Phase} = C_c = \frac{F(N_A - RN_B)W}{\varepsilon_c D} \qquad \text{Equation 5.1.,}$$

where F = chlorobenzene flow rate (molecule s^{-1}),

N_A = net counts observed in catalyst chamber,

N_B = net counts observed in gas chamber,

W = weight of catalyst used (mg),

ε_c = efficiency of catalyst counter (mg),

D = total tracer activity used (s^{-1}).

R is the proportionality factor giving the gas phase count rate observed in the catalyst chamber relative to that in the gas chamber for a given density. From figure 4.9 for the calculated gas density of 0.0926 g l^{-1}, the appropriate value of R is 0.098.

$$C_c = \frac{6.54 \times 10^{16}(2.35 \times 10^{14} - 0.098 \times 2.04 \times 10^4)250}{0.173 \times 3.7\ 10^4}$$

$$= 5.49 \times 10^{19} \text{ molecule}$$

$$\equiv \underline{2.20 \times 10^{17} \text{ molecule (mg catalyst)}^{-1}}.$$

Similarly, for B1/2, the capacity was calculated:

$$C_c = \frac{6.54 \times 10^{16}(2.46 \times 10^4 - 0.099 \times 2.38 \times 10^4)250}{0.173 \times 3.7 \times 10^4}$$

$$= 5.68 \times 10^{19} \text{ molecule}$$

$$\equiv \underline{2.27 \times 10^{17} \text{ molecule (mg catalyst)}^{-1}}$$

Figure 5.2 shows the semi-log plots of count-rate versus time for the radiotracer desorptions from the catalyst for B1/1 and 2. The reciprocals of the slopes of these plots, obtained by the least squares approximation (L S A), yield values of $1.10 \pm 0.02 \times 10^3$ s (B1/1) and $1.27 \pm 0.03 \times 10^3$ s (B1/2) for τ_s, the mean surface lifetime of a tracer molecule. Using equation 2.3, the flux of molecules through the adsorbed phase, or rate of exchange of adsorbed molecules may be calculated:

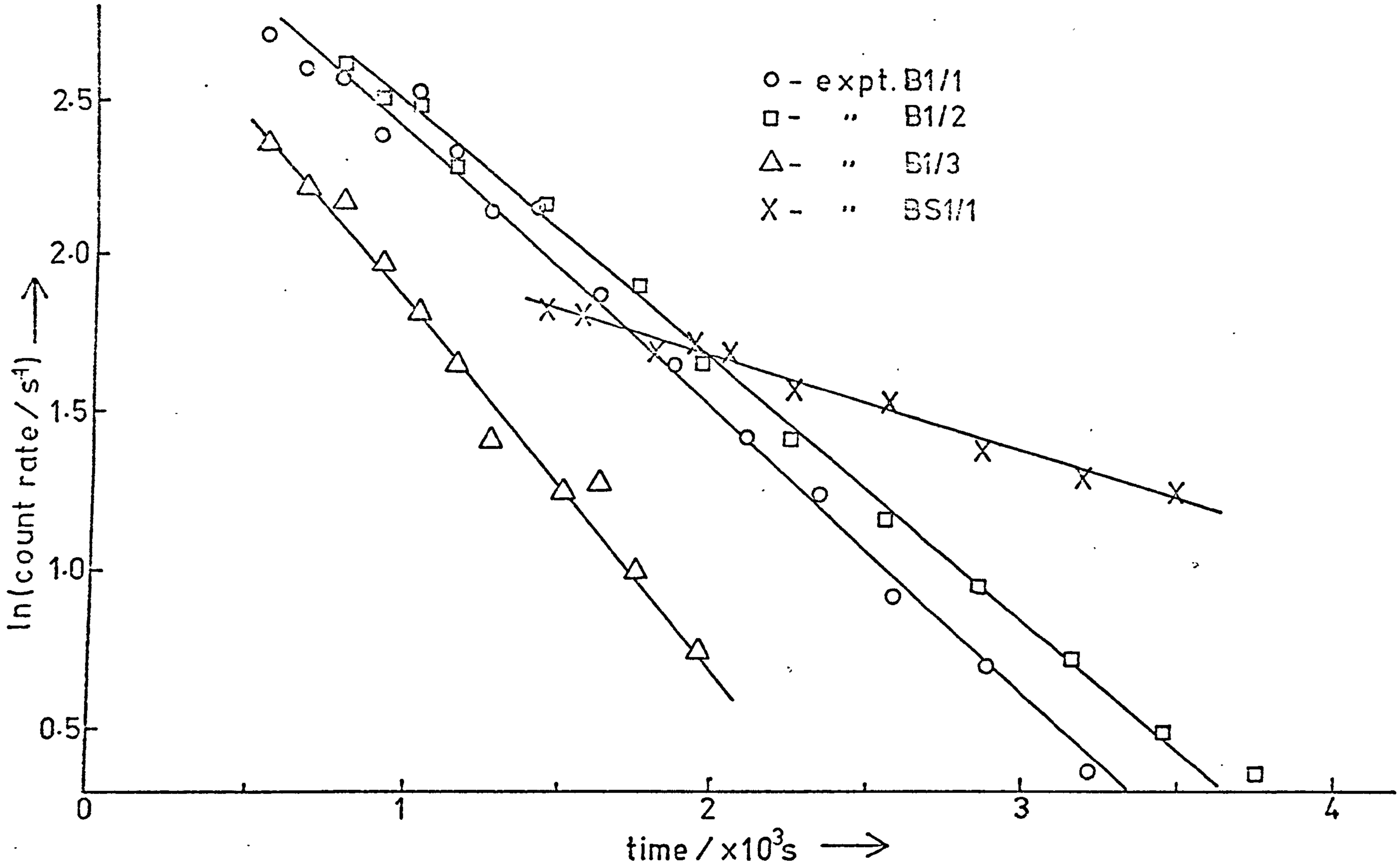

Figure 5.2. Chlorobenzene -C14 desorptions during Occupancy Principle experiments.

$$f = \frac{C_c}{\tau_s} = \frac{5.49 \times 10^{19}}{1.10 \times 10^3} = \underline{5.0 \times 10^{16} \text{ molecule } s^{-1} (B1/1)}$$

$$= \frac{5.68 \times 10^{19}}{1.27 \times 10^3} = \underline{4.5 \times 10^{16} \text{ molecule } s^{-1} (B1/2)}.$$

Experiment B1/3.

For a summary of the experimental conditions and results, see table 5.1 and 5.2. The previous experiments were repeated here, but with higher chlorobenzene flow rate and partial pressure to test the effect of the latter on adsorption. Prior to the experiment, the catalyst was left overnight in a slow H_2 flow. The semi-log plot of count rate versus time for the radiotracer desorption is shown in figure 5.2.

Experiment BS1/1.

For the experimental conditions and results, see tables 5.1 and 5.2. From the values of capacity determined in the previous experiments, it seemed probable that an extensive adsorption occurred on the silica support. The Occupancy Principle experiment was therefore repeated under similar conditions to the previous experiments, using Aerosil silica as the adsorbent to test for adsorption in the absence of the metal. While adsorption was found to occur, no reaction was observed. The semi-log plot of count rate versus time is shown in figure 5.2.

5.2. Ambient temperature chlorobenzene desorptions from Pd/SiO_2 in H_2 flow.

It was concluded from the experiments of the previous section, under constant flow conditions, that the adsorption observed related primarily to the support. The present experiments were carried out under pulsed chlorobenzene-Cl4 flow conditions in a hydrogen carrier flow. It was hoped that from the desorption kinetics it might be possible to distinghish between support and metal adsorption.

Both 1.08% (experiments B2/1, B3/1 and B4/1) and 3.93% (experiments C2/1 - 6) catalysts were studied. The other major variation between experiments was in the quantity of radiotracer chlorobenzene pulsed

over the catalyst, giving rise to different initial adsorption values. Only the catalyst chamber counter was employed as the gas phase activity during the desorptions was considered to be negligible and difficult to assess accurately. Further, in an exponential desorption process, the gas phase activity should be proportional to the surface coverage.

Table 5.3 lists the conditions pertaining to each experiment. The background count rate for each experiment is included as an indication of the contamination of the sample due to retained radioactive species from previous experiments performed with the same catalyst. Count rates of 0.3 to 0.6 s^{-1} represent the normal background obtained with a fresh sample.

Standard reduction conditions were employed for all catalysts.

The semi-log desorption curves are shown in figure 5.3 for experiments B2/1, B3/1 and B4/1, and in figure 5.4 for experiments C2/1 - 6. To facilitate comparison of the curves, the adsorption levels are given in terms of molecules adsorbed per mg rather than count rates, as the specific activity of the chlorobenzene-Cl4 was not uniform throughout the various experiments. Experiments B2/1, B3/1, C2/1 and 2 yielded less accurate data at lower surface coverages due to the lower specific activity employed.

As may be seen from figures 5.3 and 4, most of the semi-log desorption curves resolved into two approximately straight-line regions. The slopes of these lines (λ_1 and λ_2) are given in table 5.4 along with the adsorption level at the point of intersection where applicable, and the maximum adsorption level of chlorobenzene observed.

Figure 5.5 shows the complete count rate versus time curve for the catalyst and gas counters during a typical desorption experiment (C2/3).

5.3. Chlorobenzene desorptions from Pd/SiO_2 in N_2 flow.

In an attempt to gain further insight into the processes occurring during the chlorobenzene-Cl4 desorptions, it was considered desirable to study the desorption under non-reactive conditions. To this end

Table 5.3. Ambient temperature chlorobenzene desorptions. Experimental conditions.

Experiment number	B2/1	B3/1	B4/1	C2/1	C2/2	C2/3	C2/5	C2/6
Temperature / K	295	293	292	295	295	296	293	294
Pressure / torr	753	758	750	753	752	752	755	751
H_2 carrier flow rate / ml s^{-1}	2.75	2.61	2.59	2.31	2.16	2.29	2.45	2.40
Volume chlorobenzene injected / $x10^{-6}$ l	10	10	0.5	20	10	5	0.5	0.1
Specific activity / s^{-1} $mmol^{-1}$	0.376	0.376	17.6	0.376	0.376	15.1	15.1	15.1
Background count rate / s^{-1}	0.565	0.515	0.415	0.502	0.552	0.597	2.45	2.80

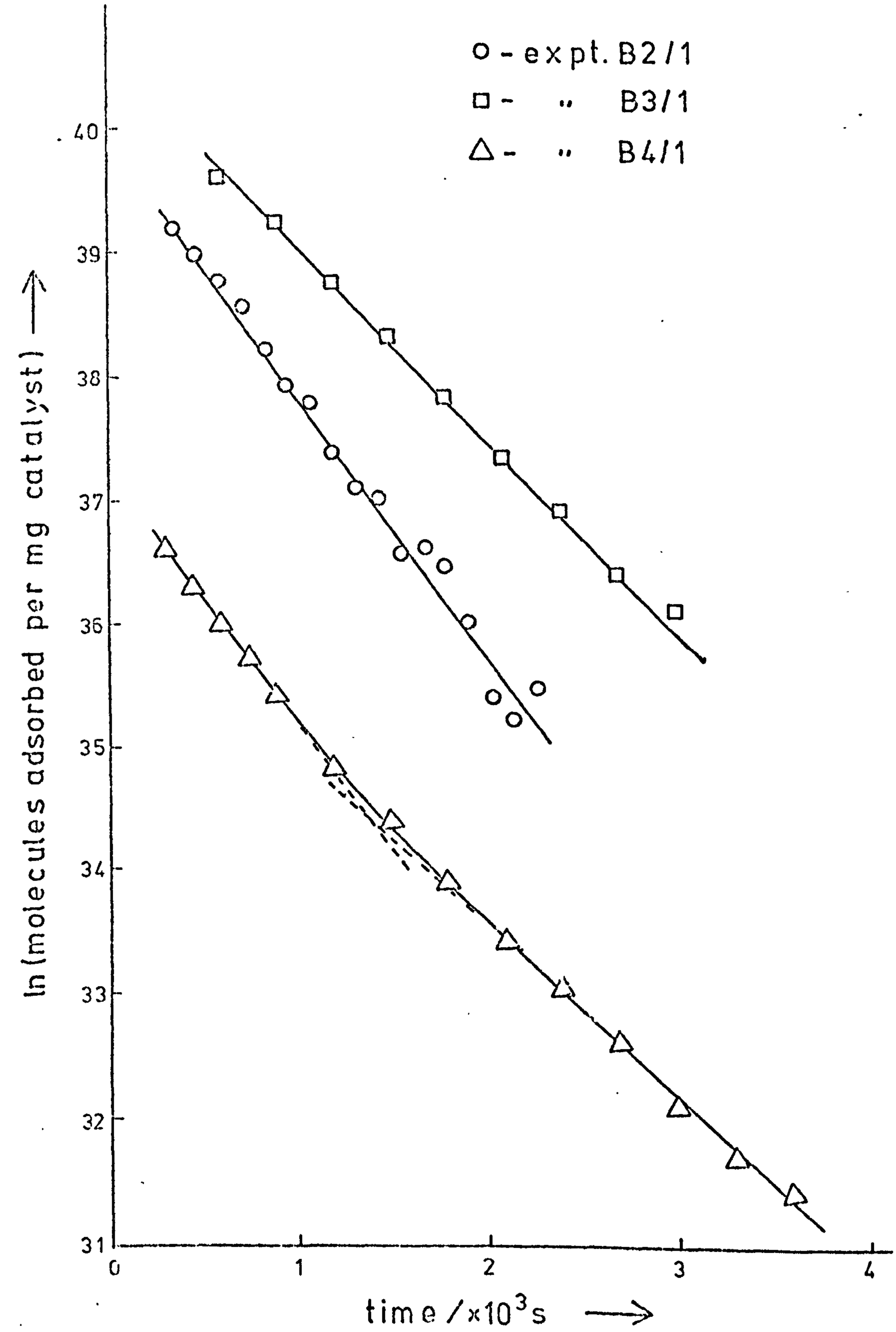

Figure 5.3. Chlorobenzene-C14 desorptions from 1% Pd/SiO_2 in H_2 flow.

Table 5.4. Ambient temperature chlorobenzene desorptions. Adsorption and kinetic data.

Experiment number	B2/1	B3/1	B4/1	C2/1	C2/2	C2/3	C2/5	C2/6
Maximum adsorption level / $x10^{16}$ molecule (mg catalyst)$^{-1}$	10.5	15.9	0.41	27.6	14.0	6.74	0.85	0.22
λ_1 / $x10^{-3}$ s^{-1}	1.94	1.55	2.04	2.2	2.5	2.9	2.1	-
λ_2 / $x10^{-4}$ s^{-1}	-	-	14.1	4.1	6.8	5.7	7.7	5.3
Intersection / $x10^{15}$ molecule (mg catalyst)$^{-1}$	-	-	1.03	4.39	4.29	3.65	3.33	0.63

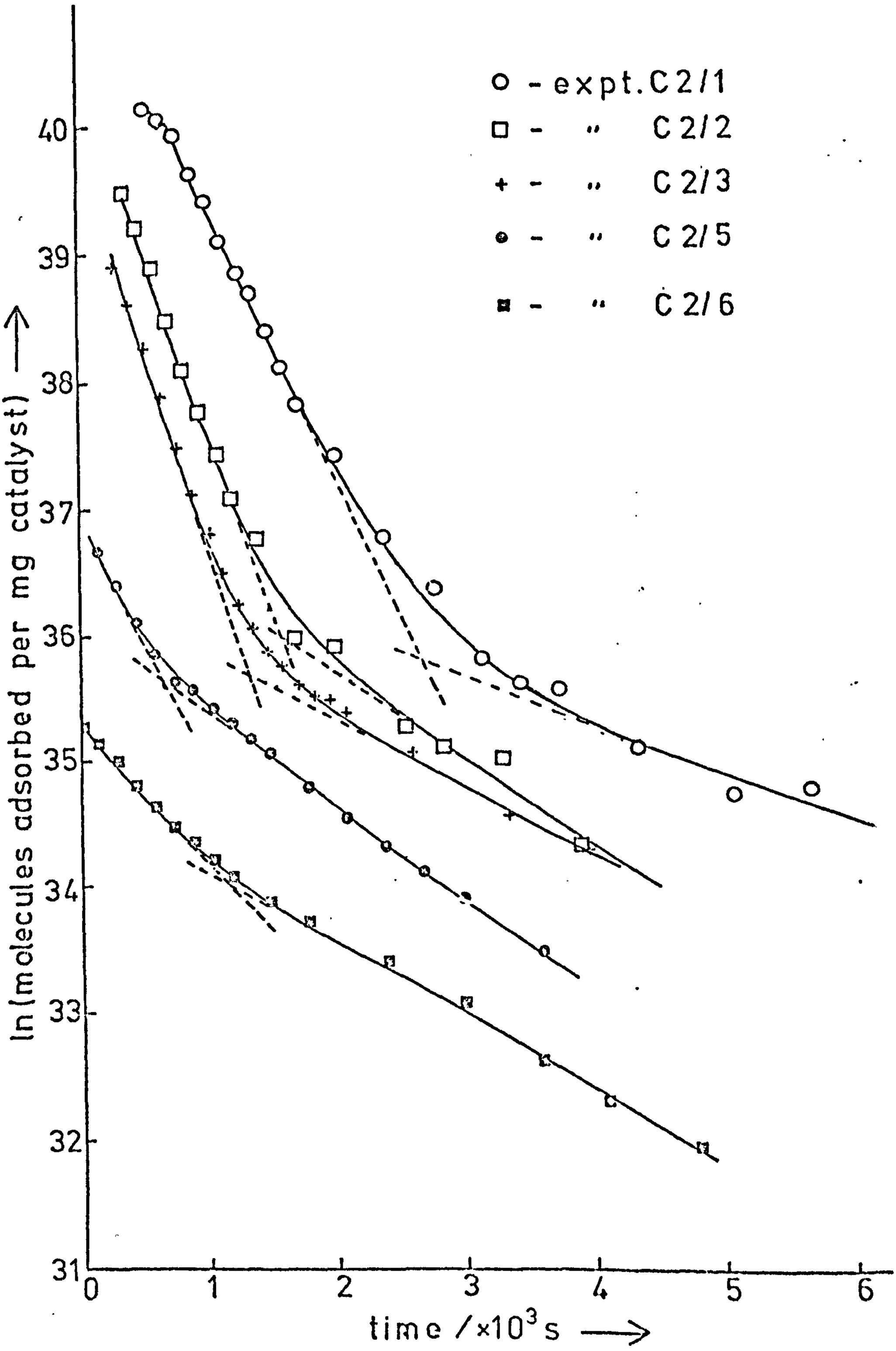

Figure 5.4. Chlorobenzene-C14 desorptions from 5%Pd/SiO_2 in H_2 flow with various values of initial adsorption.

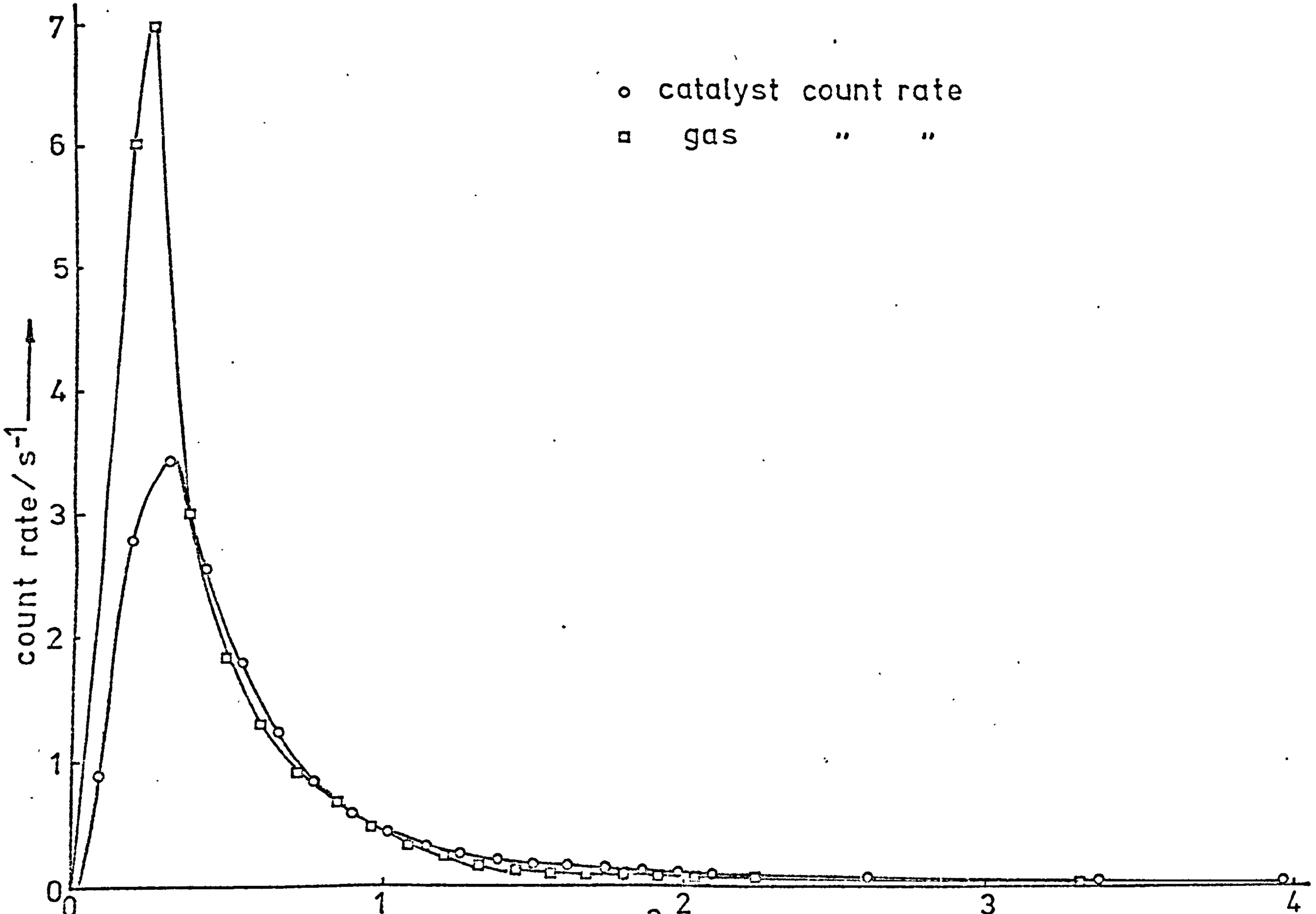

Figure 5.5. Count rate versus time for catalyst and gas chambers - experiment C2/3.

experiments were conducted under pulsed chlorobenzene-Cl4 flow conditions in a nitrogen carrier flow, when it was assumed that adsorbed chlorobenzene rather than product benzene was observed. The observed desorption kinetics were slower than those under hydrogen flow, and in several of the experiments a hydrogen flow was substituted for the initial nitrogen flow to see if the desorption kinetics would revert to those obtained with hydrogen flow throughout. The experiments were carried out with the ambient temperature reactor/counting chamber. Prior to each experiment in N_2 flow, the catalyst was left overnight in a slow N_2 flow following standard reduction procedure or an experiment in H_2 flow. For each experiment, the carrier gas flow (N_2 or H_2) was maintained at approximately 2.5 ml s^{-1}.

Experiments C1/1 and 2. (see figure 5.6).

Both experiments were run at 299 K and 750 torr. Catalyst sample C1 weighed 240 mg. In experiment C1/1, 20 µl of chlorobenzene-Cl4 (specific activity 3.76×10^5 s^{-1} $mmol^{-1}$) was introduced into the gas flow. Following the introduction of 10 µl of similar chlorobenzene-Cl4 in experiment C1/2, the N_2 flow was changed to one of H_2 during the latter part of the desorption.

Experiments C1/4 and C2/7. (see figure 5.7).

As the count rates obtained in C1/2 were considered to be unsatisfactorily low, the experiment was repeated with 0.5 µl samples of higher specific activity chlorobenzene-Cl4 (C1/4, 1.88×10^8 s^{-1} $mmol^{-1}$, C1/7, 1.51×10^7 s^{-1} $mmol^{-1}$). Experiment C1/4 was carried out at 301 K and 758 torr, and experiment C2/7 at 297 K and 745 torr. In experiment C1/4, prior to the introduction of constant H_2 flow, a 1 ml sample of H_2 was injected into the carrier N_2 flow.

Experiment 2/8. (see figure 5.8).

The experiment was carried out at 295 K and 750 torr in N_2 flow throughout. Following an initial pulse of 0.7 µl chlorobenzene-Cl4 (specific activity 1.51×10^7 s^{-1} $mmol^{-1}$), two further 0.2 µl pulses were added.

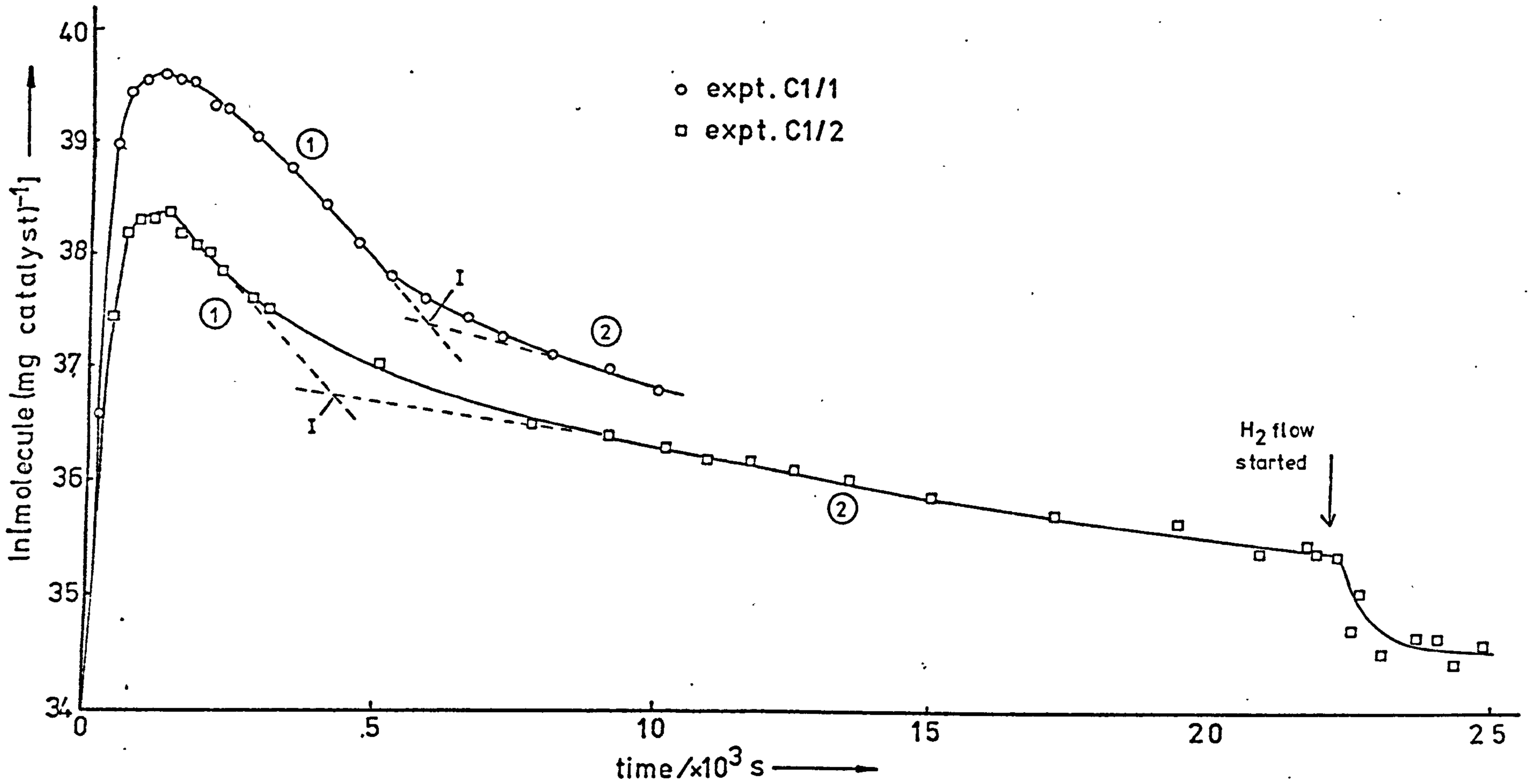

Figure 5.6. Chlorobenzene-C14 desorption from 5% Pd/SiO_2 in N_2 flow.

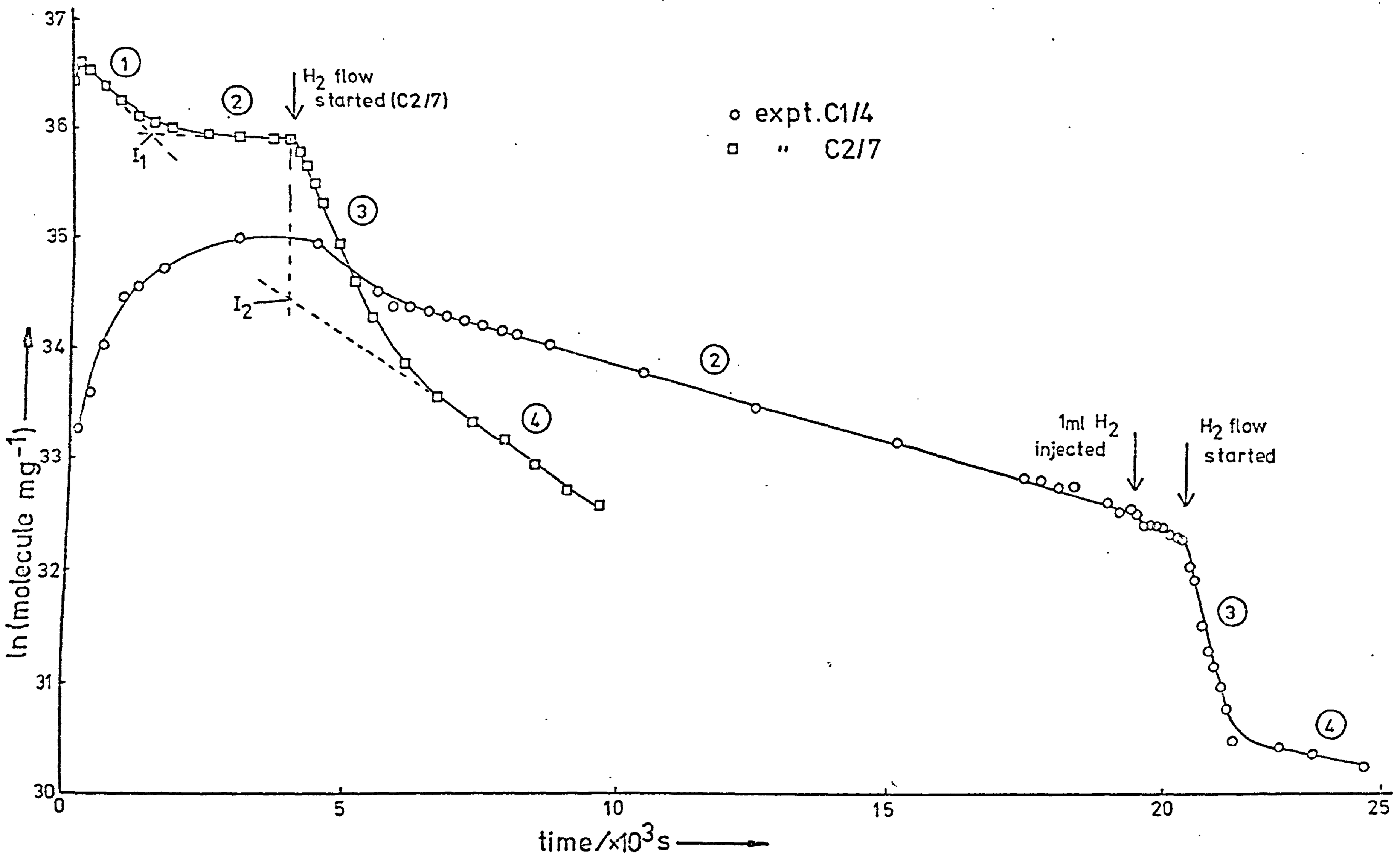

Figure 5.7. Chlorobenzene-C14 desorptions from 5% Pd/SiO_2 in N_2 followed by H_2 flow.

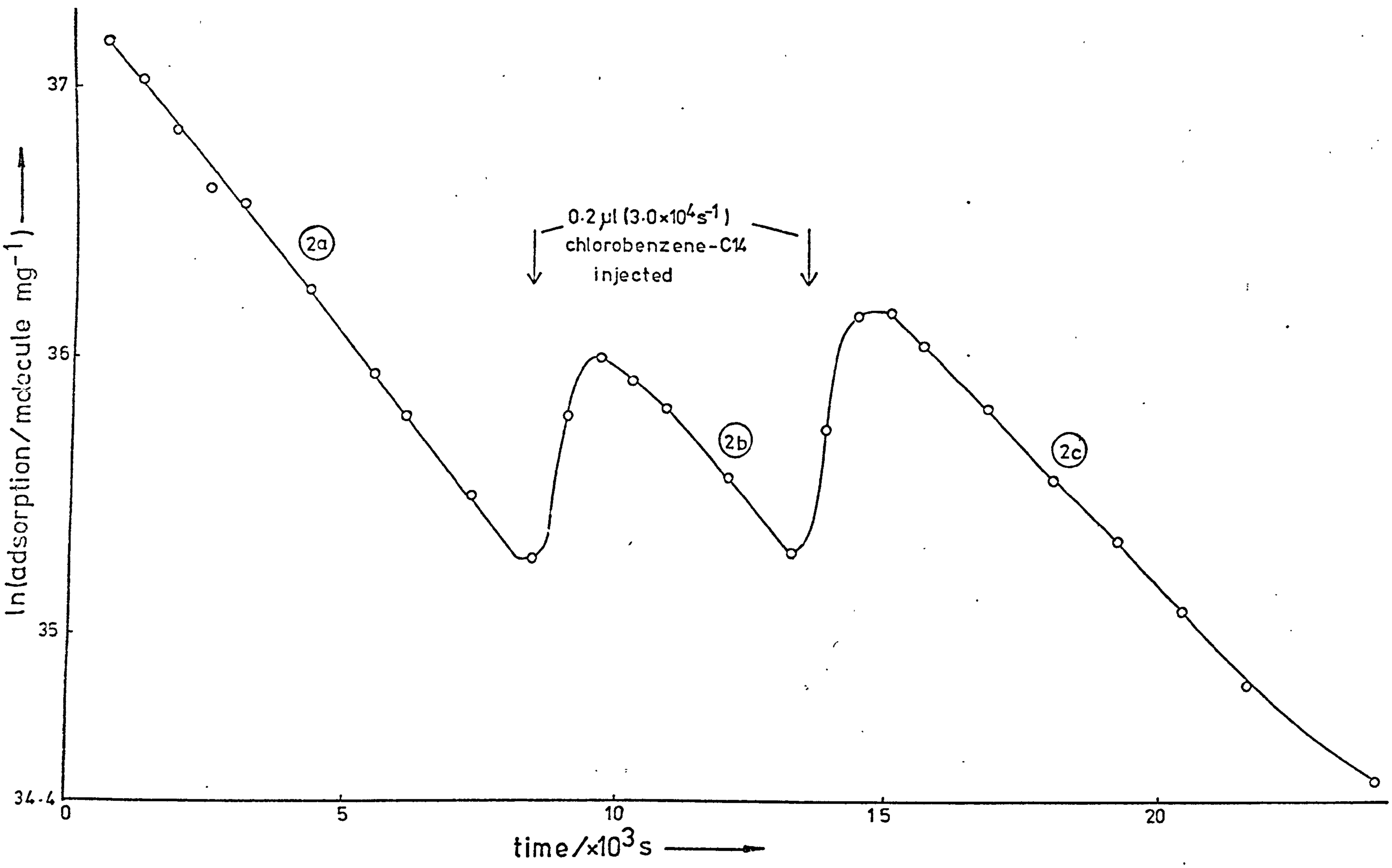

Figure 5.8. Experiment C2/3 - chlorobenzene-C14 pulses over Pd/SiO_2 in H_2 flow.

Experiment 2/10. (see figure 5.9).

The experiment was carried out at 293 K and 755 torr. The first part of the experiment was conducted as in experiments C1/4 and C2/7. 0.5 µl chlorobenzene-C14 (specific activity 1.51×10^7 s^{-1} $mmol^{-1}$) was introduced in N_2 flow followed by H_2 flow. A sample of 10 µl of non-radiotracer chlorobenzene was then introduced into the carrier flow to test for displacement of the adsorbed radioactive species.

Table 5.5 lists the data derived from the desorptions in N_2 flow. λ_1 and λ_2 are the rate constants for the fast and slow sections respectively of the desorption curves in N_2 flow. The point of intersection referred to is that of the corresponding "straight-line" sections of the curves.

Table 5.6 gives the information from the desorptions occurring after introduction of H_2 flow. λ_3 is the first order desorption rate constant immediately following the start of the H_2 flow, and λ_4 the subsequent slower rate constant observed.

The various regions of the semi-log curves, figures 5.6 - 9, have been labelled 1 - 4, corresponding to the numbering of the rate constants. The desorptions associated with these regions will henceforth be termed types 1 - 4 respectively. Table 5.6 also lists the adsorption of species giving rise to type 4 desorptions, obtained by extrapolating the type 4 curves to the time of introduction of the flow.

5.4. Benzene desorptions from Pd/SiO_2.

In these experiments, the desorption of benzene-C14 from a Pd/SiO_2 catalyst was investigated by pulsed flow experiments in hydrogen and nitrogen carrier flows. It was intended to compare the desorption kinetics with those observed with chlorobenzene-C14 to ascertain whether or not adsorbed benzene could account for the slower part of these desorptions (assumed to be from the metal).

The experiments were performed using benzene-C14 of specific activity 7.16×10^6 s^{-1} $mmol^{-1}$. The normal carrier gas flow rate was approximately 2.5 ml s^{-1}.

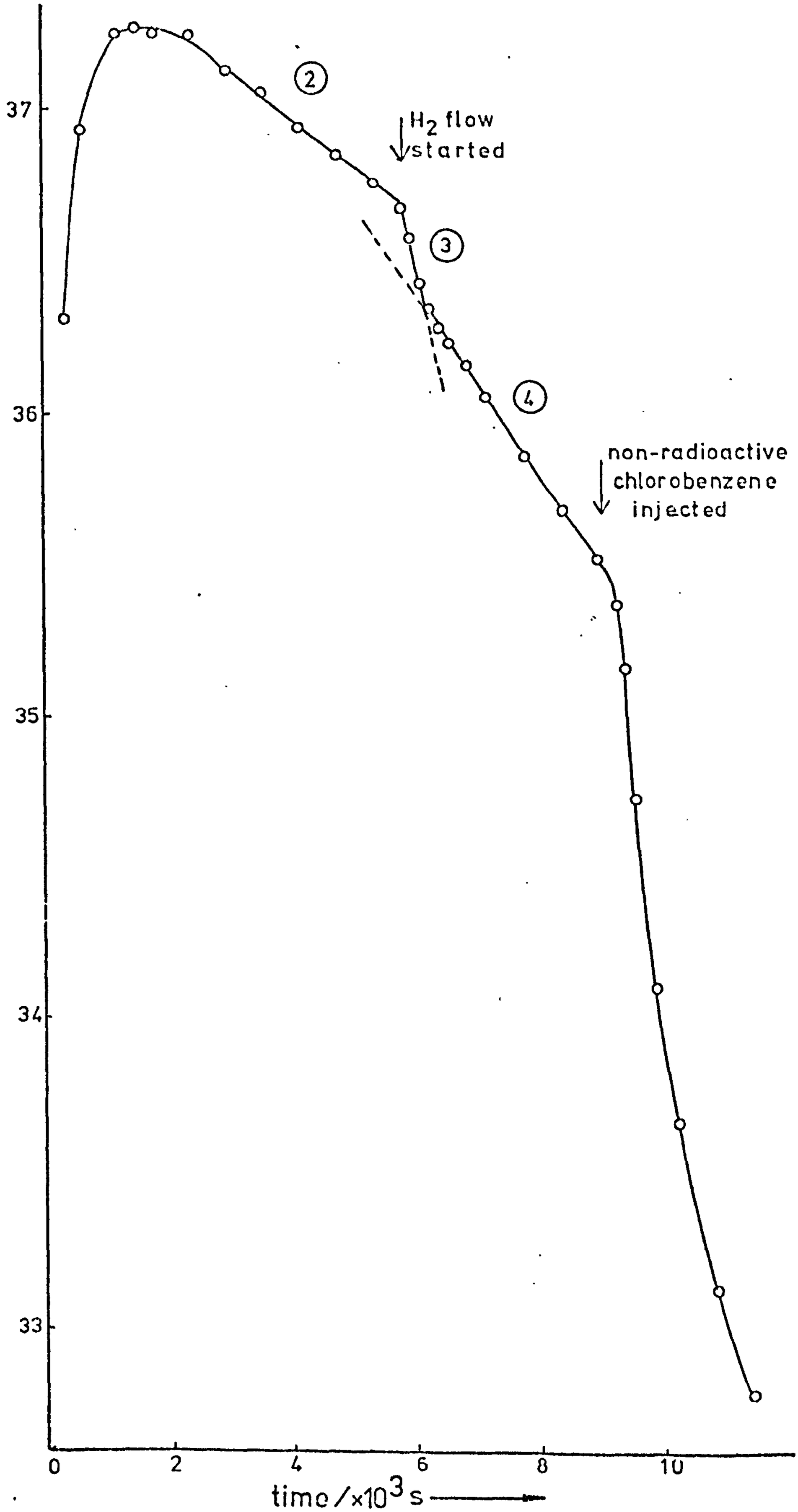

Figure 5.9. Experiment C2/10 - desorption curve.

Table 5.5. Adsorption and kinetic data from chlorobenzene-C14 desorptions in N_2 flow.

Experiment number	C1/1	C1/2	C1/4	C2/7	C2/8 A	C2/8 B	C2/8 C	C2/10
Maximum adsorption / $\times 10^{16}$ molecule (mg catalyst)$^{-1}$	16.1	4.66	0.159	0.786	1.4	0.44	0.52	1.53
λ_1 /$\times 10^{-4}$ s^{-1}	5.21	5.44	-	4.93	-	-	-	-
λ_2/$\times 10^{-4}$ s^{-1}	1.60	1.27	1.31	~0.25	2.53	2.23	2.03	1.5
Adsorption at intersection (I_1) / $\times 10^{15}$ molecule (mg catalyst)$^{-1}$	17.1	9.13	-	4.10	-	-	-	-

Table 5.6. Adsorption and kinetic data from chlorobenzene -C14 desorptions in H_2 flow, following initial desorption in N_2 flow.

Experiment number	C1/2	C1/4	C2/7	C2/10
Adsorption at start of H_2 flow / $x10^{15}$ molecule (mg catalyst)$^{-1}$	2.4	0.11	3.9	8.5
λ_3 / $x10^{-3}$ s^{-1}	-	1.8	1.2	0.93
λ_4 / $x10^{-4}$ s^{-1}	-	1.2	3.4	2.6
Extrapolated type 4 adsorption at start of H_2 flow / $x10^{15}$ molecule (mg catalyst)$^{-1}$	1.1	0.022	0.88	6.6

Experiments C2/11, 14 and 15. (see figure 5.10).

The experimental conditions were as follows: C2/11 - 292 K, 755 torr; C2/14 - 291 K, 754 torr; C2/15 - 295 K, 749 torr.

In experiment C2/11, 2.5 µl (2.02×10^5 s^{-1}) benzene-Cl4 was injected into the H_2 carrier flow, which was constant throughout.

The observed desorption curve appeared to be ill-defined and did not resolve into the clearly defined regions of the chlorobenzene desorptions. This was attributed to a reluctance of the benzene to adsorb on the metal. If this hypothesis was correct, a longer time of contact between the benzene-Cl4 and the catalyst was expected to increase the amount of slowly desorbed species. To this end, in experiments C2/14 and 15, an initially slow H_2 flow was used (approximately 0.1 ml s^{-1}), into which was injected 2 µl (1.61×10^5 s^{-1}) benzene-Cl4. The normal H_2 flow was subsequently resumed after 900 s and 2400 s respectively.

Experiment C2/16. (see figure 5.11).

The experiment was carried out at 295 K and 750 torr. 2 µl benzene-Cl4 (1.61×10^5 s^{-1}) was injected into an initially slow N_2 flow (approximately 0.1 ml s^{-1}). The flow rate was then returned to normal and a H_2 flow substituted at the point indicated in the diagram.

Experiment C2/17. (see figure 5.12).

Assuming that the observed species during the slow chlorobenzene desorptions in hydrogen flow was due to benzene or a benzene derivative adsorbed on the metal, by analogy with experiment C2/10 (see section 5.3), benzene-Cl4 adsorbed on the metal should also be displaced by non-radiotracer chlorobenzene.

The experiment was carried out at 294 K and 753 torr. 2 µl(1.61×10^5 s^{-1}) benzene-Cl4 was injected into an initially slow H_2 carrier flow, subsequently increased to the normal flow rate as in experiments C2/14 and 15. At the point indicated in the diagram, 10µl non-radioactive chlorobenzene was injected into the H_2 flow.

The slopes of the various "straight-line" sections of the

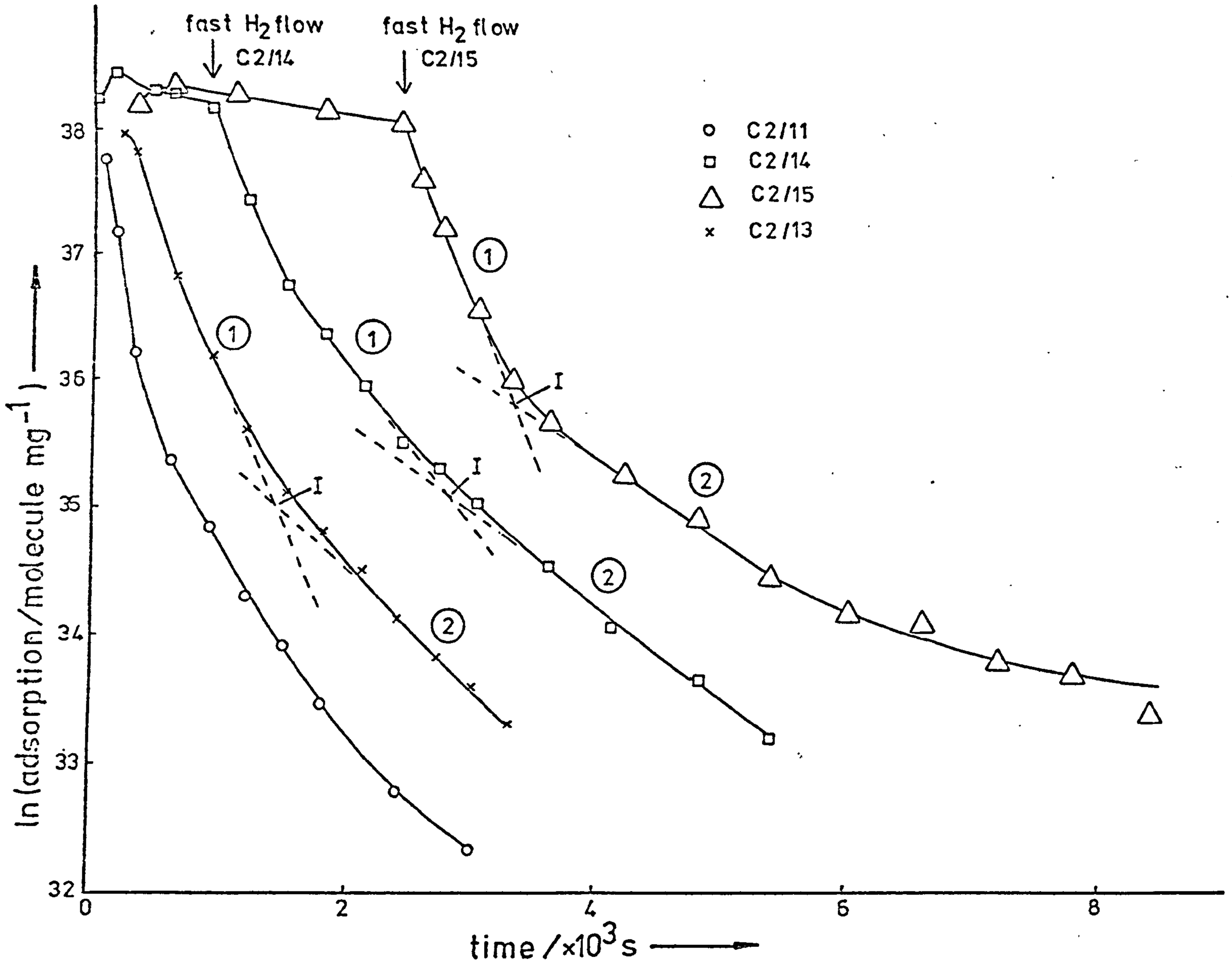

Figure 5.10. Benzene-C14 desorptions from 5% Pd/SiO_2 in H_2 flow.

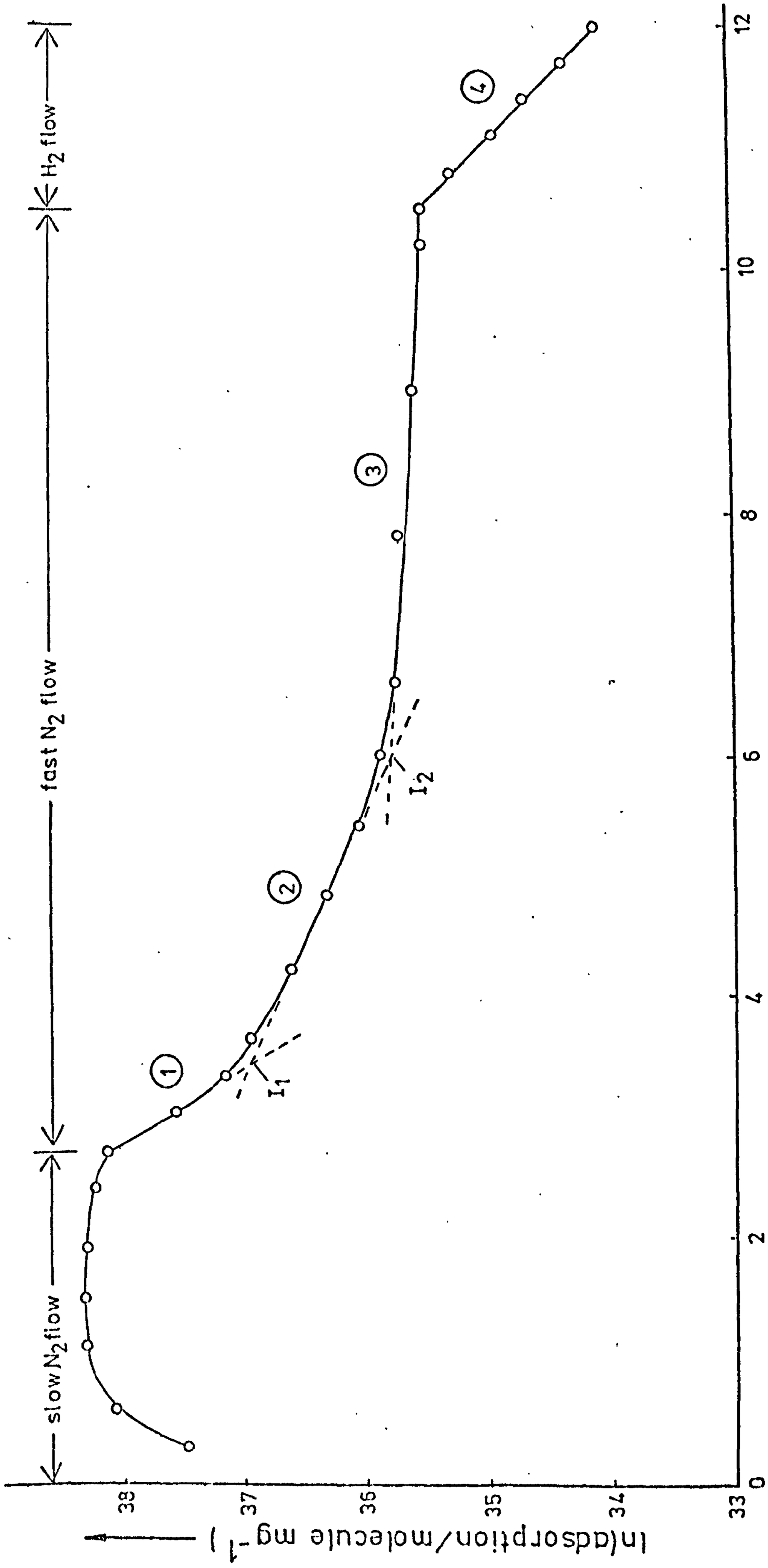

Figure 5.11. Benzene-C14 desorption from 5% Pd/SiO_2, initially in N_2 flow and subsequently in H_2 flow.

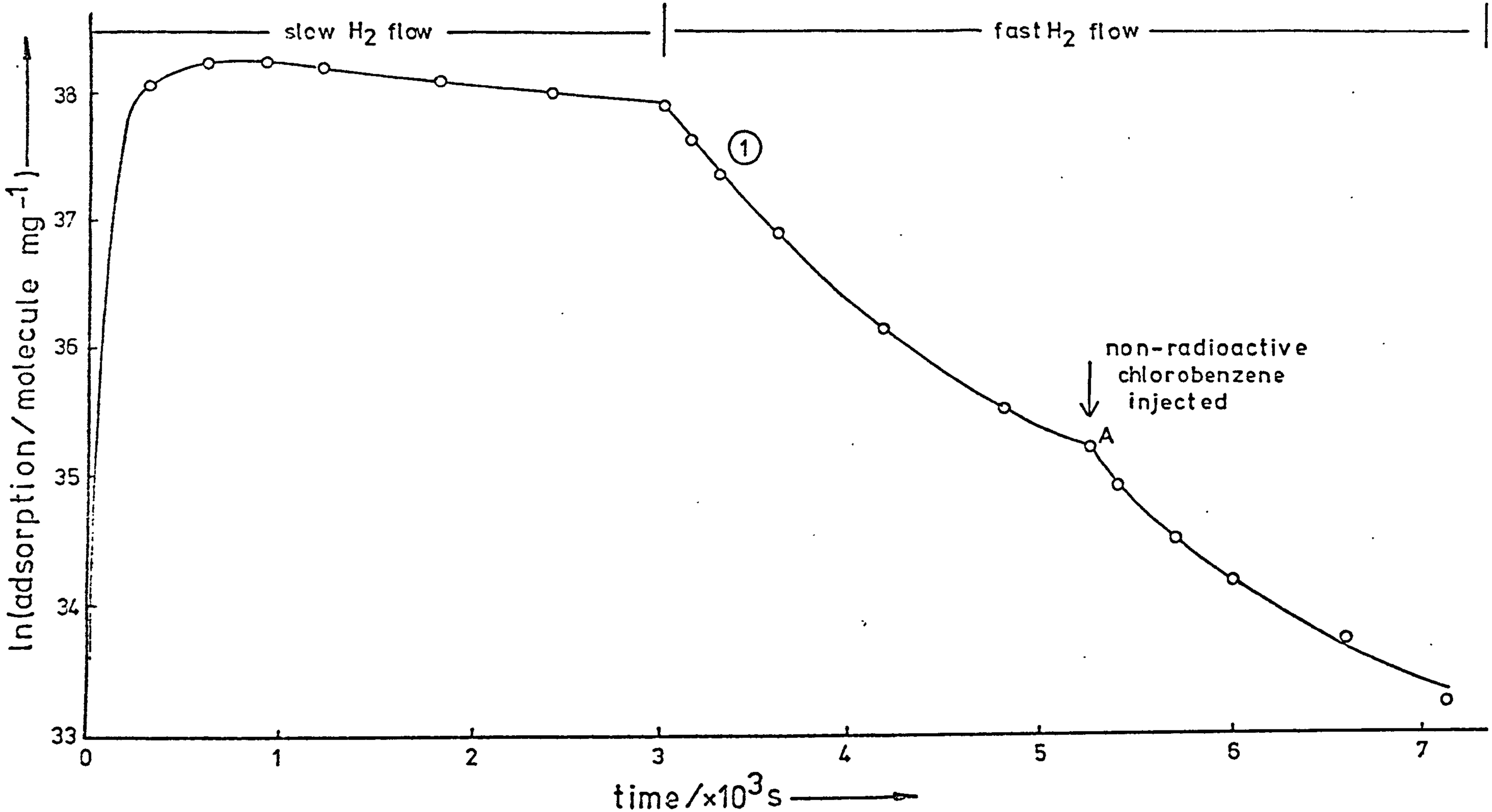

Figure 5.12. Benzene-C14 desorption from 5% Pd/SiO_2, with injection of 2µl non-radioactive chlorobenzene.

Table 5.7. Adsorption and kinetic data from benzene-C14 desorptions.

Experiment number	C2/11	C2/14	C2/15	C2/16	C2/17	C2/13
Maximum adsorption / $x10^{16}$ molecule (mg catalyst)$^{-1}$	2.5	4.9	4.5	4.4	4.1	3.0
λ_1/ $x10^{-4}$ s^{-1}	-	12.8	23.3	16.9	17.7	-
λ_2/ $x10^{-4}$ s^{-1}	-	8.62	6.45	4.65	-	9.1
λ_3/ $x10^{-4}$ s^{-1}	-	-	-	0.60	-	-
λ_4/ $x10^{-4}$ s^{-1}	-	-	-	9.78	-	-
I_1 /$x10^{15}$ molecule (mg catalyst)$^{-1}$	-	2.61	3.57	11.0	-	1.55
I_2 /$x10^{15}$ molecule (mg catalyst)$^{-1}$	-	-	-	3.41	-	-
A /$x10^{15}$ molecule (mg catalyst)$^{-1}$	-	-	-	-	1.94	-

semi-log desorption plots, figures 5. 10, 11 and 12, were measured and recorded in table 5.7. The values of λ given correlate with the numeration used in the figures. The count rates recorded in the table correspond to the features labelled in the respective plots.

Experiment C2/13. (see figure 5.10).

In a further attempt to identify the slowly removed species during the hydrogen flow chlorobenzene desorptions, a pulse composed of 2 μl non-radioactive chlorobenzene and 2 μl benzene-C14(1.61×10^5 s^{-1}) was injected into a normal hydrogen carrier flow. It was hoped to demonstrate on exchange between the radiotracer benzene and product non-radiotracer benzene adsorbed on the metal in the latter part of the desorption.

The slope of the latter part of the semi-log desorption curve and the adsorption at the start of this region are given in table 5.7.

5.5. Chlorobenzene desorptions from Pd black.

Chlorobenzene-C14 desorptions were conducted in hydrogen flow with palladium black as the adsorbent. The powdered metal was used to eliminate effects due to support adsorption.

The Pd black catalyst, sample PdBl (235 mg), was reduced under standard conditions, and the normal carrier gas flow rate employed was again 2.5 ml s^{-1}. All experiments were carried out at approximately 292 K and 757 torr.

Experiments PdBl/1, 2 and 3. (see figure 5.13).

10 μl (3.7×10^4 s^{-1}) and 0.9 μl (1.6×10^5 s^{-1}) chlorobenzene-C14 were injected into a normal H_2 carrier flow in experiments PdBl/1 and 2 respectively. In an attempt to increase the extent of adsorption experiment PdBl/3 used an initially slow (approximately 0.1 ml s^{-1}) H_2 carrier flow, into which was injected 0.5 μl (8.7×10^4 s^{-1}) chlorobenzene-C14, normal H_2 flow being resumed after 450 s.

Experiments PdBl/4 and 5. (see figure 5.14).

Here, an increased amount of adsorption was achieved by repeated dosage of radiotracer pulses.

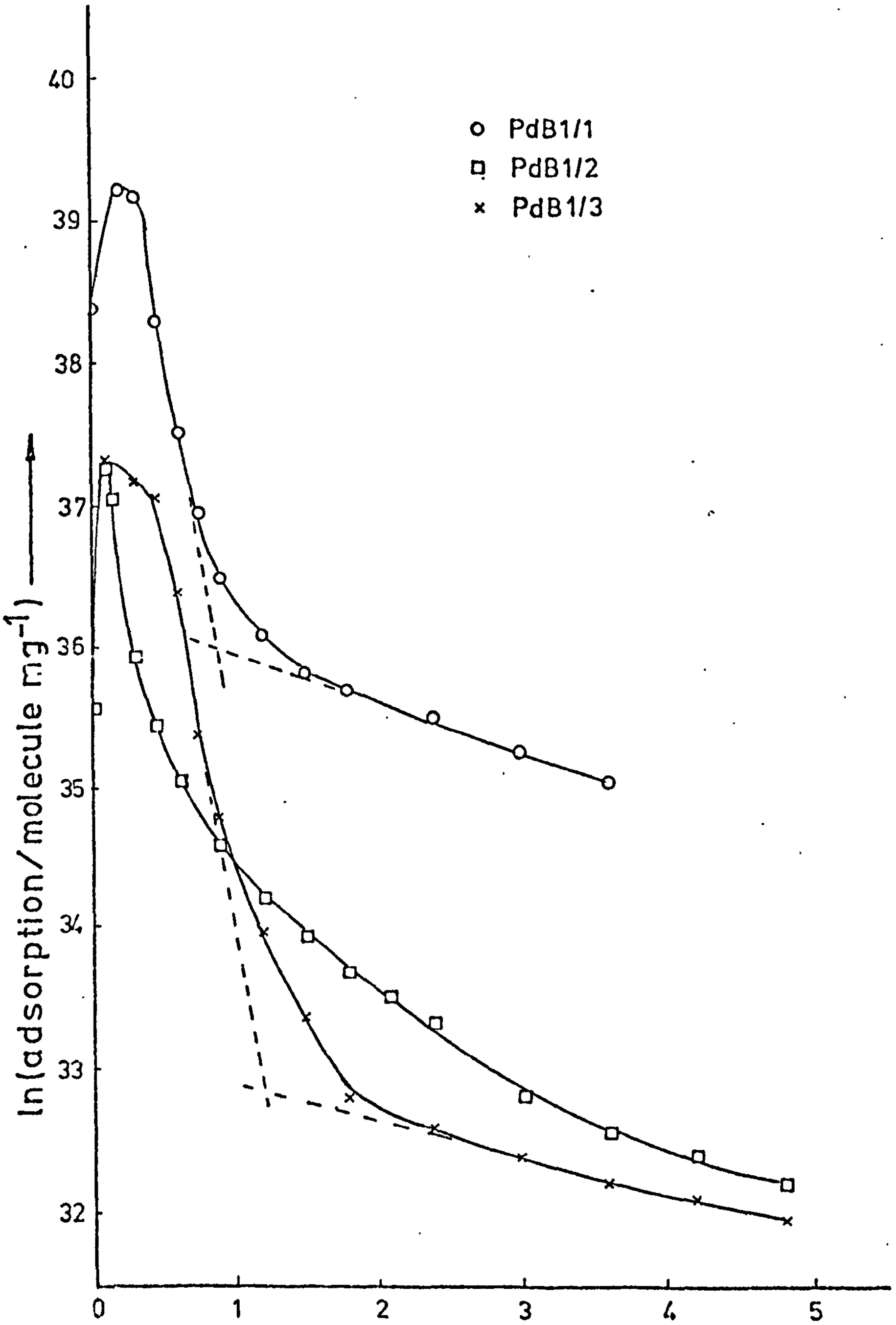

Figure 5.13. Chlorobenzene-C14 desorptions from Pd black in H_2 flow - experiments PdB1/1-3.

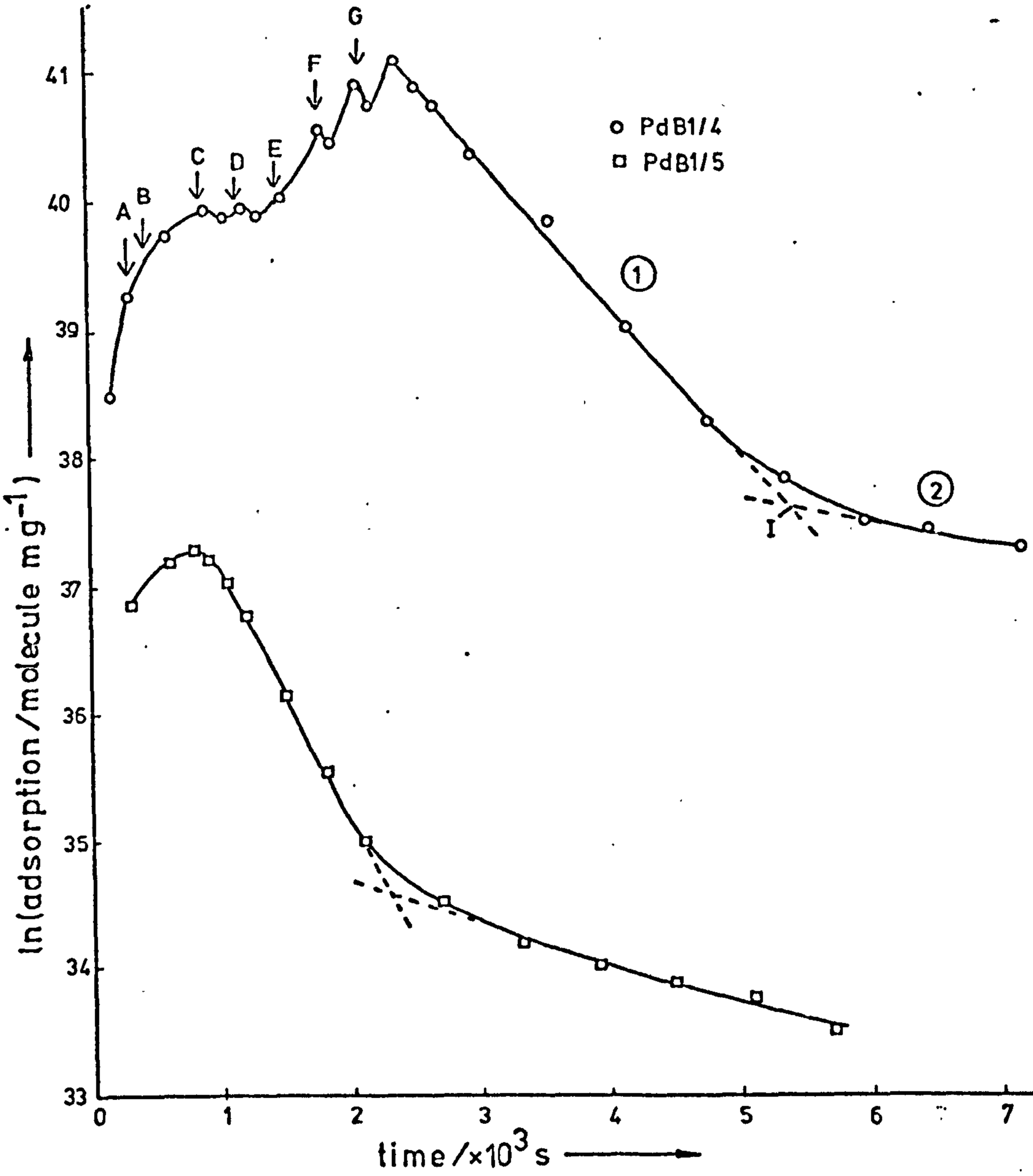

Figure 5.14. Chlorobenzene-C14 desorptions from Pd black in H_2 flow. Experiments PdB1/4 &5.

Table 5.8. Adsorption and kinetic data from chlorobenzene-C14 desorptions from Pd black.

Experiment number	PdB1/1	PdB1/3	PdB1/4	PdB1/5
Maximum adsorption / $x10^{16}$ molecule (mg catalyst)$^{-1}$	10.6	1.58	69.3	1.60
λ_1 / $x10^{-3}$ s^{-1}	5.54	5.43	1.16	1.96
λ_2 / $x10^{-4}$ s^{-1}	3.36	2.53	2.20	3.31
I / $x10^{15}$ molecule (mg catalyst)$^{-1}$	4.27	0.187	21.8	1.05

In experiment PdBl/4 a total of 110 µl (4.07×10^5 s^{-1}) chlorobenzene-Cl4 was passed over the catalyst in normal H_2 flow, in 7 x 10 µl and 2 x 20 µl samples. The rate of evaporation of the last 3 chlorobenzene-Cl4 samples was increased by warming the area of the flow system in which the liquid sample sat after injection. 3 x 0.3 µl (total 1.6×10^5 s^{-1}) chlorobenzene samples were used in experiment PdBl/5 without heating. In both experiments the times of injection of each sample are indicated by arrows in figure 5.14.

Table 5.8 lists the initial and final slopes and the surface coverage at the point of intersection between the corresponding straight-line regions of the curves of figures 5.13 and 14, excepting PdBl/2, where the semi-log plot was insufficiently resolved for meaningful analysis.

5.6. High temperature chlorobenzene desorptions.

The high temperature experiments were designed to test the variation of the desorption rates with temperature and, if possible, find values for the apparent energy of activation for the desorption from the Pd/SiO_2 catalyst and a sample of the silica support. The experiments were performed with the high temperature counting/reaction chamber (figure 4.4) at atmospheric pressure. As the component of the observed count rate due to gas phase radioactivity was difficult to assess at low surface coverages with this counting chamber, no attempt was made to follow desorption kinetics at low surface coverages. The results given relate to the initial desorption rates only.

Experiments C3/1 - 6.

Catalyst sample C3 (354 mg) was reduced under standard conditions. The desorptions were studied by passing 2 µl (7.4×10^3 s^{-1}), samples of chlorobenzene-Cl4 over the catalyst in a 2.5 ml s^{-1} H_2 carrier flow. The desorption curves obtained are shown in figure 5.15. The desorption rate constants calculated from the semi-log plots are given in table 5.9(a). Figure 5.16 shows a plot of ln (desorption rate constant) versus 1/ (temperature) for experiments C3/1 - 4. Experiments C3/5 and 6 are omitted from this plot as they probably correspond to the flow pattern of the chlorobenzene sample through the chamber rather than

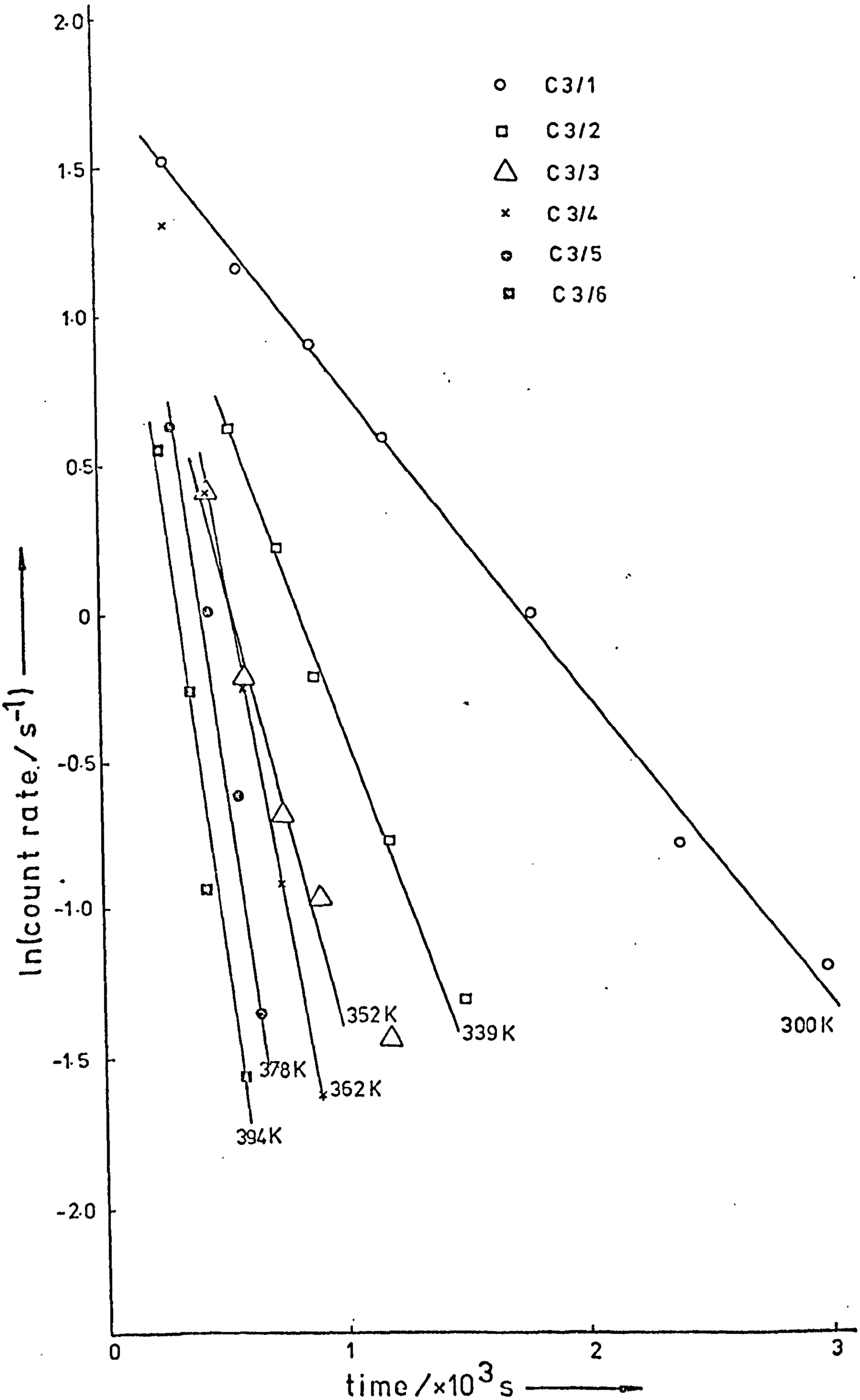

Figure 5.15. High temperature chlorobenzene-C14 desorptions from 5% Pd/SiO_2 in H_2 flow.

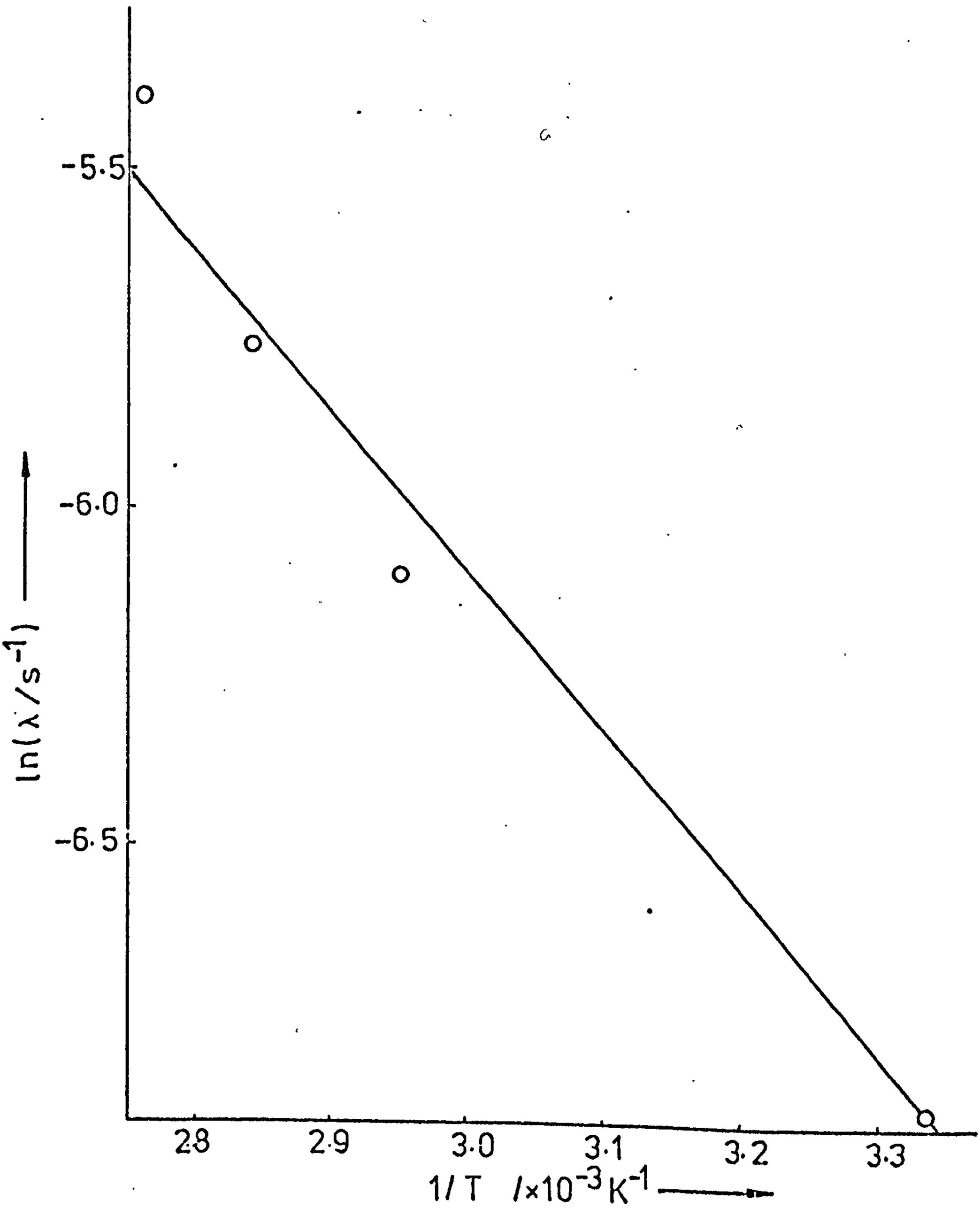

Figure 5.16. Arrhenius plot for desorption of chlorobenzene-C14 from 5% Pd/SiO_2 in H_2 flow.

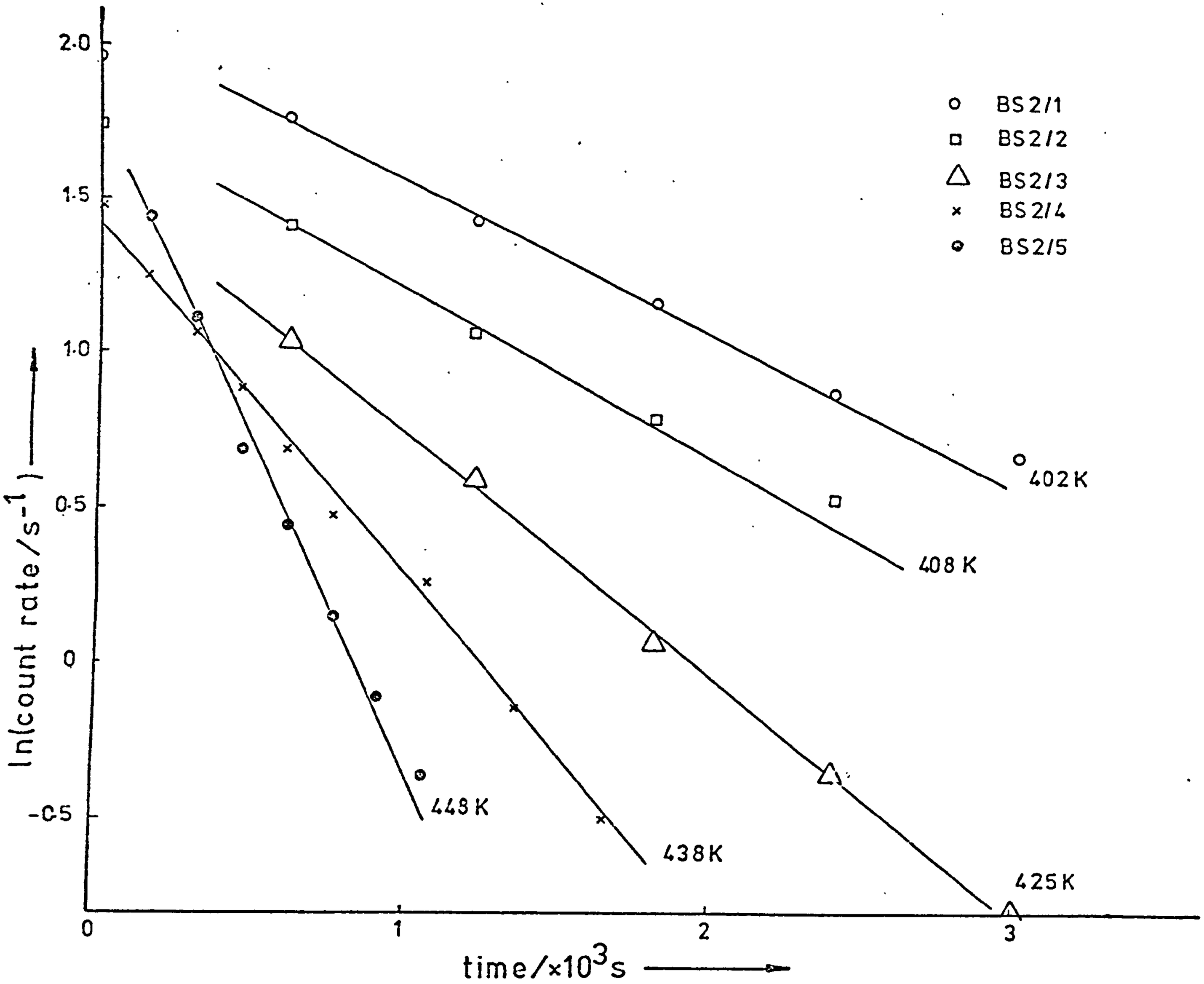

Figure 5.17. High temperature chlorobenzene-C14 desorptions from silica in H_2 flow.

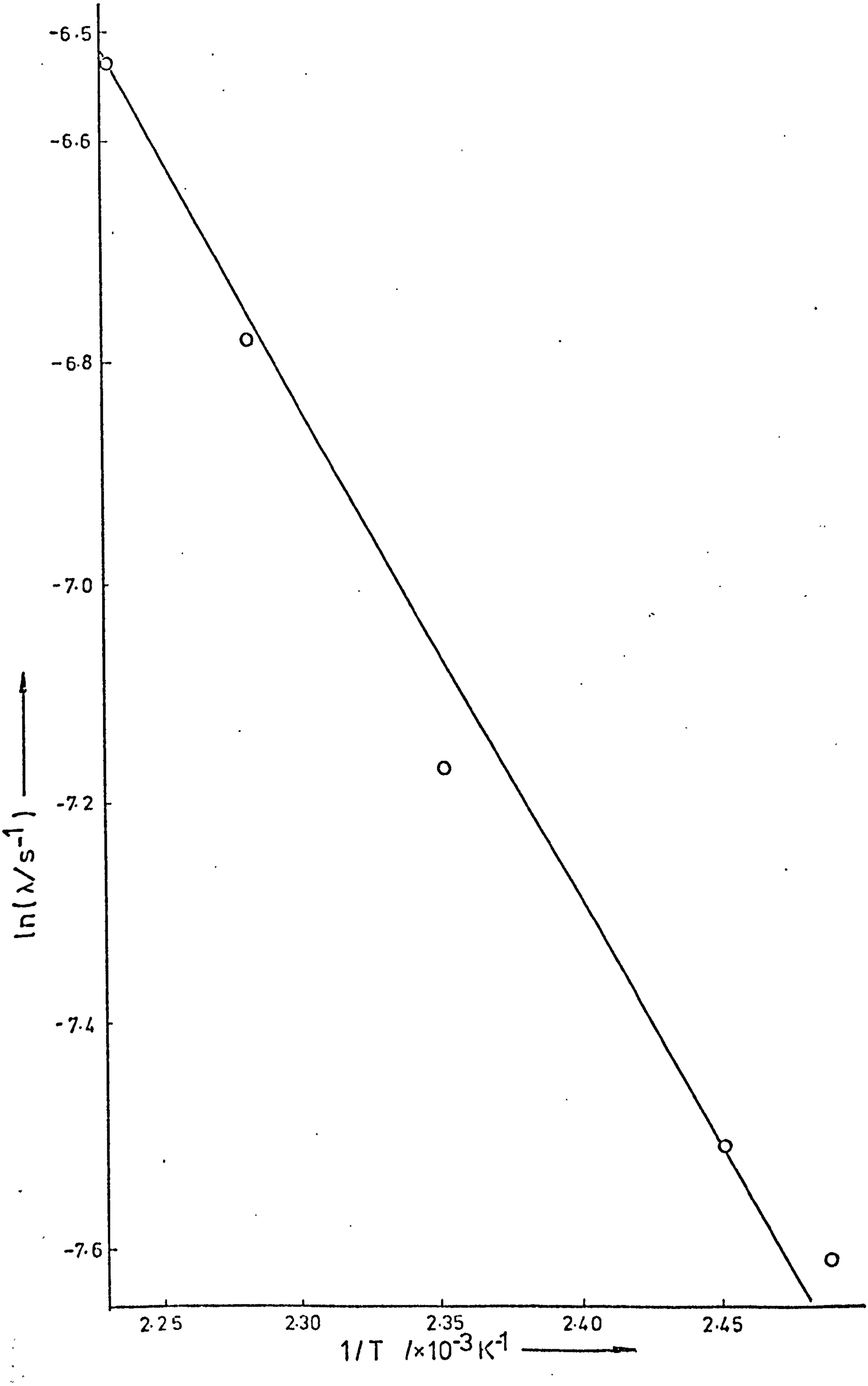

Figure 5.18. Arrhenius plot for desorption of chlorobenzene-C14 from silica in H_2 flow.

Table 5.9. High temperature desorption rate constants.

Experiment number	C3/1	C3/2	C3/3	C3/4	C3/5	C3/6
Temperature / K	300	339	352	362	378	394
λ / $x10^{-3}s^{-1}$	1.03	2.25	3.15	4.57	6.52	6.31

(a) Chlorobenzene desorption from Pd/SiO_2.

Experiment number	BS2/1	BS2/2	BS2/3	BS2/4	BS2/5
Temperature / K	402	408	425	438	448
λ / $x10^{-3}s^{-1}$	0.494	0.548	0.772	1.14	1.45

(b) Chlorobenzene desorption from silica.

the desorption process. A value for the apparent energy of activation of the desorption process was calculated by the Arrhenius equation:

$k = A \exp(- E_A/RT)$, where k = rate constant, A = pre-exponential factor, E_A = energy of activation, R = gas constant and T = temperature.

$$\text{i.e.} \quad \ln k = \frac{E_A}{-RT} + \ln A.$$

A plot of ln (rate constant) versus 1/T should therefore have a slope of $- E_A/R$. From the LSA slope of figure 5.15, the apparent energy of activation was 20.6 ± 2.5 kJ mol^{-1}.

Experiments BS2/1-5.

A 296 mg sample of Aerosil silica was used to study chlorobenzene-Cl4 adsorption over the temperature range 408 - 448 K. As the desorptions were considerably slower than from the Pd/SiO_2 catalyst, the higher temperature range used gave more convenient desorption rates. The semi-log desorption curves obtained are shown in figure 5.17. The rate constants obtained are listed in table 5.9(b), and the Arrhenius plot is given in figure 5.18. The LSA value calculated for the apparent energy of activation of the desorption was 35.3 ± 2.2 kJ mol^{-1}.

5.7. Flow patterns and catalyst reactivity.

Flow patterns.

It was necessary to determine whether or not any of the effects observed in the desorption studies could be attributed to the flow characteristics of the system rather than the desorption process under study.

Samples of 3 µl (1.11×10^4 s^{-1}) chlorobenzene-Cl4 were injected into a 2.5 ml s^{-1} H_2 carrier flow to pass through the ambient temperature and the high temperature counting/reaction chambers in separate experiments. No catalyst or adsorbent was present in either case. The resulting count rate versus time plots are shown in figure 5.19. In both cases the passage of the radiotracer pulse through the system was considerably faster than the desorption processes studied.

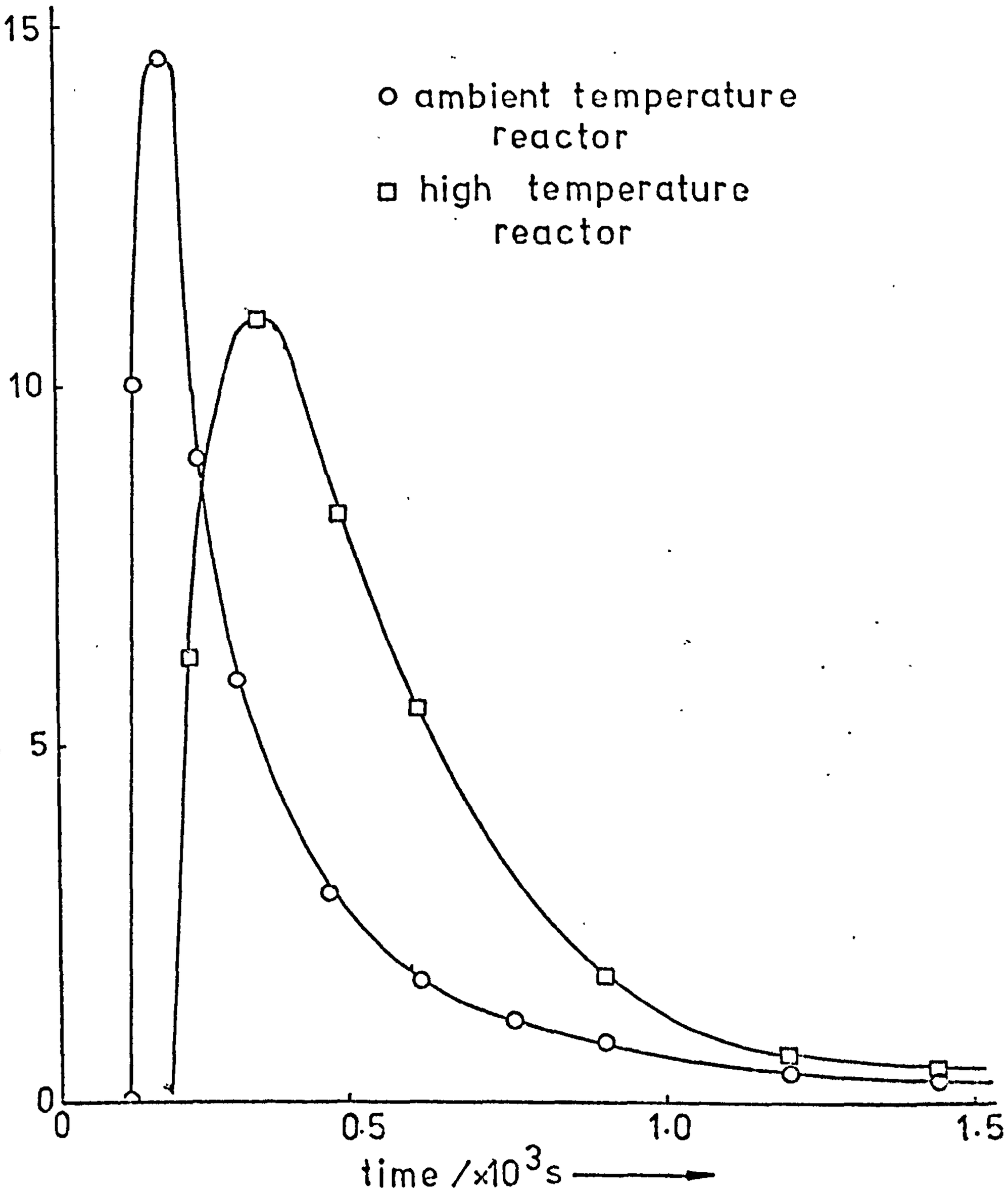

Figure 5.19. Flow patterns for passage of chlorobenzene-C14 pulse through empty counting/ reaction chambers.

Catalyst activities.

In the pulsed flow desorption experiments, no measure of catalytic activity was made.

The activities of catalysts C and PdB were therefore tested under constant chlorobenzene/H_2 flow conditions. Both catalysts were tested in the ambient temperature reactor, and catalyst C at 296 K and 425 K in the high temperature reactor. The products were collected over intervals of 36 minutes and analysed spectroscopically. The results are given in table 5.10. Each catalyst sample used was reduced under standard conditions.

Table 5.10. Catalyst activities for chlorobenzene hydrogenolysis.

Catalyst	C	C	C	PdB
Reactor	Ambient temp.	High temp.	High temp.	Ambient temp.
Catalyst weight / mg	344	483	451	420
Temperature / K	293	294	425	294
Total pressure / torr	750	752	752	754
Partial pressure chlorobenzene / torr	1.35	1.28	1.25	1.41
Chlorobenzene flow rate /x10^{17}molecule s^{-1}	1.21	1.14	1.11	1.26
Hydrogen flow rate / ml s^{-1}	2.5	2.5	2.5	2.5
Reaction rate /x10^{16}molecule s^{-1}	5.23	2.77	1.38	6.36

Part B. Ethylene Studies.

The experiments described in sections 9 to 15 made use of both counting ratemeter coupled to a chart recorder, and the fast counting system (FCS) to record experimental data. In experiments where only ratemeter data is given, this is normally due to malfunctioning of the fast counting system. Under these circumstances, the ratemeter data has been presented if it contained material of sufficient interest. The relevant sections of the fast counting system printout are given in table 5.19, experiments included in this table being marked with an asterisk in the text. No FCS data were available for the experiments of section 8.

Unless otherwise stated, standard catalyst reduction conditions were used i.e. 5 hours in H_2 flow at 423 K.

5.8. Preliminary studies on Pt/SiO_2.

Experiment F2/1.

This experiment was of an exploratory nature to find reaction conditions for an ethylene/hydrogen reactant flow passing over a sample of catalyst F(3.93% Pt/SiO_2) giving a suitable conversion to ethylene. 290 mg of catalyst were used in reactor A, and reduced at 473 K for 4 hours in H_2 flow. The pressure during reaction was maintained at 760 torr and the temperature at 292 K. The total reactant flow rate was varied between 0.83 ml s^{-1} and 7.15 ml s^{-1}, and the ethylene partial pressure from 75 torr to 350 torr. In all cases the conversion to ethane was found to be greater than 99.9%. The maximum reaction rate observed was 4.0 ml ethylene s^{-1}.

Experiments F5/1, 2, 3 and 5.

The experiments described here represent an attempt to obtain a desorption curve following the passage of ethylene-C14 pulses over the Pt/SiO_2 catalyst. The desorptions of primary interest, suitable for an application of the time dependent tracer dynamic method described in section 2.4, would have corresponded to the form of adsorbed hydrocarbon active in the hydrogenation reaction.

Such desorptions should have been rapid, forming a tail to the count rate versus time plot during the passage of the radiotracer pulse. In each experiment, only a slow desorption process was observed. Experiments with the Pt/SiO_2 catalyst were therefore curtailed and for the reasons given in section 3.3, subsequent experiments were performed with an Ir/SiO_2 catalyst.

Using reactor B, pulses of ethylene-Cl4 (specific activity 3.11×10^6 $s^{-1}m\ mol^{-1}$) in a H_2 carrier flow were passed at various temperatures over an 84 mg sample of catalyst F. A typical pair of count rate versus time plots for the catalyst and gas chambers are shown in figure 5.20 for the passage of the pulse through the system (F5/5). The conditions for each experiment and results pertaining to the passage of the initial pulses are given in table 5.11. The values R_I, given in this table refer to the ratio of the net counts observed which occurred from adsorbed species on the catalyst to the net counts observed from the gas counting chamber. Allowance was made for the gas phase counts observed from the catalyst chamber by the method described in Section 4.5. The maximum reversible adsorption values given were calculated from the maximum count rates observed in the catalyst chamber, making allowance for the gas phase count rate, as for R_I, and the count rate due to retained species. The count rate values obtained were converted to adsorption values (molecules adsorbed per mg catalyst) from the conversion factors given in table 4.3.

Following the passage of the ethylene-Cl4 pulse in each experiment, it was found that some radioactive species were retained by the catalyst. Part of this activity was slowly desorbed at the temperature of the experiment, and the respective semi-log slow desorption curves for F5/1, 3 and 5 are shown in figure 5.21. Where the semi-log curve divided approximately into two "straight-line" regions, the gradients of the slow and fast sections (labelled 1 and 2 respectively) are given in table 5.12. The adsorption at the intersection between these regions is given as I in the same table. The "contamination" value given refers to the number of ethylene-Cl4 molecules, equivalent in activity to the background count rate at the beginning of the

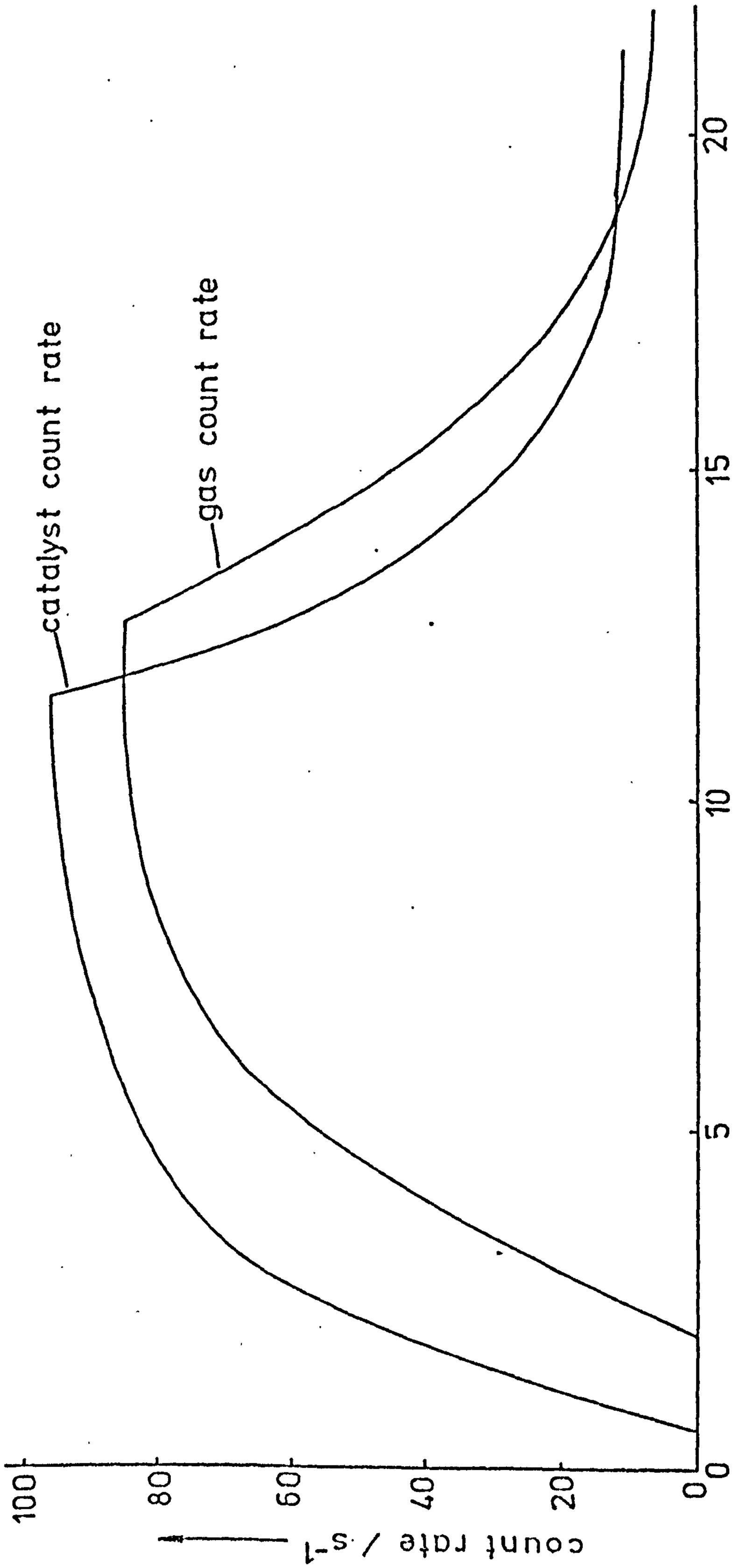

Figure 5.20. Experiment F5/5. Count rate versus time during initial ethylene-C14 pulse.

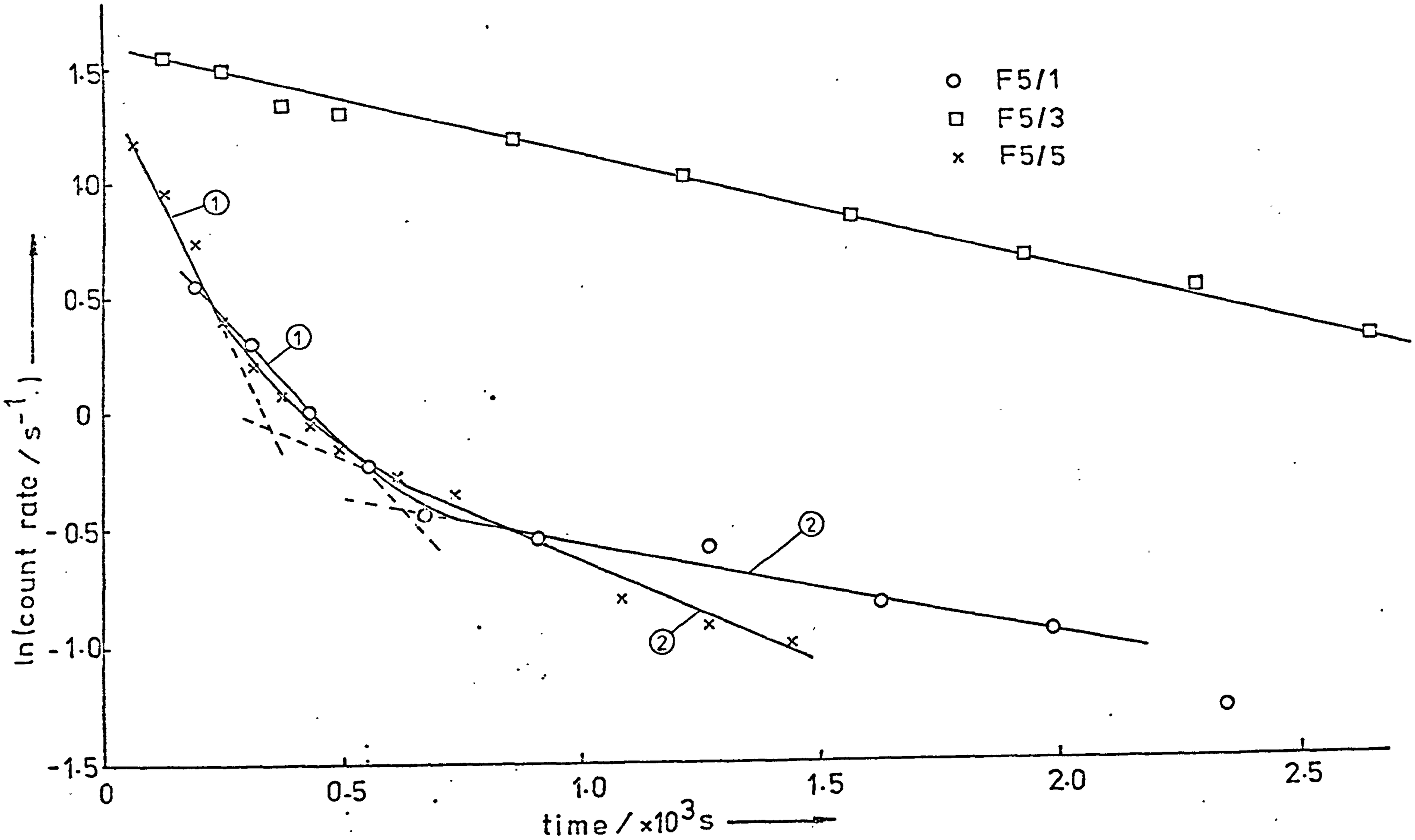

Figure 5.21. Slow desorptions following ethylene-C14 pulse.

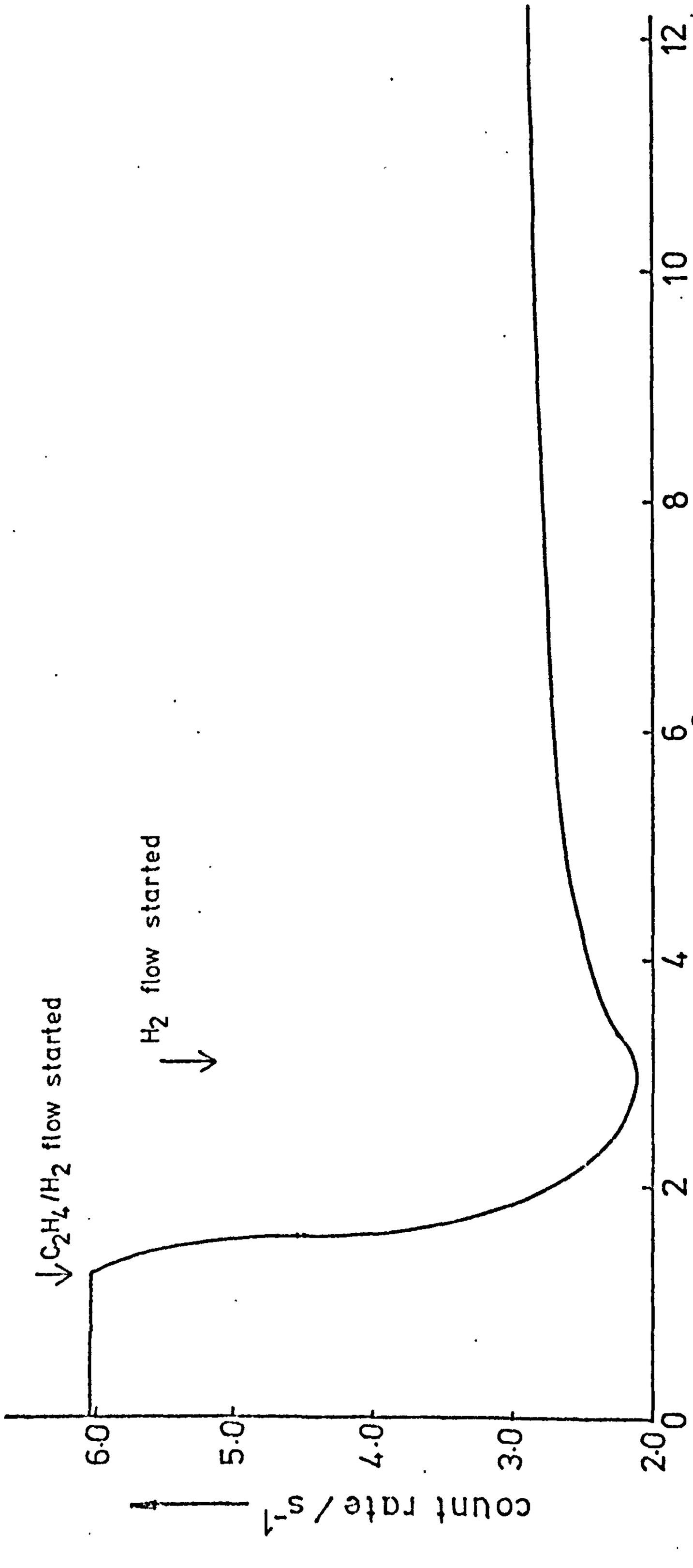

Figure 5.22. Experiment F5/2. Catalyst count rate versus time following initial ethylene-C14 pulse.

Table 5.11. F5 experiments. Conditions and data from initial ethylene-C14 pulses.

Experiment number	F5/1	F5/2	F5/3	F5/5
Temperature / K	298	296	275	268
Pressure / torr	780	780	780	780
H_2 carrier flow rate / ml s^{-1}	2.0	2.0	2.2	2.2
Ethylene-C14 partial pressure in pulse / torr	71	40	91	62
Pulse length / s	7	15	10	11
Maximum reversible adsorption/ $x10^{16}$ molecule (mg catalyst)$^{-1}$	2.8	0.44	-	2.3
R_-	0.33	-	0.49	0.83

Table 5.12. F5 experiments. Data from slow desorptions.

Experiment number	F5/1	F5/2	F5/3	F5/5
Temperature / K	298	296	275	268
Ethylene-C14 used / mmol	0.057	0.069	0.115	0.086
Contamination / $x10^{14}$molecule mg^{-1}	0	1.50	3.67	10.2
Initial retention /$x10^{15}$molecule mg^{-1}	0.96	2.50	3.26	3.09
Final retention /$x10^{15}$molecule mg^{-1}	0.10	-	0.74	1.64
λ_1 / $x10^{-3}s^{-1}$	2.2	-	0.50	4.4
λ_2 / $x10^{-4}s^{-1}$	3.8	-	-	8.9
I / $x10^{14}$ molecule mg^{-1}	3.1	-	-	5.2
Adsorption following 2 hours at 393K/ $x10^{14}$molecule mg^{-1}	1.5	3.67	6.32	12.3

experiment. The "initial retention" is the number of ethylene-C14 molecules equivalent to the count rate observed immediately following the tracer pulse, and the "final retention", that to which it falls when left in H_2 flow at the temperature of the experiment. Following each experiment, the catalyst was heated at 393 K for 2 hours in H_2 flow, and the adsorption level remaining after this treatment is given in the table.

In experiment F5/2, at the point indicated in figure 5.22, the H_2 flow was changed to one of 1 ml s^{-1} H_2, 0.6 ml s^{-1} non-radioactive ethylene. The count rate fell rapidly from the equivalent of 2.6×10^{15} molecule mg^{-1} to 6.3×10^{14} molecule mg^{-1}, and subsequently rose slowly to 9.7×10^{14} molecule mg^{-1} on resuming the initial H_2 flow.

In all experiments the conversion of ethylene to ethane was greater than 99.9%. The "tailing" found during the initial ethylene-C14 pulse could, in each case, be attributed to the ratemeter time constant rather than a desorption process. It was not possible, therefore, to distinguish any rapid desorption.

5.9. Preliminary studies on Ir/SiO_2.

These experiments were again of an exploratory nature, in an attempt to observe rapid desorption processes from an Ir/SiO_2 catalyst under a variety of flow conditions. As in the case of the platinum catalyst, these processes were not observed, although perseverence in moving to lower temperatures (see section 5.10) did eventually produce the type of curve desired.

The catalyst sample, G1, used in these experiments was 95 mg of 4.77% Ir on silica reduced under standard conditions.

Experiment G1/1.

An 11 s rectangular pulse of ethylene-C14 (85 torr)/H_2(695 torr) was passed in a 2.2 ml s^{-1} H_2 carrier flow over the catalyst bed at 267 K and 780 torr. The count rate versus time plots obtained are shown in figure 5.23. The maximum reversible adsorption observed during the initial tracer pulse was 2.5×10^{16} molecule mg^{-1}. The initial retention following this pulse was 3.9×10^{15} molecule mg^{-1},

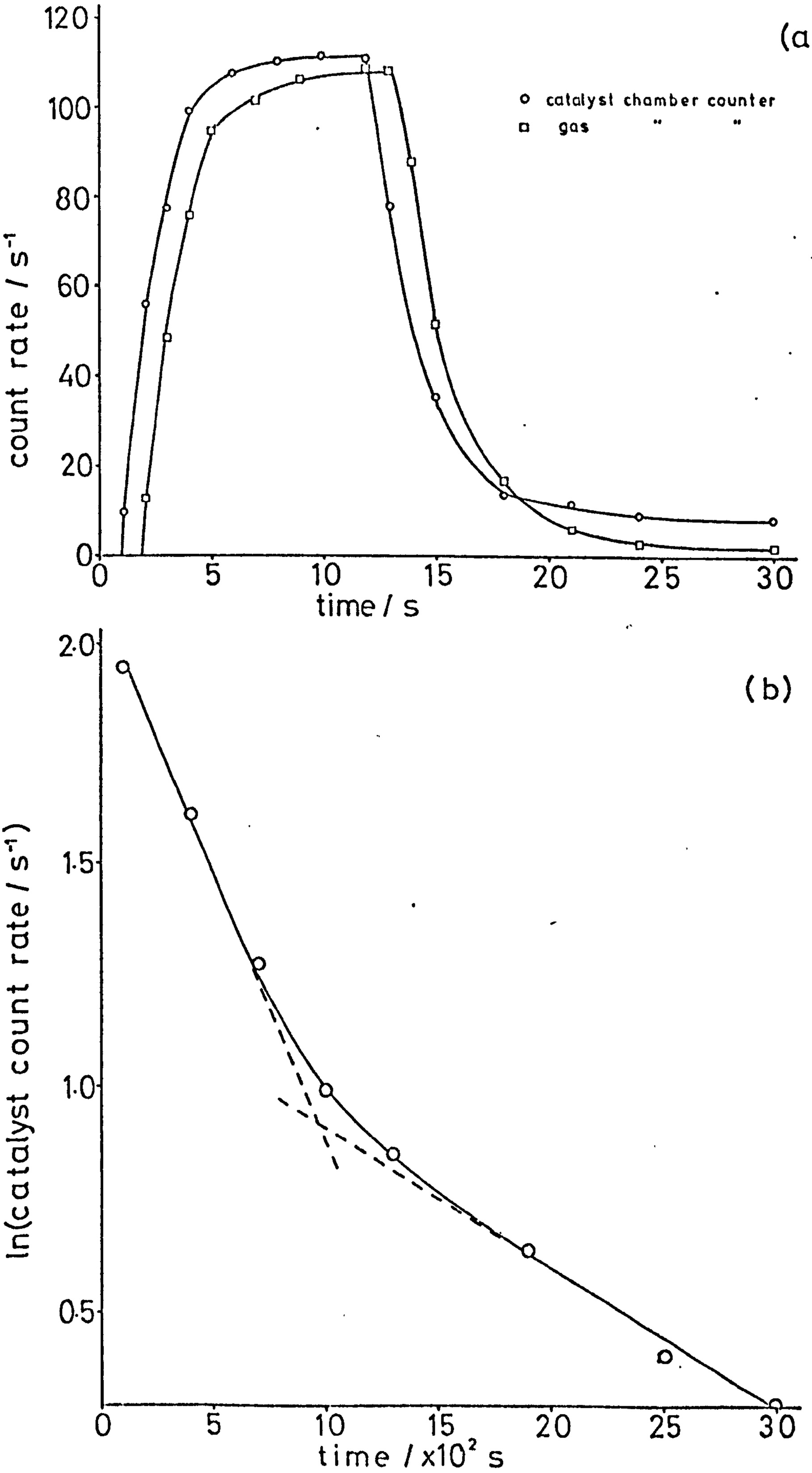

Figure 5.23. Experiment G1/1, count rate versus time plots from ratemeter output, for (a)initial ethylene-C14 pulse and (b) subsequent slow desorption.

which slowly fell to a value of 7.0×10^{14} molecule mg^{-1}. The semi-log decay curve between these values, based on a background count rate of 1.55 s^{-1} and shown in figure 5.22(b), divided into two approximately straight line regions with rate constants 1.1×10^{-3} s^{-1} and 3.1×10^{-4} s^{-1}. The intersection between these regions occurred at 1.9×10^{15} molecule mg^{-1}. The conversion of the ethylene pulse to ethane was greater than 99.9%.

Experiment G1/2. *

An 11 s rectangular pulse of ethylene-C14(99 torr)/H_2(681 torr) was passed over the catalyst in a 2.1 ml s^{-1} constant flow of ethylene(100 torr)/H_2(680 torr). Considerable difficulty was found in maintaining a constant temperature due to the exothermic reaction, so that it was not possible to monitor the desorption of retained radioactivity under these conditions. The temperature during the pulse was 301 K. The count rate versus time curve observed for the catalyst chamber is shown in figure 5.24.

The maximum reversible adsorption during the pulse was found to be 2.8×10^{16} molecule mg^{-1} and the initial retention following the pulse was 2.2×10^{15} molecule mg^{-1}. After heating the sample to 393 K for 2 hours in H_2 flow, the retained radioactivity fell to 2.4×10^{14} molecule mg^{-1}. The conversion of ethylene to ethane during the initial constant ethylene/H_2 flow was greater than 99.9%.

Experiment G1/3.

A 12 s pulse of ethylene-C14(64 torr)H_2(716 torr) was passed over the catalyst (at 268 K) in a 1.92 ml s^{-1} flow of H_2. The count rate versus time plot for the catalyst chamber is shown in figure 5.25.

The initial tracer injection is indicated by A in this figure, and B marks the time at which the unused portion of the radiotracer sample in the injection loop was passed over the catalyst. The conversion of ethylene to ethane for each of these pulses was greater than 99.9%. At C, D and E, 60 s pulses of inactive ethylene (253 torr)/H_2(527 torr) were injected into the carrier flow. Each of these

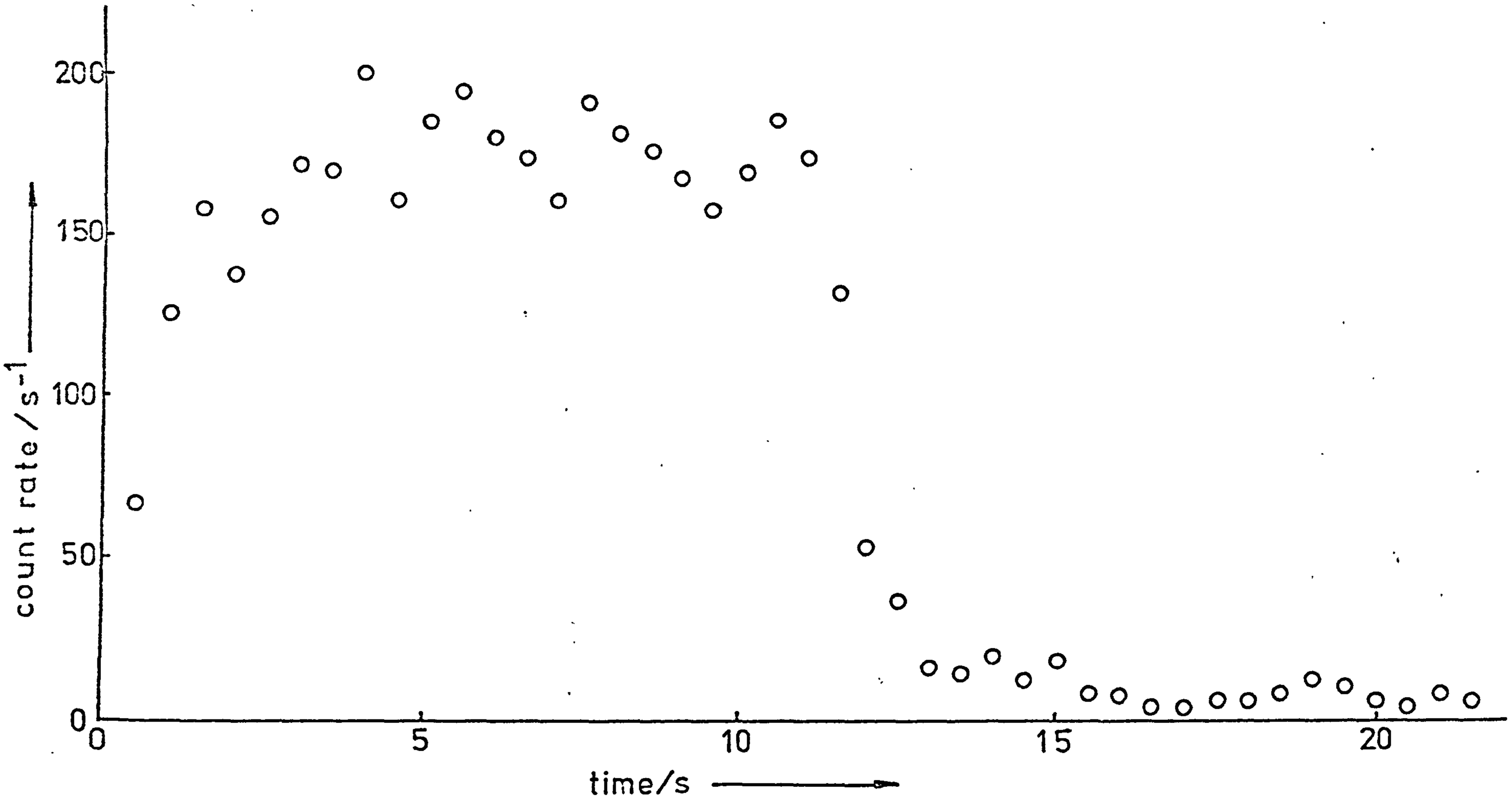

Figure 5.24. Experiment G1/2 - catalyst count rate versus time. FCS data, 0.5s resolution.

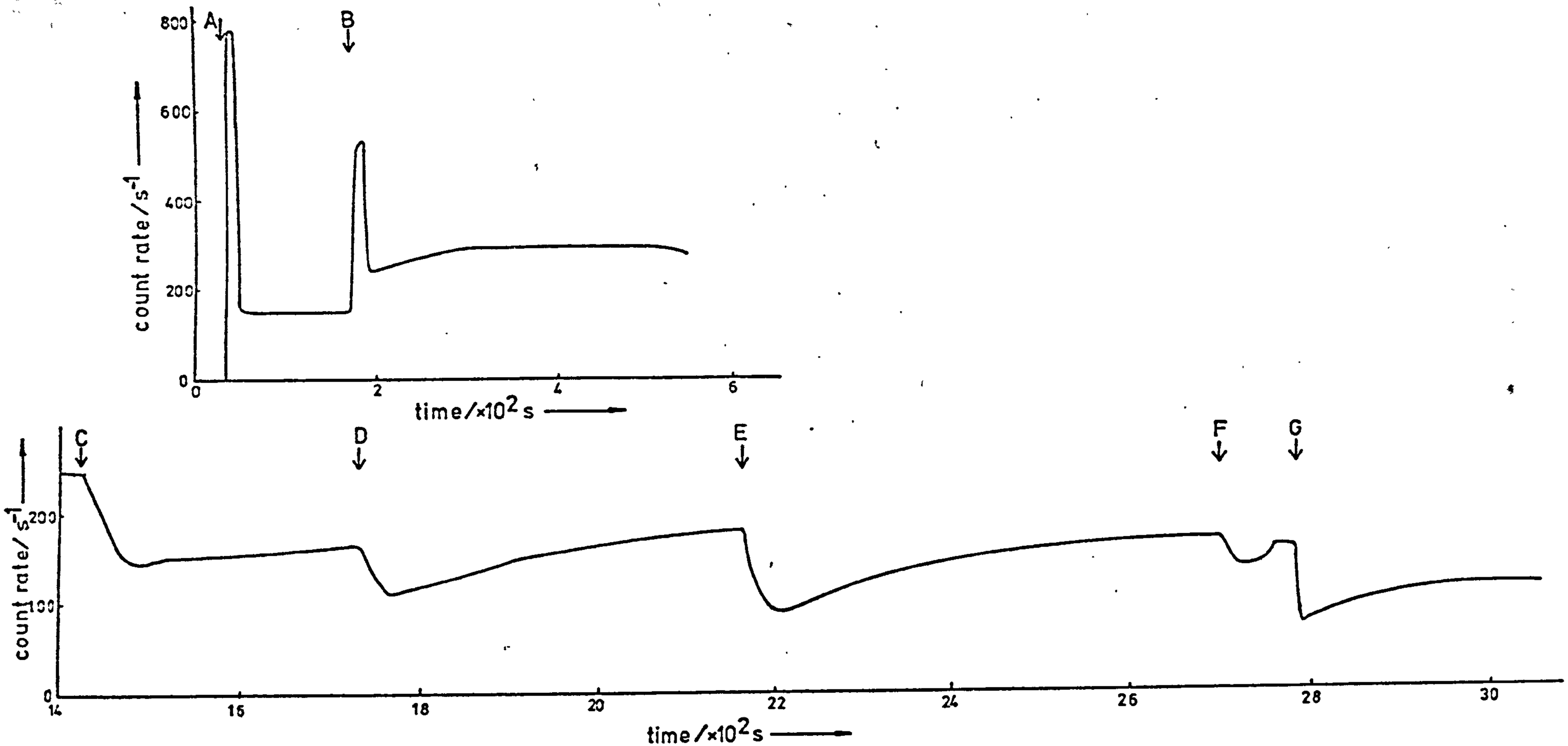

Figure5.25. Experiment G1/3 - catalyst count rate vesus time. Ratemeter plot.

pulses resulted in an initial fast reduction in the count rate followed by a slow increase. At F, an 80 s pulse of ethylene without H_2 was introduced into the carrier flow. Only a relatively small decrease in count rate was observed initially, followed by a rise almost to the original level. On resumption of the H_2 flow at the end of the pulse, marked by G in the diagram, a much larger decrease in the count rate was observed.

The reversible adsorption maximum during the ethylene-C14 pulses corresponded to 2.2×10^{16} molecule mg^{-1} and 1.5×10^{16} molecule mg^{-1} respectively. The adsorption maximum observed for the retained species was 2.1×10^{16} molecule mg^{-1}. Heating for 2 hours at 393 K in H_2 flow reduced the retained radioactive species to 1.0×10^{15} molecule mg^{-1}.

Experiment G1/4.*

A 110 s pulse of ethylene-C14(71 torr)/H_2(709 torr) was passed over the catalyst at 263 K in a 0.18 ml s^{-1} H_2 carrier flow. The conversion of the ethylene to ethane was greater than 99.9%. This pulse is indicated by A in figure 5.26. At point B, the unused tracer sample in the injection loop, of irregular composition (mean values 25 torr ethylene-C14, 755 torr H_2) was passed over the catalyst. The maximum adsorption observed during these pulses was 2.2×10^{16} molecule mg^{-1} and 1.0×10^{16} molecule mg^{-1} respectively. The retained species observed following the initial pulse corresponded to 5.8×10^{15} molecule mg^{-1}.

At C a 100 s inactive ethylene(64 torr)/H_2(716 torr) pulse was introduced, resulting in a reduction in count rate corresponding to 4.7×10^{15} molecule mg^{-1}. Corresponding to this desorption, a small peak was observed in the gas phase count rate. Between points D and E, the catalyst temperature was raised to 313 K, the retention falling to 2.2×10^{15} molecule mg^{-1}. A 100 s non-radioactive ethylene(98 torr)/H_2(682 torr) pulse introduced at F produced no observable reduction in count rate. Heating at 393 K in H_2 flow for 2 hours reduced the retention to 1.5×10^{15} molecule mg^{-1}.

Experiment G1/6.*

A 13 s pulse of ethylene-C14(75 torr)/H_2(705 torr) was passed over the catalyst at 296 K in a 1.66 ml s^{-1} flow of hydrogen, with greater than 99.9% conversion of ethylene to ethane. The count rate

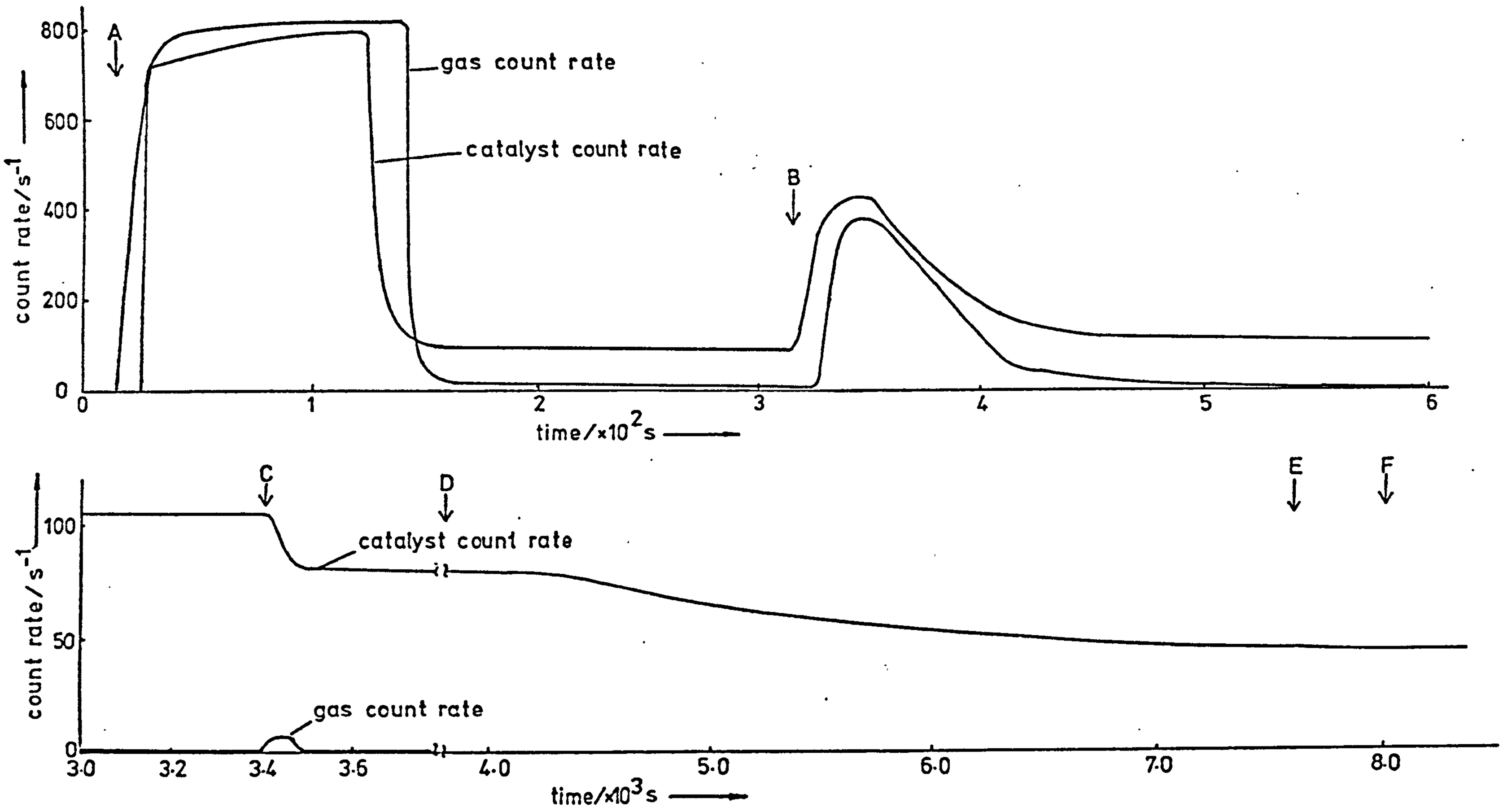

Figure 5.26. Experiment G1/4 - count rate versus time for catalyst and gas counting chambers. Ratemeter plot.

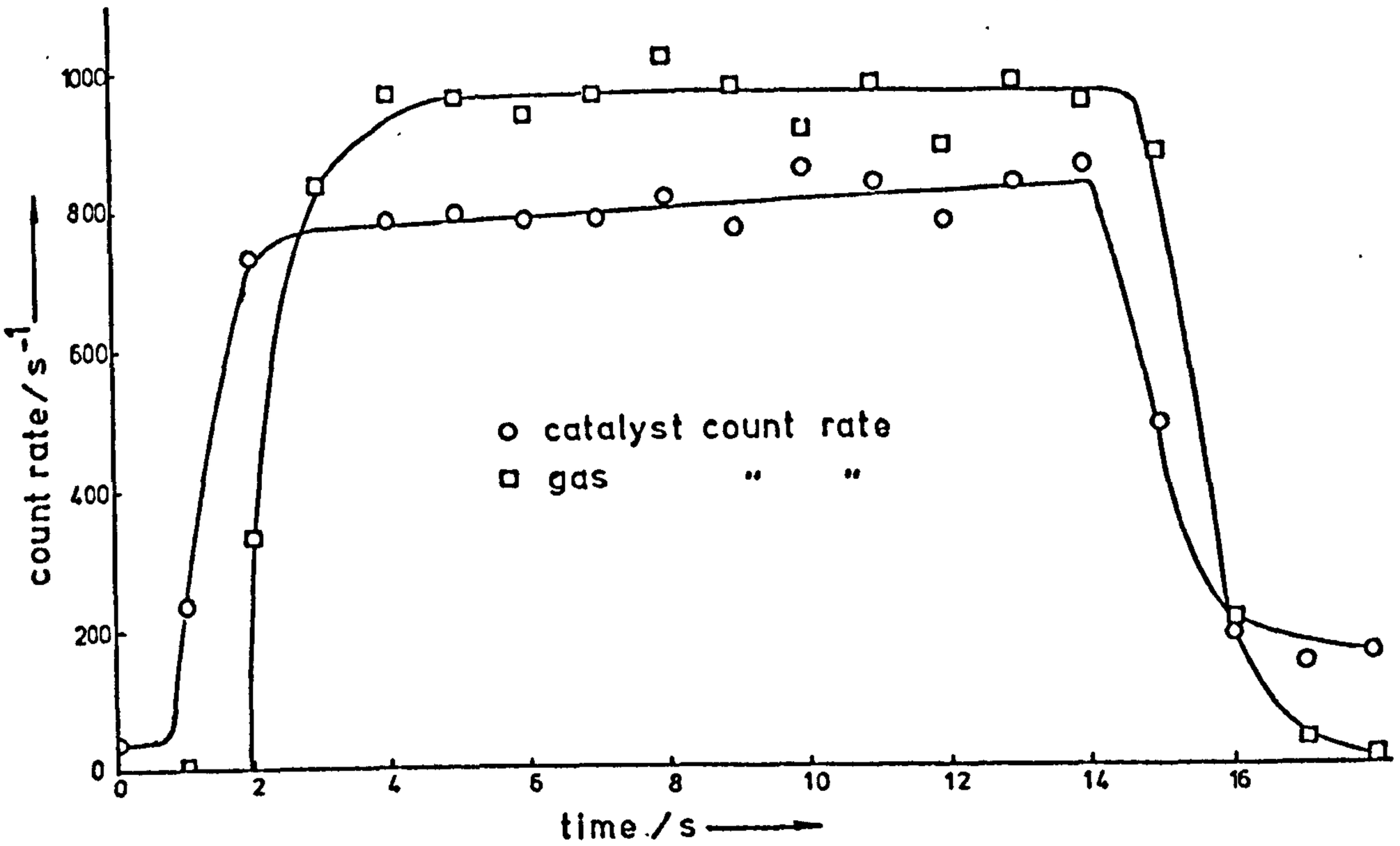

(a) Initial ethylene-C14 pulse. FCS plot, 1s resolution.

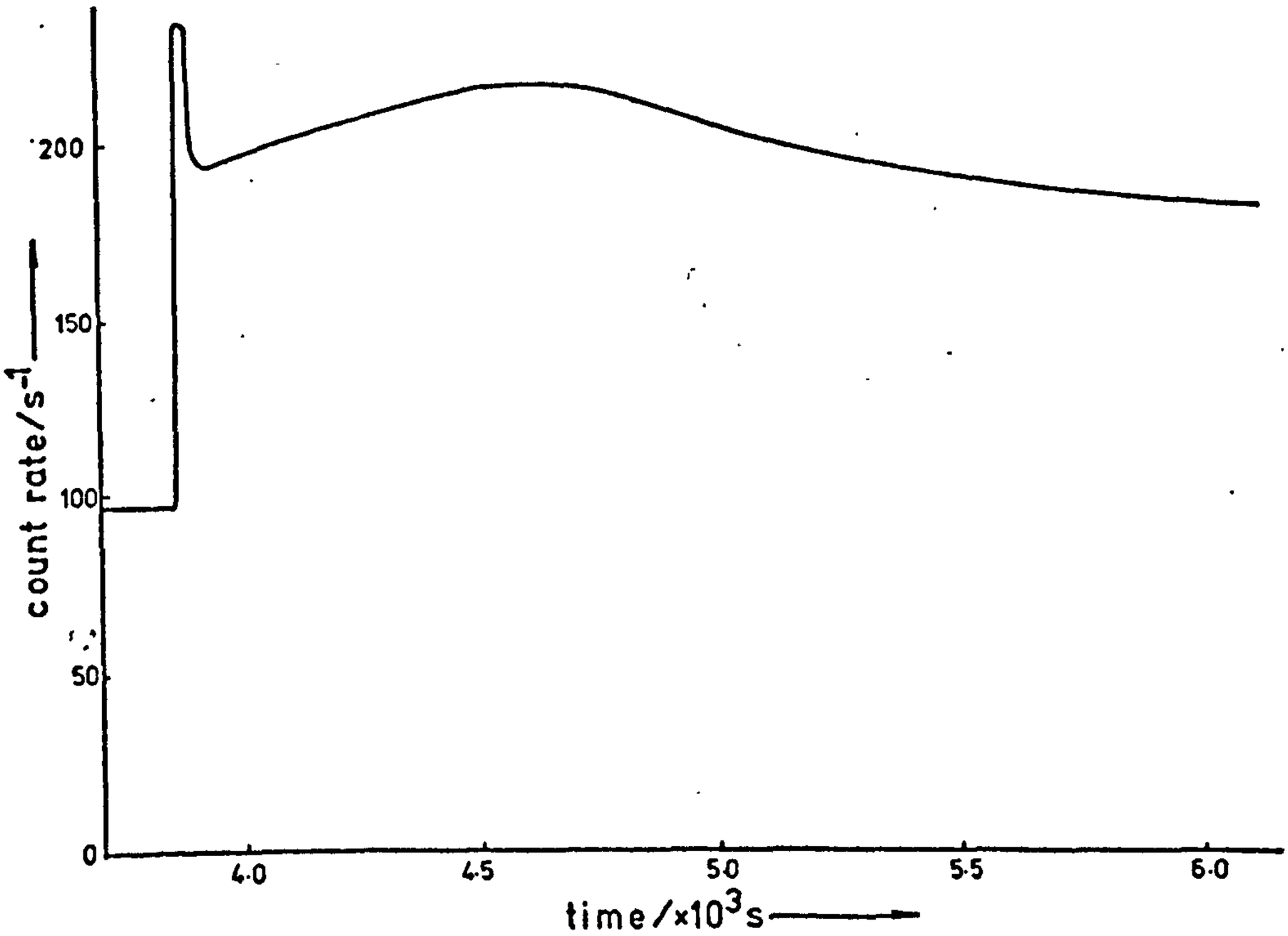

(b) Second ethylene-C14 pulse and ensuing count rate plot.

Figure 5.27. Experiment G1/6 - count rate versus time.

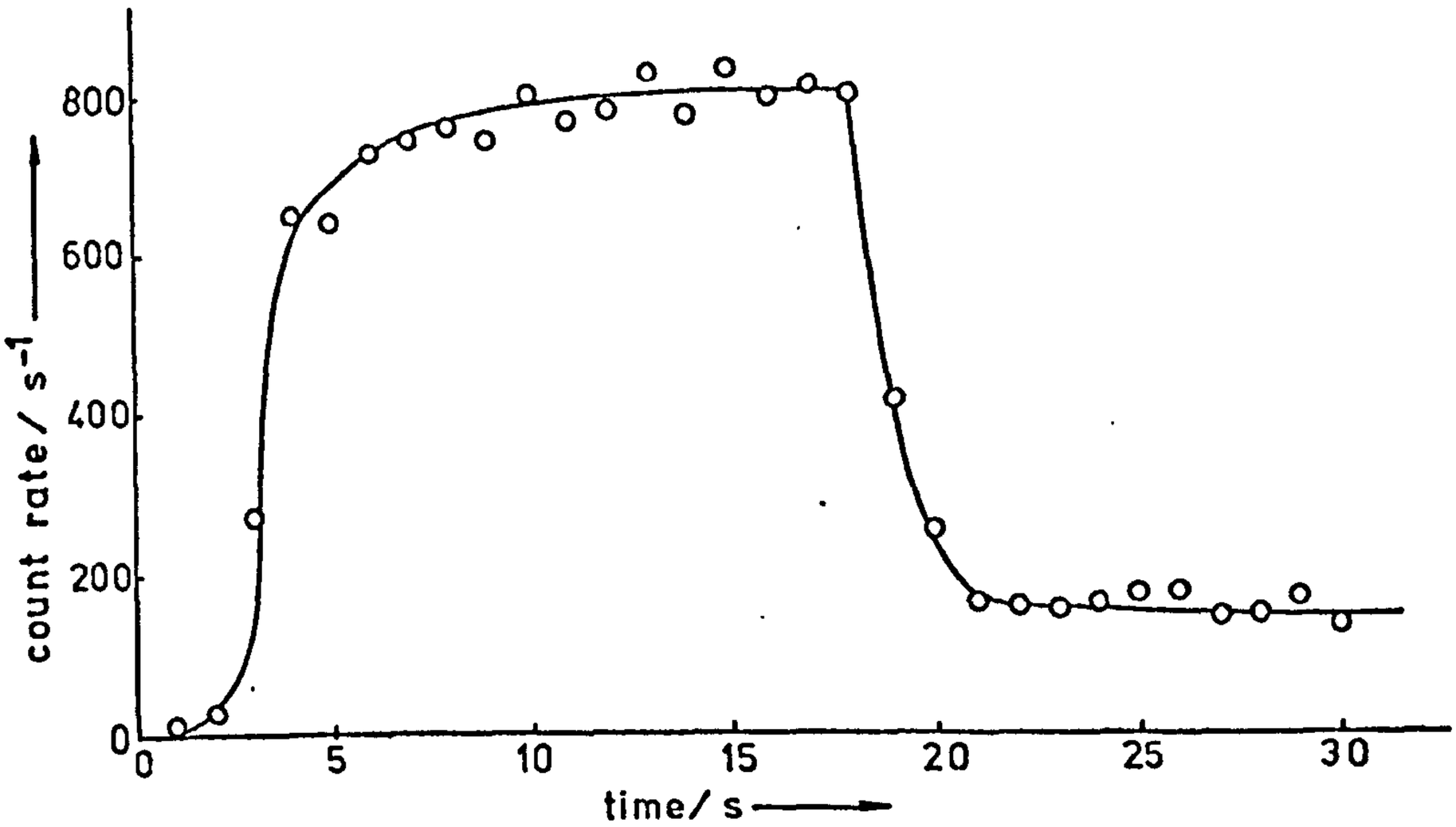

(a) Initial ethylene-C14 pulse. FCSplot, 1s resolution.

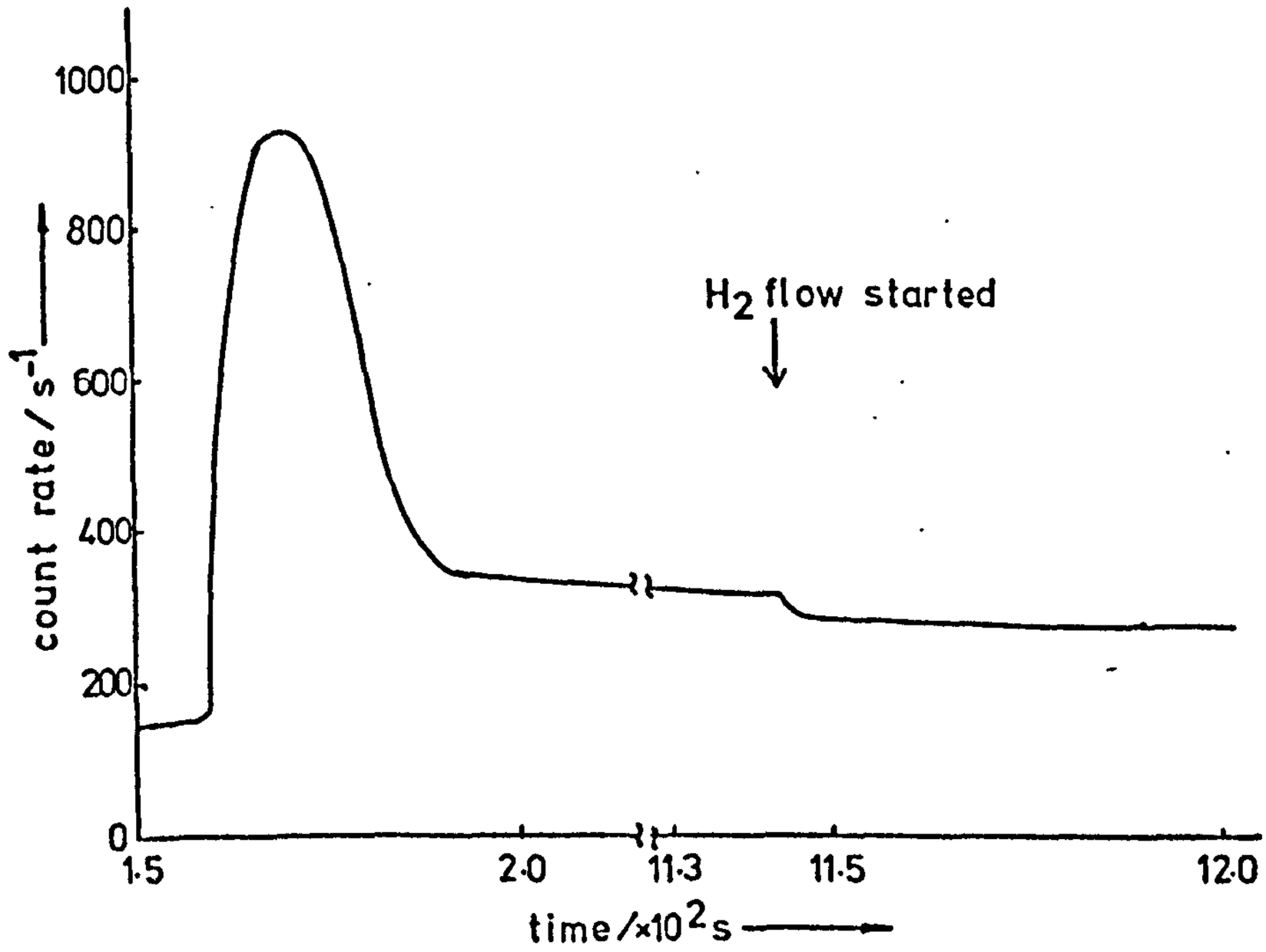

(b) Second ethylene-C14 pulse and H_2 flow introduction. Ratemeter plot.

Figure 5.28. Experiment G1/7 - catalyst count rate versus time.

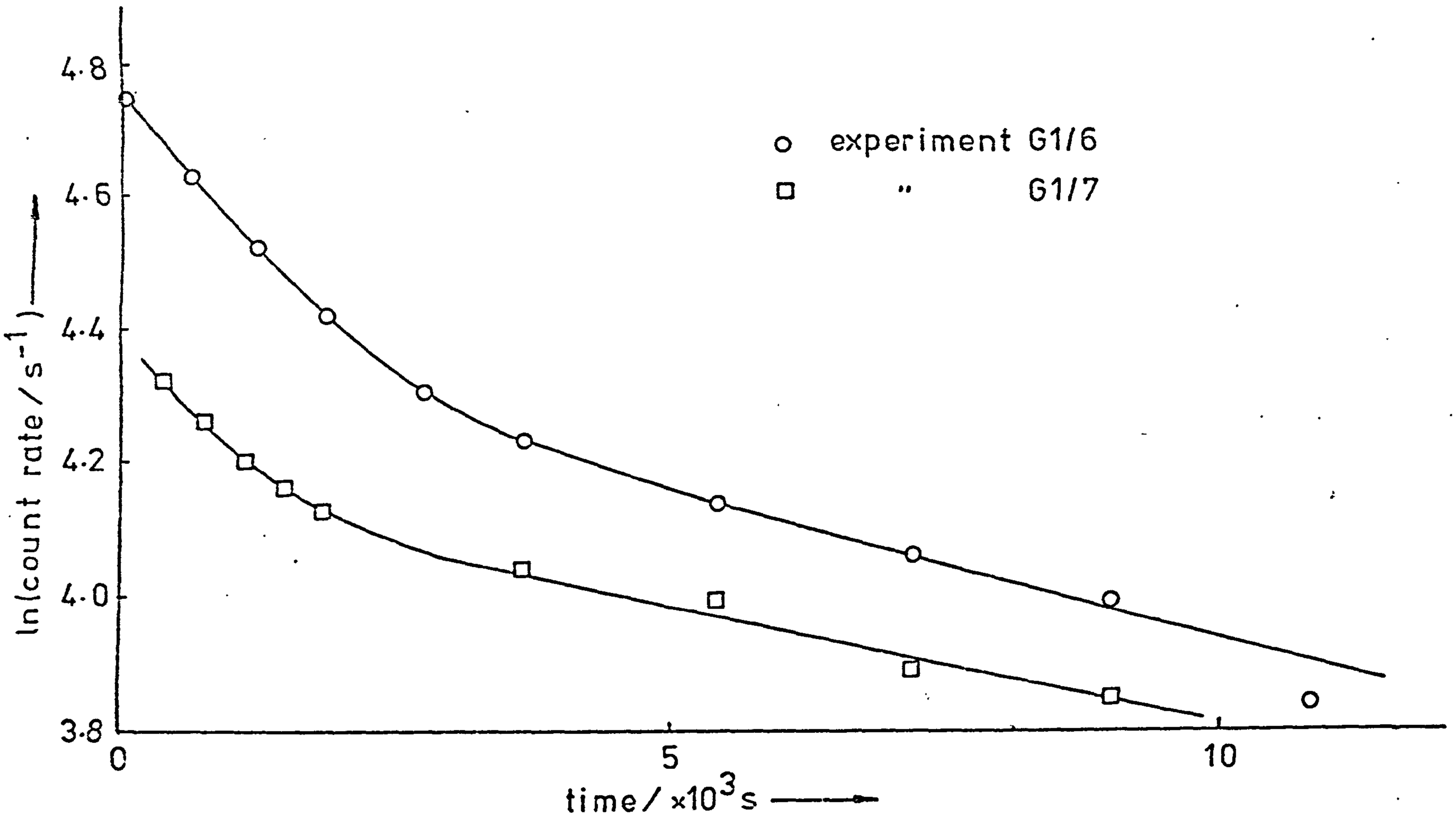

Figure 5.29. Desorption of retained radioactivity - experiments G1/6 & 7. Time zeros at 3720s for G1/6 and 1150s for G1/7.

versus time plots are shown in figure 5.27(a). The maximum reversible adsorption observed was 1.7 x 10^{16} molecule mg^{-1}, and the value of R_I calculated, 0.324.

Figure 5.27(b) shows the catalyst count rate versus time plot obtained following the introduction of the remaining tracer sample from the injection loop (average composition 30 torr ethylene, 750 torr H_2 over 18 s). The initial count rate observed following this pulse was equivalent to 1.31 x 10^{16} molecule mg^{-1}. The subsequent slow desorption process to 5.9 x 10^{15} molecule mg^{-1} is shown in figure 5.29. The initial and final first order rate constants were 1.9 x 10^{-4} s^{-1} and 5.3 x 10^{-5} s^{-1} respectively. After heating to 393 K for 2 hours in H_2 flow, the residual adsorption was reduced to 1.4 x 10^{15} molecule mg^{-1}.

Experiment G1/7.*

As this experiment was to be carried out in He flow, the catalyst was first heated to 400 K for 5 hours in He flow. A 15 s pulse of ethylene-C14(69 torr)/He(711 torr) was passed over the catalyst at 296 K in a 1.0 ml s^{-1} carrier He flow. Less than 0.1% conversion of ethylene to ethane was observed. The maximum reversible adsorption observed during this pulse (shown in figure 5.28(a)) was 1.92 x 10^{16} molecule mg^{-1}. A value of R_I was calculated as 0.41.

Following the intoduction of the remainder of the ethylene-C14 sample (mean composition 36 torr ethylene, 744 torr He over 30 s), the retention was found to be 2.08 x 10^{16} molecule mg^{-1}, which fell to 2.01 x 10^{16} molecule mg^{-1} over 900 s. The He flow was replaced with a 2.2 ml s^{-1} H_2 flow at the point indicated in figure 5.28(b), resulting in an initial, rapid drop of 1.9 x 10^{15} molecule mg^{-1}. The subsequent slow desorption is shown in figure 5.29, having initial and final first order rate constants 1.5 x 10^{-4} s^{-1} and 4.2 x 10^{-5} s^{-1}. The final adsorption value obtained was 1.1 x 10^{16} molecule mg^{-1}.

5.10. Adsorption on Ir/SiO_2 - Temperature dependence.

Experiments G2/1*, 2*, 3*, 5*, 6*, 7*, 8*.

Following the variable flow conditions of the oast section, the temperature of the above experiments was systematically varied, with the

Table 5.13. G2 experiments. Conditions and data from initial ethylene-C14 pulses.

Experiment number	G2/1	G2/2	G2/3	G2/5	G2/6	G2/7	G2/8
Temperature / K	265	292	304	251	317	239	271
H_2 flow rate / ml s^{-1}	1.85	1.56	1.85	1.85	1.85	1.85	1.85
Ethylene-C14 partial pressure in pulse / torr	75.0	76.5	75.0	72.2	25.4	74.5	23.1
Pulse length / s	13	13	12	13	17	12	17
Maximum reversible adsorption / $x10^{16}$ molecule mg^{-1}	0.67	0.15	-0.15	1.72	-0.02	3.67	0.53
Desorption rate constant / s^{-1} (LSA)	2.23 $\pm$0.29	-	-	1.31 $\pm$0.09	-	1.03 $\pm$0.10	-
R_I	0.12	0.06	~0	0.17	0.02	0.42	0.24

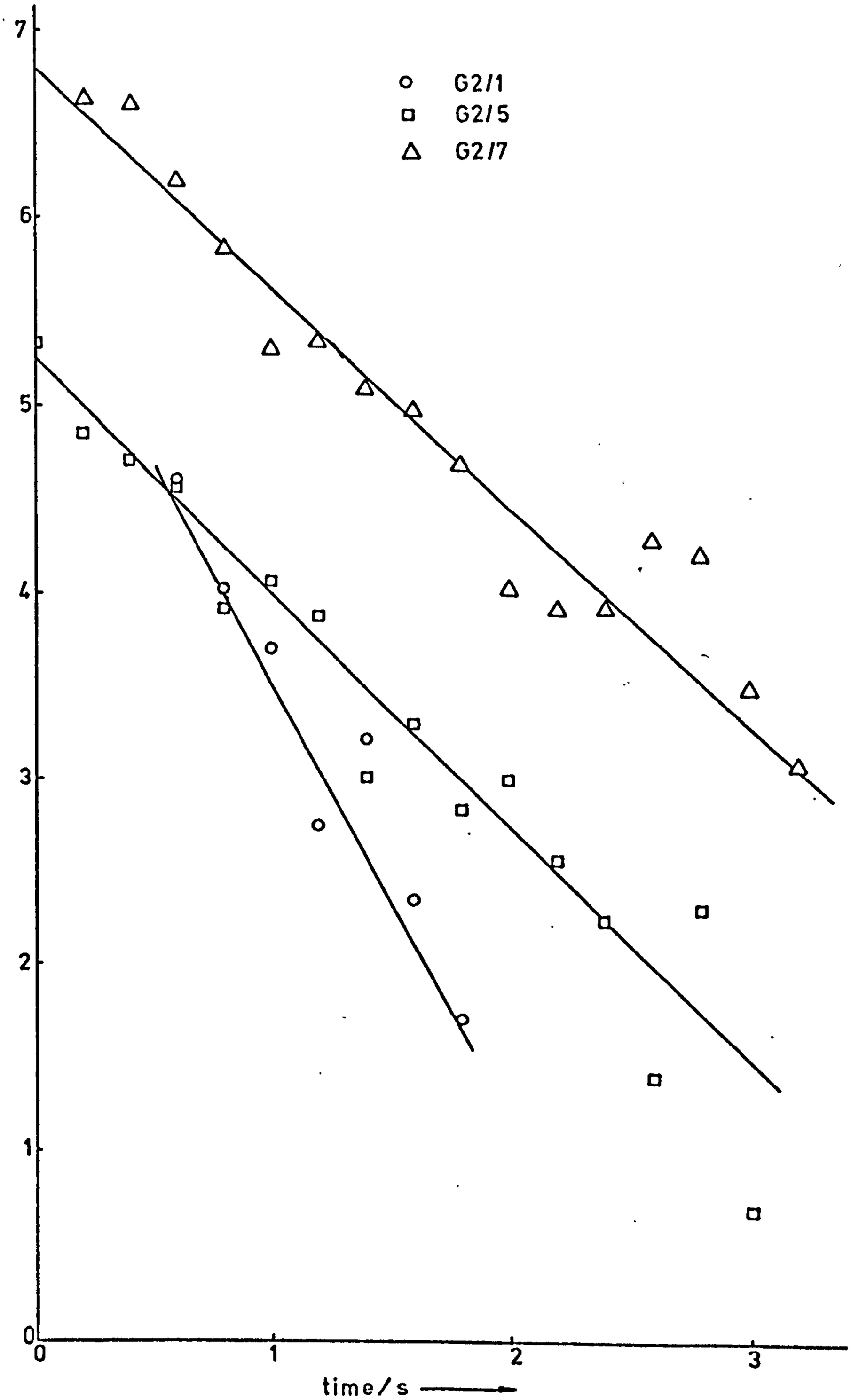

Figure 5.30. Experiments G2/1,5 & 7 - fast desorptions.

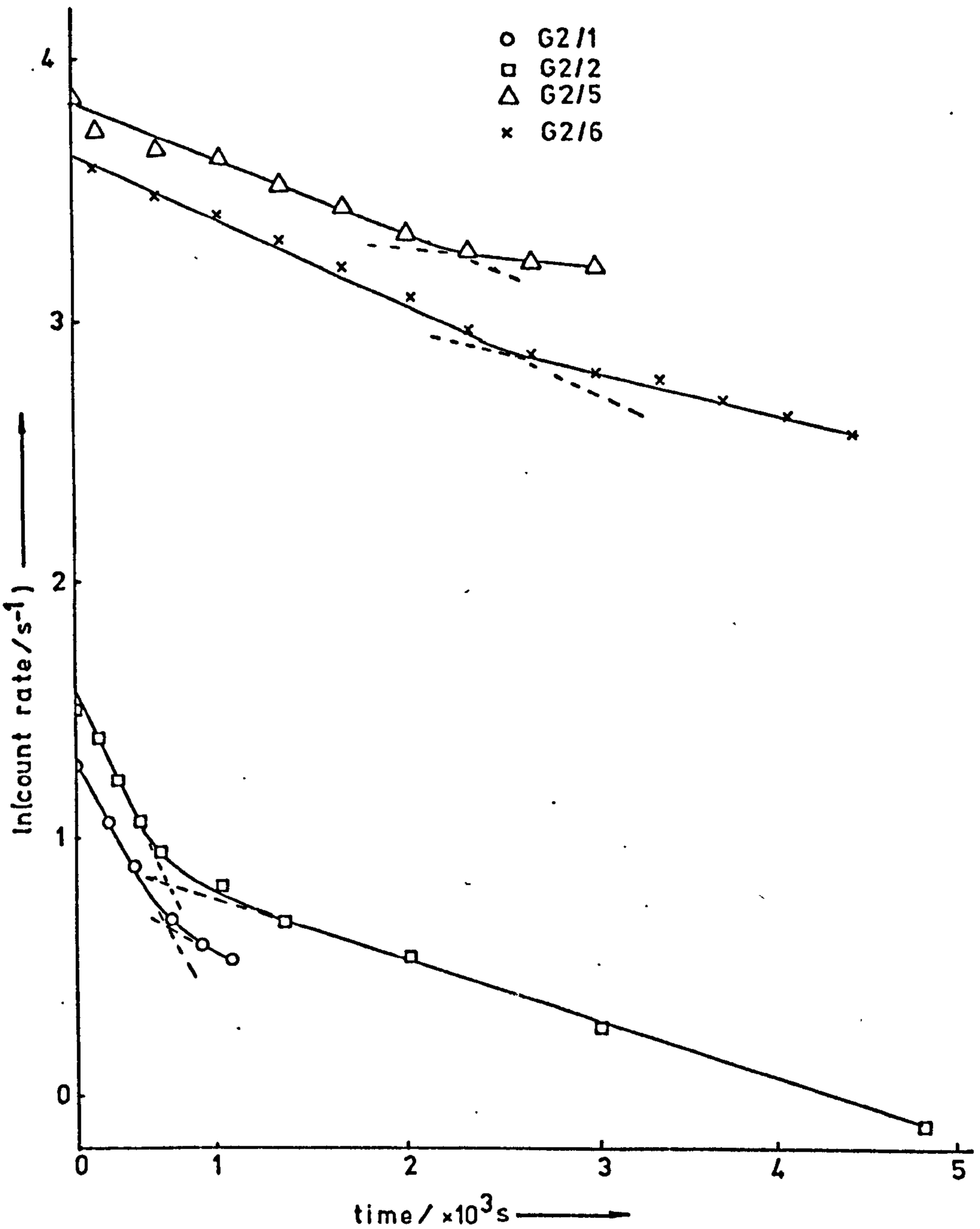

Figure 5.31. Experiments G2/1,2,5 & 6. Desorption of retained radioactivity.

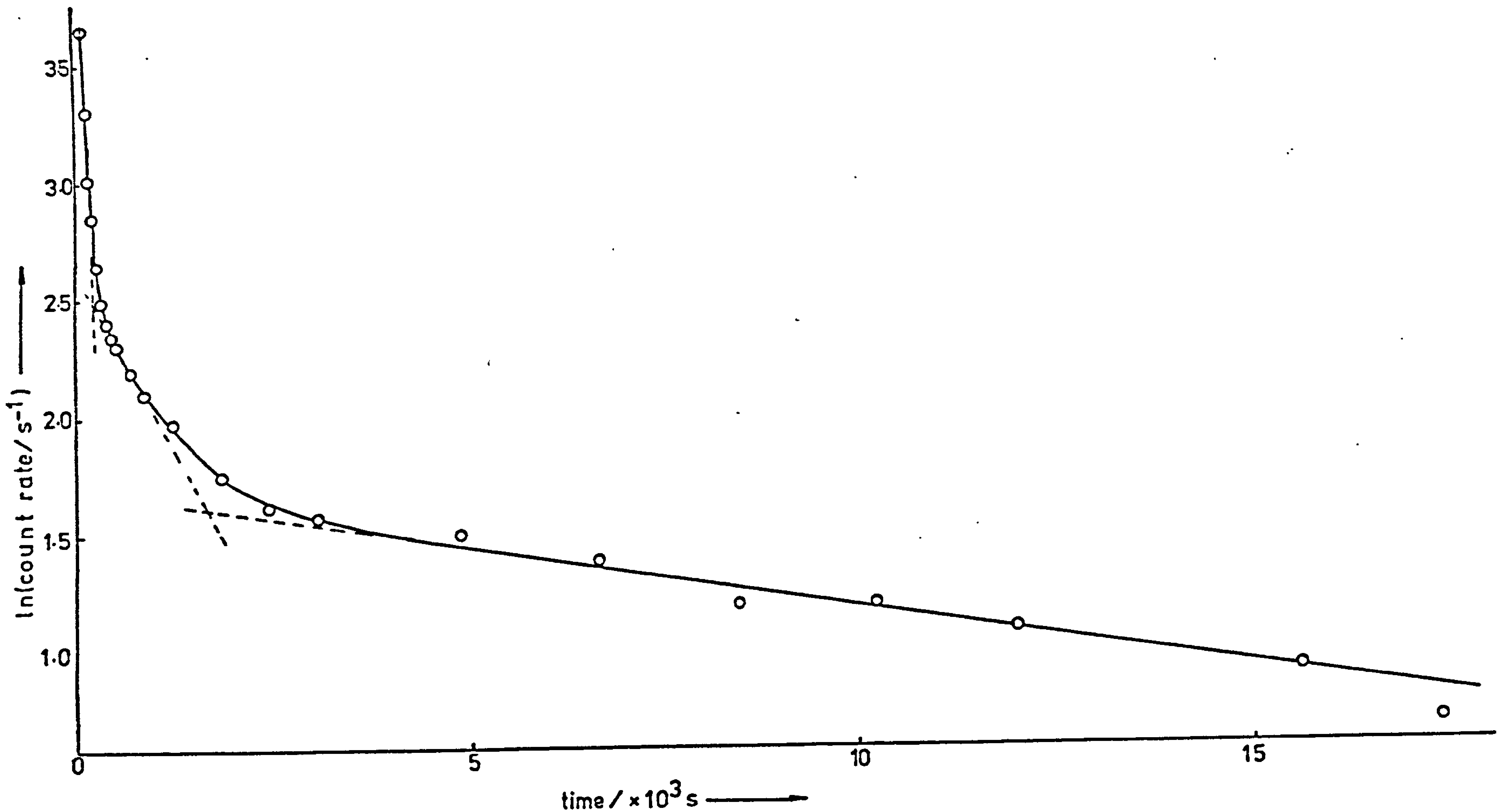

Figure 5.32. Experiment G2/3. Desorption of retained radioactivity.

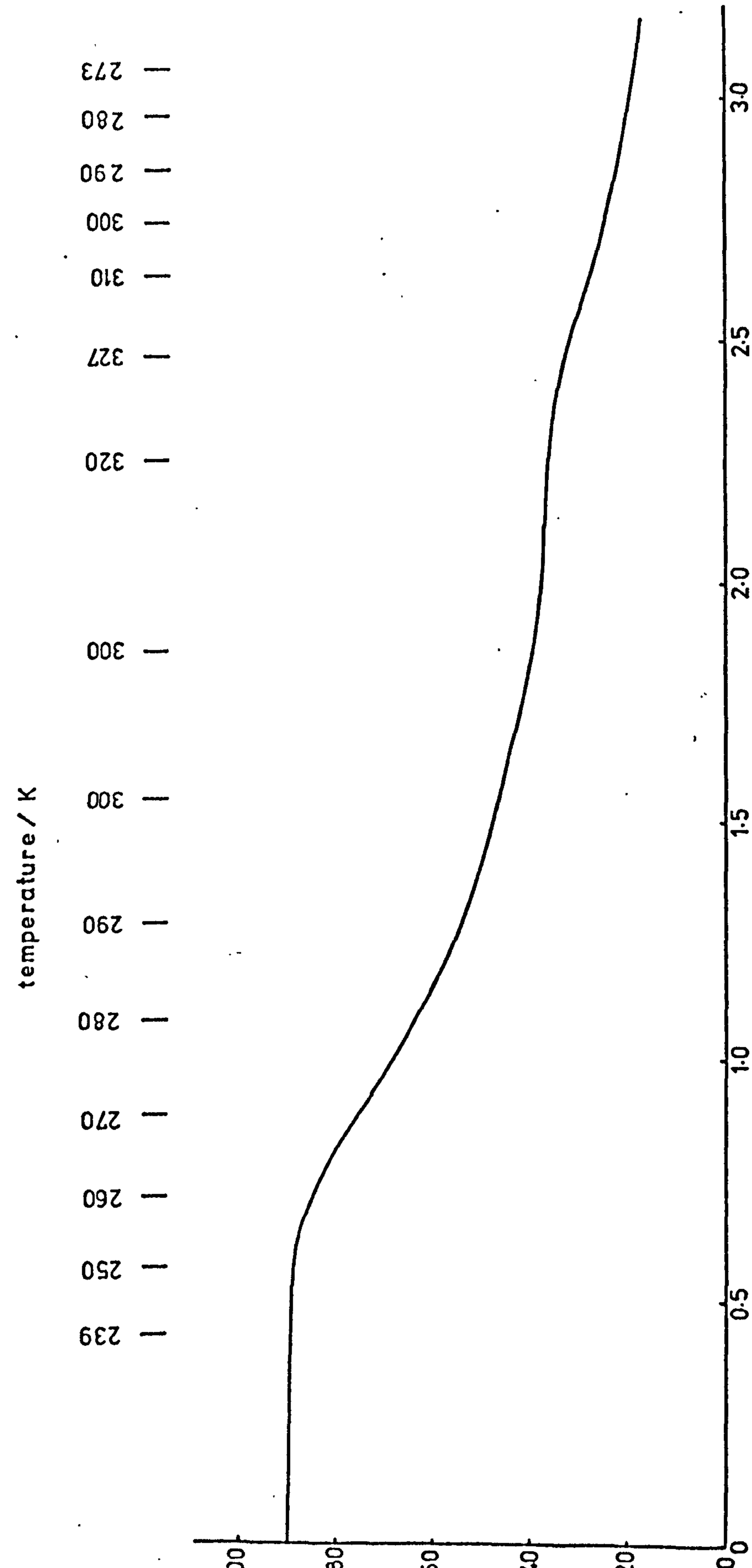

Figure 5.33. Experiment G2/7 - temperature programmed desorption of ^{3}He from Ir/SiO_2.

Table 5.14. G2 experiments. Data from slow desorptions.

Experiment number	G2/1	G2/2	G2/3	G2/5	G2/6	G2/7
Temperature / K	265	292	304	251	317	239
Contamination / $x10^{15}$molecule mg^{-1}	0	0.83	0.61	7.2	8.0	1.1
Total ethylene-C14 used / mmol	0.11	0.14	0.10	0.10	0.05	0.10
Initial retention /$x10^{15}$molecule mg^{-1}	2.3	3.5	2.2	4.2	3.3	5.8
Final retention /$x10^{15}$molecule mg^{-1}	0.70	0.69	0.71	0.73	-	-
λ_1 / $x10^{-3}$ s^{-1}	1.1	1.1	14	-	0.27	-
λ_2 / $x10^{-4}$ s^{-1}	-	1.9	4.0	2.3	1.6	-
λ_3 / $x10^{-5}$ s^{-1}	-	-	5.9	-	-	-
I_1 / $x10^{14}$ molecule mg^{-1}	8.4	7.8	4.01	17.4	12.2	-
I_2 / $x10^{14}$ molecule mg^{-1}	-	-	1.87	-	-	-

expectation that a rapid desorption process would be observed at sufficiently low temperatures. Pulses of ethylene-C14 were passed in an H_2 carrier flow over an 88 mg sample of 4.77% w/w Ir on silica catalyst, reduced under standard conditions. With the exceptions of experiments G2/6 and 8, these pulses were rectangular. In all cases, the conversion of ethylene to ethane was greater than 99.9%. The experimental conditions and data derived from the initial passage of the pulses over the catalyst are given in table 5.20.

Only in the cases of experiments G2/1, 5 and 7 was it possible to make a kinetic analysis of the desorption process immediately following the tracer pulse. These desorption curves are shown in figure 5.30, and the LSA values of the desorption rate constants calculated (k) are given in table 5.13. In other experiments, the pulse shape approximated to that expected with no adsorption occurring

The desorption curves obtained for the radioactivity retained after the passage of the tracer pulse are shown in figures 5.31 and 32. Most of the semi-log curves resolved into approximately "straight line" regions. Table 5.14 lists the data derived from these curves, with the rate constants grouped into three categories, λ_1, λ_2 and λ_3 respectively, according to their magnitude and the temperature of the experiment. The adsorption levelsat the intersection between these regions are given as I_1 (between lines of slope λ_1 and λ_2) and I_2 (between lines of slope λ_2 and λ_3).

Between experiments, the catalyst was heated to 393 K for 2 hours in H_2 flow to remove retained radiotracer.

In experiment G2/7, shortly after the passage of the tracer pulse, the temperature was raised slowly from the reaction temperature of 239 K to 327 K and then returned to 273 K. Figure 5.33 shows the resulting desorption curve, annotated at intervals with the catalyst temperature.

5.11. Adsorption on Ir/SiO_2 - Dependence on ethylene pressure.

Experiments G3/1*, G4/1*, 3*, 4 and G5/1.

It was intended in this section to study the adsorption occurring when samples of both smaller and larger partial pressures of ethylene

Table 5.15. Experiments G3/1, G4/1 and 3. Conditions and results.

Experiment number	G3/1	G4/3	G4/1
Temperature /K	253	252	252
Total pressure / torr	780	780	780
Catalyst weight / mg	86	108	108
Ethylene-C14 partial pressure in pulse /torr	9.6	14.0	81
Pulse length / s	12	11	12
Maximum reversible adsorption / $x10^{16}$ molecule mg^{-1}	0.28	0.12	24.2
R_I	0.50	0.32	2.51
Contamination / $x10^{15}$ molecule mg^{-1}	0	1.74	0
Initial retention / $x10^{15}$ molecule mg^{-1}	5.2	5.3	17.8
Maximum retention / $x10^{15}$ molecule mg^{-1}	5.6	6.4	18.2
λ / $x10^{-4}$ s^{-1}	-	-	4.2

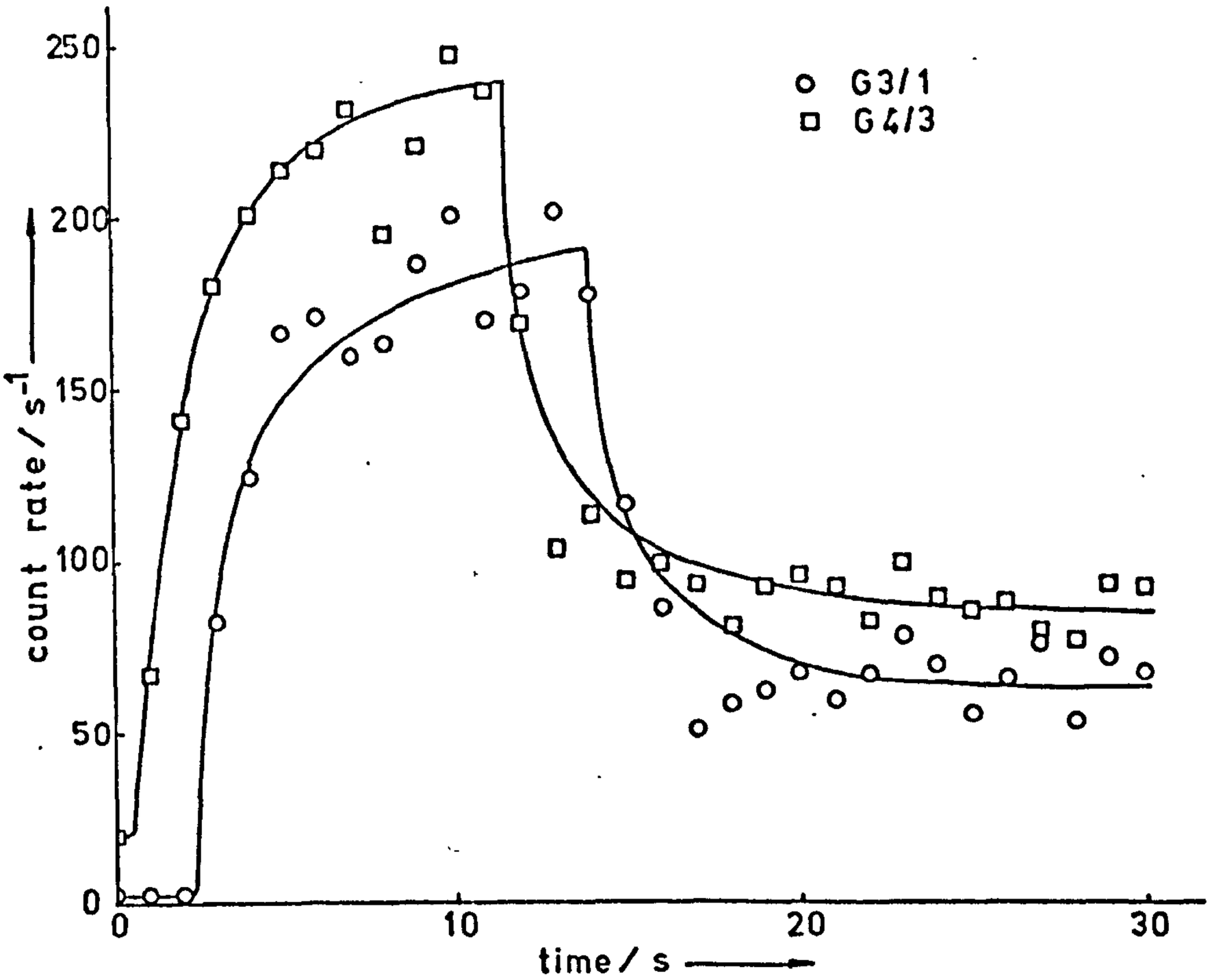

(a) Initial ethylene-C14 pulse. FCS plot, 1s resolution.

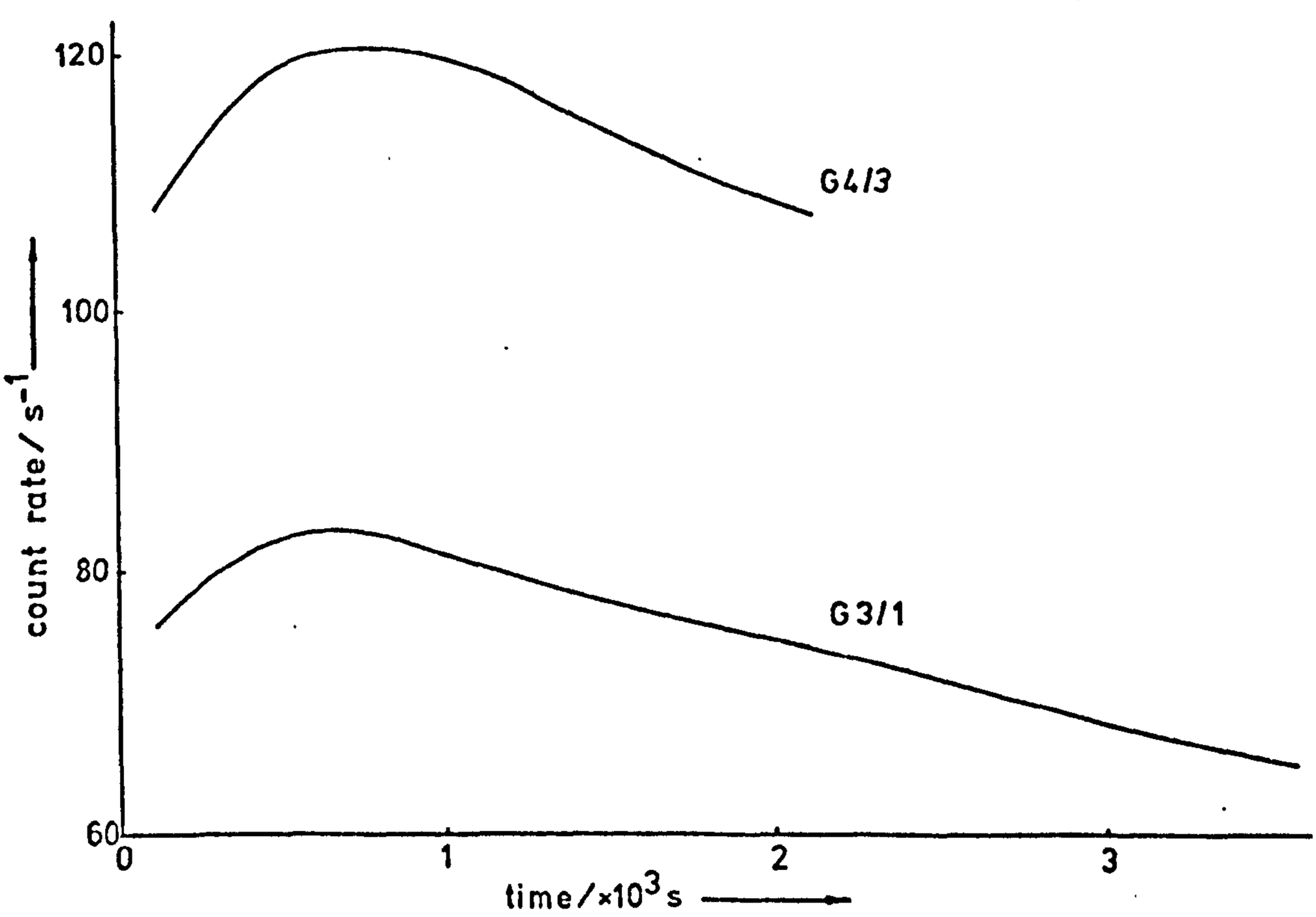

(b) Subsequent slow desorption. Ratemeter plot.

Figure 5.34. Experiments G3/1 & G4/3 - catalyst count rate versus time.

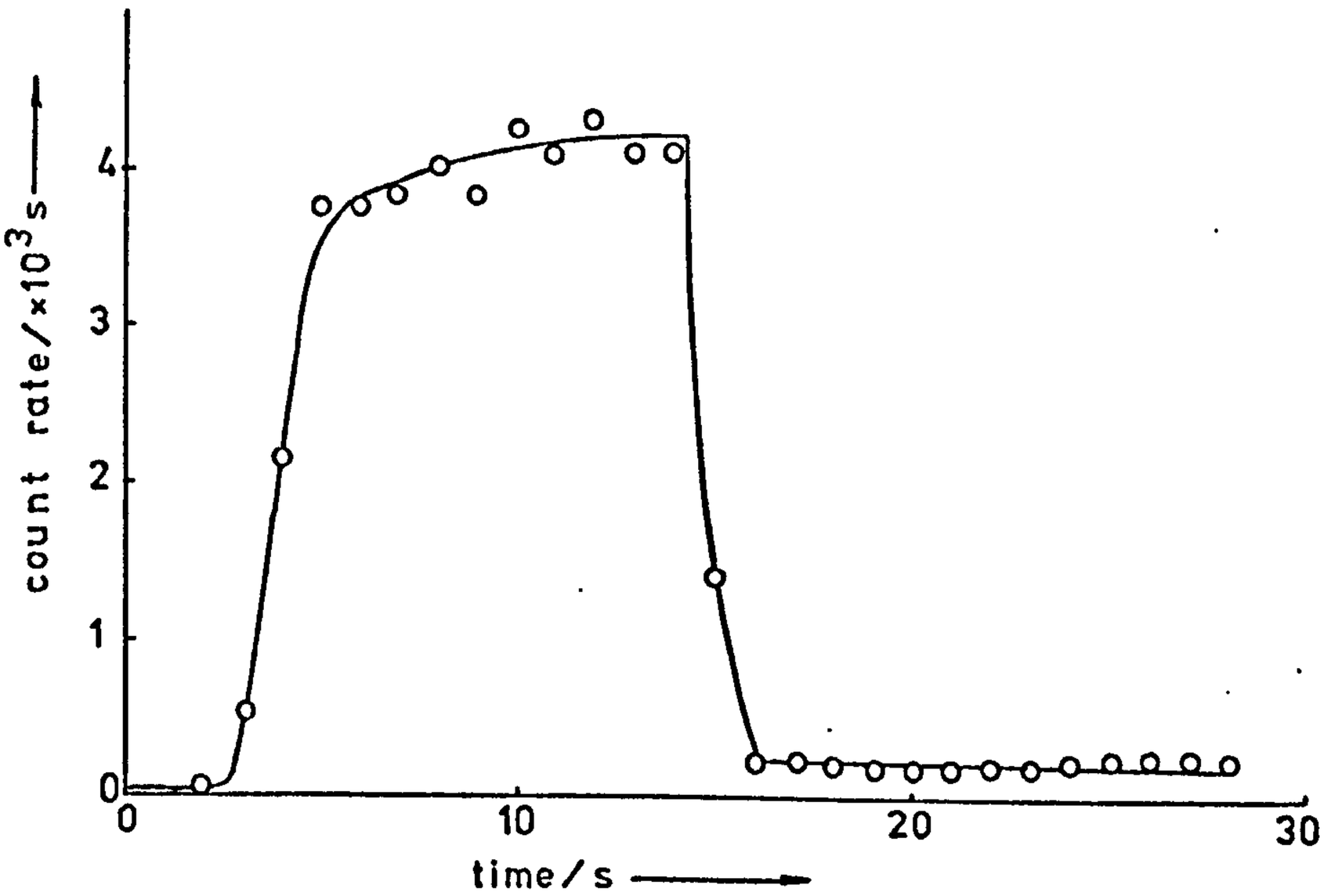

(a) Initial ethylene-C14 pulse. FCS plot, 1s resolution.

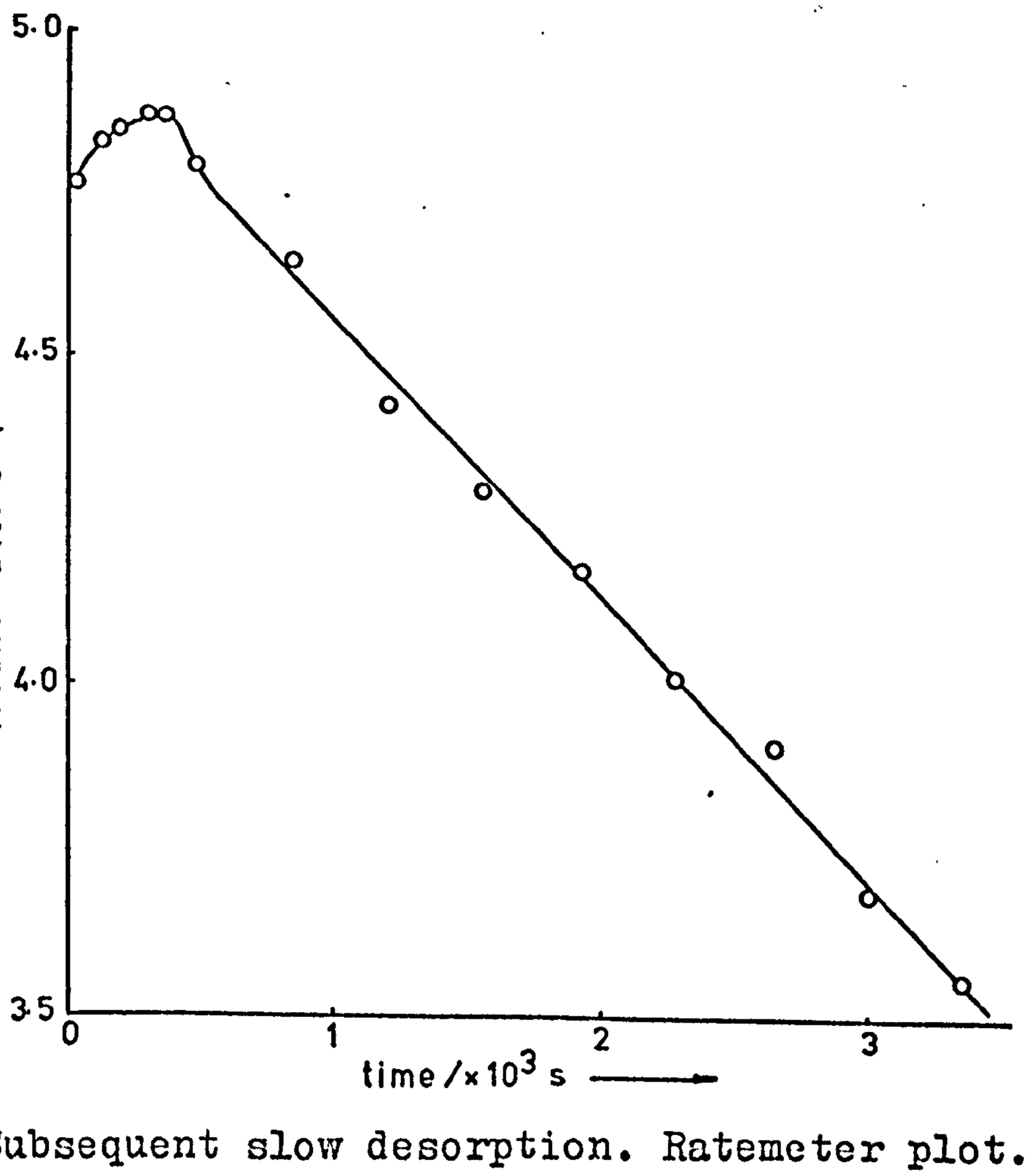

(b) Subsequent slow desorption. Ratemeter plot.

Figure 5.35. Experiment G4/1. Catalyst count rate versus time.

than used in the previous experiments were passed over the catalyst. The experimental conditions and results are given in table 5.15 for experiments G3/1, G4/1 and 3, where two samples of low and one of normal ethylene content were used. The catalyst count rate versus time plots are shown in figures 5.34 and 35.

Experiment G4/4 was carried out under similar conditions to the previous runs, at 252 K and 780 torr but with an ethylene partial pressure of 349 torr. During the passage of an 11 s pulse of this composition over the catalyst in a 2.5 ml s^{-1} H_2 carrier flow, the Melinex counting window melted, presumably due to catalyst heating (softening point of Melinex $\sim$523 K), and the experiment was abandoned. Under the same conditions, a pulse of 142 torr ethylene was used in experiment G5/1, resulting in a similar window melting and abandonment of the experiment.

5.12. Gas phase count rate contribution.

Experiments G6/2* and 4*.

During the passage of a radiotracer pulse through the catalyst counting chamber, it was desirable to know the contribution of gas phase radioactivity to the observed count rate (see section 4.5). Trial experiments with carbon dioxide-C14 had proved unsuccessful, and the following procedure was adopted.

A pulse of ethylene-C14 was passed through the reactor with the catalyst bed in the normal position, as shown in figure 4.16 (experiment G6/4). A similar radiotracer ethylene pulse was used with the reactor inverted, causing the catalyst sample to cover the counting window (experiment G6/2). The resulting curves obtained for catalyst chamber count rate versus time are shown in figure 5.36(a) for the initial etaylene-C14 pulse, and figure 5.36(b) for the ensuing slow desorptions.

In each of these experiments, the same number of counts should have been obtained from the adsorbed phase. In experiment G6/2, where the catalyst sample was in direct contact with the counting window, however, the gas phase contribution to the observed counts could effectively be neglected. The difference in the value of the ratio R_I for the two experiments should therefore give the ratio of

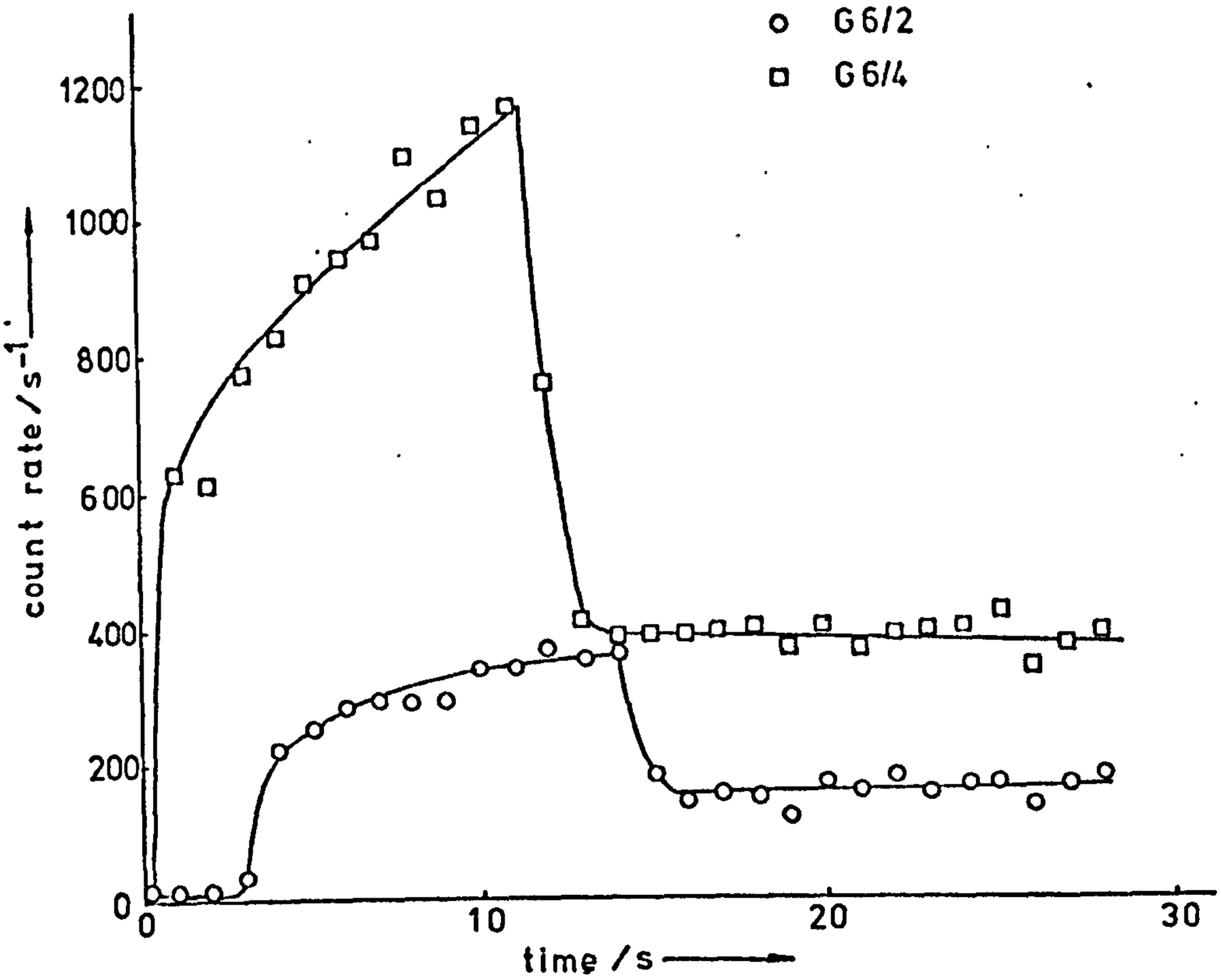

(a) Initial ethylene-C14 pulse. FCS plot, 1s resolution.

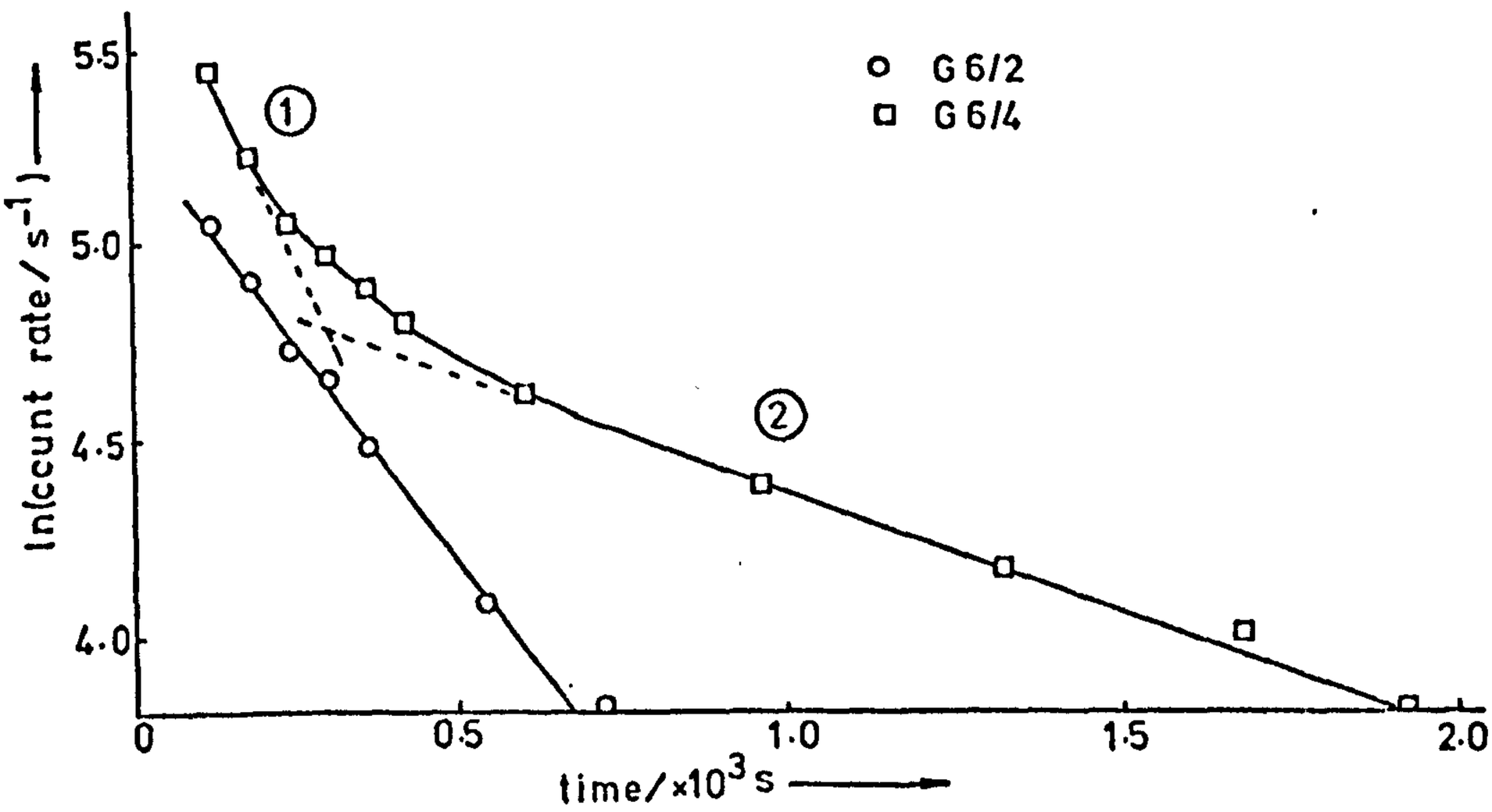

(b) Subsequent slow desorptions. Ratemeter plots.

Figure 5.36. Experiments G6/2 & 4 - catalyst count rate versus time.

Table 5.16. Experiments G6/2 and 4. Conditions and results.

Experiment number	G6/2	G6/4
Catalyst weight / mg	90	90
Temperature / K	297	297
Total pressure / torr	780	780
Ethylene-C14 partial pressure in pulse / torr	74	74
Pulse length / s	11	11
Maximum reversible adsorption/ $x10^{16}$ molecule mg^{-1}	1.30	-
$\frac{\text{Net catalyst chamber counts observed}}{\text{Net gas chamber counts observed}}$	0.222	0.693
Contamination / $x10^{15}$ molecule mg^{-1}	0.65	0.71
Initial retention / $x10^{15}$ molecule mg^{-1}	14.2	24.2
λ_1 / $x10^{-3}$ s^{-1}	2.3	3.4
λ_2 / $x10^{-4}$ s^{-1}	-	6.1

gas phase counts observed in the catalyst chamber to those observed in the gas counting chamber. The experimental conditions and results are given in table 5.16.

5.13. Adsorption on silica.

Experiments BS3/1*, 2*, 3*, 4*, 5*, 6*, 7*.

To aid interpretation of the experiments in which ethylene-C14 was adsorbed on metal-on-silica catalysts, it was necessary to determine the adsorption characteristics under similar conditions of ethylene on the support material in the absence of the metal component.

A sample of the Aerosil silica used for the catalyst preparations was subjected to the same treatment as the catalyst samples, i.e. slurry formation, drying and grinding. In experiment BS3/1, a 62 mg sample of this silica was placed in the reactor, and without further heat treatment, a pulse of ethylene-C14 was passed over it in H_2 flow. Prior to experiment BS3/2, the sample was heated to 423 K for 5 hours in H_2 flow. Five ethylene-C14 pulses were then passed over the catalyst at different temperatures. In all cases, some retention of radioactive species was observed, and the sample was heated to 393 K for 2 hours between experiments to remove as much of this contamination as possible. Experiment BS3/5 was run under similar conditions to BS3/4, with the exception of a He flow being substituted for one of H_2, and the silica sample being heated in He flow for 2 hours at 393 K prior to commencement of the experiment. The FCS fast, initial desorption curves are given in figures 5.37(a), 38(a) and 39(a), and the respective slow desorptions, when these were followed, in figures 5.37(b), 38(b) and 39(b). Table 5.17 gives the experimental conditions and data from the passage of the ethylene-C14 pulses. Data relating to the slow desorptions are given in table 5.18. Figure 5.40 shows the Arrhenius plot for the fast desorption rate constants, and yields a LSA value of 17.5 ± 2.2 kJ mole^{-1} for the apparent energy of activation.

The conversion of ethylene to ethane was found to be less than 0.1% in all experiments.

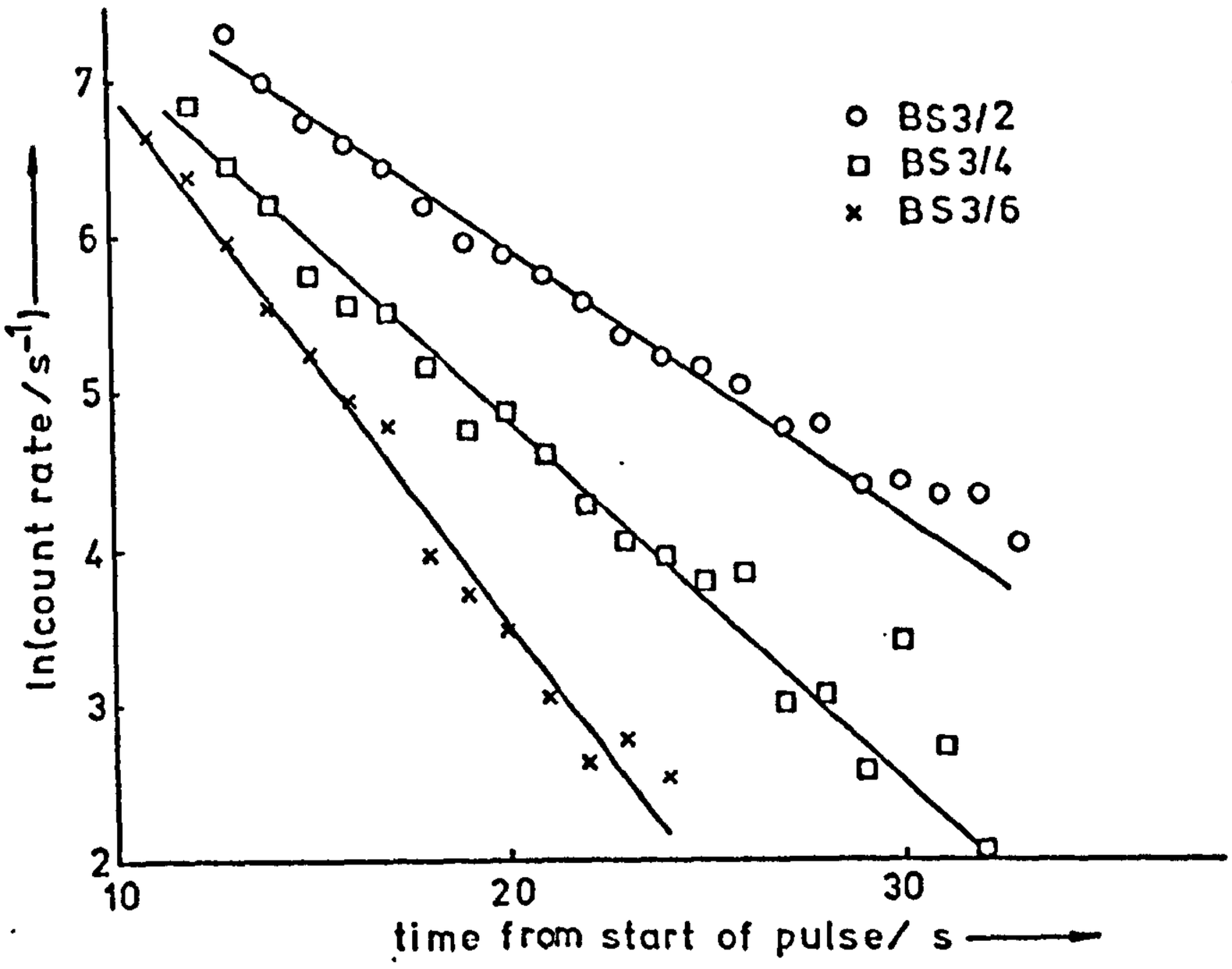

(a) Fast desorption. FCS plot, 1s resolution.

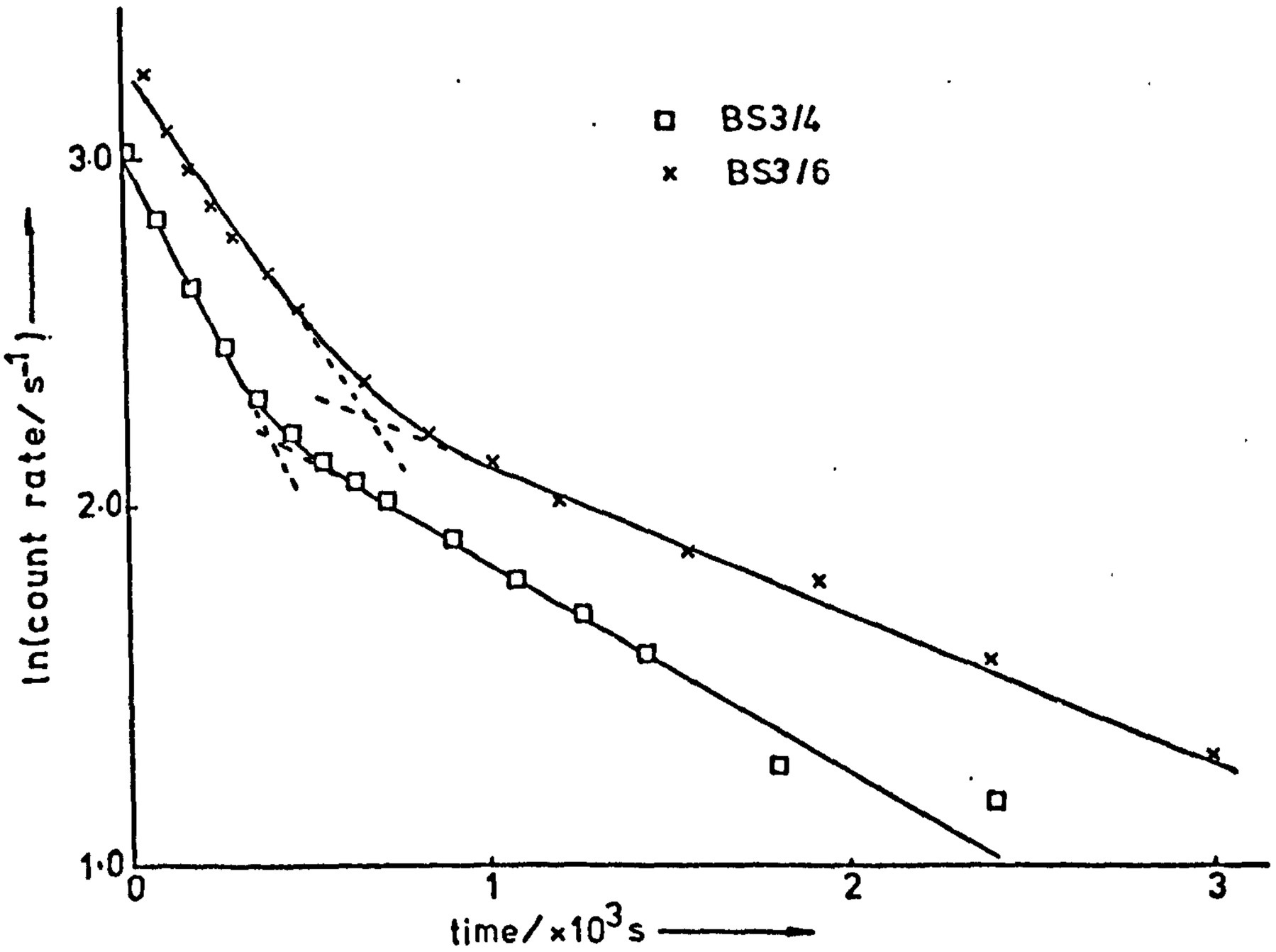

(b) Subsequent slow desorptions. Ratemeter plots.

Figure 5.37. Experiments BS3/2,4 & 6. Catalyst chamber count rate versus time.

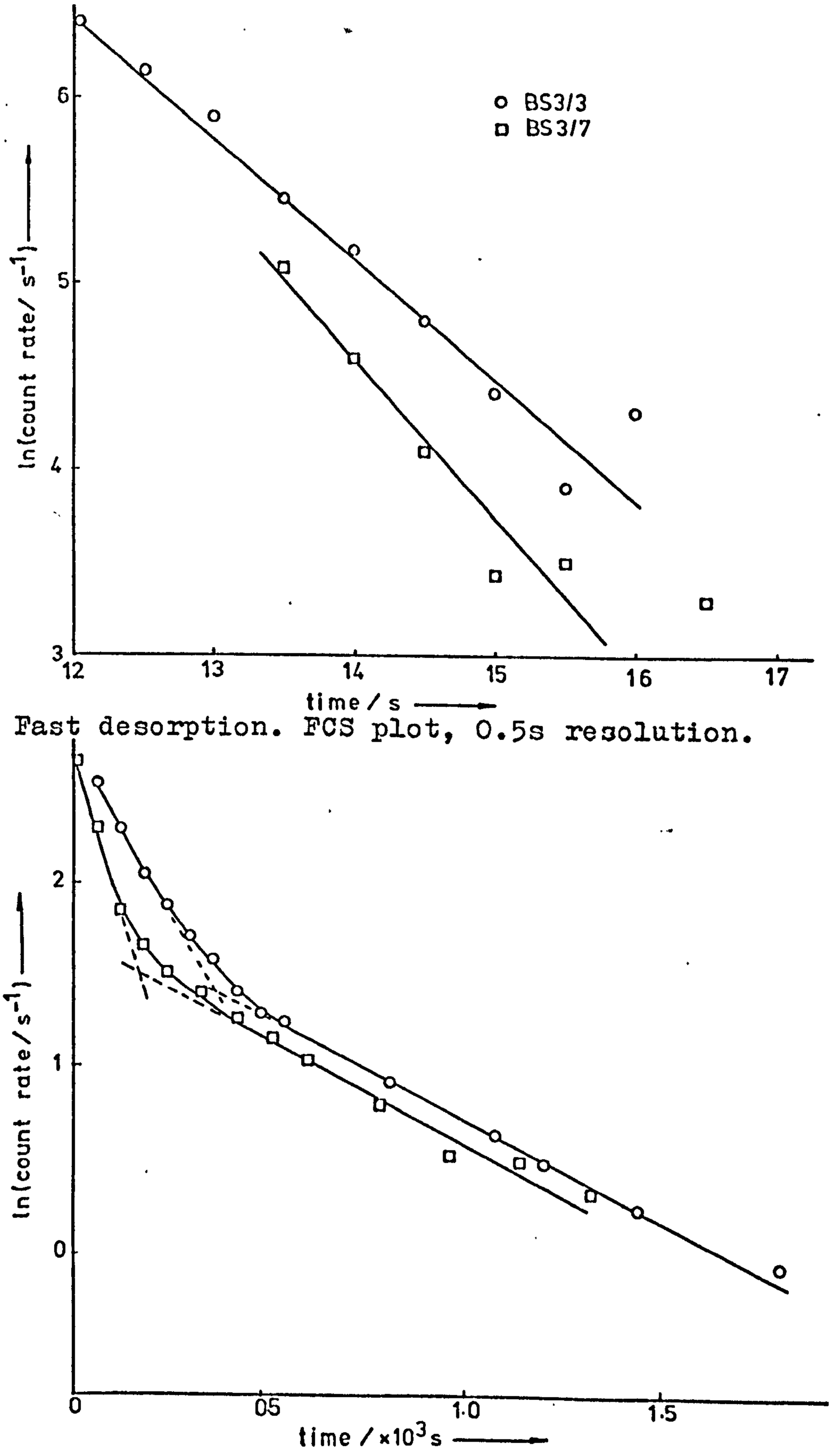

(a) Fast desorption. FCS plot, 0.5s resolution.

(b) Subsequent slow desorption. Ratemeter plot.

Figure 5.38. Experiments BS3/3 & 7 - catalyst chamber count rate versus time.

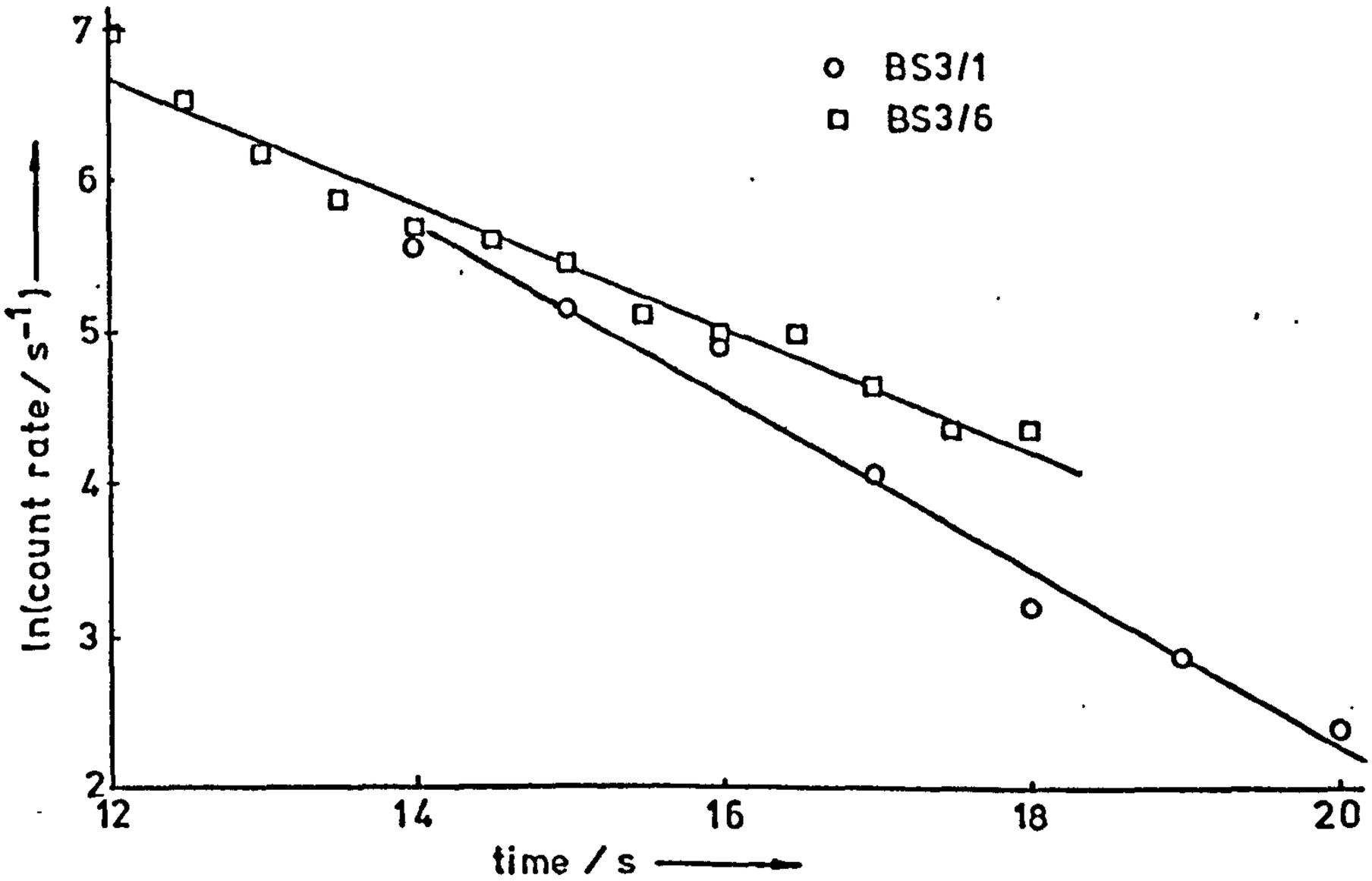

(a) Fast desorptions. FCS plots, 1s resolution BS3/1, 0.5s resolution BS3/5.

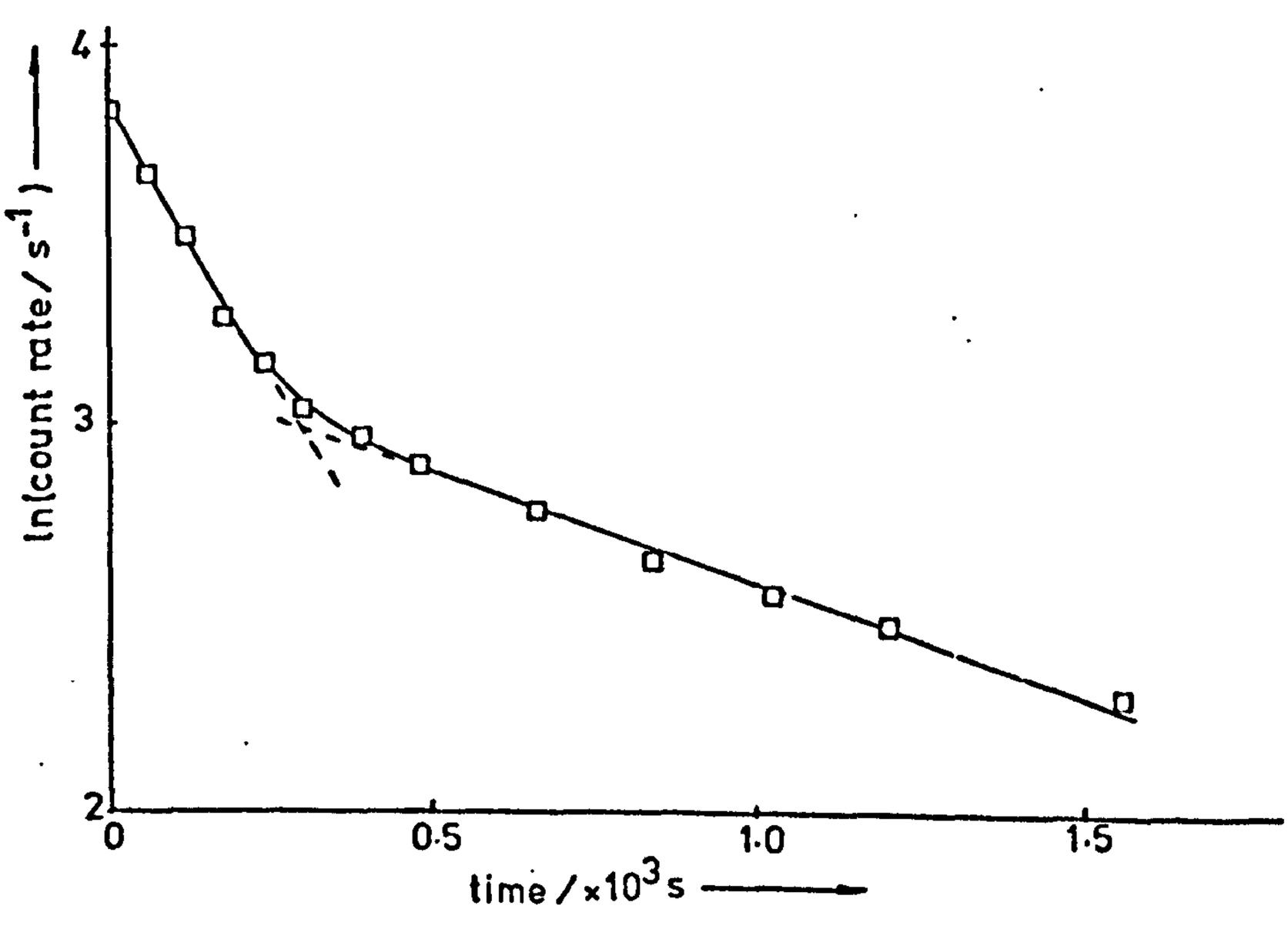

(b) Subsequent slow desorption. Ratemeter plot.

Figure 5.39. Experiments BS3/1 & 5. Catalyst chamber count rate versus time.

Table 5.17. BS3 experiments. Conditions and data from initial ethylene-C14 pulses.

Experiment number	BS3/2	BS3/4	BS3/6	BS3/3	BS3/7	BS3/1	B33/5
Temperature / K	251	273	283	302	321	251	273
Carrier gas flow rate / ml s^{-1}	1.85H_2	1.85H_2	1.85H_2	1.85H_2	1.85H_2	1.85H_2	2.0 He
Ethylene-C14 partial pressure in pulse / torr	78	72	78	77	34	25	79
Pulse length / s	12	12	11	11	12	15	11
Maximum reversible adsorption / $x10^{16}$ molecule mg^{-1}	7.8	3.4	2.3	-0.2	-0.3	1.3	3.0
Desorption rate constant / s^{-1} (LSA values)	0.16 ±0.02	0.23 ±0.01	0.34 ±0.01	0.63 ±0.05	0.96 ±0.25	0.56 ±0.04	0.41 ±0.02
R_I	1.12	0.45	0.35	0.01	-0.05	0.45	0.31

Table 5.18. BS3 experiments. Data from slow desorptions.

Experiment number	BS3/2	BS3/4	BS3/6	BS3/3	BS3/7	BS3/1	BS3/5
Temperature / K	251	273	283	302	321	251	273
Contamination / $x10^{15}$molecule mg^{-1}	0.42	0.18	0.27	0.13	0.53	0	0.23
Ethylene-C14 used / mmol	0.099	0.091	0.091	0.090	0.043	0.040	0.099
Initial retention / $x10^{15}$molecule mg^{-1}	3.89	2.11	3.34	1.14	1.41	5.88	4.84
Final retention / $x10^{15}$molecule mg^{-1}	-	0.73	1.10	0.34	0.51	-	1.46
λ_1 / $x10^{-3}$ s^{-1}	-	2.01	1.50	3.41	6.81	-	2.90
λ_2 / $x10^{-4}$ s^{-1}	-	5.8	4.1	10.7	11.0	-	5.8
I / $x10^{14}$molecule mg^{-1}	-	6.6	6.9	2.7	3.3	-	14.3

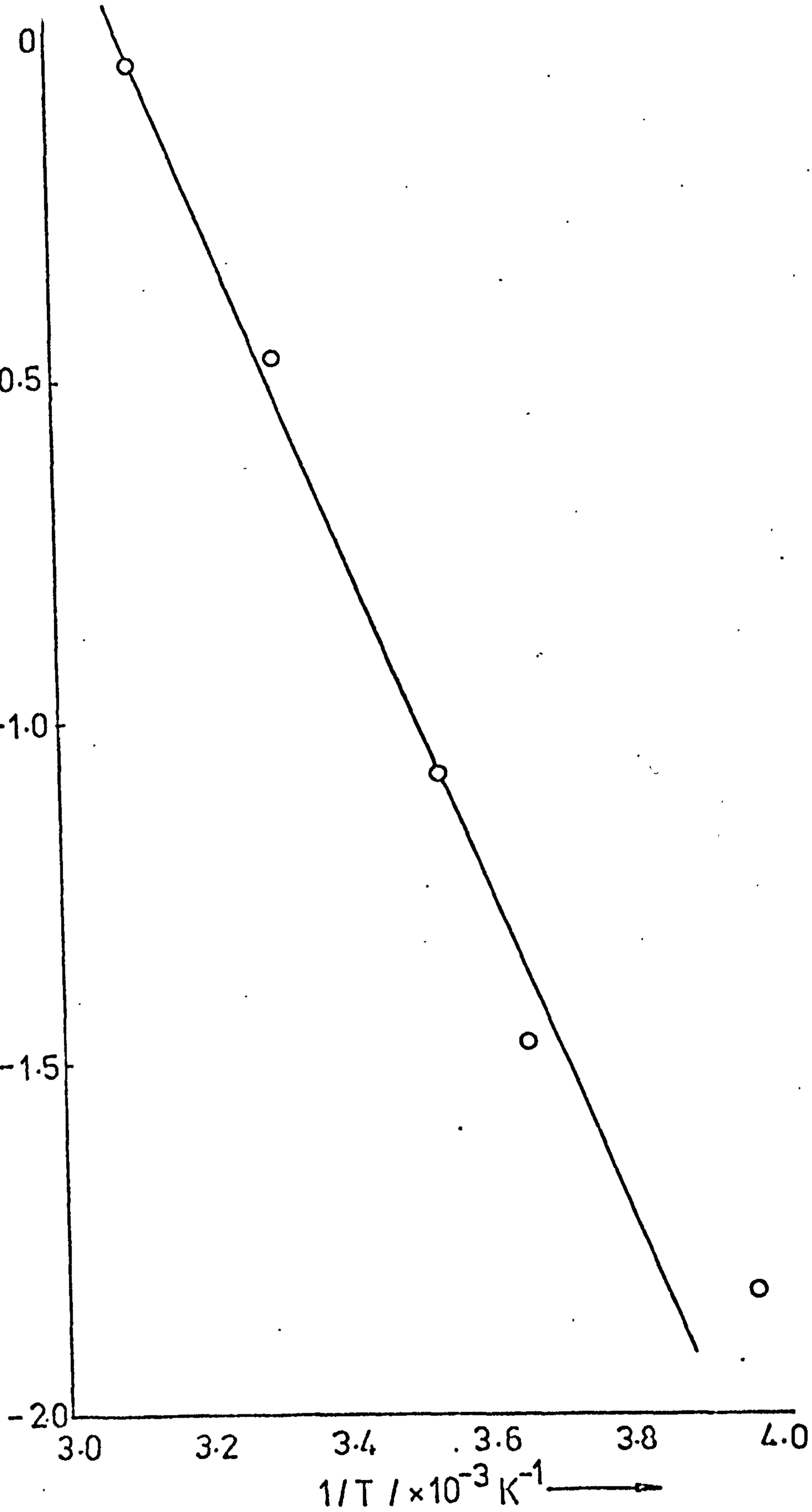

Figure 5.40. Arrhenius plot for ethylene-C14 desorptions from silica. BS3 experiments.

5.14. Ethane adsorption on Ir/SiO_2.

Experiments G6/6* and 7.

As the experiments involving the passage of ethylene pulses over Ir/SiO_2 catalyst samples in H_2 flow all gave a conversion to ethane of over 99.9%, it was possible that the observed adsorption was primarily related to ethane rather than ethylene. This possibility was therefore investigated by the use of ethane-C14 pulses.

In experiment G6/6, an 11 s pulse of ethane-C14/H_2 (74 torr ethane, 706 torr H_2) was passed over catalyst G6 in a carrier gas flow of 1.85 ml s^{-1} H_2 at 253 K. The ethane-C14 pulse was produced by passing a pulse of ethylene-C14 through a microreactor containing 25 mg of 5% Pd/SiO_2 (catalyst C). This arrangement had previously been shown to give greater than 99.9% conversion of ethylene to ethane.

The maximum reversible adsorption observed was 2.2×10^{17} molecule mg^{-1} during the tracer pulse, and the calculated value of R_I, 1.70. The LSA value for the fast desorption rate constant was 4.0 ± 0.3 s^{-1}. The count rate versus time plots for the ethane-C14 pulse are given in figure 5.41.

The initial retention following the ethylene-C14 pulse was 3.1×10^{15} molecule mg^{-1}, which rose to a maximum of 5.2×10^{15} molecule mg^{-1}, as shown in figure 5.42. This figure also gives the slow desorption curve for experiment G6/7, where a 12 s pulse of ethane-C14 (75 torr)/ H_2(705 torr) was passed over the catalyst in a 1.85 ml s^{-1} H_2 carrier flow at 294 K. The maximum reversible adsorption was 5×10^{15} molecule mg^{-1} and the initial retention was 1.3×10^{15} molecule mg^{-1}, which rose to a maximum value of 1.6×10^{15} molecule mg^{-1}. The ensuing slow desorption had initial and final rate constants 2.1×10^{-3} s^{-1} and 4.8×10^{-4} s^{-1} respectively, with a value of 4.8×10^{14} molecule mg^{-1} adsorption at the intersection of the "straight-line" regions.

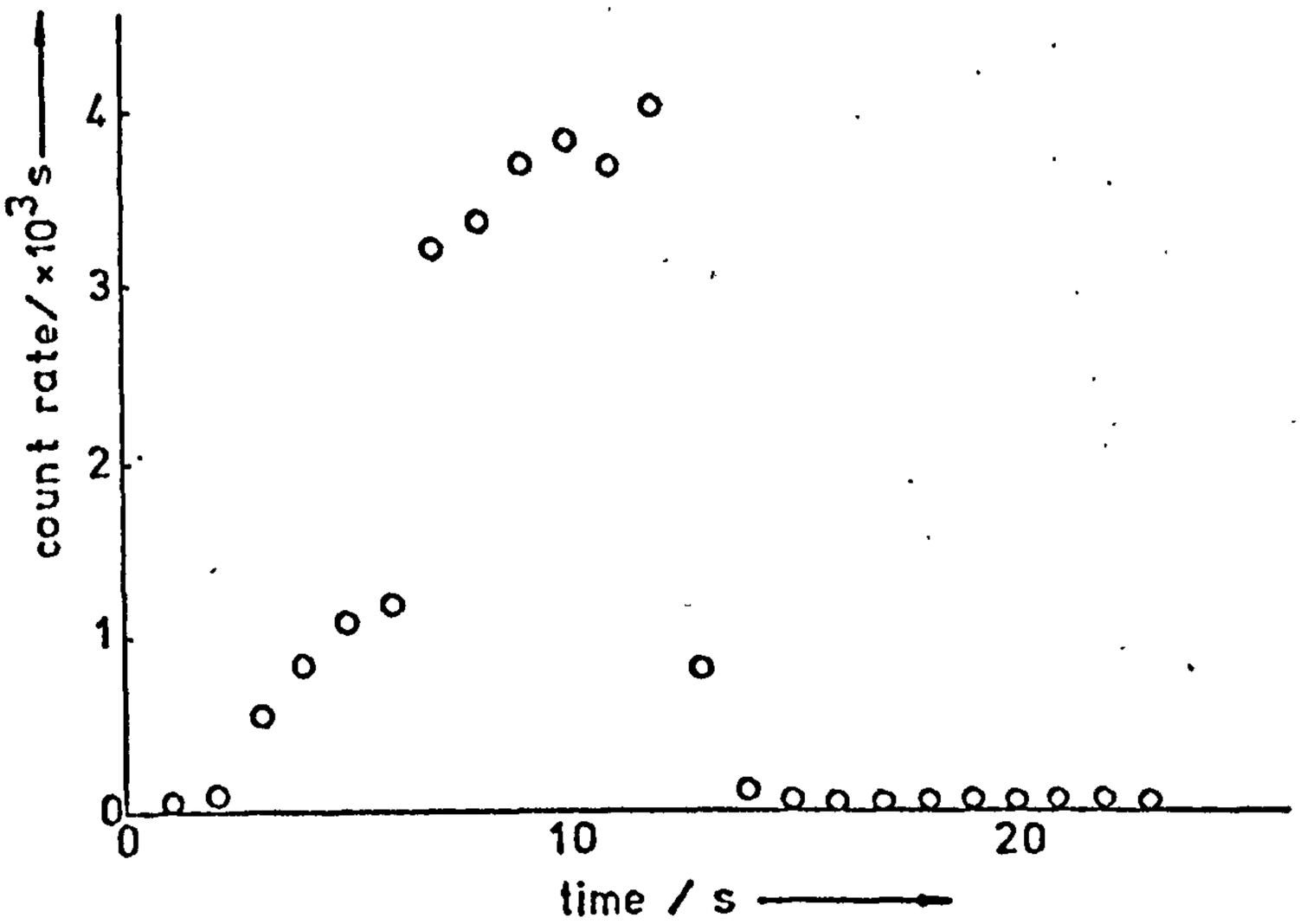

(a) Initial ethylene-C14 pulse.FCS plot,1s resolution.

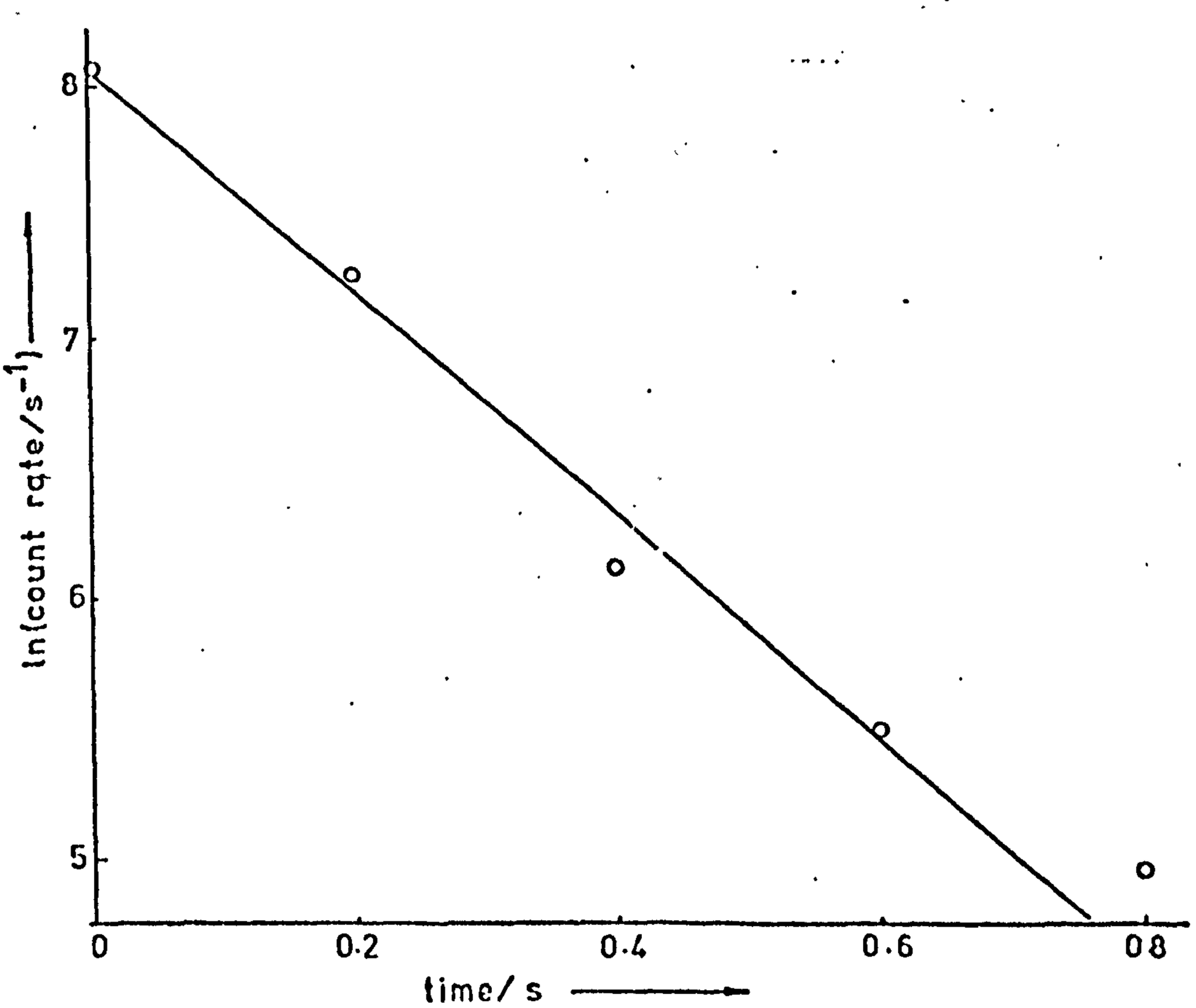

(b) Fast desorption. FCS plot, 0.2s resolution.

Figure 5.41. Experiment G6/6. Catalyst count rate versus time during initial ethane -C14 pulse.

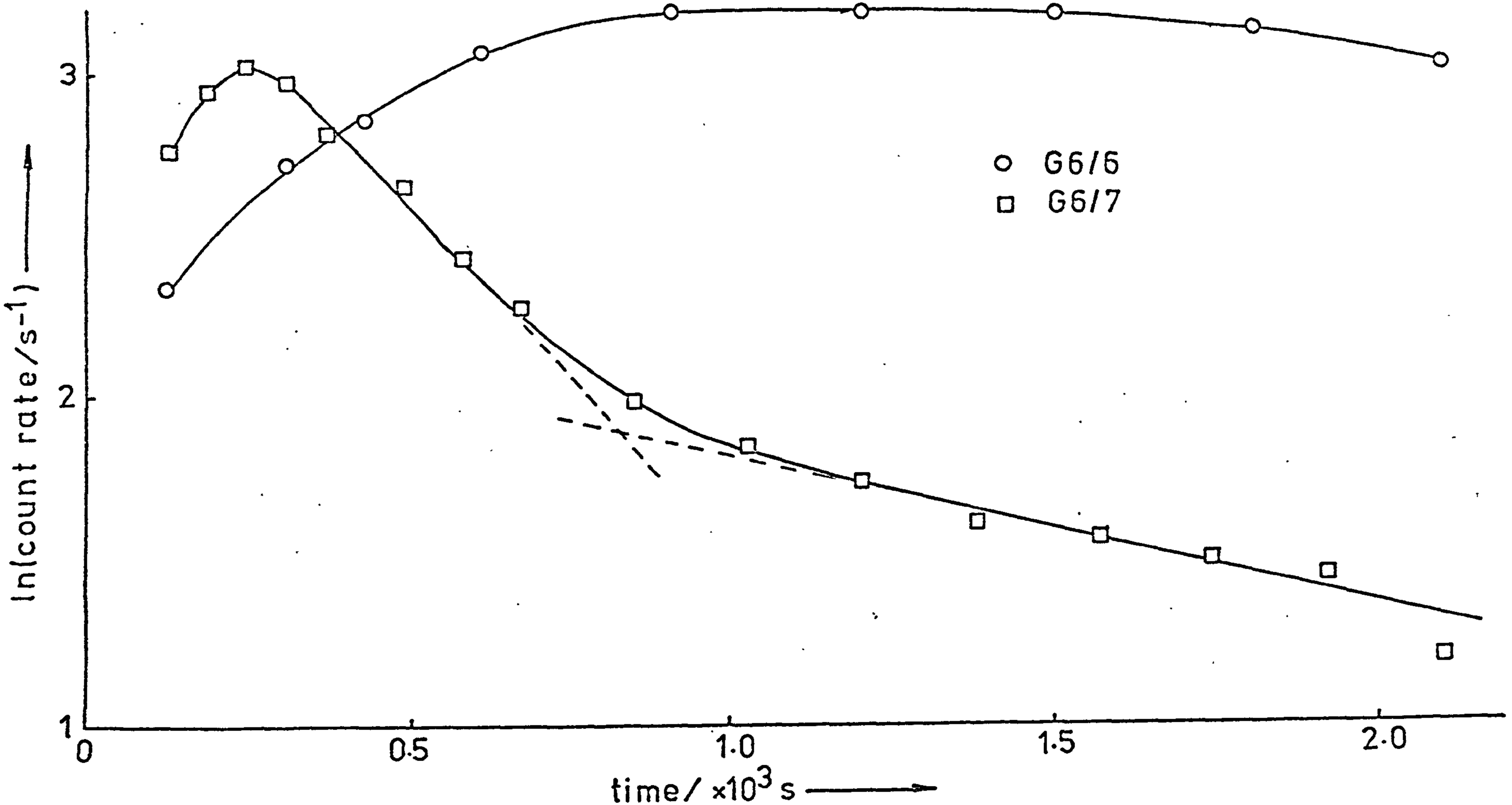

Figure 5.42. Count rate versus time following ethane-C14 pulse. Experiments G6/6&7, ratemeter plot.

5.15. Catalyst reduction temperature.

Experiment G7/1*.

In each of the previously described experiments, catalyst samples were reduced in situ in the reactor/counting chamber. The reduction temperature used was 423 K, and it was desirable to compare the results obtained with a catalyst sample pre-reduced at a higher temperature in order to eliminate the possible effects due to incomplete reduction.

Catalyst sample G7 (86 mg) was pre-reduced at 623 K in H_2 flow for 3 hours in a microcatalytic reactor. It was then transferred in air to the reaction/counting chamber, where it was reduced under standard conditions. A 12 s ethylene-C14(75 torr)/H_2(705 torr) pulse was passed over the catalyst in 1.85 ml s^{-1} H_2 flow at 253 K. The maximum reversible adsorption observed was 7×10^{15} molecule mg^{-1}, and the value of R_I calculated as 0.05. The fast desorption curve, shown in figure 5.43(a) gave an LSA desorption rate constant of $1.3 \pm 0.2\ s^{-1}$.

The initial retention was 9.0×10^{15} molecule mg^{-1}, which fell to 4.2×10^{15} molecule mg^{-1}. The intervening slow desorption curve, shown in figure 5.43(b) had initial and final first order rate constants of $7.5 \times 10^{-4}\ s^{-1}$ and $3.1 \times 10^{-4}\ s^{-1}$ respectively.

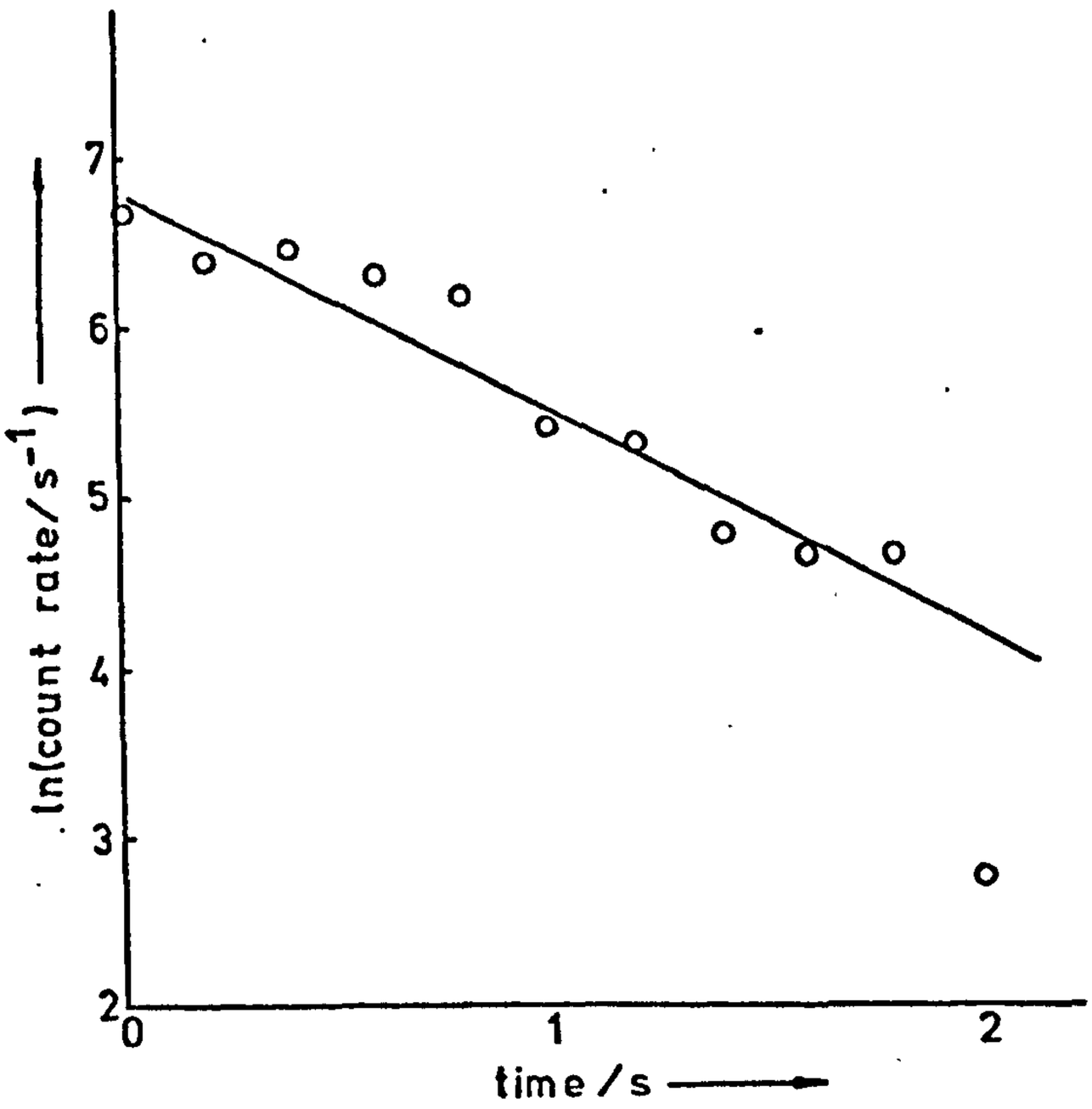

(a) Fast desorption. FCS plot, 0.2 s resolution.

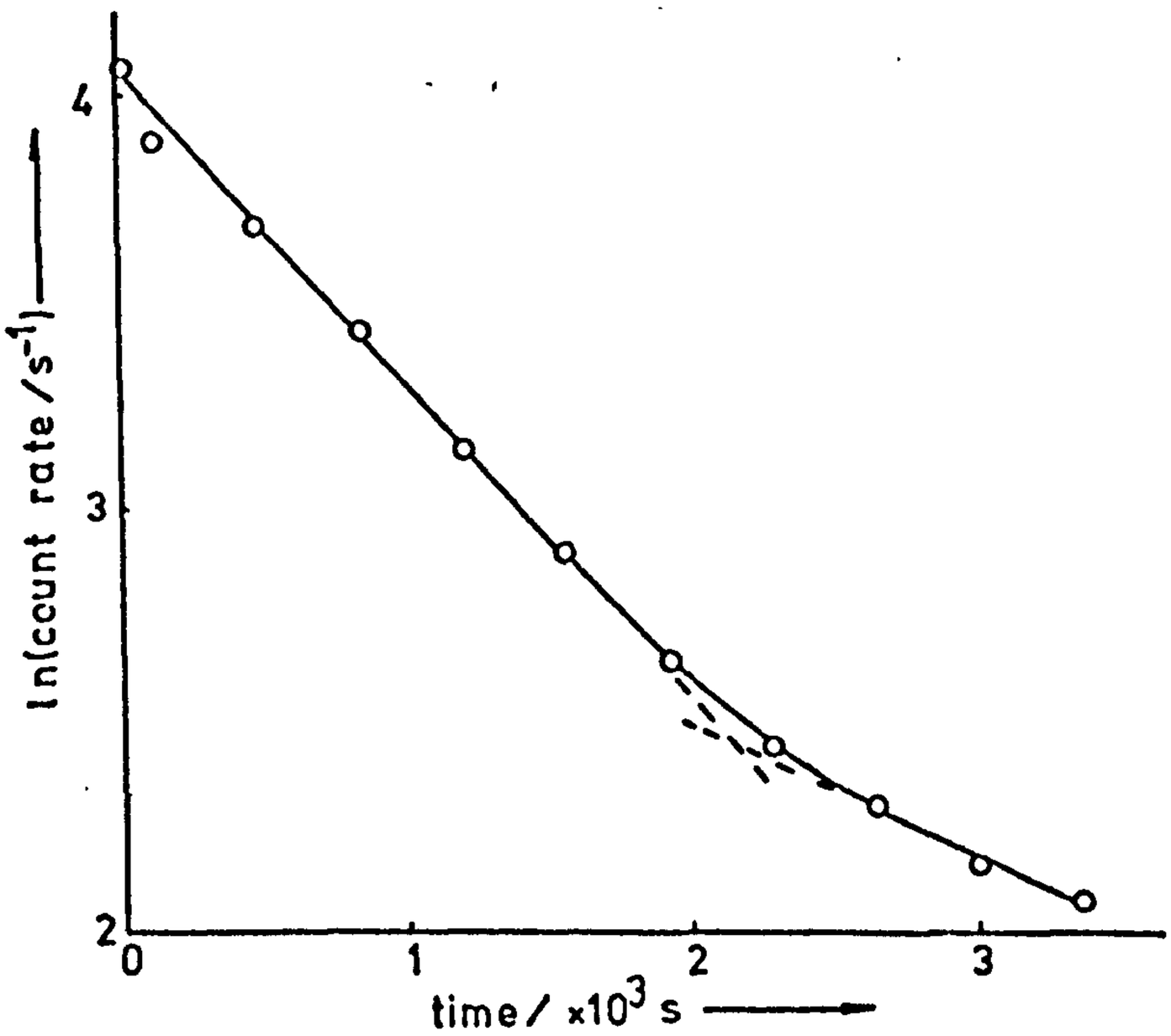

(b) Slow desorption following ethylene-C14 pulse.
Ratemeter plot.

Figure 5.43. Experiment G7/1 - catalyst count rate versus time.

Table 5.19. Fast counting system analyses.
The values of resolution given are the time intervals over which counts were taken. The order in which the figures should be read is left to right and row by row. The time corresponding to the first counting interval of each row is shown in the left hand column.

Experiment G1/2. Catalyst counts. Resolution = 0.5 s.

t(s)										
0	0	31	59	73	64	72	79	78	91	74
5	84	89	67	80	74	87	83	81	77	73
10	78	85	87	62	26	18	8	7	10	3
15	9	4	2	2	3	3	4	6	5	9

Experiment G1/4.
Catalyst counts. Resolution = 5 s.

t(s)										
0	84	68	66	146	1264	2280	2478	2652	2611	2539
50	2544	2518	2628	2658	2552	2595	2622	2620	2543	2585
100	2553	2609	2581	2265	1203	584	526	447	427	411
150	426	418	412	425	384	356	349	374	388	363

Gas counts. Resolution = 5 s.

t(s)										
0	2	3	3	40	24	171	1450	2555	2813	2687
50	2647	2721	2649	2689	2683	2686	2708	2677	2754	2685
100	2691	2765	2654	2691	2676	1983	887	253	88	41
150	35	28	32	30	25	23	21	16	21	20

Experiment G1/6.
Catalyst counts. Resolution = 1 s.

t(s)										
0	35	211	536	585	563	581	562	564	580	556
10	599	587	560	588	600	391	171	139	154	136
20	165	143	145	120	139	133	147	135	152	132

Gas counts. Resolution = 1 s.

t(s)										
0	1	5	286	588	652	650	639	651	674	655
10	626	657	614	657	644	610	192	36	10	5
20	4	3	3	3	2	1	1	1	1	3

Experiment G1/7.
Catalyst counts. Resolution = 1 s.

t(s)										
0	9	9	25	239	490	484	533	542	552	541
10	571	554	562	586	558	587	569	575	568	342
20	223	149	144	141	149	168	165	136	139	150

Gas counts. Resolution = 1 s.

t(s)										
0	1	1	0	0	18	228	410	529	567	551
10	547	554	542	580	565	556	570	584	573	567
20	464	297	131	63	25	14	11	7	6	4

(Cont.)/

/Table 5.19.(Cont.)

Experiment G2/1.

Catalyst counts. Resolution = 0.2 s.

t(s)										
0	0	0	5	10	13	14	19	24	28	27
2	28	31	20	23	25	20	22	22	23	32
4	26	24	19	32	30	29	24	18	24	21
6	30	24	21	24	24	22	22	25	31	19
8	22	22	19	33	23	26	22	24	25	26
10	24	23	20	27	24	23	33	25	26	23
12	24	18	18	20	12	9	4	6	3	2
14	2	3	3	0	3	1	1	0	2	2

Gas counts. Resolution = 0.2 s.

t(s)										
0	0	0	1	2	5	19	24	28	27	37
2	37	33	39	32	43	30	39	35	37	38
4	41	36	46	35	54	38	35	44	40	41
6	34	40	42	50	40	45	45	48	44	45
8	48	41	30	36	52	54	48	44	45	48
10	41	29	41	47	38	36	41	43	36	38
12	37	37	28	25	26	24	20	17	6	6
14	1	4	3	3	0	1	0	0	1	0

Experiment G2/2.

Catalyst counts. Resolution = 0.2 s.

t(s)										
0	0	0	0	0	8	16	17	17	13	13
2	29	18	15	18	17	25	20	20	22	18
4	21	17	24	14	31	10	15	26	25	18
6	24	19	27	17	22	24	22	18	22	28
8	22	15	18	23	30	23	30	23	30	16
10	20	19	14	18	15	15	17	25	18	22
12	25	22	13	14	27	22	24	10	13	3
14	2	2	2	1	1	2	1	0	0	2

Gas counts. Resolution = 0.5 s.

t(s)										
0	0	0	1	12	47	74	93	92	89	102
5	97	92	78	84	93	82	97	84	82	66
10	71	95	111	89	90	80	93	90	91	53
15	16	5	3	1	0	0	0	0	0	2

Experiment G2/3.

Catalyst counts. Resolution = 0.2 s.

t(s)										
0	0	0	0	2	9	29	27	16	21	24
2	14	16	17	18	17	16	18	19	17	23
4	26	27	21	26	21	17	24	25	22	18
6	25	19	19	18	25	28	15	26	23	21
8	18	22	20	18	19	19	23	16	18	14
10	22	21	20	29	23	23	20	16	30	22
12	23	20	15	10	9	1	2	2	2	0

(Cont.)/

/Table 5.19 (Cont.)

Experiment G2/3 (Cont.)

Gas counts. Resolution = 0.2 s.

t(s)										
0	0	0	0	2	2	7	13	25	30	44
2	35	28	34	38	31	40	40	36	45	32
4	35	39	33	51	41	47	38	43	40	34
6	40	33	48	41	42	48	45	43	52	37
8	50	35	42	43	45	41	49	40	39	49
10	38	35	32	30	56	31	42	44	38	44
12	38	40	32	26	18	10	6	4	6	5
14	0	1	0	1	0	0	0	0	1	1

Experiment G2/5.

Catalyst counts. Resolution = 0.2 s.

t(s)										
0	2	0	0	0	20	56	84	88	106	131
2	129	155	119	100	112	154	129	109	117	142
4	147	143	141	130	121	144	144	145	104	149
6	139	139	144	143	150	135	135	120	132	140
8	123	133	149	144	124	131	118	140	132	131
10	142	137	143	139	137	139	141	126	141	132
12	142	142	105	95	86	55	61	54	31	37
14	29	37	25	22	17	23	15	12	19	14
16	13	19	14	11	17	11	15	17	9	15

Gas counts. Resolution = 0.2 s.

t(s)										
0	0	1	0	3	21	38	81	104	97	125
2	140	140	156	152	164	154	164	158	154	146
4	169	154	167	157	167	177	161	168	171	163
6	160	165	159	170	152	153	183	163	154	163
8	139	159	155	181	147	175	151	164	166	150
10	154	156	171	153	166	164	160	182	166	163
12	173	144	118	109	100	68	48	51	40	44
14	34	21	28	18	14	21	12	12	12	6
16	8	4	4	9	2	2	3	2	3	4

Experiment G2/6.

Catalyst counts. Resolution = 0.2 s.

t(s)										
0	8	6	3	8	27	42	39	47	53	52
2	47	42	47	48	49	48	44	43	47	43
4	44	40	43	65	49	38	53	61	46	56
6	45	64	50	55	53	51	50	55	46	48
8	51	46	49	50	51	53	46	46	52	57
10	57	55	52	53	52	49	62	50	58	45
12	51	53	52	61	50	40	53	51	47	58
14	50	41	64	53	51	50	41	57	40	60
16	57	47	46	50	41	37	31	26	35	32
18	21	20	18	27	16	17	12	13	15	24
20	9	9	12	11	14	7	5	7	14	12

(Cont.)/

/Table 5.19 (Cont.)

Experiment G2/6 (Cont.)

Gas counts. Resolution = 0.2 s.

t(s)										
0	0	0	0	0	9	27	47	54	69	67
2	68	76	87	83	96	81	83	87	81	75
4	82	84	83	79	85	82	77	81	79	85
6	96	69	83	79	60	73	83	86	91	71
8	75	80	78	84	72	83	93	78	98	85
10	80	75	72	70	80	94	82	90	86	84
12	92	86	80	82	70	79	74	82	82	76
14	74	78	84	88	79	86	72	70	70	87
16	68	77	78	66	70	67	60	56	54	53
18	46	35	26	25	27	20	13	13	7	11
20	10	10	3	3	5	1	1	1	0	2

Experiment G2/7.

Catalyst counts. Resolution = 0.2 s.

t(s)										
0	1	1	6	26	60	104	118	134	113	140
2	142	141	148	153	130	147	143	137	148	153
4	149	156	140	154	153	162	166	164	160	163
6	175	158	153	152	148	156	150	162	160	146
8	147	148	161	173	152	152	160	145	152	146
10	157	164	157	159	168	162	152	147	162	140
12	143	146	118	116	88	69	49	50	43	44
14	34	25	24	24	28	27	21	19	27	22

Gas counts. Resolution = 0.2 s.

t(s)										
0	0	2	13	33	78	92	127	150	143	146
2	151	159	163	155	167	169	147	155	155	160
4	163	176	167	164	156	176	168	164	147	158
6	165	165	173	158	158	173	156	152	156	153
8	154	163	147	172	164	163	181	156	166	168
10	168	175	174	169	170	166	169	172	164	165
12	153	140	116	102	83	63	55	47	32	42
14	35	22	17	16	19	17	13	14	14	10
16	12	10	13	4	6	7	6	2	3	3

Experiment G2/8.

Catalyst counts. Resolution = 0.2 s.

t(s)										
0	1	7	9	35	41	36	52	43	41	60
2	52	42	57	52	47	55	58	57	49	56
4	54	51	51	50	45	48	63	59	56	61
6	57	56	56	60	62	65	58	48	51	48
8	53	52	55	59	58	54	53	54	64	52
10	45	50	64	69	51	51	48	67	69	47
12	50	58	58	56	63	57	61	51	55	70
14	64	53	45	53	62	51	57	59	60	48
16	41	39	42	37	38	39	42	29	21	23
18	22	22	24	11	17	13	16	12	12	11
20	11	11	14	6	9	12	11	12	9	9

(Cont.)/

/Table 5.19 (Cont.)

Experiment G2/8 (Cont.)

Gas counts. Resolution = 0.2 s.

t(s)										
0	1	0	0	0	3	7	15	26	45	46
2	52	62	58	58	71	53	60	68	76	65
4	69	66	62	69	72	64	83	71	68	78
6	59	70	70	71	88	57	72	69	66	80
8	75	73	62	68	69	68	79	64	65	67
10	59	59	64	66	70	70	65	77	79	68
12	66	68	51	62	68	63	74	76	62	72
14	64	70	67	69	64	59	63	60	72	69
16	58	53	53	58	46	45	39	42	40	34
18	40	18	17	16	17	10	12	5	9	5
20	4	2	2	6	2	1	4	1	1	3

Experiment G3/1.

Catalyst counts. Resolution = 0.2 s.

t(s)										
0	1	10	12	18	24	24	22	18	16	33
2	29	29	30	36	27	44	31	26	39	27
4	30	28	37	27	30	28	32	33	22	31
6	33	29	26	39	36	45	35	43	33	29
8	37	28	22	25	23	34	31	28	23	35
10	28	31	35	34	45	37	34	42	24	35
12	25	26	18	25	24	12	22	21	13	15
14	11	6	12	14	9	8	18	10	12	9

Gas counts. Resolution = 0.2 s.

t(s)										
0	0	0	0	1	0	4	9	14	10	21
2	20	20	19	24	26	34	28	28	34	22
4	20	33	30	36	34	33	22	34	26	32
6	18	33	26	35	39	25	30	28	38	21
8	31	28	27	22	34	29	22	26	26	35
10	29	34	30	18	34	33	31	26	25	27
12	31	31	18	23	23	15	12	15	8	7
14	5	3	4	6	2	4	2	3	0	1

Experiment G4/1.

Catalyst counts. Resolution = 0.2 s.

t(s)										
0	0	0	1	4	23	59	61	100	104	100
2	108	167	187	267	261	256	261	261	265	259
4	254	273	265	256	262	257	264	258	272	268
6	260	269	260	269	266	278	257	263	262	270
8	263	269	270	263	264	265	263	270	270	270
10	274	283	275	268	277	270	264	272	276	268
12	269	266	279	263	270	276	247	235	108	40
14	46	43	45	43	38	46	37	46	40	35
16	43	44	39	30	38	25	40	37	40	40

(Cont.)/

/Table 5.19 (Cont.)

Experiment G4/1 (Cont.)

Gas counts. Resolution = 0.2 s.

t(s)										
0	0	1	6	21	30	57	93	112	115	103
2	135	123	133	135	154	145	126	167	165	175
4	159	170	170	178	198	281	258	174	182	173
6	157	163	173	158	146	145	141	155	161	148
8	145	145	146	169	142	168	150	142	157	148
10	160	150	151	149	148	154	156	161	133	149
12	165	152	135	96	83	73	52	45	32	21
14	18	25	25	13	11	13	4	5	4	8
16	6	5	5	6	5	5	3	3	3	5

Experiment G4/3.

Catalyst counts. Resolution = 0.2 s.

t(s)										
0	3	11	6	20	18	16	30	27	27	31
2	31	31	40	23	36	36	31	41	37	37
4	41	33	39	42	41	35	39	41	48	37
6	49	40	38	37	44	41	33	31	37	35
8	44	42	30	49	36	43	54	48	41	33
10	43	45	40	49	40	36	42	24	27	28
12	20	20	20	18	26	20	21	21	16	22
14	14	24	19	13	20	16	18	21	21	19

Gas counts. Resolution = 0.2 s.

t(s)										
0	0	4	7	14	21	21	19	24	25	27
2	32	34	32	29	38	34	40	41	39	43
4	34	39	34	43	38	49	39	45	44	23
6	38	34	25	38	37	42	40	46	39	42
8	33	48	39	27	42	34	37	34	41	40
10	29	41	49	39	38	28	25	19	20	11
12	9	12	6	7	7	6	4	3	6	3
14	3	4	5	2	1	3	1	0	0	2

Experiment G6/2.

Catalyst counts. Resolution = 0.2 s.

t(s)										
0	0	3	1	3	11	33	40	42	35	46
2	54	48	42	47	40	51	55	47	46	54
4	50	60	50	51	45	36	62	60	50	48
6	50	44	48	61	55	52	56	63	55	53
8	61	48	66	62	58	60	56	69	60	54
10	57	68	64	59	64	71	61	66	68	44
12	46	27	38	37	29	31	33	30	27	22
14	20	21	25	34	36	20	31	29	30	29

(Cont.)/

/Table 5.19 (Cont.)

Experiment G6/2 (Cont.)

Gas counts. Resolution = 0.2 s.

t(s)										
0	0	0	13	27	55	93	95	112	130	128
2	121	123	147	144	129	119	126	116	128	138
4	110	135	134	138	132	131	151	135	140	131
6	132	137	141	133	138	123	130	124	133	126
8	130	134	139	131	142	153	136	139	136	138
10	127	144	151	140	127	135	121	89	71	66
12	36	16	16	11	6	7	8	1	4	7
14	9	5	7	2	0	3	6	4	2	3

Experiment G6/4.

Catalyst counts. Resolution = 0.2 s.

t(s)										
0	1	3	20	42	72	84	105	110	102	104
2	128	100	118	108	126	115	109	116	122	116
4	132	134	126	123	125	137	127	137	112	131
6	126	141	137	128	154	147	131	134	150	139
8	146	129	124	135	138	138	144	163	142	160
10	142	146	147	151	140	109	103	91	78	71
12	69	69	76	54	69	65	79	61	59	68
14	69	67	61	75	60	66	61	68	64	61

Gas counts. Resolution = 0.2 s.

t(s)										
0	0	5	21	67	92	122	141	137	156	134
2	137	140	157	148	140	140	148	153	151	161
4	146	144	151	149	151	159	155	132	143	149
6	151	154	147	144	148	152	147	152	150	151
8	141	140	149	149	150	159	152	159	163	156
10	157	148	139	145	119	93	65	47	25	19
12	24	10	15	11	9	9	11	9	3	4
14	6	6	11	0	6	4	5	2	3	3

Experiment BS3/1.

Catalyst counts. Resolution = 1 s.

t(s)										
0	3	1	1	15	170	280	291	309	345	378
10	343	354	358	356	368	364	350	354	345	300
20	234	202	139	110	104	98	76	89	73	79
30	79	66	74	64	76	68	64	68	67	57

Gas counts. Resolution = 1 s.

t(s)										
0	0	1	0	1	4	32	140	224	295	333
10	333	333	342	374	349	332	325	329	343	309
20	301	250	177	97	87	33	25	17	16	13
30	4	4	4	3	2	3	1	0	1	1

(Cont.)/

/Table 5.19 (Cont.)

Experiment B33/2.

Catalyst counts. Resolution = 1 s.

t(s)										
0	2	2	2	5	6	7	181	478	662	753
10	788	815	875	874	869	896	899	892	747	642
20	580	525	454	389	370	337	305	265	247	237
30	226	193	197	166	167	159	159	144	111	132
40	123	99	95	103	77	100	78	75	83	77
50	67	59	63	54	65	58	61	51	46	46
60	57	49	43	60	36	53	50	44	52	46
70	53	41	44	48	47	47	67	44	51	44
80	46	36	47	41	45	46	38	37	47	44

Gas counts. Resolution = 1 s.

t(s)										
0	0	4	26	105	237	352	514	573	626	717
10	699	737	692	674	544	450	391	335	280	237
20	203	189	179	135	125	118	90	98	88	68
30	66	56	58	49	36	40	42	39	35	26
40	39	24	18	16	20	16	12	11	13	17
50	9	13	8	9	7	5	7	5	2	8
60	5	11	8	3	7	5	1	2	1	2
70	4	0	0	2	1	2	3	3	0	1

Experiment BS3/3.

Catalyst counts. Resolution = 0.5 s.

t(s)										
0	2	2	45	136	192	190	202	200	221	238
5	224	221	227	215	238	229	236	228	232	229
10	242	232	217	240	191	157	108	85	61	44
15	29	41	27	23	28	24	16	11	10	16
20	16	6	12	14	15	13	8	12	15	6
25	13	13	9	4	14	16	22	6	9	9
30	9	6	13	14	9	8	5	6	14	11
35	13	5	8	13	8	9	8	11	12	6

Gas counts. Resolution = 1 s.

t(s)										
0	1	2	0	0	1	218	561	725	733	738
10	790	757	795	765	815	779	607	362	197	102
20	61	42	21	16	8	7	8	7	4	7
30	0	6	4	1	1	3	2	4	1	1

Experiment BS3/4.

Catalyst counts. Resolution = 1 s.

t(s)										
0	4	2	5	2	1	153	384	533	549	629
10	644	672	726	698	660	686	656	501	419	297
20	257	245	190	140	153	124	101	88	83	76
30	78	54	55	47	63	49	42	40	39	40
40	48	40	39	36	32	45	33	26	30	27

(Cont.)/

/Table 5.19 (Cont.)

Experiment BS3/4 (Cont.)

Gas counts. Resolution = 1 s.

t(s)										
0	0	0	0	3	45	276	495	579	660	704
10	702	688	729	742	739	695	569	404	330	267
20	207	153	141	121	95	70	50	48	48	39
30	30	26	22	22	14	12	15	11	14	11
40	11	4	7	5	7	2	3	1	3	3

Experiment BS3/5.

Catalyst counts. Resolution = 0.5 s.

t(s)										
0	1	1	3	1	4	136	239	255	281	299
5	317	345	326	338	350	348	328	329	359	336
10	375	352	341	375	362	369	367	272	214	171
15	150	142	128	102	94	93	75	64	65	64
20	62	67	50	41	56	47	35	42	56	40
25	44	34	40	61	31	42	40	32	27	44

Gas counts . Resolution = 0.5 s.

t(s)										
0	1	1	36	163	236	311	362	346	382	392
5	399	423	409	402	403	409	404	412	395	408
10	405	402	377	413	328	263	203	185	129	137
15	105	94	61	68	42	46	37	28	34	19
20	19	26	15	16	8	19	10	12	13	5
25	4	5	5	2	3	0	4	1	6	6

Experiment BS3/6.

Catalyst counts. Resolution = 1 s.

t(s)										
0	0	1	2	4	252	412	471	549	552	591
10	585	623	587	626	598	498	375	280	232	193
20	176	120	109	102	92	85	87	84	53	65
30	60	46	59	52	53	40	57	47	49	51
40	40	43	34	39	45	38	47	38	38	46

Gas counts. Resolution = 1 s.

t(s)										
0	3	0	0	30	278	502	586	626	674	695
10	694	685	679	664	625	479	337	230	193	122
20	122	80	46	56	48	41	28	25	13	19
30	10	11	10	9	10	8	11	4	5	5
40	3	6	2	0	2	2	2	5	4	2

Experiment BS3/7.

Catalyst counts. Resolution = 0.5 s.

t(s)										
0	5	3	0	6	9	44	65	73	72	71
5	75	75	77	77	80	83	105	78	79	98
10	79	87	86	78	89	98	79	89	101	83
15	82	53	37	24	25	13	22	6	10	15
20	14	14	13	9	14	13	11	13	8	13
25	13	8	4	6	9	9	5	4	7	9

(Cont.)/

/Table 5.19 (Cont.)

Experiment B33/7 (Cont.)

Gas counts. Resolution = 1 s.

t(s)										
0	3	1	0	28	241	309	322	343	342	315
10	332	317	358	360	353	357	289	122	39	23
20	7	4	3	4	2	4	1	2	1	1

Experiment G6/6.

Catalyst counts. Resolution = 0.2 s.

t(s)										
0	4	21	46	59	81	82	101	99	116	102
2	122	133	115	123	149	142	161	123	110	133
4	137	167	189	211	268	257	248	245	242	245
6	260	241	268	261	264	263	260	255	262	260
8	261	261	278	264	254	241	271	265	269	261
10	277	262	271	249	170	81	52	56	23	29
12	22	25	16	21	15	17	15	17	17	15
14	16	10	13	11	16	12	12	16	11	6

Gas counts. Resolution = 0.2 s.

t(s)										
0	1	12	27	63	93	116	102	120	124	138
2	130	125	141	128	152	148	152	144	165	139
4	154	158	153	168	170	159	147	152	137	146
6	131	145	147	144	157	157	156	160	146	143
8	151	150	137	137	144	139	143	159	142	171
10	161	146	153	125	104	82	61	47	29	36
12	23	21	23	19	21	17	9	10	8	13
14	5	7	2	2	5	3	4	4	3	3

Experiment G7/1.

Catalyst counts. Resolution = 0.2 s.

t(s)										
0	1	2	12	36	52	70	81	86	74	89
2	95	99	105	118	112	106	103	94	116	99
4	100	118	112	125	87	131	109	96	119	129
6	131	113	116	107	125	128	133	137	123	105
8	122	119	105	117	112	129	113	115	117	123
10	142	107	142	140	119	116	136	139	129	103
14	107	97	90	55	52	39	37	37	22	38
16	19	25	24	18	24	19	24	20	24	21

Gas counts. Resolution = 0.2 s.

t(s)										
0	1	1	5	22	43	61	75	92	140	134
2	148	174	150	157	170	153	159	166	171	172
4	175	154	172	167	165	165	160	175	168	174
6	174	172	165	161	167	162	163	162	185	145
8	156	158	167	177	157	165	150	163	190	177
10	170	157	161	172	176	172	158	171	168	171
12	164	160	139	111	83	71	45	40	41	33
14	25	24	16	15	11	7	9	7	5	7

(Cont.)/

/Table 5.19 (Cont.)

Blank reactor experiment.

Catalyst chamber counts. Resolution = 0.2 s.

t(s)										
0	0	0	0	0	1	8	57	92	115	155
2	151	152	149	143	160	145	156	155	145	150
4	156	157	159	157	159	156	156	145	157	145
6	153	169	146	144	160	144	145	161	153	147
8	148	168	129	153	157	145	162	147	145	141
10	146	149	136	143	146	158	150	154	141	166
12	145	159	156	168	158	119	62	23	11	2
14	3	0	6	4	2	0	2	2	0	4

Gas chamber counts. Resolution = 0.2 s.

t(s)										
0	0	0	0	0	0	0	2	14	40	77
2	115	145	147	126	159	148	145	153	137	151
4	132	150	158	147	164	143	148	147	147	153
6	123	142	141	143	143	153	163	153	140	139
8	135	143	137	148	148	143	133	129	150	139
10	152	143	145	161	146	136	158	145	143	140
12	145	140	150	152	146	144	147	97	59	26
14	7	5	1	1	2	3	0	1	1	1

Part C. General.

5.16. Catalyst characterisation.

To facilitate interpretation of the adsorption data obtained in the previous sections, it was necessary to obtain information about the metal surface areas of the catalysts used. The following determinations were made for catalysts B, C, F and G, reduced under standard conditions. A summary of the results is given in table 5.20.

Metal assays.

The assays were carried out by Johnson, Matthey and Co., Limited.

Carbon monoxide chemisorption areas.

The metal surface areas of the four catalysts were determined by carbon monoxide chemisorption in the laboratories of Johnson, Matthey and Co., Limited. The value given in table 5.20 for catalyst G (Ir/SiO_2) was based on a figure of 2.39 m^2 ml^{-1} carbon monoxide adsorbed, the value normally used for platinum. No data were available for carbon monoxide chemisorption on iridium.

Metal particle size distributions.

Electron micrographs of catalysts C and G were taken by Dr. T. Baird of Glasgow University using a Siemens Elmiskop I electron microscope, operating at 100 kV (see plates 1 and 2). Electron micrographs of catalysts B and C were supplied by British Petroleum Limited, Sunbury-on-Thames (see plates 3 and 4). All samples were prepared by drying a drop of water-suspended catalyst on a carbon film specimen grid.

The particle size distributions shown in figure 5.44 were determined by measuring approximately 150 metal particles for each sample. The metal particles on plates 1 - 4 are distinguishable as small dark areas against the background of less dense support material. It is normally recommended that at least 1000 particles be measured to obtain an accurate particle size distribution (see e.g. 28). A smaller number of measurements was used here as the results obtained were primarily intended for comparison with the metal areas determined by carbon monoxide chemisorption.

The volume weighted surface areas and mean particle diameters were calculated according to the relationships (28):

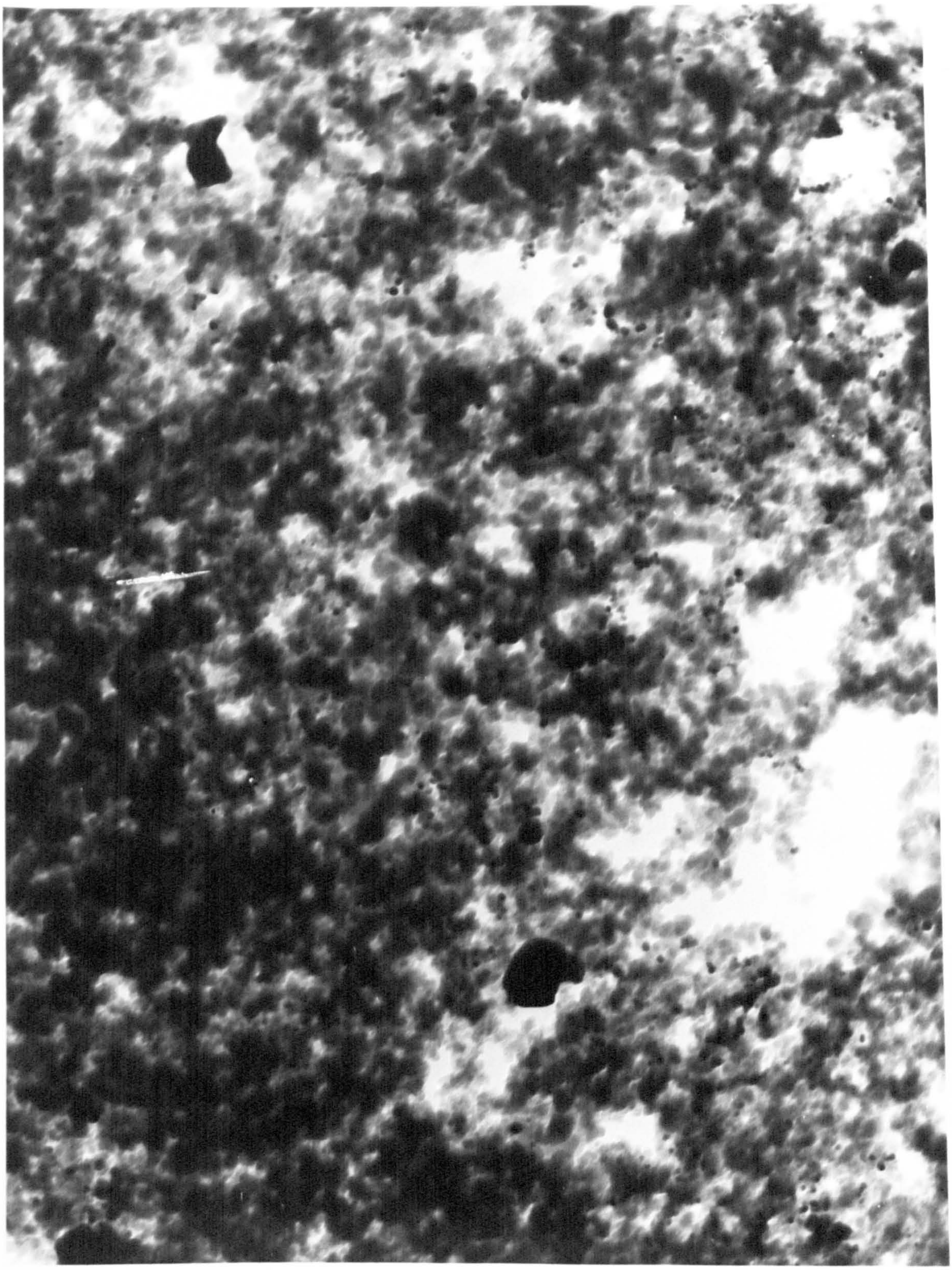

Plate 1. Catalyst C, 4.47% Pd/SiO_2. X120,000.

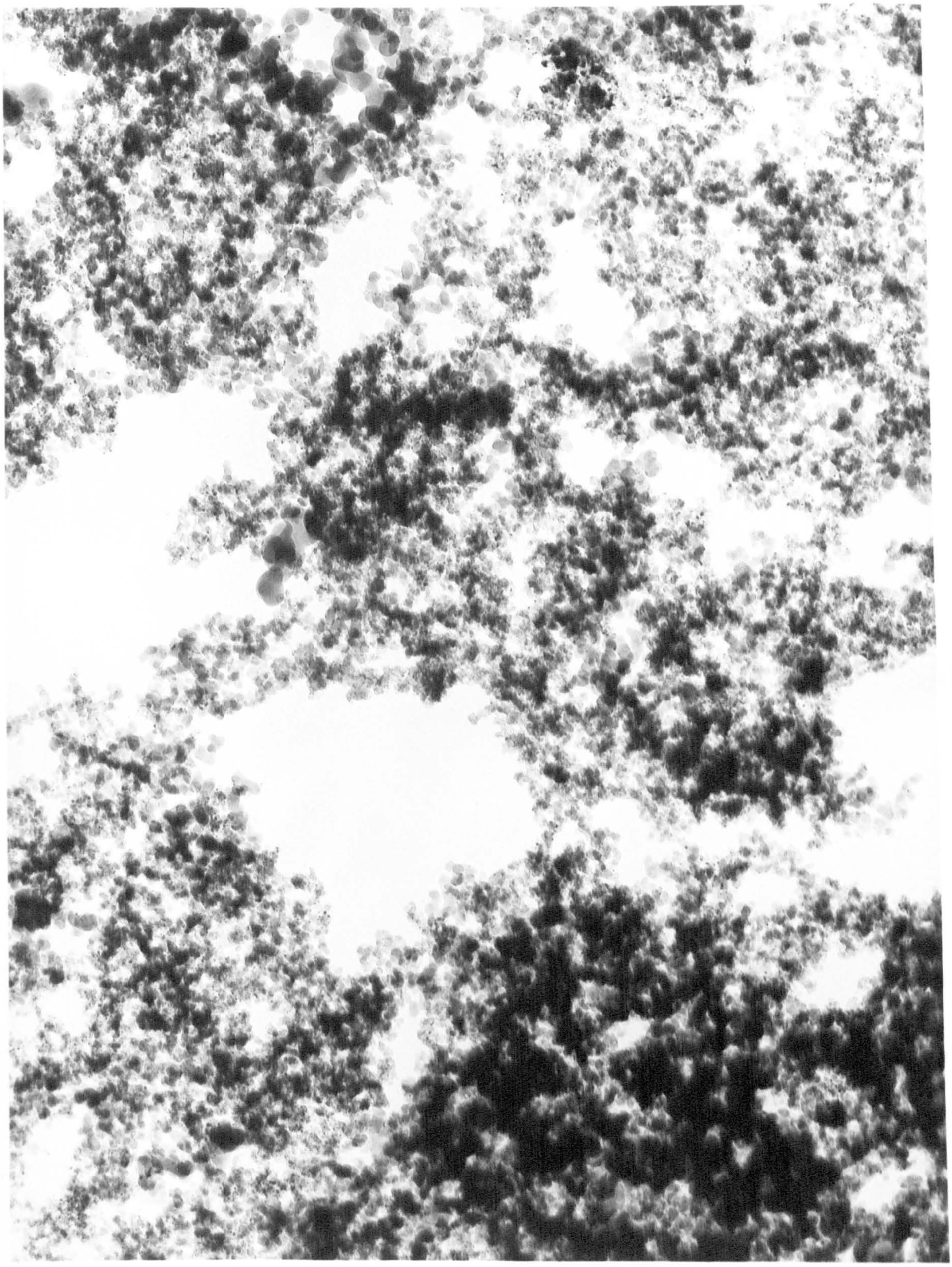

Plate 2. Catalyst G, 4.77% Ir/SiO_2. X130,000.

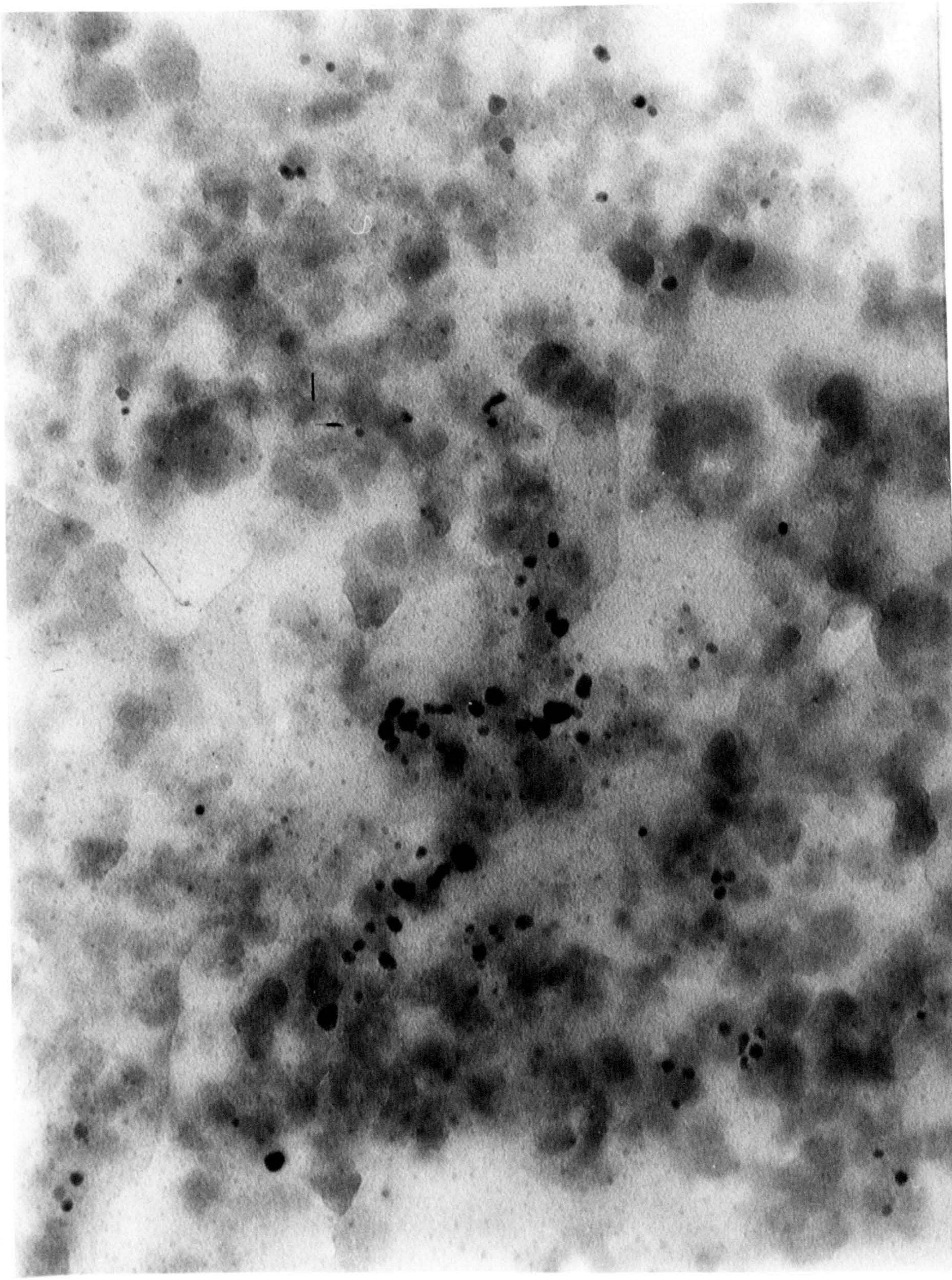

Plate 3. Catalyst B, 1.08% Pd/SiO_2. X290,000.

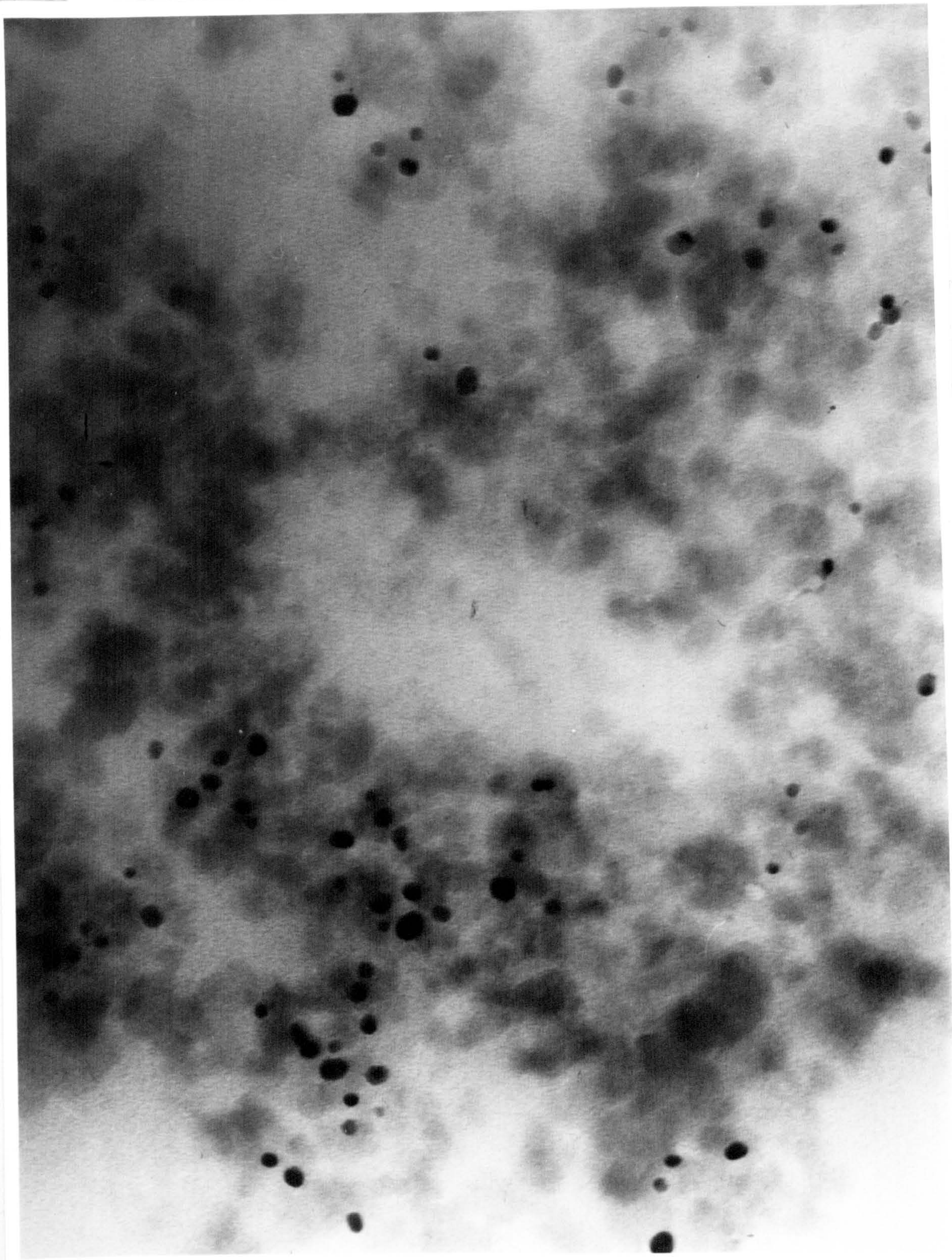

Plate 4. Catalyst C, 4.47% Pd/SiO_2. X290,000.

Table 5.20. Catalyst data.

Catalyst batch	B	C	F	G
Catalyst	Pd/SiO_2	Pd/SiO_2	Pt/SiO_2	Ir/SiO_2
Nominal metal content/ % w/w	1	5	5	5
Metal assay/ % w/w	1.08	4.47	3.93	4.77
Metal area (CO chemisorption)/ m^2 (g catalyst)$^{-1}$	1.37	6.06	3.40	5:06
Metal area (electron microscopy)/ m^2 (g catalyst)$^{-1}$	0.84	(a)2.64 (b)2.79	-	6.39
Volume weighted mean diameter/ nm	7.19	(a)9.45 (b)8.73	-	2.07

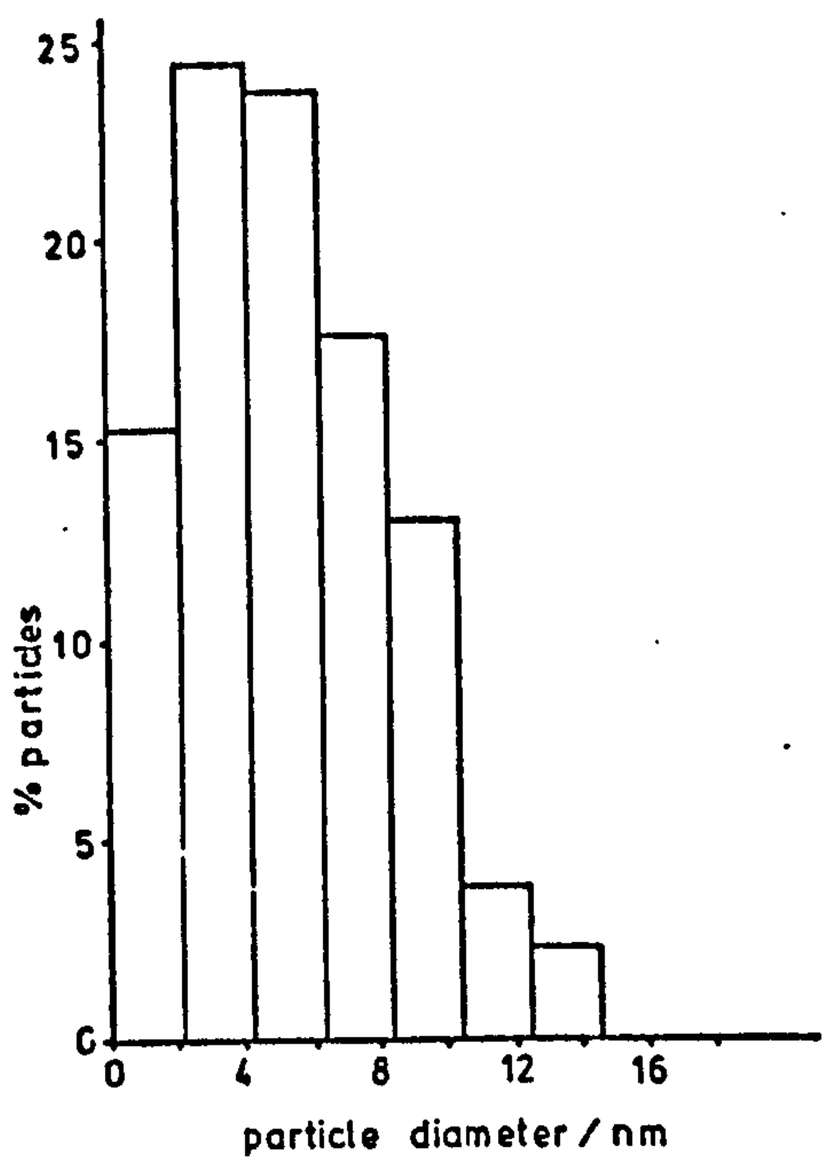

(a) 4·47% Pd / SiO_2

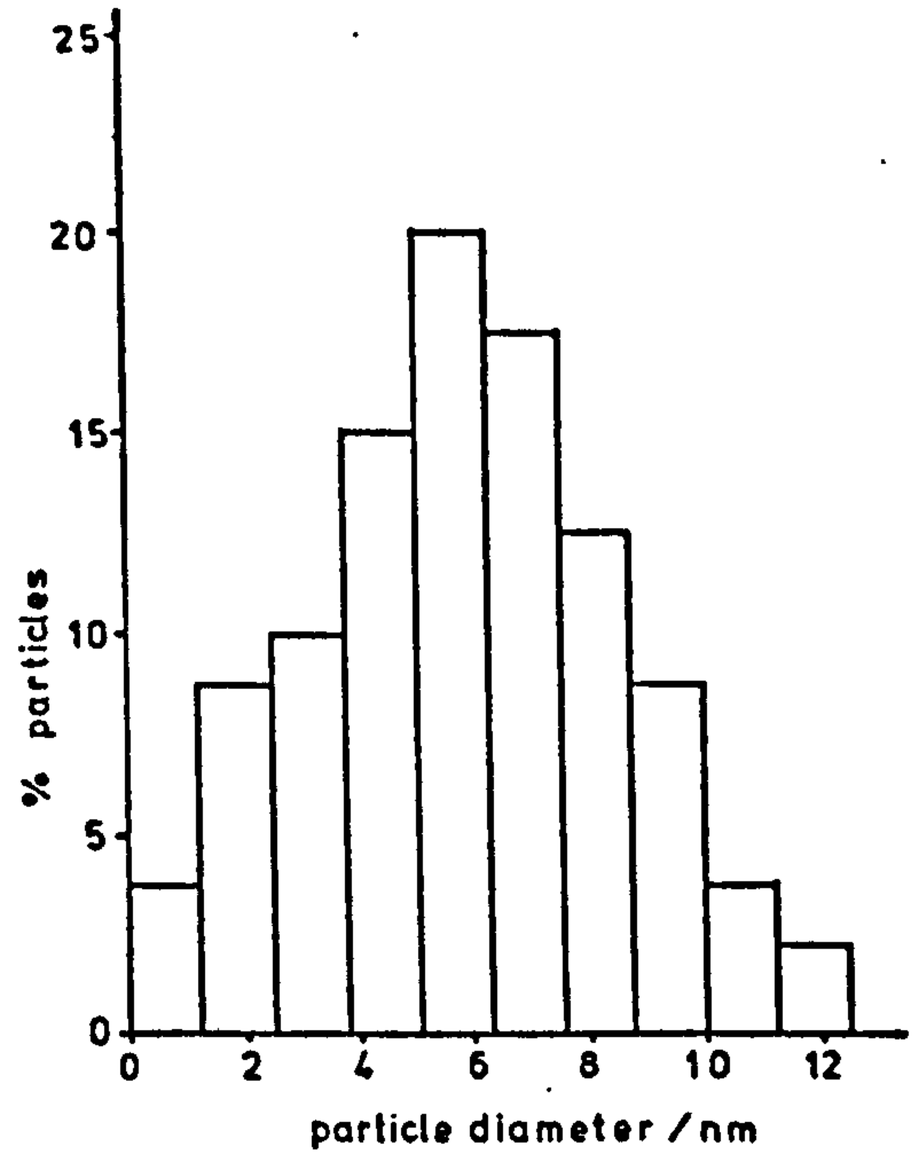

(b) 4·47% Pd / SiO_2

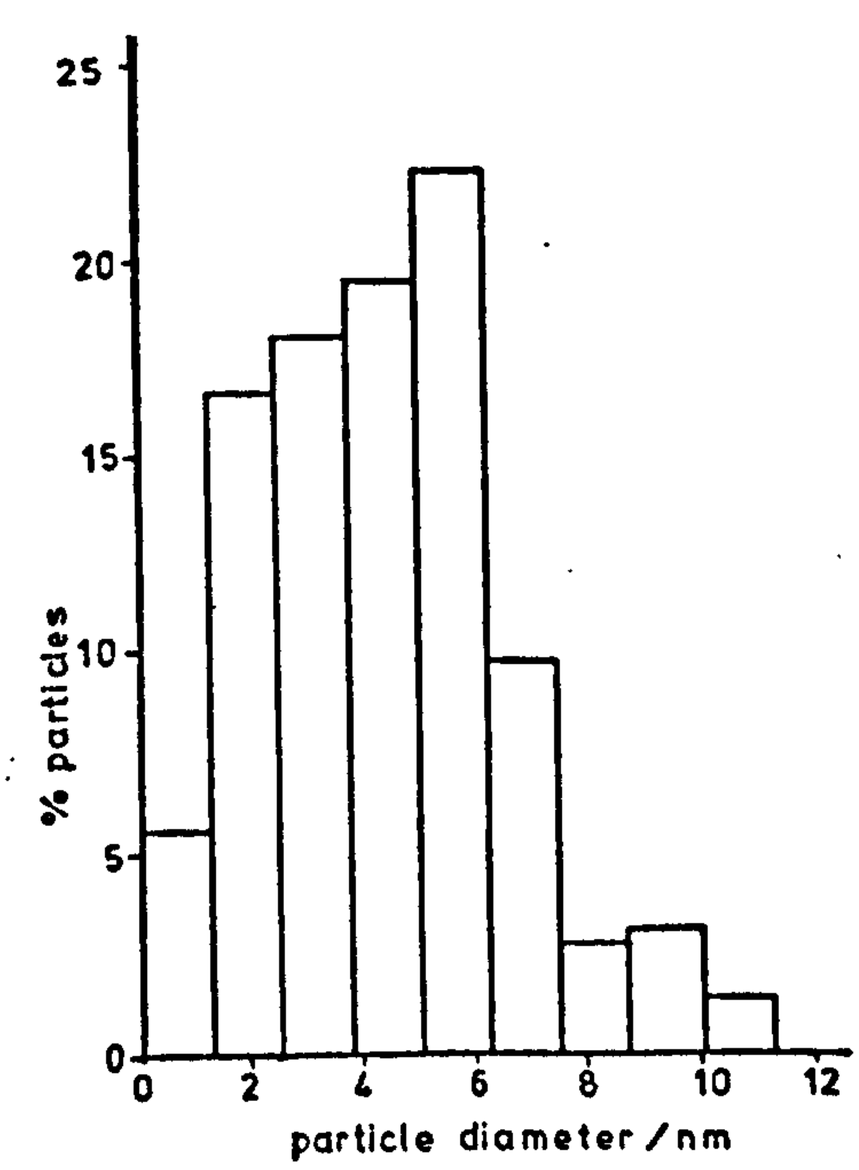

(c) 1·08% Pd / SiO_2

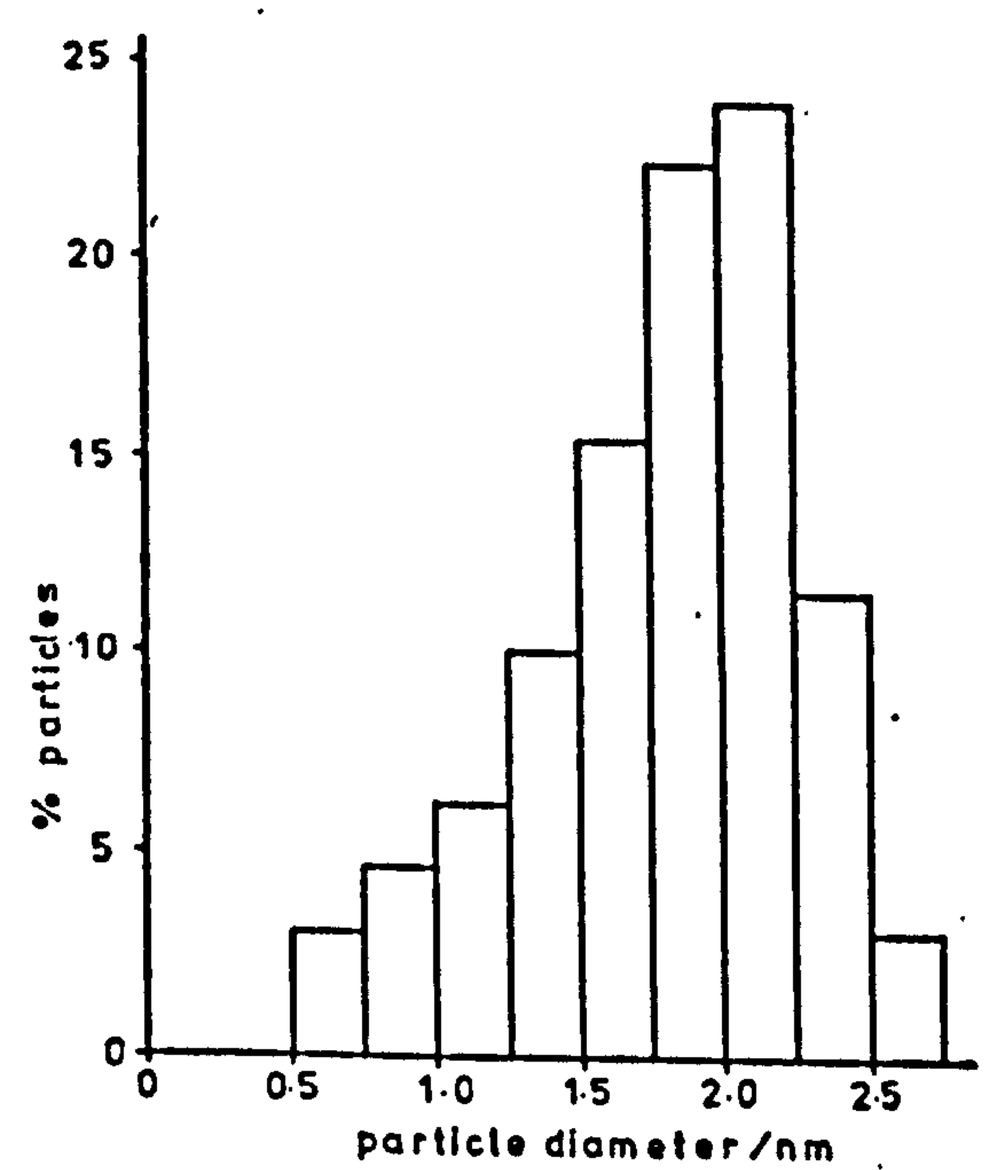

(d) 4·77% Ir / SiO_2

Figure 5.44. Metal particle size distributions from electron micrographs of (a) and (b), catalyst C, (c), catalyst B and (d), catalyst G.

$$\text{Surface area per unit volume metal} = \frac{6\,\Sigma d_i n_i^{\,2}}{\Sigma d_i n_i^{\,3}} \ m^2(m^3 \text{ metal})^{-1}$$

$$\text{Mean particle diameter} = \frac{\Sigma d_i n_i^{\,4}}{\Sigma d_i n_i^{\,3}} \ m$$

where n_i particles were measured of diameter d_i m.

The values given under (a) of table 5.20 and the size distribution shown in (a) of figure 5.44 for catalyst C were obtained by Dr. T. Baird. (b) of table 5.20 and figure 5.44 were obtained for a different sample of the same catalyst in the laboratories of British Petroleum Ltd.

Exchangeable support hydrogen.

It was of interest while considering support activity for adsorption and catalysis in the ethylene studies to determine the exchangeable hydrogen atoms on the support. Tritium exchange was coupled with flow proportional counting in a method developed by Altham and Webb (85) for detecting exchangeable hydrogen atoms on the support. By this method (180) it was found that catalyst G (4.77% Ir/SiO_2) had 4.75×10^{17} exchangeable atoms per mg at 403 K (or, alternatively 2.7×10^{14} exchangeable atoms per cm^2).

5.17. Errors and presentation of results.

Temperature measurement.

In general, where ambient temperature readings are given, these were obtained by thermometer and the values given are accurate to $\pm$ 1 K. The temperatures measured by chromel/alumel thermocouple in conjunction with a Comark Electronic Thermometer (i.e. high temperature chlorobenzene experiments and reactor temperatures for the ethylene experiments) were accurate to within $\pm$ 2 K of temperatures measured by mercury thermometer. From the experiments of section 5.11, some temperature rise was expected during the passage of ethylene/hydrogen pulses over the catalyst in the Part B experiments. While it was not possible to quantify this catalyst

bed temperature variation, the observed temperature readings were constant to within ± 2 K of the stated value during such experiments.

Pressure measurement.

For the chlorobenzene experiments, atmospheric pressure was normally employed. The values given were read from a mercury barometer and are accurate to within ± 1 torr of the stated values. The major errors in the values of flow system pressures measured by pressure transducer during the ethylene studies originated in two ways, viz. (a) Non-linearity and hysteresis of the transducer response, quoted by the manufacturers as less than ± 1% of the full scale reading; (b) readings from the scale of the galvanometer. This error was estimated as ± 10 torr, and considered to be more important as it affected the transducer calibrations in addition to the readings of experimental pressure. The pressure variation during an experiment was normally less than the estimated error.

The major source of error in the radiotracer dilutions and making up tracer samples for the ethylene studies flow system arose from the spiral gauge pressure readings. The estimated error on readings of the light beam deflection was ± 0.5 mm, giving rise to an error of ± 0.25 torr on the pressures measured in the vacuum system manifold. This was equivalent to an error of approximately ± 0.5 torr on the partial pressure of an ethylene sample after freezing into the tracer injection loop. For the tracer dilutions, similar errors arose and the specific activities quoted for the samples used were estimated to be within ± 1% of the values stated.

Gas flow rates.

During the chlorobenzene experiments, fluctuations of about ± 5% in the carrier flow rates in the course of an experiment were found to be greater than the uncertainty in the flow rate measurement. With the greater flow rate stabilisation used in the ethylene studies, rotameter readings were found to be effectively constant during the course of an experiment. The error originating from the flow rate readings was estimated as ± 3%.

Tracer pulse sizes.

The liquid injections by syringe during the chlorobenzene studies were estimated to be within ± 2% of the stated values, based on the accuracy of the scale readings. The partial pressures of the ethylene - C14 pulses have been discussed above. The duration of these pulses could not be measured with any degree of precision, as it was governed by the opening and closing of a stopcock for a period of about 10 s. The duration of the pulses so achieved was normally measured from the count rate versus time date and the values given are accurate to ± 1 s.

Product analysis.

From the analysis of five standard benzene/chlorobenzene/ethanol solutions by ultra-violet spectrophotometry, the error in calculating the conversion and chlorobenzene flow rate was less than ± 3%.

No attempt was made to accurately assess the limits of detection of the gas chromatograph. As the experimental conversions observed were generally zero or ~100%, the limiting factor in detection was the background noise. This was estimated as ca. 0.5% of the usual peak height.

Counting efficiencies and statistics.

In section 4.2, a standard deviation of ± 3.1% was calculated for the counting efficiency from a series of standard, radioactively doped catalyst sources. Taking into consideration the probable error on the specific activity of these sources, determinations of adsorption level may be estimated as accurate to within ± 5% before considering the counting statistics.

The standard deviation of an observed number of counts, N, may be calculated as $\pm \sqrt{N}$ (181). Thus, if 10,000 counts are collected during a single count rate determination and we assume no error to be present in the time of the determination, the value of count rate calculated would have a standard deviation of ± 1%. In the Occupancy Principle experiments of section 5.1, where the integrated counts formed the basis of the calculations, this method of determining standard deviations could be applied. In cases where the count rate versus time curves were analysed, the situation is considerably more complex, as the

accuracy of a single reading is enhanced by its relationship with adjacent points on a curve of this type. In this case it was not practicable to determine standard deviations or to make generalisations with regard to an estimated error. Where the semi-log plot yielded a single straight line, however, it was possible to determine the slope of the line and its standard deviation by the method of the least squares approximation (LSA). In such cases, the calculated values of standard deviation have been given.

Where count rate versus time curves have been taken from counting-ratemeter traces, no attempt has been made to reproduce the observed noise levels. The normal procedure has been to "smooth" such curves by visual examination. The smoothed curves have either been used directly, or where semi-log plots have been given, a number of points have been used from the smoothed curve. As an example, the catalyst count rate versus time plot from experiment C2/5 is given in its original form in figure 5.45, along with the points taken for the semi-log plot.

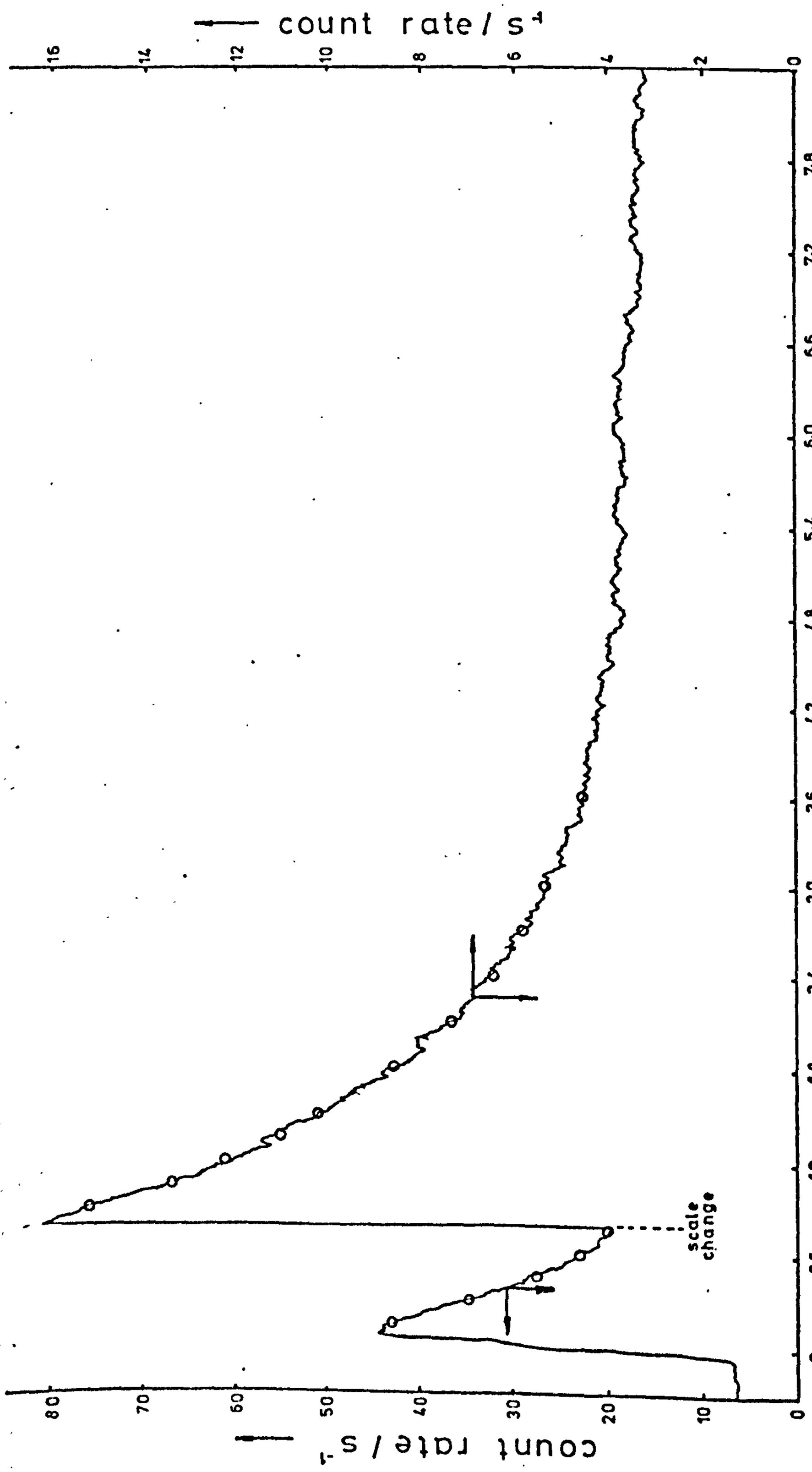

Figure 5.45. Count rate versus time for the catalyst chamber in experiment C2/5. The open circles represent points used in the semi-log plot.

C H A P T E R 6

Discussion

Chapter 6.

Discussion.

Part A. Chlorobenzene Studies.

6.1. Occupancy Principle experiments and desorptions under constant flow conditions.

Occupancy Principle calculations.

The primary aim of these experiments was to establish a number of exchangeable adsorbed molecules (or the capacity of the adsorbed phase) taking part in the hydrogenolysis reaction. This aim was indeed fulfilled, good reproducibility being demonstrated in experiments B1/1 and 2, and an approximately proportional relationship between chlorobenzene partial pressure and adsorption by a comparison with experiment B1/3. Further, it may be seen from tables 5.1 and 2 that an increase in chlorobenzene (or benzene) adsorption by a factor of 2 is accompanied by an increase in reaction rate by a factor of 1.5.

The value of capacity calculated from experiment BS1/1, using blank silica as adsorbent, was, however considerably greater than from B1/1 and 2 under similar conditions. We must, therefore, consider the probability that a large part of the adsorption observed on the Pd/SiO_2 arose from adsorption on the support.

Comparison of results with surface areas.

Let us assume for the present that the adsorption observed on catalyst B occurred on the metal. If we take an approximate value of 1 m^2(g catalyst)$^{-1}$ as the palladium metal area (see table 5.20), we may calculate an area per adsorbed molecule of ca.4.5×10^{-3} nm^2, based on the values of capacity from experiments B1/1 and 2 (2.2×10^{17} molecule (mg catalyst)$^{-1}$). This value is much lower than can be considered acceptable.

If on the other hand we assume that the adsorption occurred primarily on the silica support of surface area 175 m^2 g^{-1}, then the average area occupied by an adsorbed molecule would be 0.80 nm^2.

Comparing this value with the van der Waal's area of a chlorobenzene molecule, adsorbed with the aromatic ring parallel to the surface, of ca. 0.43 nm^2, a much better fit is achieved. The increased amounts of adsorption observed in experiments B1/3 and BS1/1 may indicate the occurrence of multilayer adsorption.

Radiotracer desorption rates.

The Occupancy Principle calculations provided us only with values for the capacity of the adsorption system. Analysis of the desorption curves gave us values of the mean surface lifetime, $\bar{\tau}_s$, and the flux of molecules through the adsorbed phase, f. The latter quantity may be considered as the rate at which molecules leave the adsorbed phase, with or without first reacting.

Comparing the values of reaction rate (table 5.1) with those for the flux (table 5.2), in each case the latter is seen to be greater. It appears that a simple chlorobenzene molecular exchange process occurred in addition to the reaction to benzene. A comparison of the values of flow rate with those for molecular flux shows that a considerable fraction of the chlorobenzene molecules passed through the reaction chamber without adsorbing. The possible surface processes may be quantified by considering turnover numbers for the adsorbed molecules. The total surface turnover number, $\lambda_s\ s^{-1}$, is the reciprocal of the mean surface lifetime, $\bar{\tau}_s$, and represents the total probability of a molecule desorbing in unit time. The turnover number for reaction, $\lambda_r\ s^{-1}$, is the probability that an adsorbed molecule will be desorbed as product benzene in unit time and is given by the relationship

$$\lambda_r = \frac{r}{c}$$

where r is the reaction rate (molecule s^{-1}). The turnover number for exchange, λ_e, is given by the difference between λ_s and λ_r. It is the probability that a molecule will desorb in unit time without first reacting.

The values calculated for the various turnover numbers are given in table 6.1. While those for λ_r for experiments B1/1 - 3 are comparable, the values of λ_e require further explanation. The relatively high value for experiment B1/3 may be attributed to an increase in the chlorobenzene flow rate effectively decreasing the number of gas phase radiotracer molecules which may exchange back into the adsorbed phase. The value of λ_e for experiment BS1/1 is not directly comparable with those for catalyst B. As "desorption" of a radiotracer molecule may be the result of several adsorption/desorption steps rather than a single process, the precise structure of the adsorbent will be of importance. In spite of this difficulty, we may attribute the high value of capacity observed in experiment BS1/1 to a smaller desorption probability than in experiments B1/1 - 3. Assuming that benzene desorption is more rapid than that of chlorobenzene, the hydrogenolysis reaction provides an alternative desorption mechanism in the case of the Pd/SiO_2 catalyst.

Table 6.1. Turnover numbers for constant flow chlorobenzene experiments.

Experiment number	B1/1	B1/2	B1/3	BS1/1
λ_s / x 10^{-4} s^{-1}	9.1	7.9	12.3	3.3
λ_r / x 10^{-4} s^{-1}	4.0	3.9	2.8	0
λ_e / x 10^{-4} s^{-1}	5.1	4.0	9.5	3.3

Limitations of the constant flow method.

In section 2.1, we set as our major objective in the present study, a determination of the size of the active pool of molecules adsorbed on a catalyst surface in the course of a catalytic reaction. While the Occupancy Principle experiments have achieved this objective, the values obtained appear to be of little value in relation to the study of the catalytic processes. We have found the number of molecules adsorbed on the catalyst during reaction and the proportion of these which undergo reaction. Reaction, however, appears to occur only on the metal component of the catalyst and most of the observed adsorption may be attributed to the support. There can, therefore, be little fundamental relationship between the size of this active pool of molecules and the catalytic activity. It is worthwhile noting that even in the case of a catalytic system for which one observed adsorption only on the active portion of the catalyst, catalytic reaction may be confined to a small number of active sites on this portion of the surface. The experiments discussed in this section serve as a good illustration of the difference between the active pool of adsorbed molecules and the number of active sites.

It appears that the constant flow method has, in this case, provided no direct information about the active catalyst surface. It might, however, be hoped that a pulsed flow technique, where a net desorption rate is studied rather than an exchange of labelled molecules, might yield information about adsorption on the metal in the lower regions of surface coverage.

6.2. Desorptions under pulsed flow conditions.

In this section, the various desorption experiments will be considered in turn and the implications of each towards an understanding of the desorption processes occurring. At the beginning of the next section we shall try to use this evidence in formulating a general picture of the desorption mechanism and the hydrogenolysis reaction.

Chlorobenzene desorptions from Pd/SiO_2 in hydrogen flow.

We noted in section 5.2 that most of the semi-log plots for these desorptions took the form of two "straight-line" sections. If we consider first the data from the 5% $PdSiO_2$ desorptions (C2 experiments) given in table 5.4, we see that over a range of initial adsorption of chlorobenzene from 2.76×10^{17} to 8.5×10^{15} molecule (mg catalyst)$^{-1}$, covered by experiments C2/1, 2, 3 and 5, there is little variation in the point of intersection between the two straight-line regions. Only when the initial adsorption falls below this value of ca. 4×10^{15} molecule (mg catalyst)$^{-1}$ (in experiment C2/6) does the point of intersection change substantially. In spite of a degree of scatter in the desorption rate constants, λ_1 and λ_2 for the two regions of these curves, it is reasonable to assume that the same types of process are observed in each experiment.

The most obvious explanation of these phenomena is to attribute the initial fast desorption to material adsorbed on the silica support and the slower process to desorption from the metal. If it is assumed that the species adsorbed on the metal are continually replenished by those from the support, we may explain the change in kinetics as the point at which the rate of desorption from the support is exceeded by the rate of desorption from the metal. This model allows for almost complete metal coverage until very low levels of support coverage are reached. In this case we may associate the surface coverage at the change in kinetics with the metal coverage during the initial desorption period, although a precise determination of the metal coverage would depend on a precise knowledge of the desorption kinetics.

Assuming that the adsorption level at the transition between the two types of kinetics is dependent on the adsorption on the metal, we should expect this point to vary with the available metal surface area. Of the experiments with catalyst B(1.10% Pd/SiO_2), only B4/1 showed the change in kinetics at low surface coverage found in experiments with catalyst C. As we may see from figure 5.3, this may be attributed to an inability to follow the adsorption to

sufficiently low surface coverage in B2/1 and B3/1, due to the low specific activity of the chlorobenzene-Cl4 used. Experiment B4/1 shows a transition point in the semi-log plot at an adsorption of 1.03×10^{15} molecule (mg catalyst)$^{-1}$ compared with the average figure of ca. 4×10^{15} molecule (mg catalyst)$^{-1}$ from the C2 experiments. This is in remarkably good agreement with the carbon monoxide chemisorption values of metal areas given in table 5.20, which differ by a factor of 4.4 for the two catalysts. (We shall discuss the differences in metal surface area values from carbon monoxide chemisorption and electron microscopy in section 6.5).

It is of interest to note that the initial desorption rate constants, λ_1, observed for the experiments with catalyst B are lower than those with catalyst C where the metal area is higher. It was suggested in section 6.1 that the desorption from the support may proceed either directly or via reaction on the metal surface. In this case, a reduction in metal surface area should proportionally decrease the desorption rate via reaction, leading to a reduction in the overall desorption rate as found experimentally. The only apparent inconsistency in the results from the two catalysts is that the slow desorption rate constant, λ_2, is considerably higher for experiment B4/1 than those found with catalyst C.

Chlorobenzene desorptions from Pd/SiO_2 under N_2 flow.

In common with the desorptions in hydrogen flow, the chlorobenze-Cl4 desorptions from Pd/SiO_2 in nitrogen flow displayed distinct fast and slow sections on examination of the semi-log desorption curves (see section 5.3). While the curves were qualitatively similar to those under hydrogen flow, the values of the desorption rate constants and the adsorption at the intersection between the two regions of the curves, differed considerably.

A comparison of tables 5.4 and 5.5 shows that the values of λ_1 and λ_2 are consistently smaller under nitrogen flow conditions. In both cases, the reduction in desorption rate may be explained in terms of a lack of catalytic activity in the absence of hydrogen. It was noted in section 6.1 that the radiotracer desorption rate was slower for the silica adsorbent than the Pd/SiO_2 catalyst under constant flow

conditions. We attributed this to the absence of the hydrogenolysis reaction as an alternative mechanism to desorption. A similar situation pertains in the case of a Pd/SiO_2 adsorbent in nitrogen flow.

If we assume that the radioactive species observed during the slower part of the desorption curves are adsorbed on the metal, then various possible explanations may be given for the desorption retardation under nitrogen flow. Under hydrogen flow, the slow desorption may be brought about by three possible means: (a) a simple desorption process of the adsorbed species, (b) a displacement of the adsorbed species by hydrogen, and (c) reaction of the adsorbed species with hydrogen to give a more readily desorbed molecule.

In the absence of hydrogen, (b) and (c) are not possible unless a dissociative adsorption occurs. This in turn would be expected to give a more firmly held species and further retardation of the desorption. In experiment C2/8 (see figure 5.8), where three successive pulses of chlorobenzene-Cl4 were admitted to the catalyst under nitrogen flow, the desorption rate constant fell with each successive pulse (see table 5.5). The lack of any distinct change in the desorption kinetics at a particular surface coverage, however, indicates that no new, more firmly held species were present in significant amounts. The gradual slowing of the desorption rate might more readily be attributed to incomplete removal of hydrogen from the catalyst prior to the introduction of the chlorobenzene-Cl4 pulses. The hydrogen may conceivably have been held on the support by a "spillover" mechanism or by aosorption by the palladium metal (see section 1.2 for a discussion of these phenomena), and slowly released to react with the adsorbed species.

While the nature of the adsorbed species during the latter part of the desorptions must remain in doubt, it might be speculated that if, for example, adsorbed chlorobenzene is observed under nitrogen flow and adsorbed benzene under hydrogen flow, the difference in their respective desorption rates without hydrogen interaction might equally well account for the difference in the desorption kinetics.

In several of the experiments, the maximum observed adsorption attributable to the metal component of the catalyst exceeded that

observed under hydrogen flow. In experiment C1/1, the intersection between the slow and fast regions of the semi-log curve occurred at an adsorption of 1.71×10^{16} molecule (mg catalyst)$^{-1}$, compared with the maximum value of 4.39×10^{16} molecule (mg catalyst)$^{-1}$ observed in C2/1. This phenomenon, together with the effects observed in changing from nitrogen to hydrogen flow, will be discussed in section 6.5.

Benzene desorptions from Pd/SiO_2.

Although both fast and slow types of desorption process could be distinguished in some of the desorption curves for benzene-C14 in hydrogen flow, the nature of the curve was found to be dependent on the period of exposure of the catalyst to the initial benzene-C14 pulse. In experiment C2/11, where the tracer pulse was admitted to a normal hydrogen carrier flow, no distinct regions were observed in the semi-log desorption plot (figure 5.10). Prolonged exposure of the catalyst to the tracer pulse in experiment C2/14 however, gave more readily discernible straight-line regions of the semi-log desorption plot, the entire desorption being slower than observed in experiment C2/11. We may explain the difference in the kinetics by assuming that the adsorption rate of benzene on the metal was slow compared with that of chlorobenzene under similar conditions, and that in experiment C2/11 only a small amount of metal adsorption occurred on the metal. In experiment C2/15, the initial period of contact with the catalyst was further extended. Once again fast and slow regions of first order desorption were observed, but a tailing was found at the end of the second region, which might again be ascribed to the metal adsorbed species. The tailing may be attributed to a further reaction of the adsorbed molecules to a more stable surface species, brought about by the prolonged exposure to the high benzene concentrations.

These considerations aside, the primary purpose of the benzene desorption studies was to ascertain whether or not the slow desorption observed in the chlorobenzene experiments in hydrogen flow could be attributed to adsorbed benzene or a derivative. The values of λ_2

obtained in experiments C2/14 and 15, respectively 8.6×10^{-1} s^{-1} and 6.4×10^{-4} s^{-1}, compare well with the value of ca. 6×10^{-4} s^{-1} obtained for the chlorobenzene desorptions from the same catalyst sample (experiments 2/1 - 6). Comparing the intersections between fast and slow desorption regions, the benzene desorption following the longest initial radiotracer/catalyst contact period (C2/15) gave an adsorption value similar to the chlorobenzene desorptions C2/1 - 6 (i.e. 3.6×10^{15} molecule (mg catalyst)$^{-1}$). In experiment C2/14, with a shorter contact period, the value was somewhat smaller (2.6×10^{15} molecule (mg catalyst)$^{-1}$), which agrees with the proposed slow benzene adsorption.

The benzene desorption under nitrogen flow (C2/16) was rather more complex than those for chlorobenzene (see figure 5.11). The desorption curve appeared to be divided into three regions, as opposed to the two observed with chlorobenzene. The second region had a rate constant only marginally smaller than the slow region under hydrogen flow, but faster than the chlorobenzene desorptions under nitrogen flow. The third part of the desorption curve was considerably slower than the slow chlorobenzene desorption under nitrogen flow. The adsorption at the intersection between regions (2) and (3) of this curve, I_2, was comparable with that for the desorptions under hydrogen flow, suggesting that it is region (3) of the curve which should be used in comparing the desorption rates under nitrogen and hydrogen flows. The intersection between regions (1) and (2), I_2, was a factor of ca. 3 higher, suggesting that region (2) of the curve represents a process which has no direct analogue under hydrogen flow. The significance of these findings will be more fully discussed in section 6.5.

It is worthwhile noting here, however, that region (3) of this curve has a rate constant approximately an order of magnitude lower than those for the slow benzene and chlorobenzene experiments in hydrogen flow. We may once again interpret these findings in terms either of an enhanced desorption rate due to further reaction of associatively adsorbed benzene with, or displacement by, hydrogen, or alternatively, a dissociatively adsorbed benzene which requires the presence of hydrogen to effect desorption.

In experiment C2/13, a pulse of a mixture of non-radioactive chlorobenzene and benzene-C14 was passed over the catalyst in hydrogen flow. Comparing the resulting desorption curve with that from experiment C2/11 where only benzene-C14 was used (both experiments were conducted with a normal hydrogen flow throughout), the mixed pulse gave greater benzene adsorption on the metal. We may conclude that product benzene adsorbed on the metal derived from the non-radiotracer chlorobenzene, was exchangeable with the tracer benzene. Two conclusions may be drawn from this experiment. Firstly, that the slow desorption during chlorobenzene experiments is attributable to benzene or a derivative, and secondly, that the desorption of this species occurs in a step-wise fashion, involving a number of adsorption-desorption steps.

Chlorobenzene desorptions from Pd black.

From the previous desorption experiments, it was expected that the desorption rate of chlorobenzene from Pd black in hydrogen flow should correspond to the slow desorption rate constants observed under similar conditions for Pd/SiO_2 catalysts. In experiment PdBl/1, a two component semi-log desorption curve was found with a slow desorption rate constant of $3.4 \times 10^{-4}\ s^{-1}$, rather slower than the values obtained with catalyst C (4.47% Pd/SiO_2), and substantially slower than that obtained in experiment B4/1 with 1.08% Pd/SiO_2. The difference observed with varying Pd content might be explained by assuming that benzene or a derivative desorbs by a multi-step, adsorption-desorption mechanism in the absence of chlorobenzene. This process was also deduced from the desorption of a non-radiotracer chlorobenzene/benzene-C14 pulse. Under these circumstances, the desorption process would be retarded by increasing the available metal area.

Most of the adsorbed material, however, was desorbed at a much faster rate, and by analogy with the benzene desorption experiments, increasing the length of initial contact of radiotracer and catalyst was tried in experiment PdBl/3. This procedure was found to have the opposite effect in this case, the proportion of slowly desorbed radio-tracer being substantially reduced. Increasing the amount of radio-tracer initially adsorbed was found to increase the quantity of slowly desorbed species, but this fraction of the initially adsorbed molecules was never greater than 10%.

In spite of the difficulties involved in explaining the initial rapid desorption process from this catalyst, we may conclude that at least part of the observed desorption is compatible with metal adsorption being responsible for the slow desorptions under similar conditions from the Pd/SiO_2 catalysts.

Radiotracer displacements.

If we are to assume that the active part of Pd/SiO_2 surface is that on which the slow chlorobenzene and benzene desorptions are observed, then during the constant flow reaction and the initial part of the chlorobenzene desorption in hydrogen flow product molecules adsorbed on this part of the surface must be readily displaced by those from the support. If the desorption process was the rate determining step in the hydrogenolysis reaction, the reaction rate should be given by the product of the metal surface coverage and the desorption rate constant. This product gives a value of ca. 2×10^{12} molecule s^{-1} (mg catalyst)$^{-1}$ compared with an observed reaction rate of 1.52×10^{14} molecule s^{-1} (mg catalyst)$^{-1}$ for the same catalyst, calculated from the data of section 5.7. Product molecules adsorbed on the metal must therefore be displaced by unreacted or reacting chlorobenzene to account for the reaction rate.

To confirm this theory, in experiment C2/10 (see figure 5.9), a pulse of non-radioactive chlorobenzene was passed over a catalyst bearing the long lived radiotracer species in hydrogen flow. The radiotracer pulse was initially adsorbed under nitrogen flow to allow desorption from the support before hydrogen flow was introduced. The non-radioactive chlorobenzene pulse was introduced during the later, slow region of the desorption curve in hydrogen flow ((4) of figure 5.9). The ensuing rapid fall in count rate indicates a ready displacement of adsorbed radiotracer. More than 95% of the adsorbed tracer was displaced.

A similar experiment was conducted with an initial pulse of benzene-C14 adsorbed over a contact period of 3000 s. While a noticeable increase was observed in the desorption rate following the addition of non-radioactive chlorobenzene, this was less marked than in experiment C2/10. As noted previously, the initial long contact period of the benzene pulse with the catalyst produced a tailing during the slow desorption section of the curve which we

ascribed to the formation of more strongly bonded species on the metal. It may be concluded that such species are not readily displaced by chlorobenzene.

High temperature chlorobenzene desorptions.

The activation energy of desorption, E_d, may be expressed in terms of the heat of adsorption, ΔH_a, and the activation energy of adsorption, E_a (e.g. 182).

$$E_d = -\Delta H_a + E_a$$

For a non-activated chemisorption or physisorption, E_a is zero and the activation energy of desorption may be equated with the heat of adsorption. In all cases, the activation energy of desorption gives an upper limit for the heat of adsorption.

In the chlorobenzene desorptions from silica, the activation energy of desorption was calculated as 35.3 ± 2.2 kJ mol^{-1}. As this value is close to that of the heat of vaporization of chlorobenzene (ca. 36 kJ mol^{-1}), we may surmise that physically adsorbed chlorobenzene was observed. It is therefore somewhat surprising to find that the calculated value for the apparent activation energy of desorption for chlorobenzene from 4.77% Pd/SiO_2 was 20.6 ± 2.5 kJ mol^{-1}.

It was suggested earlier that chlorobenzene desorption from the support occurred largely via hydrogenolysis on the metal surface, direct desorption of chlorobenzene from the support to the gas phase playing a subsidiary role. We should therefore look for the rate determining step of the desorption in terms of the transfer of molecules from the support to the metal and hence to the gas phase. As the activation energy of desorption of a chemisorbed molecule must be at least as large as the heat of physical adsorption, we may conclude that the rate determining step of the desorption is not the desorption itself. Rather, the low value of activation energy suggests that surface migration of chlorobenzene from support to metal may be the rate determining step. The alternative mechanism for this transfer would be a desorption of chlorobenzene from the support followed by readsorption on the metal, but the activation energy for this process should be at least as large as that for the desorption from the support.

In conclusion, we may write three possible mechanisms for the chlorobenzene desorption:

(a) desorption from the support;

(b) desorption from the support followed by readsorption and reaction on the metal, the molecule finally being desorbed as benzene;

(c) surface migration from the support to metal, followed by reaction and desorption as benzene.

Mechanism (a) occurs in the absence of the metal, and may therefore be assumed to occur to some extent with metal present. This in turn indicates the probability of step (b) occurring. Process (c) is also necessary to explain the low value of activation energy of desorption observed.

6.3. Mechanism and kinetic analysis of chlorobenzene desorptions in hydrogen flow.

The desorption mechanism.

Having discussed the observations from the different types of desorption experiment performed, we wish now to assemble an overall picture of the various possible processes occurring as a basis for a kinetic analysis. Figure 6.1 gives an outline of the processes necessary to explain the experimental observations, primarily relating to the desorption rather than constant flow conditions. The evidence for each of the steps as labelled in the diagram may be summarised as follows:

A: Adsorption of chlorobenzene from the gas phase on the metal. While this adsorption can presumably take place, as in the palladium black experiments, it may be of little importance when large amounts of chlorobenzene are adsorbed on the support. The reverse reaction, the desorption of chlorobenzene from the metal, is probably of little consequence in the presence of hydrogen, as we may see from the slow desorptions under nitrogen flow.

B: Adsorption/desorption of chlorobenzene on the support. From the constant flow experiment with a silica sample (BSl/1) and the pulsed flow experiments under nitrogen flow, both processes may be assumed to take place in the desorption experiments. The observed desorption process may well consist of a series of desorption -

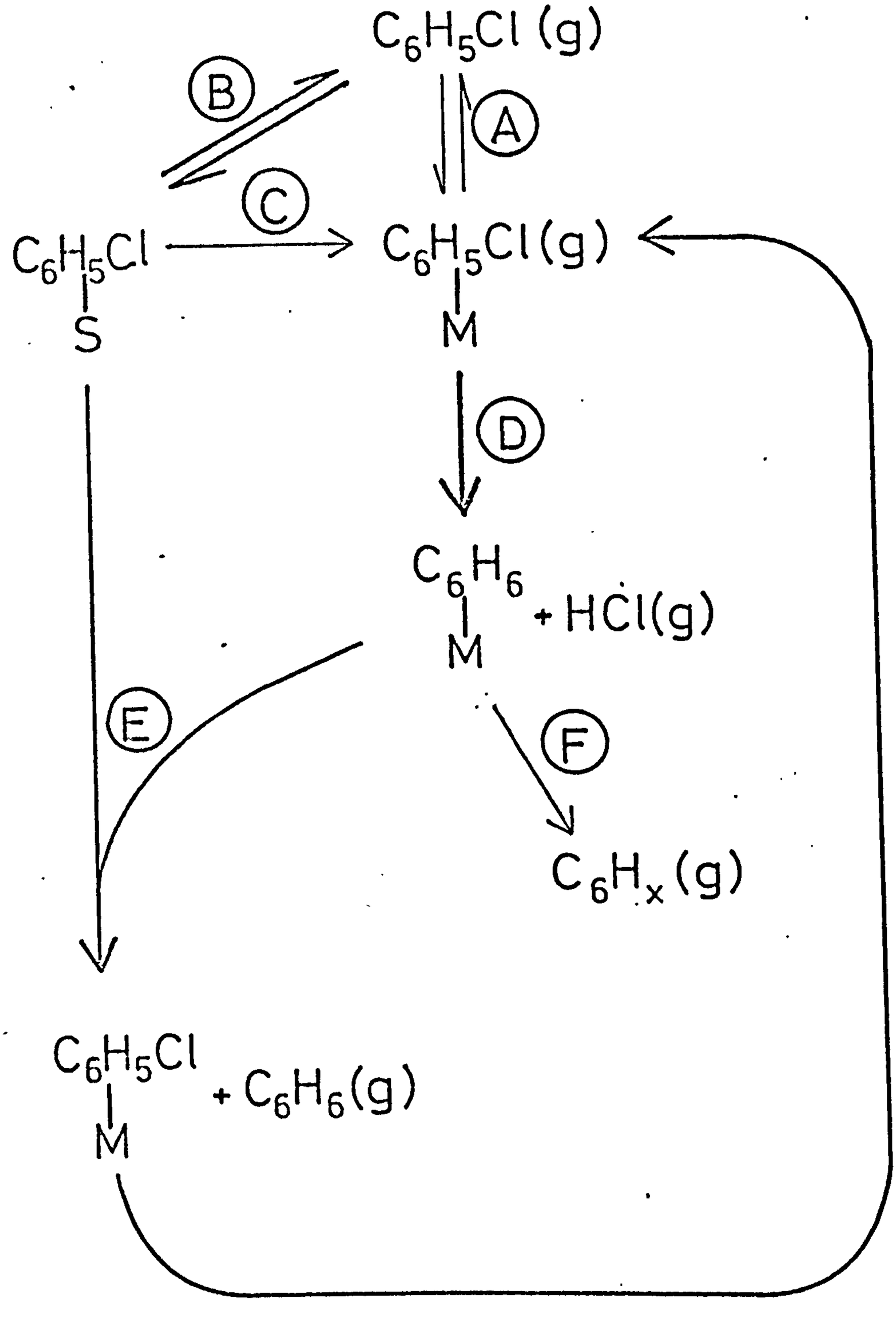

Figure 6.1. Outline of the processes occurring during the desorption of chlorobenzene from Pd/SiO_2 in H_2 flow. The heavy lines indicate the most probable route during the constant flow reaction.

adsorption steps culminating in removal from the catalysis chamber in the carrier gas flow.

C: Adsorption of chlorobenzene on the metal from the support. As chlorobenzene may desorb from the support and separately adsorb on the metal, part of the transfer from support to metal must occur via the gas phase. We have, however, seen that the apparent activation energy for the desorption process from the catalyst is lower than that from the support. This result suggests that a significant part of the support to metal transfer occurs by surface migration.

D: Hydrogenolysis reaction. In figure 6.1 we have represented this reaction as occurring between adsorbed chlorobenzene and adsorbed hydrogen. From section 3.2, however, the kinetics observed by Kraus and Bazant (131) allow the possibility of gas phase reaction of chlorobenzene with adsorbed hydrogen, i.e. a Rideal-Eley type mechanism. In this case the initially adsorbed species on the metal in step C may not be chlorobenzene but an intermediate formed by addition of a hydride ion. Steps C and D would then become indistinguishable but the overall kinetics of the desorption would be unaffected.

E: Displacement of metal-adsorbed benzene by chlorobenzene from the support. We have seen that the species slowly desorbed from the metal may be rapidly displaced by chlorobenzene. As the hydrogenolysis reaction occurs relatively rapidly, the rate controlling step may be attributed to the benzene displacement by chlorobenzene. Assuming high active surface coverage, if the hydrogenolysis reaction were rate controlling the desorption should be zero order with respect to support coverage. From the hydrogen flow chlorobenzene desorptions following various initial adsorption levels, the initial desorption rates have an approximately first order dependence on the support adsorption, showing the rate of supply of chlorobenzene to be rate limiting. The hydrogen chloride produced by the reaction has been shown as a gas phase product. From the results of the present study it was not possible to determine the presence of any intermediate adsorbed species or any obvious effect on the desorption kinetics due to adsorbed hydrogen chloride.

F: Desorption of hydrocarbon from the metal. The nature of the material desorbed in the latter, slow part of the desorption curves was not determined. We may, however, assume this to be benzene or a hydrogenated derivative. The process is in any case relatively slow, and should play little part in the reaction scheme under constant flow conditions or with high support coverage.

We have so far neglected the possible contribution of product benzene adsorbed on the support to the observed desorptions. We may conclude, however, that if benzene was held on the support to an extent comparable with chlorobenzene, the overall desorption rate should not be dependent on the reaction rate. Comparing the desorption experiments under nitrogen and hydrogen flows, benzene desorption must be rapid relative to that of chlorobenzene.

We may now give a sequence of steps which a chlorobenzene molecule is most likely to undergo in reaction under constant flow conditions or during the initial part of the desorption under hydrogen flow (shown in figure 6.1 with heavy arrows): B - E (as chlorobenzene) - D - E (as benzene).

The desorption rate equation.

The significant steps in the proposed desorption scheme may be listed as follows:

(1) $C_6H_5Cl\text{-}S \xrightarrow{k_1} C_6H_5Cl\ (g)$

(2) $C_6H_5Cl\text{-}S + M \xrightarrow{k_2} C_6H_5Cl\text{-}M + S$

(3) $C_6H_5Cl\text{-}M + 2\,H\text{-}M \xrightarrow{k_3} C_6H_6\text{-}M + HCl + 2\,M$

(4) $C_6H_5Cl\text{-}S + C_6H_6\text{-}M \xrightarrow{k_4} C_6H_5Cl\text{-}M + C_6H_6\ (g) + S$

(5) $C_6H_6\text{-}M \xrightarrow{k_5} C_6H_x\ (g) + M$

where $|_S$ represents a support adsorption site and $|_M$ a metal adsorption site. (g) indicates a gas phase species.

Before formulating a desorption rate equation, we should first consider the possible effects of surface heterogeneity on the rate constants for the above processes. It is a notable feature of the chlorobenzene desorption curves under hydrogen flow, that a fairly strict first order relationship exists between adsorption level and desorption rate for each region of the curves, indicating a possible lack of surface heterogeneity. We have, however, seen that some of the results obtained point to a multi-step desorption process which may result in only the "average" process being seen. For the regions of the surface on which adsorption was detected we shall therefore neglect effects due to heterogeneity.

Let x be the number of tracer bearing support adsorbed molecules and y the total number of tracer bearing molecules adsorbed on the metal at time t, and M the number of available metal adsorption sites. For the support desorption rate we may write

$$-\frac{dx}{dt} = k_1 x + k_2 x\,(M-y) + k_4 xy \qquad \text{Equation 6.1}$$

Assuming that the rate of adsorption of chlorobenzene on vacant metal sites and the displacement of benzene adsorbed on the metal by chlorobenzene adsorbed on the support are both controlled by the transport of chlorobenzene from the support to the metal, we may equate the rate constants k_2 and k_4. Equation 6.1 then simplifies to

$$-\frac{dx}{dt} = (k_1 + k_2 M)x \qquad \text{Equation 6.2}$$

The rate of change of the total metal adsorption may be given as

$$-\frac{dy}{dt} = k_5 y - k_2 x\,(M - y) \qquad \text{Equation 6.3}$$

This equation assumes that step (3) above is fast compared with steps (2) and (4). The overall desorption rate may be obtained by addition of equations 6.1 and 6.3:

$$-\frac{dz}{dt} = -\frac{dx}{dt} - \frac{dy}{dt} = k_1 x + k_5 y + k_4 xy \qquad \text{Equation 6.4}$$

where z = total number of tracer bearing molecules adsorbed on the catalyst = x + y.

During the initial part of the desorption curve, assuming that the fractional metal coverage is almost unity (i.e. $y \approx M$) and $k_5 y$ is small, we may approximate the desorption rate to

$$-\frac{dz}{dt} = (k_1 + k_4 M)x \qquad \text{Equation 6.5}$$

In the latter part of the desorption, the support adsorption may be assumed negligible and equation 6.4 becomes

$$-\frac{dz}{dt} = k_5 y \qquad \text{Equation 6.6}$$

Equations 6.5 and 6.6, which indicate an approximately first order relationship between the total adsorption level and desorption rate at the beginning and end of the desorption curves agree well with the experimental semi-log plots.

Since it was not possible to derive an integrated form of the total desorption rate equation, 6.4, directly, this was done by separately deriving integrated forms for x and y.

Equation 6.2 is a standard first order differential equation, having a solution

$$x = x_o \exp(-Kt) \qquad \text{Equation 6.7}$$

where $K = k_1 + k_2 M$

and x_o = value of x at time zero.

To integrate equation 6.3 it is simplest to proceed by elimination of t between equations 6.2 and 3 rather than x between equations

6.3 and 7. Since

$$-\frac{dy}{dt} = -\frac{dy}{dx} \cdot \frac{dx}{dt}$$

and $$\frac{dx}{dt} = -Kx \quad \text{(from equation 6.2)},$$

$$\frac{dy}{dt} = \frac{dy}{dx} \cdot Kx$$

i.e. from equation 6.3

$$\frac{dy}{dx} \cdot Kx = k_5 y - k_2 x\,(M - y)$$

or, rearranging

$$\frac{dy}{dx} - y\left(\frac{k_2}{K} + \frac{k_5}{Kx}\right) = -\frac{k_2 M}{K} \qquad \text{Equation 6.8}$$

This is a standard differential equation of the form

$$\frac{dy}{dx} + P(x)y = Q(x)$$

(see e.g. 183), which has the solution

$$y = I^{-1}\ [\ \int IQ(x)dx + C\ ] \qquad \text{Equation 6.9}$$

where $I = \exp\left(\int P(x)dx\right)$

and C = constant of integration.

Relating the symbols of equations 6.8 and 6.9

$$P(x) = -\left(\frac{k_2}{K} + \frac{k_5}{Kx}\right)$$

$$Q = -\frac{k_2 M}{K}$$

If $A = -\frac{k_5}{K}$, $B = -\frac{k_2}{K}$ and $D = -\frac{k_2 M}{K}$

then $I = \exp\left\{\int\left(\frac{A}{x} + B\right)dx\right\}$

i.e. $I = x^A e^{Bx}$ Equation 6.10

In order to evaluate the expression

$$\int IQdx = D\int x^A e^{Bx} dx \qquad \text{Equation 6.11}$$

we must first express $x^A e^{Bx}$ as an infinite series

$$x^A e^{Bx} = x^A \sum_{n=0}^{\infty} \frac{(Bx)^n}{n!}$$

$$= \sum_{n=0}^{\infty} \frac{B^n x^{n+A}}{n!}$$

From equation 6.11,

$$\int IQdx = D\int \sum_{n=0}^{\infty} \frac{B^n x^{n+A}}{n!} dx$$

$$= D\sum_{n=0}^{\infty} \frac{B^n x^{(n+A+1)}}{(n+A+1)n!}$$

i.e. $\int IQdx = DS(x)$ Equation 6.12

where $S(x) = \sum_{n=0}^{\infty} \frac{B^n x^{(n+A+1)}}{(n+A+1)n!}$.

Substituting equations 6.10 and 6.12 into 6.9, we obtain

$$y = x^{-A} e^{-Bx} (DS(x) + C) \qquad \text{Equation 6.13}$$

At time t = o, if $S(x) = S_o$, $y = y_o$ and $x = x_o$, rearranging equation 6.13 we have

$$C = y_o x_o^{\Lambda} e^{Bx} - DS_o \qquad \text{Equation 6.14}$$

Expanding equation 6.13 in terms of the rate constants gives us

$$y = x^{k_5/K} e^{k_2 x/K} \left(- \frac{k_2 M}{K} S(x) + C \right) \qquad \text{Equation 6.15}$$

where $$S(x) = \sum_{n=o}^{\infty} \frac{-\left(\frac{k_2}{K}\right)^n x^{\left(n - \frac{k_5}{K} + 1\right)}}{\left(n - \frac{k_5}{K} + 1\right) n!}$$

and $$C = y_o x_o^{-k_5/K} e^{- k_2 x_o/K} + \frac{k_2 M}{K} S_o$$

The expression for x, equation 6.7, may be substituted to give y in terms of t, and the total adsorption at time t is given by the equation

$$z = x_o e^{-Kt} + x_o^{k_5/K} \exp\left\{ - k_5 t + \frac{k_2}{K} e^{-Kt} \right\} \left\{ - \frac{k_2 M}{K} S(x) + C \right\}$$

Equation 6.16

Before proceeding to the direct application of this equation to the experimental desorption curves, we shall first describe a graphical approach using the differential forms of the rate equations.

Preliminary graphical analysis.

In section 5.2 values were recorded for the initial and final first order rate constants for the chlorobenzene desorptions in hydrogen flow, λ_1 and λ_2 respectively. From equations 6.5 and 6.6 respectively, we may interpret these values in terms of the rate constants for the proposed desorption mechanism:

$$\lambda_1 \approx k_1 + k_4 M = K$$

$$\lambda_2 \approx k_5 y$$

In an attempt to obtain a value of M, the number of metal adsorption sites, the following graphical procedure was adopted (figure 6.2 gives a schematic representation of the various plots used).

(1) A value of M was chosen initially as the point of intersection of the two "straight-line" regions of the semi-log desorption curve (see figure 6.2(a)).

(2) During the initial part of the desorption curve, the adsorption level on the metal, y, was assumed to be approximately equal to the number of metal adsorption sites, M. The initial value of M was therefore subtracted from the initial total adsorption values, z, and ln(z - M), plotted against time to give the type of plot shown in figure 6.2(b). The initial value of the slope of this plot was taken as - K.

(3) Assuming that the desorption from the support was a first order process throughout the experiment, the initial linear region of the ln(z - M) versus time plot was extrapolated to give values of x (the support adsorption) at later times in the experiment (see figure 6.2(b)).

(4) The values of x so obtained were subtracted from the values of total adsorption, z, to give a curve of the type shown in figure 6.2(c) for ln y (metal adsorption) versus time. The final slope of this curve was taken as - k_5.

(5) The value of k_1 was estimated from the initial chlorobenzene desorption rate from the same catalyst in nitrogen flow. As no reaction occurred in this case, the only major desorption process should be the direct desorption of chlorobenzene from the support. A value of k_2 was then calculated from the relationship

$$K = k_1 + k_2 M$$

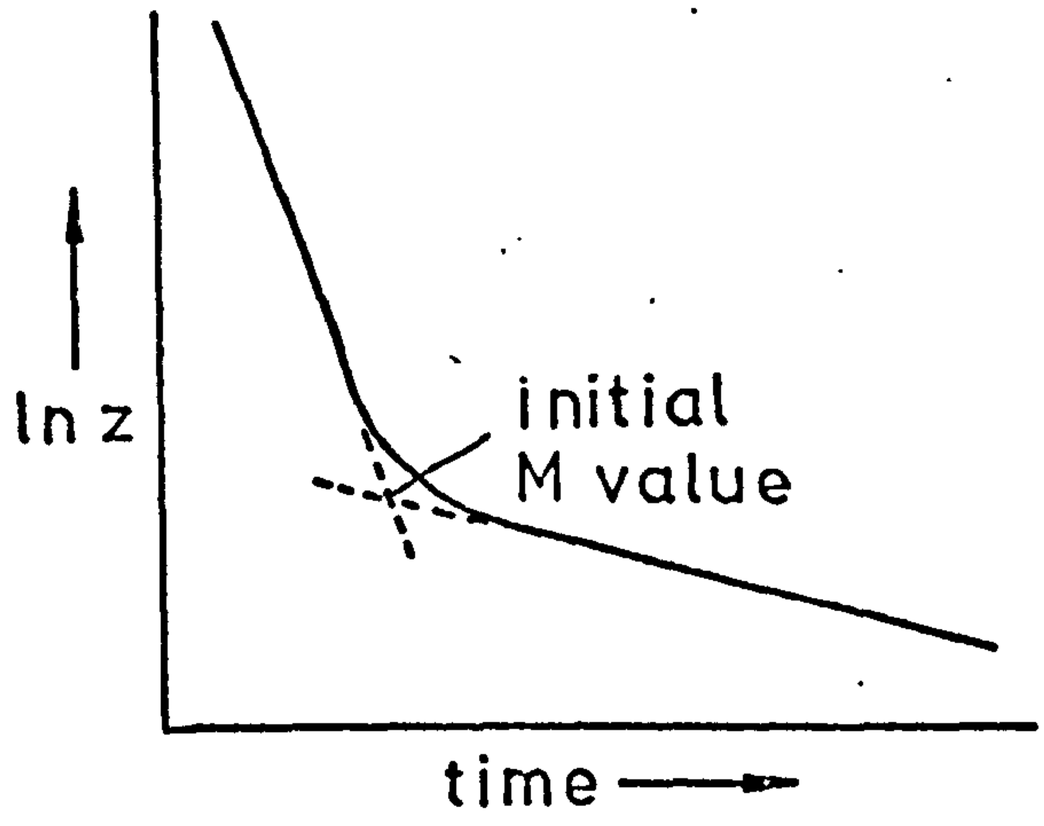

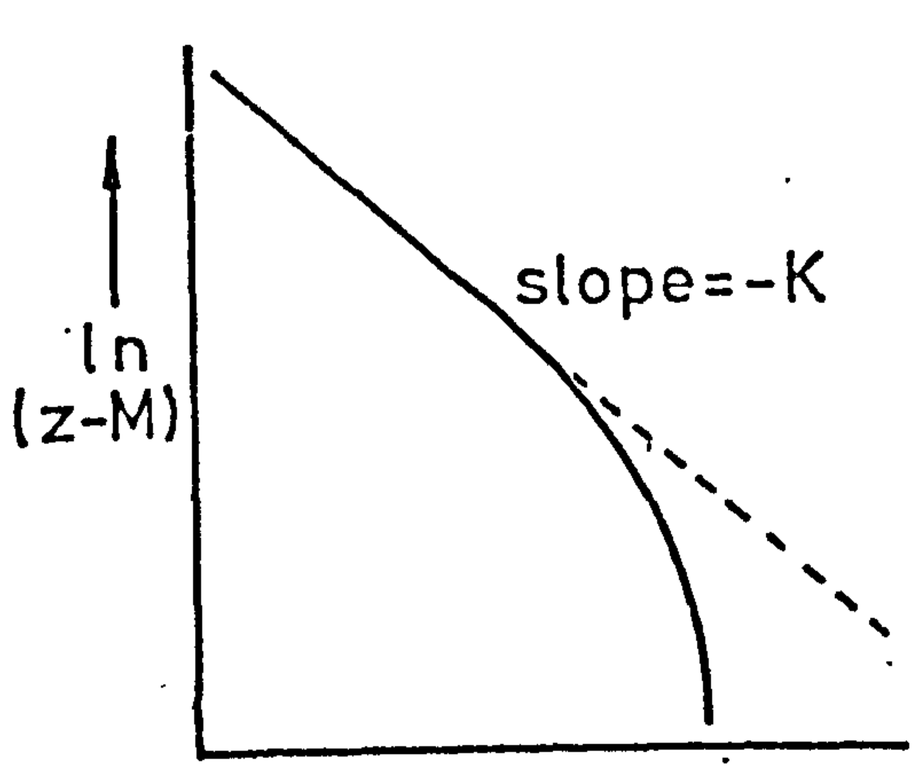

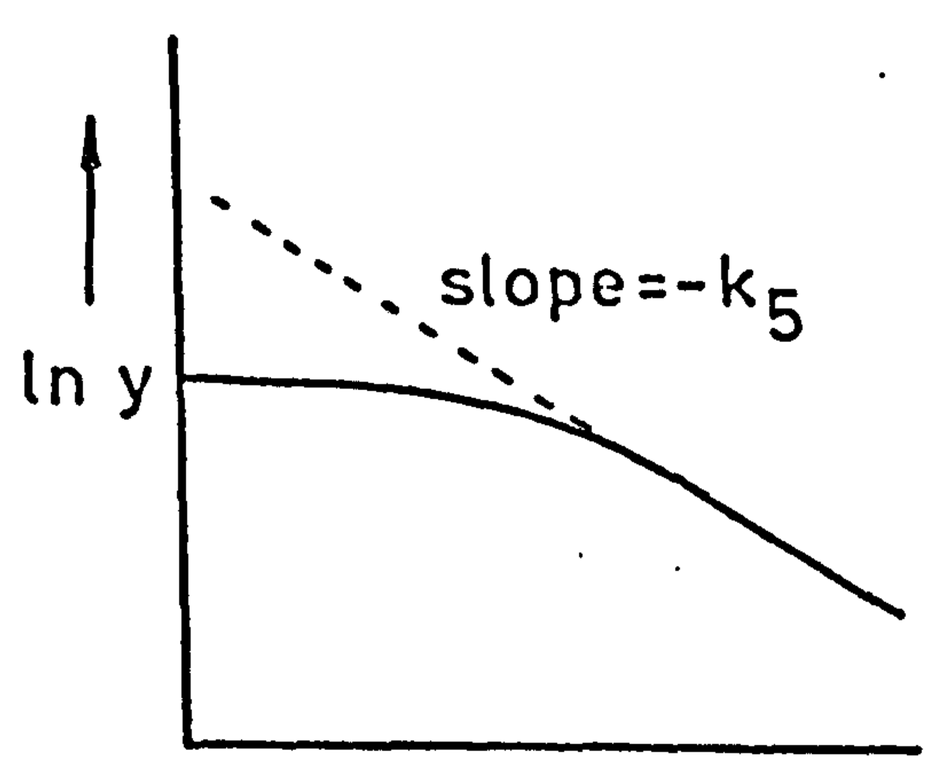

Figure 6.2. Schematic representation of the plots used in the graphical analysis of the chlorobenzene desorptions.

(6) The calculated values of the rate constants and the support and metal adsorptions were inserted into equation 6.4 to obtain values of the desorption curve gradient at various values of time, and compared with the values of the gradient measured from the experimental curve.

(7) (1) - (6) were repeated for different values of M chosen in the region of the initial value.

Since experiment C2/3 represented the most complete desorption curve from high to low coverage and had the greater accuracy inherent in the use of high specific activity radiotracer, the method of analysis outlined above was applied primarily to this curve. The optimum values obtained were: $M = 3.3 \times 10^{15}$ sites (mg catalyst)$^{-1}$, $K = 3.7 \times 10^{-3}$ s^{-1}, $k_1 = 5.2 \times 10^{-4}$ s^{-1}, $k_2 = 9.4 \times 10^{-19}$ s^{-1} site^{-1} (mg catalyst), $k_5 = 5.8 \times 10^{-4}$ s^{-1}.

As this method of analysis was felt to be rather cumbersome it was not extended to the other desorption experiments. The values of the rate constants and M calculated for C2/3 were, however, used as a basis for calculations from the integrated rate equation.

Desorption simulation.

As a first step towards finding the optimum values of M and the rate constants to fit equation 6.16, a computer program was written to calculate values of z for given values of M, K, k_2, k_5 and z_o. This program, "ØCL PLOT", written in language suitable for a Hewlett-Packard HP9320 programmable calculator (as was the program " ØCL FIT" discussed below), is given in appendix III.1. The program calculated values of z at 200 s intervals from t = o to t = 4000 s. Figure 6.3 shows the plot obtained using the values of M and the rate constants obtained by the graphical method from C2/3. This curve compares favourably with the type obtained experimentally, and shows that equation 6.16 is a good model for the observed surface processes.

Iterative curve fitting.

The program "ØCL FIT", given in appendix III.2, was designed to iteratively obtain optimum values for M, k_2 and k_5 for a given value of k_1 and a set of four points on the experimental desorption curve. The program functioned as follows:

(1) Initial values of k_1, k_2, k_5 and M were chosen, based on those from the graphical solution of experiment C2/3. Values of z

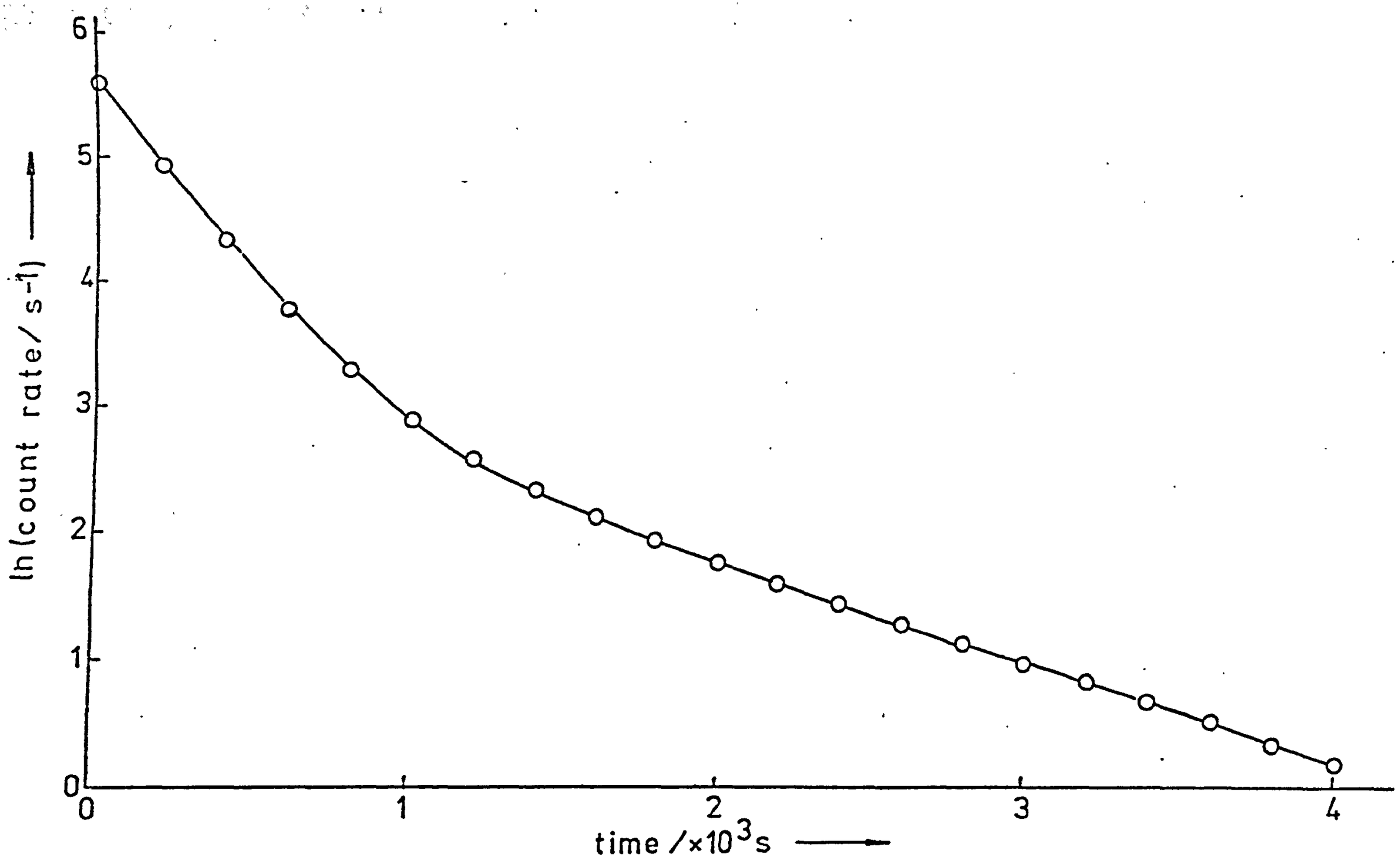

Figure 6.3. Calculated desorption plot using constants from the graphical analysis of experiment C2/3 by the program "ØCL FIT".

were taken from the experimental desorption curve for t = 0,600, 1400 and 3000 s. The time zero was chosen at a convenient point near the beginning of the desorption.

(2) Values of z were calculated by a subroutine based on the program "ØCL PLOT" for values of t at 600, 1400 and 3000 s respectively, using the initial values of k_1, k_2, k_5, M and z_o.

(3) The calculated value of z at t = 600 s was compared with the experimental value. If these values were within 0.3% of each other, the value of k_2 was accepted and the program passed to the next step. If the difference exceeded this value, k_1 was adjusted to an extent depending on the discrepancy and (2) repeated with the new value of k_1.

(4) The calculated value of z at t = 1400 s was compared with the experimental value. If the values differed by more than 0.3%, a new value of M was chosen based on the magnitude of the discrepancy, k_2 adjusted to maintain k_2M constant and the program returned to (2).

(5) Having obtained a satisfactory fit for z at t = 600 and 1400 s, the calculated and experimental values of z at t = 3000 s were compared. The difference was used to compute a better value for k_5. If the difference was greater than 0.3% the program once again returned to step (2) above, to calculate values of z with the improved values of k_2, k_5 and M.

(6) Having achieved agreement between the calculated and experimental values of z to within 0.3%, the final values of k_2, k_5 and M were printed out.

During the above procedure, the initial value of k_1 was maintained throughout. Table 6.2 gives values of k_2, k_5, M and K calculated in this fashion for a range of initial values of k_1. As it was found that a satisfactory curve fit could be obtained with any of these values of k_1, this type of analysis could not provide a unique set of rate constants. An inspection of the values given in table 6.2, however, shows little variation in the values of k_5, M and K over the range of k_1 values used.

In order to fix the values of k_1 and k_2 more definitely, a value of k_1 was sought from the chlorobenzene desorptions from catalyst C in nitrogen flow. The desorption plot from experiment C1/1 was chosen for this purpose, having the longest initial fast desorption section

Table 6.2. Rate constants and adsorption site densities calculated for experiment C2/3 using various values of k_1.

k_1 /	k_2 /	k_5 /	M /	K /
$x10^{-4}s^{-1}$	$x10^{-19}s^{-1}site^{-1}$ (mg catalyst)	$x10^{-4}s^{-1}$	$x10^{15}sites$ (mg catalyst)$^{-1}$	$x10^{-3}s^{-1}$
2.5	10.23	6.88	3.38	3.71
5.0	9.36	6.88	3.44	3.72
7.5	8.35	6.83	3.49	3.73
10.0	7.73	6.80	3.52	3.72
12.5	6.92	6.78	3.59	3.37
6.12	6.12	6.77	3.67	3.74

in the semi-log plot. By a method similar to the graphical approach outlined above, a value of M was chosen at the intersection of the slow and fast sections of this curve and subtracted from the initial values of adsorption, z. The initial slope of the curve, $\ln(z - M)$ versus t was taken as the rate constant for desorption from the support in the absence of reaction, i.e. k_1. The calculated value of k_1 was $8.11 \times 10^{-4}\ s^{-1}$.

With this value of k_1, the iterative curve fitting program was applied to the desorption curves from experiments C2/1, 2, 3 and 5 (experiment C2/6 was omitted as the initial adsorption level was less than the estimated value of M for the other curve). The constants calculated for each of the experiments are given in table 6.3. As an example of the agreement between the calculated and experimental adsorption values, figure 6.4 shows the experimental points from experiment C2/3 and the points calculated by the program "ØCL PLOT", based on the constants derived from "ØCL FIT" with $k_1 = 8.11 \times 10^{-4}\ s^{-1}$.

The values of M given in table 6.3 do not appear to vary regularly with the maximum adsorption level for the experiment. We may therefore attribute the variation to experimental error and assign a mean value to M of $(4.1 \pm 0.8) \times 10^{15}$ sites (mg catalyst)$^{-1}$. Similarly, k_5 appears to vary randomly. K, however, shows a definite trend to higher values with decreasing initial adsorption. As $K = k_1 + k_2M$, the variation must be attributable to one or more of k_1, k_2 and M. k_1 is the desorption rate constant for chlorobenzene from the support and is therefore unlikely to vary, and M, as mentioned above, shows no obvious trend. We may therefore ascribe the variation in K to that of k_2, the values for which do show a trend, although not as definite as that for K. As the value of k_2 is essentially calculated from K using k_1 and M, we may attribute the lack of clarity in the trend of k_2 to the inaccuracy of the individual M values.

If we therefore accept that k_2 increases with decreasing adsorption, may we reconcile this phenomena with the proposed desorption mechanism? The process governed by k_2 under this scheme is the displacement of product benzene adsorbed on the metal by chlorobenzene from the support. If this process was indeed controlled by the migration of chlorobenzene from support to metal, we would expect it to be first order with respect to the support adsorption. In this case the value of k_2 should be

Table 6.3. Rate constants and adsorption site densities for ambient temperature chlorobenzene desorptions in hydrogen flow calculated using $k_1 = 8.11 \times 10^{-4} s^{-1}$.

Experiment number	Max.adsorption $\times 10^{16}$ molecule (mg catalyst)$^{-1}$	k_2 / $\times 10^{-19} s^{-1} site^{-1}$ (mg catalyst)	k_5 / $\times 10^{-4} s^{-1}$	M / $\times 10^{15}$ sites (mg catalyst)$^{-1}$	K / $\times 10^{-3} s^{-1}$
C2/1	27.0	3.57	3.95	3.37	2.01
C2/2	14.0	5.44	7.02	4.66	3.34
C2/3	6.74	8.33	6.83	3.50	3.73
C2/5	0.85	7.37	6.27	4.81	4.35

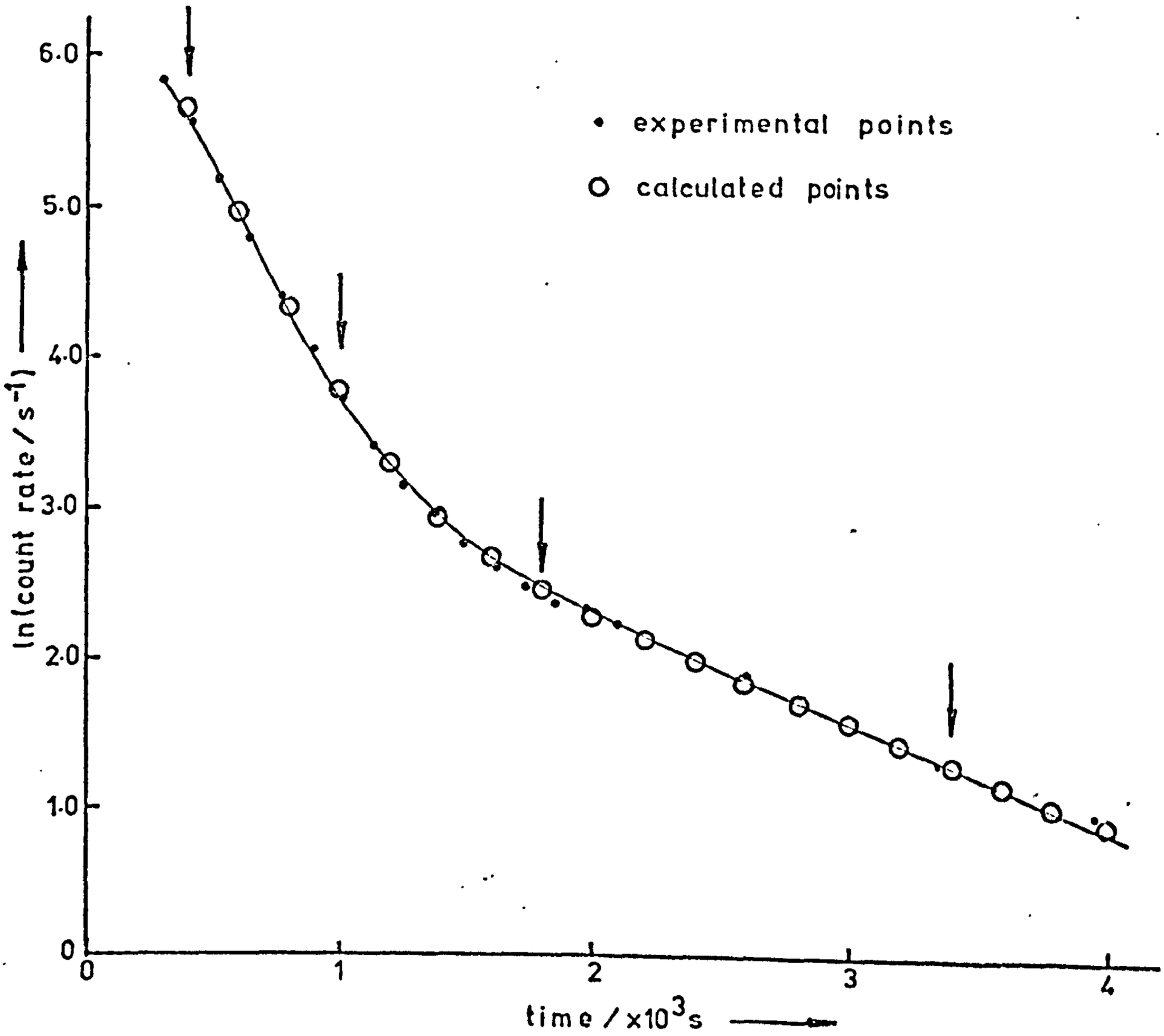

Figure 6.4. Experimental and calculated points from the experiment C2/3 desorption, with $k_1 = 8.11 \times 10^{-4} s^{-1}$. The arrows indicate the points to which the calculated curve was fitted.

independent of surface coverage. If, on the other hand, the process was controlled by the reaction of chlorobenzene to benzene on the metal, then the process might be expected to conform to zero order kinetics with respect to support coverage, assuming most of the metal sites to be occupied. This mechanism would result in an inverse proportional relationship between the adsorption and the value of k_2, taking k_2 as a first-order rate constant. As the value of k_2 varies by less than a factor of 3 over a corresponding change in maximum adsorption of a factor of ca. 33, we may assume only a slight deviation from a first-order dependence of the rate on the support coverage. It may be, however, that as the support adsorption is increased, with a corresponding increase in the rate of supply of chlorobenzene to the metal, the rate of exchange of benzene adsorbed on the metal with chlorobenzene from the support becomes comparable with the rate of the hydrogenolysis reaction. Under these circumstances, we would expect a falling off in the rate of exchange at high surface coverages, producing the type of reduction in k_2 shown in the values of table 6.3.

6.4. Correlations between desorption and reaction mechanism.

In the previous section we formed a kinetic scheme for the desorption of chlorobenzene from a Pd/SiO_2 catalyst and obtained a value for the number of adsorption sites taking part in this process. Before assuming that this value is equivalent to the number of sites taking part in the constant flow reaction, we should first attempt a correlation with the results obtained in the mechanistic studies of Kraus and Bazant (131) and Harper and Kemball (130).

In the kinetic studies of Kraus and Bazant (131) at 473 K, the hydrogenolysis reaction was found to be first order with respect to the chlorobenzene partial pressure. The results from the constant flow experiments of this investigation, at ambient temperature, tend to confirm this dependence. In our chlorobenzene desorption experiments, we observed an approximately first order relationship between the initial desorption rate (largely related to the reaction rate) and the support chlorobenzene adsorption. We may therefore interpret the first order kinetics in terms of the supply of chlorobenzene to the metal as the

rate determining step. Had the rate determining step been the surface reaction, we would have expected the adsorbed species to be largely chlorobenzene or an intermediate, resulting in zero order kinetics with respect to the support chlorobenzene adsorption. On the other hand, a fractional coverage of the active surface by chlorobenzene or an intermediate substantially less than unity would mean that the surface reaction proceeded more rapidly than the rate of supply of substrate chlorobenzene. In this case the observed first order kinetics should be found. Furthermore, we have seen that the slow desorption from the metal surface following a chlorobenzene pulse may be interpreted as the desorption of benzene or a hydrogenated derivative, substantiating the above proposal which requires that the surface be largely covered by product rather than reactant.

In the study of the deuterium/p - chlorotoluene reaction at 473 K by Kraus and Bazant (131), deuteration was found to occur only at the site on the aromatic ring vacated by chlorine during the deuterolysis, no deuterated reactant or further deuterated product being found. These findings were interpreted in terms of a charge-transfer chemisorptive bond primarily through the chlorine, of the type proposed by Matsen, Makrides and Hackermann (136) and Garnett and Sollich-Baumgartner (137). A bond of this type would allow little further interaction of the aromatic ring with the metal surface. Our observation that substantial benzene adsorption appears to take place during the reaction at 295 K indicates the possibility of deuteration of the product benzene. In their study of the deuterium/chlorobenzene reaction at 273 and 298 K, Harper and Kemball (130) also found no deuterated chlorobenzene over palladium films with static reaction conditions. It was found, however, that the amount of deuterated benzene product increased slowly as the reaction progressed and evidence was found in the latter part of the reaction for decomposition of the benzene. In our model for the reaction system, increasing amounts of benzene adsorption should have occurred as the chlorobenzene partial pressure was reduced, permitting further reaction and exchange. While the poisoning effect of chlorine or hydrogen chloride, proposed by Harper and Kemball, might explain the lack of further reaction or exchange by benzene in the initial stages of reaction, the concept is unnecessary with regard

to the absence of chlorobenzene deuteration if the chlorine charge-transfer bond is accepted.

Kraus and Bazant (131) proposed two possible mechanisms for the hydrogenolysis reaction: (a) gas phase chlorobenzene reacting with adsorbed hydrogen and (b) reaction of adsorbed chlorobenzene with adsorbed hydrogen.

Mechanism (b) requires the presence of adsorbed chlorobenzene, assumed to be in the form I below.

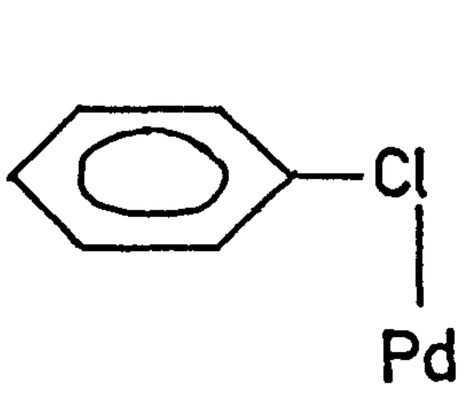

I

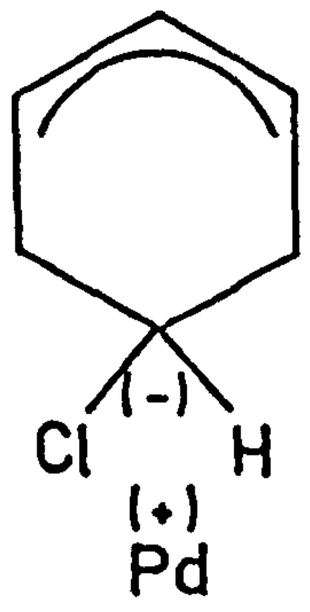

II

By applying the Hammett equation (132) to various substituted halogenobenzenes , analogy with the homogeneous reaction with bis (2 - methoxyethoxy) aluminium hydride, and the order of reactivities of the halogen substituents, Kraus and Bazant concluded that the reaction occurred by nucleophilic attack of a hydride ion on the halogen bearing carbon atom by an S_N2 mechanism. This process can be accommodated in either of the mechanisms (a) and (b) above, both requiring the formation of an intermediate of the type II above. An attempt to distinguish between mechanisms (a) and (b) must therefore rest on the presence or absence of adsorbed chlorobenzene (I).

The only circumstances under which we can be reasonably certain of the existence of the species I, are for chlorobenzene adsorption in the absence of hydrogen (i.e. in our experiments under nitrogen flow). On introducing hydrogen flow to chlorobenzene adsorbed under nitrogen flow, an initial rapid desorption was followed by a slow desorption with a rate constant smaller than that observed for the desorption under hydrogen flow throughout. We shall return to the

initial rapid desorption in the next section, but the slow desorption rate constant was comparable to that for the preceding desorption under nitrogen. In a similar nitrogen/hydrogen flow desorption experiment with benzene (C2/16), the desorption rate on hydrogen introduction was considerably higher, more readily comparable with the chlorobenzene/hydrogen flow experiments. It therefore appears that if reaction of the type I species to benzene does occur, the reaction is slow. While this evidence is not by any means conclusive, it does support the mechanism with gas phase (or support adsorbed) chlorobenzene reacting with adsorbed hydrogen (i.e. a Rideal-Eley type mechanism).

To explain the difference in slow desorption rates from catalysts with different metal contents, we postulated a multi-step desorption process. If this is the case, the mechanism for displacement of adsorbed benzene by chlorobenzene may take place by vacation of a site by product benzene (or a derivative) followed by hydrogen adsorption on the vacant site and subsequent reaction with chlorobenzene from the gas phase or support.

6.5. The active metal surface.

The first step which we should take in assessing the value of the adsorption site densities obtained in the desorption studies is a comparison with the metal surface areas. A difficulty arises here, however, in the discrepancies found in the figures of table 5.20 between the areas derived from CO chemisorption and electron micrograph particle size distributions. The figures are most readily explained by assuming a large number of small particles not detected by electron microscopy, but giving the large area measured by carbon monoxide chemisorption. It may also be noted, that for the Ir/SiO_2 catalyst, where higher resolution electron micrographs were obtained, the particle size distribution gave a larger area than that from chemisorption. For these reasons, and others which will become apparent later, we will accept the values obtained by carbon monoxide chemisorption.

For the number of adsorption sites active in the hydrogenolysis reaction, we will take the mean value of M given in table 6.3 for the desorptions from catalyst C(4.47% Pd/SiO_2) i.e. $(4.1 \pm 0.8) \times 10^{15}$ sites $(mg\ catalyst)^{-1}$. Comparing this figure with the value of 6.06 $m^2\ g^{-1}$ for the CO metal area yields an area of 1.47 nm^2 per adsorption site,

if complete metal coverage is assumed. Since the van der Waal's area of a chlorobenzene molecule is ca. 0.43 nm^2, the calculated value seems very high. Before coming to any conclusions, however, we must first examine the possible adsorption modes on the Pd surface.

The value of M used was obtained during desorption experiments where we expect benzene to be the major adsorbed molecule. We may therefore consider an adsorption model such as that proposed by Bond (184), where the benzene molecule lies parallel to the surface with the aromatic ring centred over a surface metal atom. This arrangement is necessary if we assume that the bonding occurs via a π - complex. The geometric arrangement shown in figure 6.5(a) for a Pd(111) surface, with no overlapping of the hydrogen van der Waal's radii, gives an area per molecule of ca. 0.59 nm^2. A similar area is obtained from the closest possible packing without distortion for benzene on the (100) face (figure 6.5(b)). The precise orientation of the molecule in this type of model is difficult to assess (see e.g. 185). Further complications arise when the nature of the metal particles is taken into account. In their study of benzene adsorption on supported platinum under a nitrogen carrier flow, Pitkethly and Goble (186) concluded that some compression of the type of models shown in figure 6.5 was necessary to give the observed surface Pt:benzene ratio of 6.1. These results suggest that the Pd surface of our catalyst was only partly covered by benzene.

In the chlorobenzene desorption experiments under nitrogen flow, one of the major differences from the results obtained under hydrogen flow was the larger adsorption noted in some cases at the onset of the slow desorption. In experiments C1/1 and 2, where the initial adsorption figure substantially exceeded the value of M for the hydrogen flow experiments (4.1×10^{15} sites mg^{-1}), the slow desorptions started at 1.7×10^{16} and 9.1×10^{15} molecule mg^{-1} respectively. Assuming that both of these figures correspond to metal adsorption, the former gives an area of 0.35 nm^2 per adsorbed molecule, much closer to the expected maximum adsorption. In this case, however, we are probably dealing with an associatively adsorbed chlorobenzene molecule. Although this molecule has a greater van der Waal's area, as the chemisorptive bond is thought to be largely through the chlorine atom, the steric

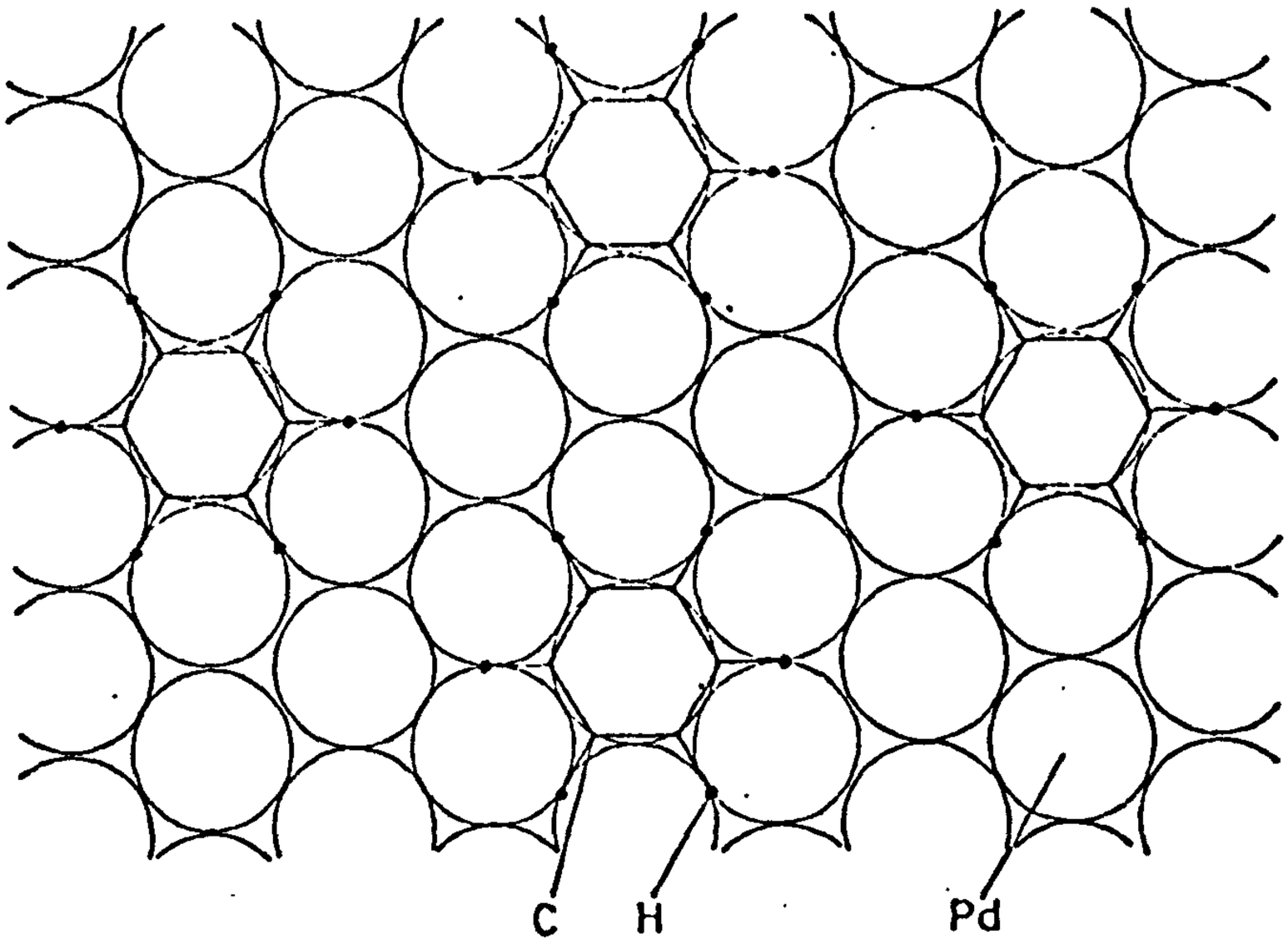

(a) Pd (111) face.

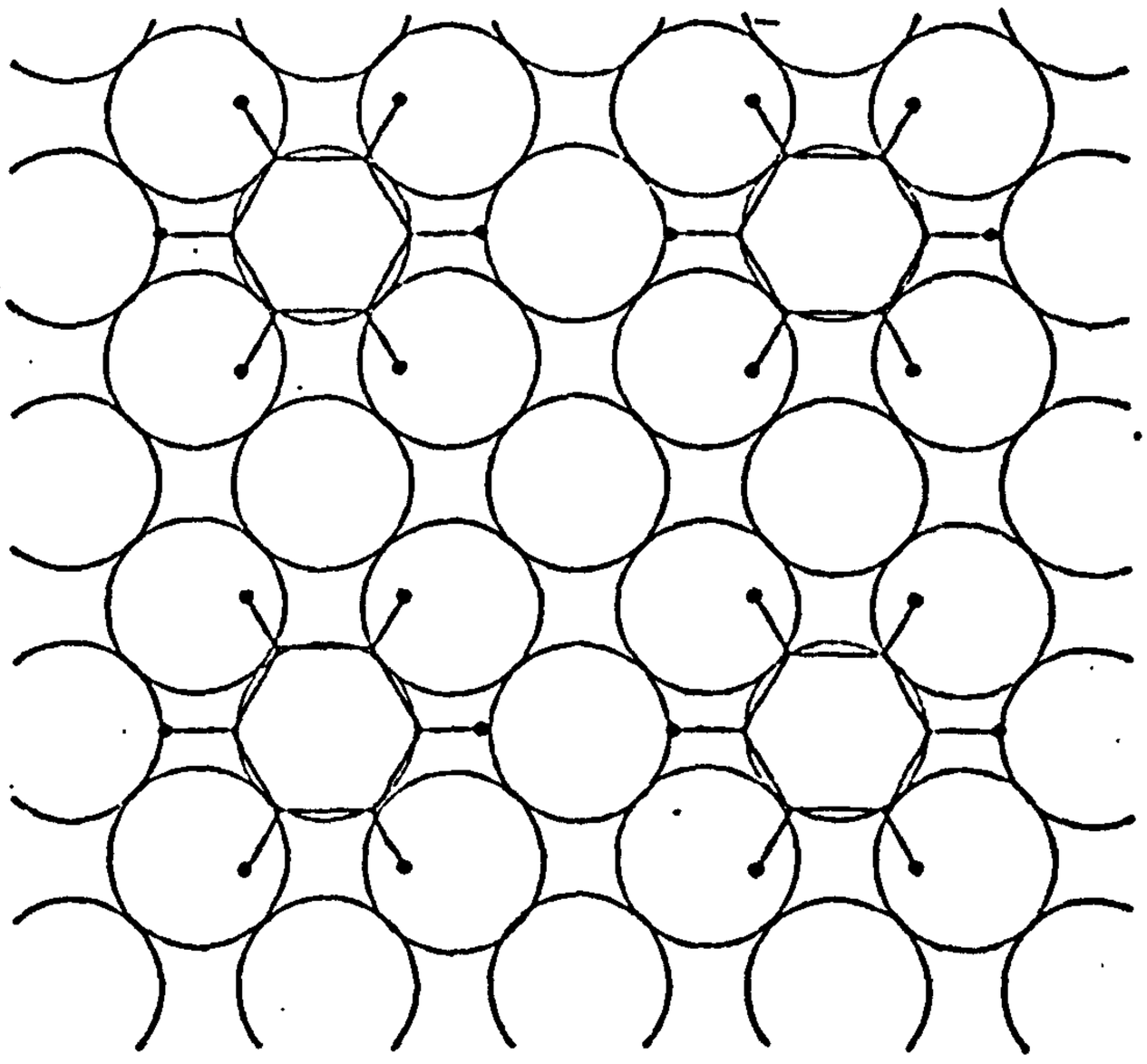

(b) Pd (100) face.

Figure 6.5. Possible benzene adsorption modes on Pd surfaces. Pd nearest neighbour spacing = 0.274 nm.

requirements for adsorption may be less stringent than for benzene. If, however, we consider the equivalent adsorption figure at the onset of slow desorption kinetics for benzene in nitrogen flow (C2/16), at 1.1×10^{16} molecule mg^{-1}, we see that the difference cannot be entirely explained by e.g. chlorobenzene adsorption with the aromatic ring perpendicular to the surface.

For the sake of clarity, we shall designate two types of adsorption site on the metal surface. The adsorption sites which are filled during the hydrogen flow chlorobenzene desorptions we shall name type A, and the remainder of the sites, on which we presume adsorption to occur under nitrogen flow, type B.

On introducing hydrogen flow to the chlorobenzene adsorbed on the metal during the slow desorption under nitrogen, in all cases an initial rapid desorption resulted, followed by a slower process. In each case, the onset of this latter, slow desorption occurred at adsorption levels comparable with or lower than the number of type A sites. It may be concluded that only part of the chlorobenzene adsorption under nitrogen flow was stable in the presence of hydrogen. The fact that this two-fold desorption was observed in all experiments, including those for which the adsorption level prior to hydrogen introduction was less than the number of type A sites, indicates that the desorption under nitrogen flow occurred with approximately equal facility from both types of site. During the course of the slow desorptions under nitrogen flow, no apparent differentiation was observed between sites of types A and B.

In contrast to these results, the slow desorption of benzene under nitrogen flow showed a distinct retardation at an adsorption level of 3.41×10^{15} molecule (mg catalyst)$^{-1}$, remarkably similar to the value of M from the chlorobenzene desorptions under hydrogen. The subsequent introduction of hydrogen flow showed only one type of desorption process. We may interpret this result as a preferential adsorption of benzene on type A sites under both nitrogen and hydrogen flow conditions.

The two types of adsorption site may also provide the clue to the chlorobenzene desorptions from palladium black. The small amount of slow desorption observed in these experiments may simply be attributed to a low concentration of type A sites. The initial fast desorptions

from this catalyst may be due to physisorption occurring over the chemisorbed hydrogen monolayer on the type B sites.

Having discussed the evidence for two types of adsorption site on the metal surface, we must now ask whether or not reaction may occur on the type B sites under hydrogen flow. We have so far assumed reaction to occur only at the type A sites for which adsorption was observed under hydrogen flow. The possibility arises that reaction may occur sufficiently rapidly on the type B sites to make the detection of the adsorbed species impossible in our experiments. If this was the case we should expect to observe a desorption process comparable to that immediately following the introduction of hydrogen flow in the nitrogen desorption experiments. In each experiment, this desorption was slower than the initial support desorption under hydrogen flow, and since it should occur at higher adsorption levels than the onset of the observed slow desorptions, would result in a region of intermediate desorption kinetics. Since no such process was observed, we may conclude that the hydrogen covered type B adsorption sites were unable to interact with chlorobenzene.

A possible alternative explanation of the two types of adsorption site would be to regard them essentially as the equilibrium coverages of an effectively homogeneous surface by hydrogen and adsorbed reactants or products, rather than being related to different types of metal surface. We may reject this proposal mainly on the grounds of two considerations. Firstly, if an equilibrium process was involved, as we move to lower support chlorobenzene adsorptions during the experiments under hydrogen flow, we should expect the equilibrium to favour hydrogen adsorption. The observed desorption curves show that the metal coverage is independent of the initial chlorobenzene adsorption where this is greater than a certain minimum value. Secondly, under nitrogen flow, the benzene desorption experiment clearly differentiates between the two desorption regions.

If the type B sites are hydrogen covered during the hydrogenolysis reaction, may we regard this region as the source of hydrogen which participates in the reaction? From hydrogen adsorption studies on palladium catalysts, e.g. by Sermon (187), the surface coverage should

be essentially complete in the pressure region under study at room temperature. The kinetic studies of Kraus and Bazant (131), conducted at 473 K, show that the reaction rate is dependent on a dissociative hydrogen adsorption. If the type B sites act as a hydrogen reservoir for the reaction, then this should be independent of the hydrogen pressure. If we assume a similar distribution of adsorbed hydrogen at 473 K as at room temperature, we should expect a zero order dependence on hydrogen pressure. We previously proposed a model for the reaction in which the product benzene desorbs, permitting hydrogen adsorption on the vacated site and subsequent reaction with gas phase or support adsorbed chlorobenzene. The dissociative adsorption process would provide the required order for hydrogen pressure of 0.5.

The final, and perhaps most important, question we shall ask concerning the active surface is whether or not our type A and B sites may be given a more fundamental assignment in terms of surface metal structures. It might be argued that the strong benzene adsorption on the type A sites is compatible with the surface geometry of the (111) palladium surface. The indiscriminate adsorption of chlorobenzene under nitrogen flow might indicate the relative unimportance of surface geometry when the aromatic ring is not directly involved in the chemisorptive bond. Assignments of this type are, however, highly speculative. To achieve any degree of certainty, it would be necessary to study the adsorption/desorption of chlorobenzene and benzene on either orientated metal films or single metal crystal surfaces, both in the presence and absence of hydrogen.

6.6. Conclusions on chlorobenzene studies.

Several major points emerge from the discussion of the previous sections, primarily related to the conditions employed in the present study, i.e. a total pressure of one atmosphere, with low chlorobenzene partial pressures, room temperature and a supported palladium catalyst.

(1) Only part of the metal surface (ca. 30%) appears to be active in the hydrogenolysis reaction, the remainder of the surface being hydrogen covered.

(2) The rate determining step of the reaction is controlled by the rate of supply of chlorobenzene to the metal surface, probably occurring

by a Rideal-Eley type mechanism with chlorobenzene reacting from the gas phase, and negatively charged hydrogen adsorbed on the metal.

(3) A significant fraction of the molecules adsorbed on the active metal surface is benzene or a benzene derived adsorbed hydrocarbon species.

(4) A substantial fraction of the reacting chlorobenzene is transported to the metal reaction sites by surface migration over the support in a physisorbed state.

An understanding of the specific types of metal surface site involved in the reaction might best be obtained from studies of adsorption on orientated palladium films or palladium single crystals surfaces. Infra-red spectroscopy and mass spectrometric analysis of the desorbed products may make a more positive identification of the adsorbed species participating in the reaction.

More generally, three aspects of the present study may be of a wider interest in the field of catalysts. Firstly, a comparison of the processes occurring during the hydrogenolysis and competitive reactions of chlorobenzene over other metal catalysts might be of interest with regard to the relative reactivities and selectivities in the reaction. Secondly, application of the desorption technique to other reactions, e.g. benzene hydrogenation, might be a useful tool in elucidating the relationship between adsorption and catalysis. Finally, if it proved possible to correlate our different adsorption site types with specific surface structures, studies of this type might prove valuable as a probe for characterising the surfaces of finely divided metal catalysts. The classification of reactions according to Boudart's terminology (53) as structure-sensitive or facile might then be given a more fundamental significance.

Part B. Ethylene Studies.

6.7. Short-lived adsorbed species - adsorption levels.

The greatest problem in interpretation of the count rate versus time data during the passage of ethylene-Cl4 pulses was to achieve an accurate assessment of the gas phase contribution to the catalyst chamber count rate. In presenting the results in the previous chapter, it was assumed that this contribution was constant for each catalyst sample used. Clearly, however, this was not the case. In certain experiments (see tables 5.13 and 17) this assumption led to the calculation of negative adsorption values. Experiments run under similar conditions but with different catalyst samples (e.g. G1/6 and G2/2) gave large discrepencies in the maximum reversible adsorption values calculated.

The method used in calculating gas phase count rate contributions may be regarded as giving values of the correct order, but as these were frequently found to be considerably larger than the estimated adsorbed phase count rates, a more accurate method of determining the adsorbed counts must be found within the data from individual catalyst samples. As a first step in this direction, we shall analyse the adsorption data on silica which, as a single component adsorbent, should be the most straightforward system.

Adsorption on Silica.

In section 5.13 we saw that the Arrhenius plot of the desorption rate constants for the short-lived species adsorbed on silica gave a value for the energy of activation of the desorption of 17.5 kJ mol^{-1}. This figure corresponds closely to that given by Ross and Oliver (138) for the limiting isosteric heat of physical adsorption of ethylene on graphite (18.4 kJ mol^{-1}). If we assume that physical adsorption of ethylene on silica was observed, we may apply the adsorption isobar given by de Boer (139):

$$\sigma = \frac{k\ e^{\Delta H_a/RT}}{\sqrt{(T)}}$$

where σ is the number of adsorbed molecules per unit area and k is a constant. Taking logarithms:

$$\ln \sigma = \ln \frac{k}{\sqrt{(T)}} + \frac{\Delta H_a}{RT} \qquad \text{Equation 6.17.}$$

Over a small range of temperature, changes in $\ln(k/\sqrt{(T)})$ should be negligible compared with those in $\Delta H_a/RT$. An Arrhenius type plot of ln(adsorption) versus 1/T should yield a straight line of slope $\Delta H_a/R$. From the plot given in figure 6.6, the equation appears to be obeyed at lower temperatures but rapidly falls away as the temperature is increased. If we assume that this deviation is due to an overestimation of the gas phase count rate, we may extrapolate the low temperature, linear section of the curve to give more acceptable values of adsorption at higher temperatures.

As a check on the validity of the equation, the slope of the curve at low temperatures gives a value for heat of adsorption of 19.5 kJ mol^{-1}, in good agreement with that obtained from the desorption rates. Further evidence for a substantial amount of adsorption at the higher temperatures comes from the fact that desorption rates were measureable in these experiments. Had little or no adsorption taken place, the ethylene-C14 pulses should have shown substantially less tailing.

From the extrapolated plot of figure 6.6, a new value of the ratio of gas phase counts in the catalyst chamber to those in the gas chamber was calculated, based on the experimental count rates from experiment BS3/3. As a new value of this ratio required the recalculation of adsorption values for the other experiments, the ln(adsorption) versus 1/T plot was still non-linear. After three such recyclings of the data, an acceptable straight-line plot was achieved. The calculated adsorption values from this plot and an extrapolated curve to higher temperatures are represented in figure 6.7 as open circles. The maximum reversible adsorption value for experiment BS3/7, based on the same gas count rate ratio, is shown as a filled circle. In this experiment a lower partial pressure of ethylene-C14 was used (34 torr) than in the other experiments (ca. 75 torr). The adsorption calculated was correspondingly lower.

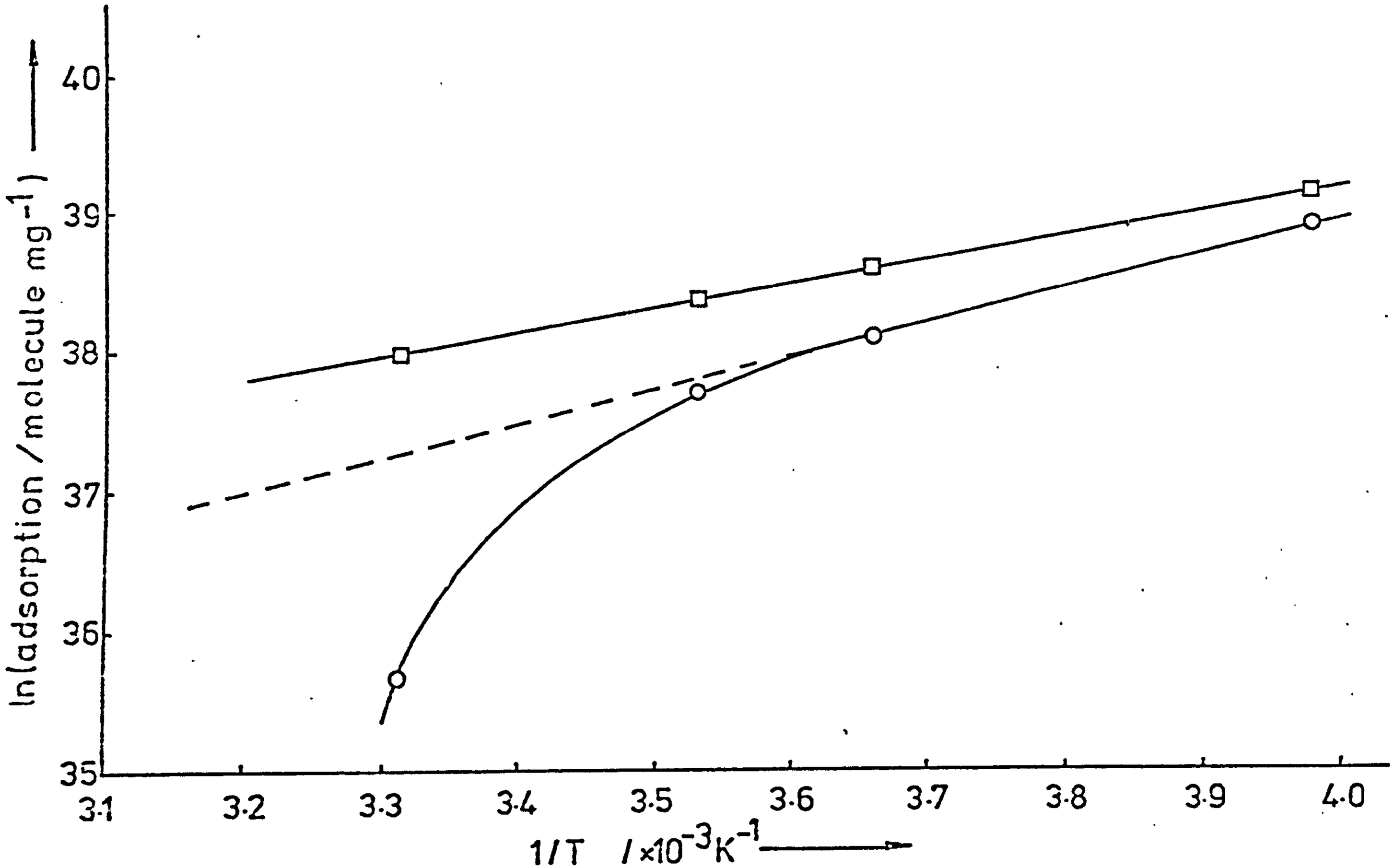

Figure 6.6. ln(adsorption) versus 1/T for ethylene-C14 on silica. o - original data; □ - 3rd. recycling (see text).

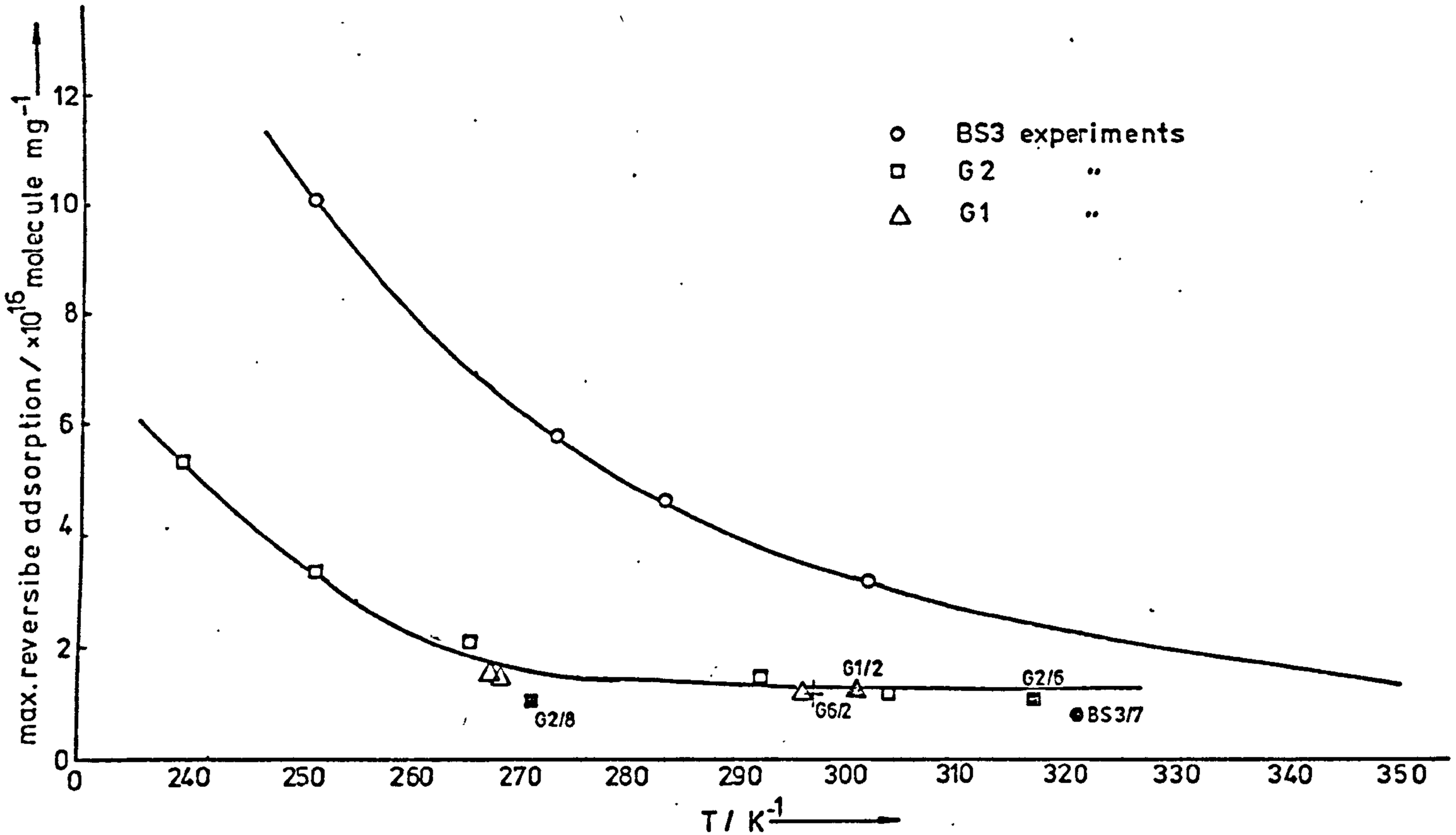

Figure 6.7. Corrected values of maximum reversible adsorption at various reactor temperatures during passage of ethylene-C14 pulses over Ir/SiO_2 and silica. For explanation of symbols, see text.

Adsorption on Ir/SiO_2.

The method used to determine the short-lived adsorption of ethylene on silica is obviously not applicable in the case of a metal bearing adsorbent where at least two distinct types of adsorption may occur. Another means must therefore be sought to determine adsorption levels.

The most complete sets of count rate versus time data for the Ir/SiO_2 catalyst were obtained with samples G1 and G2. There is, however, no direct means of relating this data to adsorption values in an absolute sense. We require at least one absolute value on the adsorption versus temperature curve. If we assume that under similar conditions adsorption occurred to the same extent on different catalyst samples, we may make use of experiment G6/2, where, with the reactor inverted and the observed gas phase count rate reduced to negligible proportions, the adsorbed radioactivity was measured directly. Comparing this value with the observed catalyst chamber count rate at the same temperature and with similar ethylene-Cl4 partial pressure, in the G1 and G2 experiments, we may calculate the gas phase contribution to the observed count rates. The calculated adsorption values based on this standard (gas phase counts in catalyst chamber: gas chamber = 0.346) are shown in figure 6.7 as open squares (G2 experiments) and triangles (G1 experiments). The adsorption value on which these calculations were based (experiment G6/2) is shown as a cross.

The shape of the resulting adsorption isobar differs considerably from that derived for adsorption on silica. In place of the steady fall in adsorption with increasing temperature, the Ir/SiO_2 catalyst gave a curve which appears to be assymptotic to an adsorption value of ca. 1×10^{16} molecule mg^{-1}. In experiments G2/8 and G2/6 where lower ethylene-Cl4 partial pressures were used, (23 torr and 25 torr respectively), the adsorption values calculated (shown in figure 6.7 as filled squares) were only slightly lower than those for the normal ethylene-Cl4 partial pressures of ca. 75 torr.

The most obvious interpretation of these adsorption values is to relate the constant adsorption at higher temperatures to adsorption on the metal, and those at low temperatures largely to support adsorption.

From experiments G4/4 and G5/1 (see section 5.11), where large ethylene partial pressures were used, melting of the plastic counting window indicated a catalyst temperature considerably in excess of that measured for the reactor body during passage of the ethylene pulses. The adsorption at low temperatures (below 270 K) might be largely explained by physisorption on the support if the catalyst temperature was in the region of 40 K higher than the measured values. At higher temperatures, however, we must assume an alternative type of adsorption.

The metal surface area of our Ir/SiO_2 catalyst, as determined by carbon monoxide chemisorption, was 5.06 m^2 (g catalyst)$^{-1}$, and 6.39 m^2 (g catalyst)$^{-1}$ by electron microscopy. Sinfelt and Yates (190) studied the adsorption of hydrogen and carbon monoxide on Ir/SiO_2, concluding that at "monolayer" coverage, the CO:surface Ir ratio was 0.58 and that for H:surface Ir, 0.78. Moyes et al. (191) have also studied iridium surface areas, in this case using the metal powder. They found that oxygen chemisorption was considerably in excess of carbon monoxide chemisorption. Thus, it appears that the actual iridium surface area may be considerably in excess of that measured by carbon monoxide chemisorption. If we accept the hydrogen chemisorption value of Sinfelt and Yates (190), then our surface area should be increased by a factor of 1.34 over the carbon monoxide value, i.e. 6.78 m^2 (g catalyst)$^{-1}$, a value similar to that obtained by electron microscopy. From the value of 2.12 ml carbon monoxide (at STP) adsorbed per g catalyst at monolayer coverage, we may similarly calculate the number of exposed Ir atoms as 4.2×10^{16} atoms(mg catalyst)$^{-1}$. While realizing that this value must be at best approximate, we shall accept it as the best available data for a comparison with ethylene adsorption.

If we now assume that the adsorption observed on the Ir/SiO_2 catalyst between 280 and 320 K(ca. 1×10^{16} molecule mg^{-1}) was largely due to adsorption on the metal, the ratio of adsorbed hydrocarbon to surface metal atoms is about 1:4. This value seems acceptable, and if we compare it with that of Reid et al. (95) for ethylene and carbon monoxide adsorption on Rh/SiO_2, where a 1:2, ethylene:metal atom ratio was found, we may have observed only partial metal coverage.

In their infra-red study of ethylene hydrogenation over Pt/SiO_2

under constant flow conditions, Sheppard et al. (116) observed physisorbed ethane at temperatures of ca. 200 K. Under their reaction conditions the hydrogenation rate appeared to be diffusion limited, and it is to be expected that this resulted in an environment largely of product ethane in the vicinity of the catalyst sample. In this respect, their conditions may be compared with those employed in the present study with effectively 100% conversion of ethylene to ethane. It is therefore plausible that the adsorption observed on our Ir/SiO_2 catalyst at lower temperatures was largely due to physically adsorbed ethane on the silica support.

Reid et al. (95) also observed support adsorption of ethylene in their radiotracer adsorption study on Rh/SiO_2 and Rh/Al_2O_3 catalysts. In this case, however, the quantity of ethylene adsorbed was relatively large for the pressure region studied (<6 torr), giving rise to the equivalent of several monolayer coverages of the metal by ethylene. The results were interpreted in terms of a spillover of hydrocarbon species from metal to support. We must not, therefore, neglect the possibility of a similar phenomenon occurring in the present study. Such a process is likely to be relatively slow, however, and the temperature range in which it was observed (ambient temperature) is considerably higher than that for which we observed large amounts of rapid, reversible adsorption. It seems more probable that if such a process was observed, it should be sought in the slowly removed adsorbed species rather than the transient species at present under discussion.

From these various considerations, we must conclude that the adsorption of primary catalytic interest is that observed above 270 K.

Constant flow ethylene-C14 adsorption.

We have seen that ethylene adsorption at our higher temperatures was largely independent of the ethylene partial pressure and the temperature. Experiment G1/2, which was carried out under constant, non-radiotracer ethylene/hydrogen flow conditions at 310 K gave rise to a similar adsorption of 1.2×10^{16} molecule mg^{-1}. This figure was calculated with the same gas count rate ratio as used for the other G1 experiments. This result indicates that the reversible adsorption data from the pulsed flow experiments is representative of the situation pertaining under constant flow conditions.

Ethane - C14 adsorption.

One of the principal questions to be asked about the calculated adsorption values is whether they are related primarily to ethylene adsorption and the hydrogenation reaction, or to adsorption of the ethane product.

In experiment G6/7, ethane-C14 was passed over the catalyst under conditions similar to those employed with ethylene-C14 pulses, at 294 K. 5×10^{15} molecule mg^{-1} reversible adsorption was observed. We may therefore conclude that, at this temperature, only part of the observed reversible adsorption with ethylene pulses may be attributed to ethane adsorption. At least part of the adsorption must have originated in adsorbed ethylene or a surface intermediate arising from ethylene.

Greater difficulty is found in the interpretation of the results from experiment G6/6, where an ethane-C14 pulse was passed over the catalyst at 253 K. Here, an adsorption of 2.2×10^{17} molecule mg^{-1} was observed, considerably higher than most adsorptions observed for the passage of ethylene pulses. Taken at face value, this result implies that the lower temperature adsorptions during the passage of ethylene pulses may be attributed to ethane adsorption, presumably on the support. Taken in conjunction with the anomalous adsorption value calculated for experiment G4/1, of 2.4×10^{17} molecule mg^{-1}, for the passage of an ethylene pulse over the catalyst at 252 K, both of these results must be rendered suspect. Previous experiments in the temperature range of G4/1 had shown much lower ethylene adsorptions (ca. 3.2×10^{16} molecule mg^{-1}). These results may have arisen from similar instrument malfunctions and we shall therefore not attempt to draw any firm conclusions from either experiment.

Ethylene-C14 adsorption in helium flow.

The reversible adsorption observed on the passage of an ethylene-C14 pulse over the catalyst in helium flow at 298 K (G1/7) was found to be 1.0×10^{16} molecule mg^{-1}. This value is similar to the adsorption observed at similar temperatures under hydrogen flow, and might therefore be attributed to adsorption on the metal component of the catalyst. Adsorption of ethylene on silica at the same temperature (see above)

may, however, have produced a larger adsorption than that observed in the present experiment. We must, therefore, regard this experiment as inconclusive.

Adsorption on Pt/SiO_2.

The methods used for estimating the gas phase contribution to the catalyst count rate were not applicable to these experiments, as no experiment was available with a known reversible adsorption on the catalyst. Had studies with Pt/SiO_2 been persued further, it would have been necessary to perform an experiment with the reactor reversed, as in experiment G6/2, followed by a comprehensive series of adsorptions over a series of temperatures. With the data available, however, no conclusion may be drawn with respect to any short-lived species which may have occurred.

6.8. Short-lived adsorbed species - tracer dynamics.

Desorption rates.

The basic equation of the time dependent radiotracer method was given in section 2.4 as:

$$\ln x = - \lambda t + \ln x_o \qquad \text{Equation 2.8}$$

where the first order desorption rate constant, λ , may be expressed as r/C_c. Here r is the reaction rate and C_c the number of exchangeable molecules taking part in the reaction. The assumptions made in deriving this equation may be stated as follows:

(a) the system is under constant flow conditions, i.e., chemically in a steady state.

(b) each adsorption of a reactant molecule is followed by subsequent reaction.

(c) only reactant molecules adsorb - product molecules having left the surface may not readsorb.

(d) either the surface on which the adsorption occurs is homogeneous, or the various types of adsorbed species are in rapid equilibrium compared with the adsorption/desorption rate.

In most of the experiments performed, condition (a) was not met. If the equation is to be applied under pulsed flow conditions, then we must assume that the observed desorption is representative of the molecules in the earlier part of the pulse as well as the "tail". It should be possible to check the validity of the assumptions made by comparing the calculated values of catalyst capacity with the observed adsorption values.

In the ethylene hydrogenation experiments over Ir/SiO_2, as the conversion to ethane was ca. 100%, we may take the ethylene flow rate during the pulse as our reaction rate. For experiments where a measurable desorption rate was observed we may now calculate values of C_c according to the relationship

$$\lambda = \frac{r}{C_c} \qquad \text{Equation 2.9}$$

Values of C_c calculated according to this equation are listed in table 6.4 along with the maximum reversible adsorption values, as calculated in the previous section. The agreement of the two sets of values is excellent, taking into account the method used in calculating adsorption data from the observed count rates. Apart from the implications

Table 6.4. Values of C_c calculated from desorption rates and maximum reversible adsorption values for the passage of ethylene-Cl_4 pulses over Ir/SiO_2 in H_2 flow at various temperatures.

Experiment number	Temperature/ K	Cc/ $\times 10^{16}$ molecule mg^{-1}	Maximum reversible adsorption/ $\times 10^{16}$ molecule mg^{-1}
G2/1	265	2.4	2.1
G2/5	251	4.0	3.4
G2/7	239	5.2	5.3

of the figures in deducing the nature of the surface processes occurring, they serve as a verification of the method used to obtain adsorption information from observed catalyst chamber count rates. We may deduce from these results that every molecule of ethylene is adsorbed on the catalyst, and that all adsorbed molecules are equivalent on the time scale of the desorptions (excluding the more firmly held species discussed in the following section).

It should be noted that, as the formation of ethane results in a reduction of the overall gas volume, a fall in the flow rate is to be expected over the length of the catalyst bed. With the initial ethylene pressures used, however, this should amount to less than a 10% deviation from the initial flow rate and a correspondingly small error in the calculated value of C_c. As this factor is difficult to assess and would result in no significant change in the agreement between observed and calculated values, it has been ignored.

In the case of ethylene-Cl4 adsorption on silica, the situation regarding the calculation of C_c values is somewhat different. With Ir/SiO_2, the flux of molecules through the adsorbed phase must have been at least equal to the reaction rate. For silica, this limitation does not apply, and we cannot therefore use the ethylene flow rate as a measure of this flux. Using the observed adsorption values, however, we may calculate values of the flux, f, with a relationship similar to equation 2.9. i.e.

$$f = \lambda C_c \qquad \text{Equation 6.18}$$

The values of f calculated by this equation are given in table 6.5. Values of the ratio of flux to total flow rate (f/F) are also listed, the units of f and F used being in terms of 1 mg of adsorbent. This ratio effectively gives the fraction of the ethylene molecules which enter the adsorbed "pool" on the silica surface, and is almost constant over the values of temperature and ethylene partial pressure studied, i.e. only about one molecule in five adsorbs on the silica.

Table 6.5. Values of the flux, f, of molecules through the adsorbed phase during the passage of ethylene-Cl4 pulses over silica in H_2 flow

Experiment number	Temperature/ K	Ethylene partial pressure/torr	f/ x 10^{16} molecule mg^{-1}	f/F
BS3/2	251	78	1.61	0.201
BS3/4	273	72	1.33	0.180
BS3/6	283	78	1.56	0.195
BS3/3	302	77	1.54	0.194
BS3/7	321	34	0.60	0.173

The results of these experiments with silica have obvious implications for the adsorption observed on Ir/SiO_2. We must conclude that the large adsorptions observed at low temperatures cannot be attributed to ethylene adsorption prior to reaction. At most, this could account for only 20% of the molecules participating. Initial adsorption on the metal presumably accounts for at least 80% of the molecules adsorbing. Adsorption of ethylene on the support following desorption from the metal seems improbable as the chances of adsorption should be no greater than that for molecules adsorbing directly from the gas phase. Two possible explanations may be advanced for the observed process:

(a) following reaction to ethane, the molecules are desorbed from the metal and readsorb on the support.

(b) some form of adsorbed hydrocarbon species on the metal migrates over the catalyst surface to the support, subsequently desorbing either directly or via the metal.

Support adsorbed species of the type (b) might be of a similar nature to those observed by Reid et al. (95). On introducing hydrogen to a

Rh/SiO_2 catalyst precovered with species ascribed to this type of adsorption, they found a rapid desorption corresponding to the amount of ethylene adsorbed on the metal surface, desorption of material from the support being a slower process. On the other hand, physically adsorbed ethane has been detected by Sheppard et al. (6.17) during ethylene hydrogenation. This type of adsorption, arising from species which have desorbed from the metal and been readsorbed, or from surface migration from the metal to support, therefore seems more plausible.

The above considerations have been primarily concerned with the nature of support adsorbed species. Although the nature of the metal adsorbed species may be of greater relevance in the catalytic reaction, there is no obvious way of correlating the data available in the present study with their structure. The fact that a constant adsorption of ca. 1×10^{16} molecule mg^{-1} was observed between 270 and 317 K suggests that a constant fraction of the metal surface is covered by hydrocarbon species over this temperature range. As demonstrated by Kemball (153), ethylene adsorption appears to occur more readily than that of ethane. If ethylene and ethane are present in the system, we should expect that at least a significant part of the observed adsorption will be due to ethylene. With a conversion of ethylene to ethane of ca. 100% however, if the conversion occurs rapidly enough we expect the ethylene to be but a transient species. While the adsorption is constant over the temperature range quoted, the desorption rate constant becomes too large to be measurable, and we may reasonably suppose it to increase with temperature. A constant value of reaction rate cannot give rise to a constant value of adsorption if we have a variable desorption rate. The flux of molecules through the adsorbed phase must therefore be greater than the reaction rate at higher temperatures to account for the increasing desorption rates. We may therefore expect a multiple adsorption/desorption process for molecules passing through the system. Under these circumstances the most probable surface species must originate from ethane.

At this point, we may take note of the results obtained with the catalyst reduced at high temperature (623 K). The extent of the short-lived adsorption was not measurable directly in a reliable manner, no standard being available for calculation of the gas phase contribution

to the observed count rate. As the experiment was conducted at 253 K, however, a desorption curve was obtained. Thus, we may calculate a value for the catalyst capacity from equation 2.9 of 4.1×10^{16} molecule mg^{-1}. This figure is almost identical with that obtained in experiment G2/5 (4.0×10^{16} molecule mg^{-1}) where the catalyst was reduced at the normal temperature of 423 K. We may also note that the value of initial retention following the tracer pulse was 9.0×10^{15} molecule mg^{-1}, which is typical of similar experiments on the catalyst samples reduced under normal conditions (see section 6.8). We may therefore conclude that the normal reduction procedure employed was adequate.

Adsorption rates.

In chapter 2 the possibility was mentioned of deriving information from adsorption rate plots in a fashion similar to that discussed above for the desorption plots. Equation 2.10, however, was derived for a constant flow situation, where tracer and non-tracer molecules are interchangeable, the processes occurring during adsorption therefore being similar to those during desorption. For a pulsed flow situation we cannot make this assumption. Any equation used in analysing adsorption processes must be derived for the particular system under study.

Let us first consider the adsorption process for the passage of an ethylene-Cl4 pulse over the Ir/SiO_2 catalyst. We saw previously that the rate of adsorption on the catalyst may be equated to the initial ethylene flow rate, i.e. the reaction rate, r. Simultaneously, the desorption rate may be given by $k_d x$, where k_d is the desorption rate constant and x the number of molecules adsorbed at time t. The rate equation for the adsorption can now be given:

$$\frac{dx}{dt} = r - k_d x \qquad \text{Equation 6.19}$$

or

$$\frac{dx}{r - k_d x} = dt$$

Integrating this equation between times 0 and t gives

$$\ln(r - k_d x) = k_d t + \ln r$$

or, rearranging

$$\ln(r/k_d - x) = k_d t + \ln(r/k_d) \qquad \text{Equation 6.20}$$

At time infinity, the system is at equilibrium with an adsorption x_{max}. From equation 6.19 we may therefore write

$$r - k_d x_{max} = 0$$

$$\text{i.e.} \quad x_{max} = r/k_d$$

Substituting into equation 6.20:

$$\ln(x_{max} - x) = - k_d t + \ln x_{max} \qquad \text{Equation 6.21}$$

This equation is identical with the integrated form of equation 2.10, derived for constant flow conditions. The observed slope, λ_a, of the $\ln(x_{max} - x)$ versus t plot should be identical to the desorption rate constant k_d.

The $\ln(x_{max} - x)$ versus t plots for the three G2 experiments in which measurable desorption rates were found are shown in figure 6.8. Table 6.6 compares the values of λ_a calculated from these plots with the previously determined values of the observed desorption rate constant , λ_d. As the two sets of rate constants agree to within the calculated standard deviations, we have further substantiation of proposed surface processes.

Table 6.6. Comparison of the observed adsorption and desorption rate constants during the passage of ethylene-Cl4 pulses over an Ir/SiO_2 catalyst in H_2 flow at various temperatures (LSA values).

Experiment number	Temperature/ K	λ_a/ s^{-1}	λ_d/ s^{-1}
G2/1	265	1.8 ± 0.4	2.2 ± 0.3
G2/5	251	1.5 ± 0.2	1.3 ± 0.1
G2/7	239	1.2 ± 0.2	1.0 ± 0.1

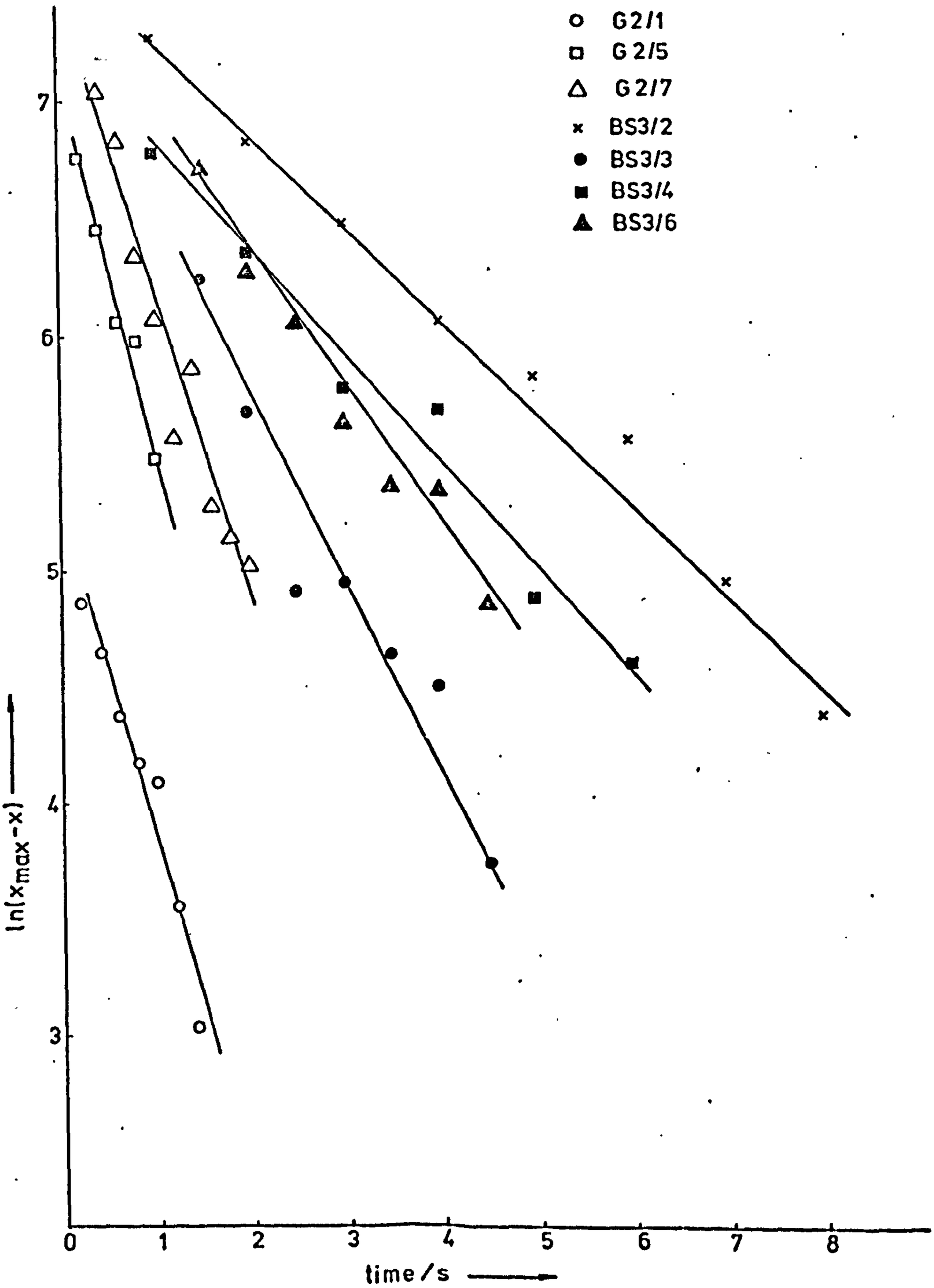

Figure 6.8. Adsorption plots for ethylene-C14 pulses on Ir/SiO_2 (G2 experiments) and silica (BS3 experiments).

In the case of ethylene adsorption on silica, the flux of molecules through the adsorbed phase was seen to be approximately proportional to the ethylene partial pressure, although less than the ethylene flow rate. We may therefore write an expression for the adsorption process:

$$\text{rate of adsorption} = k_a p_e (S - x)$$

where k_a is the adsorption rate constant, p_e the ethylene partial pressure, S the monolayer adsorption and x the number of adsorbed molecules at time t. We may assume the desorption rate to be simply $k_d x$, where k_d is the desorption rate constant. The overall rate may then be expressed:

$$\frac{dx}{dt} = k_a p_e (S - x) - k_d x$$

i.e. $$\frac{dx}{dt} = k_a p_e S - (k_a p_e + k_d) x \qquad \text{Equation 6.22}$$

This equation is in a form similar to equation 6.19 and may be integrated to give

$$\ln \left\{ \frac{k_a p_e S}{(k_a p_e + k_d)} - x \right\} = - (k_a p_e + k_s) t + \ln \left\{ \frac{k_a p_e S}{k_a p_e + k_d} \right\}$$

Equation 6.23

At equilibrium, $x = x_{max}$ and we may equate adsorption and desorption rates:

$$k_a p_e (S - x_{max}) = k_d x_{max}$$

i.e. $$x_{max} = \frac{k_a p_e S}{k_a p_e + k_d}$$

Substituting into equation 6.23 gives

$$\ln(x_{max} - x) = - (k_a p_e + k_d) t + \ln x_{max} \qquad \text{Equation 6.24}$$

Once again, the $\ln(x_{max} - x)$ versus t plot should give a straight line, but here the observed adsorption rate constant, λ_a, may not be equated with the desorption rate constant. The plots from the BS3 experiments with sufficient data are shown in figure 6.8. Table 6.7 gives the values of the observed adsorption and desorption rate constants, λ_a and λ_d respectively. The values of k_a are also listed, calculated according to the relationship

$$k_a = \frac{\lambda_a - \lambda_d}{p_e}$$

The values of k_a appear to be constant within the calculated standard deviations over the temperature range studied. This result confirms the assumption made in using equation 6.17 to extrapolate the adsorption isobar to higher temperatures.

It should be noted that adsorption and desorption rates are normally many orders of magnitude faster for physical adsorption on a plane surface than those found in these experiments (192). The observed rates are probably due rather to diffusion through the silica pore structure.

Occupancy Principle.

We have seen that the flux of molecules through the adsorbed phase during ethylene hydrogenation was equal to the flow rate of ethylene, F, throughout the pulse. This criterion is the principal requirement for an application of the Occupancy Principle. We may therefore proceed in spite of the normal requirement for a continuous reactant flow. Before assessing the value of Occupancy Principle calculations of the catalyst capacity, C_c, let us first consider the method of calculation. From equation 2.5 we have

$$C_c = F. \frac{I_c}{D}$$

where I_c is the total number of disintegrations occurring on the catalyst during the radiotracer pulse. D may be calculated using the length of the radiotracer pulse, t_p, the specific activity of the radiotracer, S_a, and the ethylene flow rate, F.

$$\text{i.e.} \qquad D = F_p S_a$$

Table 6.7. Adsorption and desorption rate constants for the passage of ethylene-C14 pulses over silica in hydrogen flow at various temperatures.

Experiment number	Temperature/ K	p_e / torr	λ_a / s^{-1}	λ_d / s^{-1}	k_a / $x10^{-3} s^{-1}$ $torr^{-1}$
BS3/2	251	78	0.43±0.04	0.16±0.02	3.5±0.5
BS3/4	273	72	0.50±0.04	0.23±0.01	3.7±0.5
BS3/6	283	78	0.58±0.04	0.34±0.01	3.1±0.5
BS3/3	302	77	0.80±0.11	0.63±0.05	2.2±1.6

Substituting into equation 2.5 we obtain

$$C_c = F.\frac{I_o}{\varepsilon_c}.\frac{1}{Ft_pS_a}$$

$$\text{i.e.} \quad C_c = \frac{I_o}{\varepsilon_c t_p S_a} \qquad \text{Equation 6.25}$$

where I_o is the total observed catalyst counts and ε_c the catalyst counting efficiency.

In effect, equation 6.25 simply averages the observed catalyst adsorption over the duration of the rectangular pulse. Any advantage gained by this approach over a simple calculation of adsorption at a given point in the tracer pulse must arise from taking a mean value for the total pulse. The method also incurs a disadvantage, however, in calculation of the count rate contribution from long-lived radioactive species on the catalyst. This contribution varied over the length of the radiotracer pulse (see section 6.9) and is therefore difficult to assess accurately when considering the total counts. On the other hand, the contribution at the end of the pulse may be accurately determined from the remaining activity following the passage of the pulse. Hence the reversible adsorption at the end of the pulse may be calculated more accurately.

Table 6.8 compares values of C_c calculated according to equation 6.25 for the G2 experiments with the maximum reversible adsorption values as shown in figure 6.7. The gas phase count rate contribution to the catalyst chamber counts was calculated by the method previously employed in determining the reversible adsorption values, i.e. the adsorption of 297 K was set equal to that observed in experiment G6/2 and the ratio of gas phase counts in the catalyst chamber : counts in the gas chamber (0.346) applied to the remaining experiments.

The similarity of the two sets of values obtained indicates that both of the methods of calculation are satisfactory. The maximum reversible adsorption values of section 6.7 are probably to be preferred, representing a more direct measure of the adsorption.

Table 6.8. Values of capacity calculated by the Occupancy Principle, C_c, and observed values of the maximum reversible adsorption for the G2 experiments.

Experiment number	C_c / $x10^{16}$ molecule mg^{-1}	Maximum reversible adsorption / $x10^{16}$ molecule mg^{-1}
G2/1	2.1	2.1
G2/2	1.3	1.4
G2/3	1.2	1.2
G2/5	2.9	3.3
G2/6	0.9	1.0
G2/7	5.3	5.3
G2/8	1.0	1.0

6.9. Long-lived adsorbed species.

In the present study, experiments were aimed primarily towards the short-lived species on the catalyst surface during ethylene hydrogenation. None the less, information has emerged on the hydrocarbon species retained on the catalysts. We shall attempt to draw some general conclusions about the formation and nature of the species.

Initial retentions.

A survey of trends in the initial radiotracer retention values with reaction conditions has to be made in the light of the different treatments to which the various catalysts were subjected in previous experiments. In the G2 series of experiments, however, the only major variables between experiments were the temperature and amount of ethylene-C14 pulsed over the Ir/SiO_2 catalyst. Even under these conditions, scrutiny of table 5.14 shows no obvious correlation between temperature or the amount of ethylene-C14 used and the initial retention. A good correlation may, however, be obtained by examining the values of "contamination" preceeding each experiment. These values represent a measure of the amount of retained radiotracer remaining from previous experiments. Table 6.9 lists these values along with the percentage of ethylene-C14 molecules in the original pulse retained by the catalyst. While the relationship between contamination and retention is clearly not linear, higher levels of contamination do appear to give higher values of retention. These results point to the possibility of a polymerisation process where molecules originating in the pulse may

Table 6.9. Catalyst contamination and percentage ethylene-C14 molecules initially retained after passage over Ir/SiO_2 in H_2 flow.

Experiment number	Temperature/ K	Contamination/ $\times 10^{15}$ molecule mg^{-1}	Molecules retained/ %
G2/1	265	0	0.31
G2/3	304	0.61	0.33
G2/2	292	0.83	0.37
G2/7	239	1.1	0.49
G2/5	251	7.2	0.62
G2/6	317	8.0	0.97

react with those previously adsorbed. Had the passage of previous pulses given rise to new adsorption sites, the amount of retention should have risen with successive experiments.

The above correlation gives no indication of the nature of the retained molecules, except that at least a proportion of them should be larger than C_2. The desorption curves show that at least three different types of adsorption occur, i.e. corresponding to the two regions of the semi-log desorption curve generally observed and those species which do not appear to be removed by hydrogen at all, at least on the time scale of the experiments. Each of these adsorbed species may arise from different adsorption sites with the same mode of adsorption, different modes of adsorption on similar sites or a combination of the two.

We can, perhaps, obtain some information about the possible location of the observed adsorption by examining the experiments with silica. Table 6.10 lists the values of contamination and percentage retention for each of these experiments. The first five listed were carried out under similar conditions and, with the exception of BS3/7, a correlation exists between the contamination and the retention, similar to that for the Ir/SiO_2 catalyst. The retention also appears to be enhanced in BS3/1 where the normal reduction procedure was not used. This may be due to the presence of water.

Reid et al. (95) adsorbed ethylene on silica and analysed the thermally desorbed species mass spectrometrically following evacuation of the sample at room temperature. It was concluded that the range of products formed (apparently including a substantial fraction of C_4 species) corresponded to alcohols rather than hydrocarbons. These results tend to confirm the proposed polymerisation process as being responsible for at least a proportion of the retained molecules on silica. Adsorbed water may enhance the alcohol formation. We may also conclude that a substantial proportion of the retained species observed in the G2 experiments are attributable to support rather than metal adsorption.

In several experiments, however, the initial retention values obtained with Ir/SiO_2 were considerably higher than those observed with silica, up to a maximum of 2.4×10^{16} molecule mg^{-1} (G6/4). The range of values obtained indicates that the retained species are not confined simply to a definite fraction of the surface. Rather

Table 6.10. Contamination and percentage of ethylene-C14 pulse initially retained on silica.

Experiment number	Carrier flow	Temperature / K	Contamination / $x10^{14}$ molecule mg^{-1}	Molecules retained / %
BS3/3	H_2	302	1.3	0.13
BS3/4	H_2	273	1.8	0.23
BS3/6	H_2	283	2.7	0.37
BS3/2	H_2	251	4.2	0.39
BS3/7	H_2	321	5.3	0.21
*BS3/1	H_2	251	0	1.51
BS3/5	He	273	2.3	0.50

* "Wet" silica sample i.e. not subjected to normal heat treatment prior to the experiment.

the uptake of retained species appears to take place throughout the ethylene-C14 pulse. If, for example, we scrutinise the count rate versus time plots during the ethylene-C14 pulse in experiments G6/2 and 4 (figure 5.36), we see that following the initial sharp rise in count rate at the beginning of the pulse, the subsequent, slower rise can be equated with the uptake of long-lived surface species. Particularly in G6/4, this uptake appears to cease only at the termination of the pulse. The addition of a second ethylene-C14 pulse before removal of retained species arising from the earlier pulse led to increased retention (e.g. experiment G1/6, figure 5.27).

At this point we must return once again to the migration of adsorbed hydrocarbon from metal to support described by Reid et al. for Rh/SiO_2 catalysts (95). The maximum retention observed in any experiment with Ir/SiO_2 was 2.4×10^{16} molecule mg^{-1} (G6/4) which, compared with the estimated number of surface Ir atoms, gives a ratio of surface metal atoms : retained ethylene of 1.74. We have previously estimated that the number of short-lived hydrocarbon species on the metal was about 1×10^{16} molecule mg^{-1}, which would tend to reinforce the idea that a significant proportion of the retained species must migrate to the support. On the other hand, we have also seen that some retention can be attributed to ethylene adsorbing directly on the support. The figures are inconclusive.

A major difficulty concerning the origins of the long-lived species is whether these may be attributed primarily to ethylene or ethane as precursor, both being present under hydrogenation conditions. Experiment G1/7 was performed with an ethylene-C14 pulse in helium flow, thus minimising the possibility of retained species arising from ethane. In this case, a high value of retention was recorded and introduction of a second ethylene-C14 pulse led to a total value of retention of 2.1×10^{16} molecule mg^{-1}. Under hydrogen flow, coverage of the metal surface by hydrogen and a rapid reaction to ethane may result in a considerably smaller effect due to ethylene.

A phenomenon not observed in helium flow, but observed in all experiments with hydrogen flow where a similar value of retention was observed , was a slow rise and fall in the count rate following the passage of the ethylene-C14 pulse (e.g. experiments G1/3, G1/6 and G4/1).

The precise origin of this effect is obscure, but must arise from preferential formation of long-lived species in selected areas of the catalyst bed "not seen" by the detector. Following the passage of the ethylene pulse, we may assume a diffusion, either via the gas phase or surface migration, to give a uniform distribution over the whole catalyst sample. It is interesting to note that this effect was also observed with ethane-Cl4 in experiments G6/6 and 7. We may take this as evidence for ethane giving rise to a significant portion of the retained species during the passage of ethylene pulses in hydrogen flow. The retention of ethane by supported metal catalysts has, in the past, been largely neglected in favour of the olefins. Ethane retention was, however, studied by Taylor, Thomson and Webb on a Pd/Al_2O_3 catalyst (45). On passing a series of ethane pulsed over the catalyst sample in helium flow, they found that the total ethane retention was only slightly less than that for ethylene at room temperature, but at higher temperatures, that of ethane fell while the amount of ethylene retained rose.

In conclusion, several processes appear to give rise to long-lived species during ethylene hydrogenation. While a certain fraction of the observed species may be attributed to direct adsorption of ethylene on the support, the nature and location of other species is uncertain. From the infra-red studies of Sheppard et al. (116) of ethylene hydrogenation over Pt/SiO_2, the same types of long-lived, σ-bonded species appear to be present on the metal as were observed from simple ethylene adsorption. It therefore seems probable that some of our long-lived species were of the type associated with ethylene on the metal.

Removal of long-lived species.

In several experiments, the desorption of retained species was monitored with time under hydrogen flow and at the temperature of the ethylene pulse. In the G2 series of experiments with Ir/SiO_2, 63-33% of the initially retained material was removed at temperatures between 251 and 304 K. Similarly, in experiments with silica, 64-70% of the retained activity was removed, although at 251 K (333/2) the desorption was extremely slow. In experiments with higher initial values of retention, e.g. G6/2 and 4, once again ca. 70% of the long-lived species were removed in hydrogen flow.

In comparing these experiments, the effect of temperature is not obvious. The desorption rates appear to vary randomly with temperature and separate experiments run at similar temperatures gave rise to different desorption rates. The only correlation between rates and temperature is found with silica experiments where a general tendency toward faster desorption at higher temperatures was observed. In experiment G2/7, however, where the initial temperature of 239 K gave rise to an extremely slow desorption rate, the temperature was raised to 327 K and then lowered to 273 K. Desorption proceeded from ca. 250 K with no other obvious enhancement at any particular temperature, but was retarded at ca. 315 K (see figure 5.33). On subsequently lowering the temperature, the desorption rate was again enhanced. The retardation of desorption as the temperature was raised might readily be explained by reaction of the surface species to give more firmly held molecules. The reversal of this trend on lowering the temperature again is not so readily explained, as there is no obvious reason for molecules which have reacted to more strongly adsorbed species reverting to their original form at lower temperatures. A possible explanation might again be found in terms of the metal-silica migration mechanism of Reid et al. (95). If we assume that the observed adsorption arose primarily from molecules adsorbed on the support which must migrate to the metal in order to desorb, then at higher temperatures they may undergo further reaction on the metal giving rise to more strongly adsorbed species. On subsequent lowering of the temperature, only molecules which had already reached the metal and reacted would be affected, the remaining support adsorbed molecules once again following the previous pattern of behaviour.

By analogy with the desorption of chlorobenzene from Pd/SiO_2, discussed previously, we might also interpret the two "straight-line" regions of most of the semi-log desorption curves in terms of this type of migration. The same type of desorption curve was also obtained, however, in the desorptions of retained species from silica. Obviously, this point is not conclusive.

On adsorbing ethylene-Cl4 on Ir/SiO_2 in helium flow at 296 K (G1/7), the initial desorption rate was considerably slower than for those experiments conducted under hydrogen flow. On introduction of hydrogen

flow, the desorption rate became comparable with those experiments performed in hydrogen flow throughout. An interesting feature of the experiment was the initial, rapid fall in count rate, immediately after the introduction of hydrogen flow, by 1.9×10^{15} molecule mg^{-1}. The extent of adsorption on the metal during the ethylene pulse is uncertain in this case, as ethylene adsorption on the support would probably have occurred. It seems possible, however, that the fraction of molecules rapidly desorbed by hydrogen could take part in the hydrogenation reaction. Less strongly adsorbed ethylene may only have been observed transiently during the passage of the ethylene pulse. In this case, we would expect that fraction also to be active in hydrogenation. Thus, we may not equate the number of ethylene molecules rapidly desorbed by hydrogen with the total number of molecules active during the hydrogenation reaction. We might, however, take the figure of ca. 2×10^{15} molecule mg^{-1} as a lower limit to the size of the active pool of molecules.

The effect of non-radiotracer ethylene on the retained radiotracer species was investigated in experiments G1/3 and 4. In each experiment, a pulse of non radiotracer ethylene in hydrogen flow produced a fairly rapid removal of part of the radioactivity, the larger pulse used in G1/3 having the greater effect. It is interesting that a smaller amount of ethylene was used in G1/4, but the pulse was of a greater duration (100 s as opposed to 80 s in G1/3). The longer duration was achieved by use of a slower carrier flow rate. This pulse would therefore have been largely ethane, while in G1/3, run under normal flow rate conditions, a greater concentration of ethylene was probable. It appears that ethylene is more efficacious in removing the retained material than ethane. A further point of interest in experiment G1/4 was the absence of any effect of non-radioactive ethylene on the remaining radioactivity after warming the catalyst to 313 K and allowing the system to come to an apparent steady state. This result is in agreement with the general observation of Cormack, Thomson and Webb (49), who found that ethylene-Cl_4 adsorbed on a variety of alumina supported metals (including iridium) was displaced to the same extent by treatment with hydrogen, non-radioactive ethylene, or a mixture of both.

The introduction of each non-radiotracer ethylene pulse in G1/3 resulted in an initial fall in count rate followed by a slower rise (see figure 5.25). We might explain this phenomenon in the same way as the rise and fall in the initial retention immediately following the passage of ethylene-C14 pulses. We previously attributed this phenomenon to surface species formed from gas phase ethane. The introduction of a pulse of non-radioactive ethylene without hydrogen at F in figure 5.28 supports this view. The pulse appears to have had effect only at its beginning and end. During the central section of the pulse a small rise in count rate was observed. If we assume small amounts of hydrogen to be present at either end of the pulse, due to mixing with the carrier gas, then we would expect ethane to be present at the appropriate times. An alternative explanation may, however, be given in terms of hydrogen being necessary for the desorption process.

In experiment G1/2, an ethylene-C14 pulse was passed over the Ir/SiO_2 catalyst in a constant ethylene/hydrogen flow and resulted in a retention of 2.2×10^{15} molecule mg^{-1} of the radiotracer. Whether or not this represents a constant build up of retained species, even after several minutes of reaction, it is difficult to decide. The result may simply be due to a constant exchange of a fraction of the long-lived species, similar to the displacement of retained ethylene-C14 by non-radioactive ethylene described previously.

Long-lived species on Pt/SiO_2.

The values of retention observed here (see table 5.12) were similar to those for the Ir/SiO_2 catalyst. The same types of slow desorption process were observed (F5/1, 3 and 5) and a similar displacement of retained radioactivity by non-radioactive ethylene (F5/2). Within the limits of the small number of experiments performed, we may accept most of the conclusions of the foregoing discussion on Ir/SiO_2 as applying also to Pt/SiO_2.

6.10. The reaction mechanism.

From the discussion on the short-lived species observed on Ir/SiO_2 during ethylene hydrogenation, two major points emerge:

(1) Over the range of temperature and ethylene partial pressures used, the adsorption of hydrocarbon on the metal appears to be approximately constant with a ratio of adsorbed hydrocarbon to surface metal atoms of ca. 1:4.

(2) At lower temperatures (< 270 K), substantial amounts of product ethane are adsorbed on the support. The desorption curves make no apparent distinction between metal and support adsorption, so that rapid interconversion of the two types of adsorbed species is probable.

The apparently constant metal coverage by hydrocarbon is in accord with the low order of the reaction with respect to ethylene observed by many workers (see section 3.3). Let us first consider the assignment of this adsorption primarily to species which may originate from ethane.

In their infra-red study of adsorption on supported nickel catalysts, Eischens and Pliskin (10) found no absorption spectrum when ethane was admitted to a hydrogen covered nickel surface. On admission of ethane to a bare nickel surface, however, absorption bands similar to those obtained with ethylene were observed. Kemball (153) found that the deuterium content of the ethanes produced from the deuterium-ethylene reaction at 173 K over tungsten, nickel, rhodium and iron films was attributable to the deuteration and ethylene/deuterium exchange reactions rather than ethane - deuterium exchange. These results suggest the improbability of ethane adsorption occurring under conditions of ethylene hydrogenation, although the same situation may not occur on an iridium surface.

Bond, Phillipson, Webb, Wells and Winterbottom have studied the deuterium - ethylene reaction over the Group 8 metals supported on alumina (193, 194). Their analysis of the initial product formation was based on that of Kemball (153) which assumes a steady state reaction scheme:

$$C_2X_4(g) \rightleftharpoons C_2X_4(a) \underset{-X}{\overset{+X}{\rightleftharpoons}} C_2X_5(a) \xrightarrow{+X} C_2X_6(g)$$

where (g) represents a gas phase molecule, (a) an adsorbed species and X may be either H or D. For iridium, it was calculated that 97% of the surface species were ethyl radicals at 257 K, due to the low probability of olefin desorption. The scheme, however, takes no account of the possibility of ethane adsorption to give adsorbed ethyl radicals. Even if the probability of ethane adsorption is low in the presence of significant amounts of ethylene, it may well be higher under conditions of total conversion to ethane. In the present study, we have seen that ethane adsorption on a hydrogen covered iridium catalyst is only about half of that occurring with ethylene at 294 K and may be due to support adsorption. A possible explanation might be found in the state of the catalyst surface under our reaction conditions. It is possible that adsorption sites vacated by adsorbed ethyl radicals on reacting to give ethane may be filled more rapidly by ethane than by hydrogen. In this case, when substantial amounts of ethylene are available for adsorption, ethane adsorption probably competes unfavourably with that of ethylene. In other words, the ethane adsorption which we suspect takes place may occur only in the time interval as the system relaxes between ethylene adsorption during the hydrogenation reaction and hydrogen adsorption following the reaction.

The above discussion has assumed that the hydrogenation reaction involves associatively adsorbed ethylene, a conclusion which seems inescapable from the deuterium exchange occurring during ethylene hydrogenation (153, 193, 194). The question of the form of hydrogen participating in the reaction is not clear from previous studies. While from the above mentioned ethylene - deuterium studies it appears certain that dissociatively adsorbed hydrogen is involved, this may occur either by dissociative adsorption on the metal preceeding reaction or by a reaction of associatively adsorbed ethylene with molecular hydrogen to give an ethyl radical and adsorbed hydrogen atom (159). The present experiments suggest a 1:4 hydrocarbon to surface metal atom ratio which may be compared with the value of 1:2 observed by

Reid et al. for ethylene on Rh/SiO_2 (95). The possibility exists, therefore, of a substantial area being available for hydrogen adsorption. From the results of Bond et al. (194) we must expect a high surface coverage of our iridium catalyst by ethyl radicals. Twigg's hypothesis (159) does not account for atomically adsorbed hydrogen to be present in greater amounts than ethyl radicals, so that the adsorbed hydrocarbon to surface metal atom ratio suggests the presence of at least some dissociative hydrogen adsorption independent of any reaction with adsorbed ethylene.

Koh and Hughes (158) studied the kinetics of ethylene hydrogenation over a silica - alumina supported nickel catalyst in a constant flow system. They constructed kinetic equations based on the various possible reaction mechanisms and found that three possibilities fitted the results, viz:

(a) reaction between adsorbed ethylene and molecularly adsorbed hydrogen with ethane desorption as the rate determining step.
(b) reaction between adsorbed ethylene and gaseous hydrogen when the rate determining step is the impact of hydrogen upon adsorbed ethylene.
(c) as for (b) but with ethane desorption as the rate determining step.

(a) was rejected because of reports of low hydrogen adsorption (159, 149), and (c) due to reports of rapid ethane desorption (160, 152), (b) therefore being accepted. Similar kinetic results had previously been interpreted by Pauls, Comings and Smith (157) and Koosternblatt and Ziegler (140) as a reaction between a small amount of adsorbed hydrogen with gas phase ethylene. For the reasons stated above, this mechanism seems implausible, but we must consider those of Koh and Hughes more carefully.

Both from our own observations and those of Bond et al. (193) there appears to be a substantial coverage of the surface by ethyl radicals. Ethane appears to give rise to an adsorption which persists at least on the time scale of the hydrogenation reaction. Combining this factor with the observation of a seemingly large number of metal adsorption sites available for hydrogen adsorption, we may conclude

that mechanism (a), the reaction between adsorbed ethylene and adsorbed hydrogen is most likely.

Since, under our experimental conditions, it was not possible to obtain conversions of ethylene to ethane of less than 100% in hydrogen flow, it is not possible to draw direct conclusions on the effect of the long-lived species on the reaction rate. We may observe, however, that no significant effect due to retained material was found on the short-lived adsorption. Beeck (151) and Jenkins and Rideal (152) have suggested that dissociatively adsorbed ethylene, whether in the form of "acetylenic complexes" or "surface carbide" result in poisoning of the hydrogenation reaction. Koestenblatt and Ziegler (140) studied this effect in a constant flow system with a Ni/Al_2O_3 catalyst operating at ca. 315 K. The various catalyst pretreatments employed, including hydrogen, ethylene and high temperature reaction, resulted in a reaction rate which, in the first two cases, took several hours to stabilise. This was interpreted in terms of slow changes in the extent of strongly adsorbed species. A considerable proportion of the retained species in the present study appear to be labile to an ethylene - hydrogen reaction mixture, and we may conclude that any equilibrium process involving such species would occur relatively rapidly. In all experiments, a small amount of retention was observed and the retained species were not removed on the time scale and at the temperatures employed. This type of adsorption probably corresponds to that responsible for poisoning in the study of Koestenblatt and Ziegler (14), although part of our observed radioactivity could be attributed to the support.

Perhaps the most important conclusion we may draw concerning the long-lived species during ethylene hydrogenation, is that at least one, and possibly several types of adsorption occur of a duration intermediate between those giving rise to the greater part of the ethane formed and the more traditional type of "acetylenic complex". Sheppard et al. (116) concluded that the normally observed, σ - bonded molecules were removed too slowly by hydrogen to participate in the hydrogenation reaction, so that these may well correspond to at least part of our "intermediate" duration adsorption.

6.11. Conclusions on ethylene hydrogenation.

In chapter 3 it was suggested that many of the inconsistencies and difficulties in interpretation of previous studies of ethylene hydrogenation might be attributed to a variety of possible surface processes occurring simultaneously. From the present study there appear to be at least ten different types of adsorption which probably occur during the hydrogenation reaction under our conditions viz:

(1) physical adsorption of ethylene on the support

(2) physical adsorption of ethane on the support

(3) transitory adsorption of ethylene on the metal, corresponding to the form active in hydrogenation

(4) transitory adsorption of ethane on the metal on a time scale similar to (3) - (3) and (4) combined give rise to a total adsorption equivalent to approximately one molecule adsorbed to four surface metal atoms

(5) and (6) retained species on the support, corresponding to the fast and slow sections, respectively, of the semi-log slow desorption curve - these may well be polymeric

(7) retained species on the metal, arising from ethylene adsorption, slowly removed by hydrogen and displaced by ethylene - these species may be subdivided as for (5) and (6) on the support, but there is no direct evidence for these two types

(8) retained species arising from ethane which may diffuse freely over the catalyst bed - these may be due either to metal or support adsorption

(9) species not removed from the support under hydrogen flow at room temperature

(10) species not removed from the metal under hydrogen flow or during ethylene hydrogenation at room temperature.

Species of types (3) and (4) are clearly the most important in the hydrogenation reaction. Combining our own evidence with that of other workers, the reaction probably occurs between associatively adsorbed ethylene and adsorbed hydrogen.

It is obvious, however, that from the variety of possible adsorption types, future concomitant studies of adsorption and catalysis alone will not be sufficient to gain insight into the mechanism of ethylene hydrogenation over metal catalysts. Any such study must include some means of distinguishing between the different adsorption types. The present attempt to differentiate on the basis of kinetic behaviour has shown clearly the complexities of the problem. These complexities will remain so long as methods are used which only measure adsorption rather than methods which will reveal the nature of individual species. Infra-red spectroscopy may eventually provide a more adequate means of studying the reaction, provided that samples can be prepared in such a way that diffusional limitation of the kinetics is avoided.

Part C. General.

6.12. Conclusions.

The tracer dynamics methods.

In each of the catalytic systems studied, it has been possible to obtain certain information about the processes occurring on the catalyst surface during reaction. The basic aim of each method described in this chapter was an estimation of the size of the "active pool" of molecules adsorbed on the catalyst surface during reaction. Given that this quantity does not differentiate between different forms of adsorbed material, there is no reason to doubt the validity of the calculations used. In both systems studied, however, it was necessary to remove the constant-flow limitation on reaction conditions originally envisaged. In the ethylene studies this was largely due to practical considerations, i.e. temperature control. In the chlorobenzene studies the difficulty was of a more fundamental nature, arising from the need to distinguish between active (chemical) adsorption and inactive (physical) adsorption. Indiscriminate use of this type of study may, therefore, give rise to values of adsorption bearing little relationship to the catalytic reaction. The Occupancy Principle method is particularly prone to this defect as it does not allow any distinction to be made between different types of adsorption. The time-dependent method, on the other hand, does allow some differentiation, particularly when applied to a pulsed flow system. This latter method therefore appears to be of greater utility than a straightforward application of the Occupancy Principle.

With regard to the applicability of the methods to catalytic systems in general, the most fundamental limitation may be the ability to detect rapid surface processes. The measurement of adsorption by radiotracer means must be limited by the number of disintegrations occurring on the catalyst surface within the duration of the experiment. Values of the mean surface lifetime of ca. 0.2 s probably represent the lower limit with an apparatus such as that used for the ethylene studies. The most likely area for improvement is in the detector sensitivity. Use of a scintillation counter such as that described by Candy, Fouilloux and Bussiere (195) should reduce the minimum acceptable surface lifetime by a factor of at least ten.

Concomitant studies of adsorption and catalysis.

The necessity for concomitant studies of adsorption and catalysis, stressed by Tamaru (98), is undeniable. Indeed, any rigorous understanding of a heterogeneous catalytic system must eventually include a knowledge of the surface concentrations of the reactive species. The present study, however, emphasises the need to discriminate between the different modes of adsorption occurring during catalysis. Apart from the physically adsorbed species observed in both catalytic systems studied, long-lived surface species may also be of considerable importance. In the study of homogeneous reaction kinetics, secondary processes giving rise to small amounts of reaction may frequently be neglected. In a heterogenous system, the surface species involved in such secondary processes may occupy a significant fraction of the catalyst surface and give rise to disproportionate effects on the overall reaction rates. It is therefore necessary to find methods capable of determining the fraction of adsorption which gives rise to the greater part of the observed reaction. In the present study, discrimination was achieved by the comparative kinetics of the observed processes. An improvement would probably be found in the use of spectroscopic techniques, as it is obviously desirable to identify each of the surface species involved in the system in addition to their concentrations.

The active surface.

From the results of the two systems studied, it appears that a substantial proportion of the metal surface is active in catalysis. We therefore have no evidence that the low site densities proposed for non-metallic catalysts by Maatman (51, 52) are also to be found on metallic surfaces.

From the observation that only about 30% of the metal surface is active in chlorobenzene hydrogenolysis over Pd/SiO_2, the reaction appears to fall into Boudart's class of "structure-sensitive" or "demanding" reactions (53). Ethylene hydrogenation over Ir/SiO_2 also appears to take place on only part of the metal surface, but may be classified as a "structure-insensitive" or "facile" reaction (4, 5). In a reaction labelled as "facile" following studies of reaction rates over different types of metal surface, it is therefore still possible for less than

the total surface to form the active sites. It would be wise, therefore, to redefine a "facile" reaction as one in which the fraction of the surface active in catalysis is independent of the surface geometry.

It is interesting to note that Taylor's concept of "active centres" due to surface heterogeneity (1) appears to have been upheld in the case of chlorobenzene hydrogenolysis over Pd/SiO_2.

A P P E N D I C E S

Appendices

Appendix I. Nomenclature.

Principal symbols and abbreviations used.

The symbols which are not listed here have been used only for isolated equations and are explained in the text at the appropriate point. Certain of the symbols which are listed have a conventional usage other than that given below. Where such cases arise, these symbols have also been explained in the text and apply only to that particular section.

A	number of molecules in the active pool adsorbed on the catalyst surface (molecule)
C	capacity of specified chamber (molecule)
D	total radioactivity of a given pulse (s^{-1})
E_a	activation energy of adsorption (kJ mol^{-1})
E_d	activation energy of desorption (kJ mol^{-1})
FCS	fast counting system
f	flux of molecules through the adsorbed phase (molecule s^{-1})
f(t)	fraction of total tracer pulse present in defined chamber at time t
F	total flow rate of reactant and product (molecule s^{-1})
$-\Delta H_a$	heat of adsorption (kJ mol^{-1})
I	total number of counts observed from a specified part of the system in a complete experiment
k, K	rate constants
LSA	least squares approximation
M	number of metal adsorption sites
n	number of tracer molecules adsorbed at time t (molecule)
N	total number of counts occurring over a given time

r	reaction rate (molecule s^{-1})
R	gas constant (JK^{-1} mol^{-1})
R_I	ratio of total adsorbed phase counts to total gas chamber counts observed
t	time (s)
T	temperature (K)
x, y, z	count rates from specified types of adsorbed species (s^{-1})
ε	extinction coefficient (l mol^{-1} cm^{-1})
ε_c	catalyst counting efficiency (mg)
ε_g	gas counting efficiency
λ	turnover number for adsorbed molecules (s^{-1})
$\bar{\tau}$	mean surface lifetime or occupancy (s)
$\bar{\tau}_g$	mean lifetime of a molecule in the gas phase for a given compartment (s)
$\bar{\tau}_v$	mean lifetime per visitation (s)

Units

Most of the units used are in accordance with the Systeme International (d'Unites). The principal exceptions are the units used for pressure (1 torr ≡ 133.322 Nm^{-2}) and volume (1l ≈ $10^{-3}m^3$).

Experiment numbers

Take as an example the experiment C2/5. Here the letter (C) represents the catalyst batch from which the sample was taken. The types of catalyst corresponding to each letter used are given in section 4.6. Additionally, experiments with blank Aerosil silica were labelled "BS". The number following the letter (2) represents the particular catalysts sample and the final number, after the stroke (5), the experiment performed with that sample.

Appendix II. Tracer Dynamics for Catalytic Flow Systems.

II. 1. Time independent tracer dynamics.

One compartment, no net flow.

Consider a compartment, A, of arbitrary shape which holds a certain number of molecules, C, where each molecule may leave or enter A in equilibrium with the environment of A (figure II. 1.) The value C molecules is defined as the capacity of A, with respect to a particular chemical species or group of chemical species. E.g. for a system containing a radioactive element as a tracer, all molecules containing the tracer element would be considered a part of this group.

Consider the movement of the molecules entering and leaving A at any point on the boundary. In unit time, a number of molecules, f_I, will pass the boundary in an inward direction, this movement being exactly balanced by the passage of f_O molecules in the outward direction in the same time interval. If f_I and f_O are considered vectors of opposite sense, the total Flux, f, of molecules, which we shall say "passes through" A, may be defined as the magnitude of $\vec{f_I}$ or $\vec{f_O}$:

$$f = |\vec{f_I}| = |\vec{f_O}|$$

$$\vec{f_I} + \vec{f_O} = 0 \qquad \text{Equation II. 1.}$$

This system may be exemplified by the case of an adsorbent in a static environment of adsorbate, the gas phase constituting the environment, and the adsorbed phase the compartment A. Although the adsorbent may influence the system, it cannot itself be considered a part of the system.

Since no net movement of molecules occurs in this system, (it is at equilibrium), we cannot consider a mean lifetime for a molecule in any part of the system. We may, however, define a mean lifetime per visitation of a molecule to A. If we designate this time $\bar{\tau}_v$, the the probability that a molecule will leave A in unit time is $1/\bar{\tau}_v$. As C molecules are present in A, $C/\bar{\tau}_v$ molecules will leave A in unit time, hence:

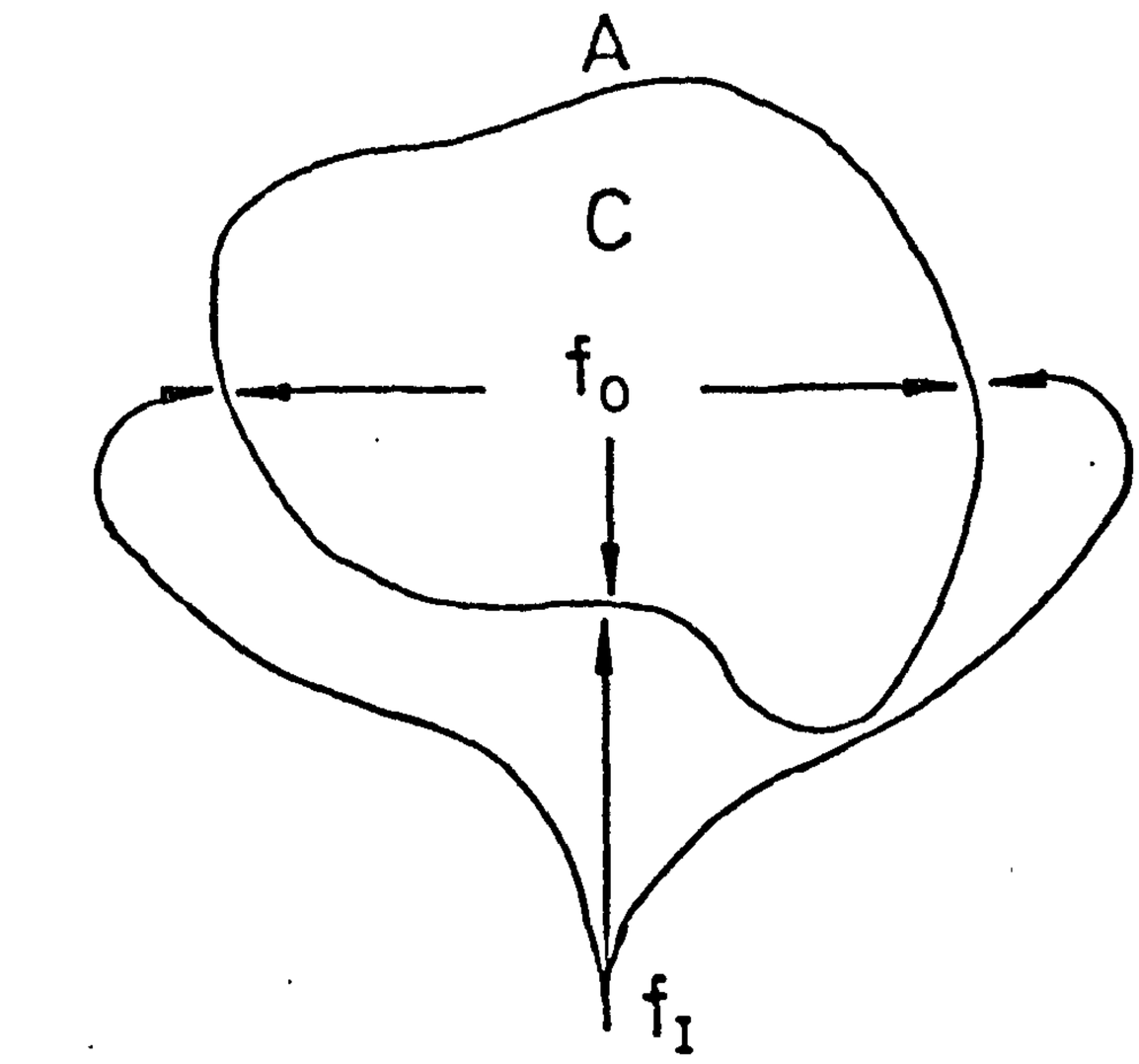

Figure II.1. Time independent tracer dynamics - case of one compartment with no net flow.

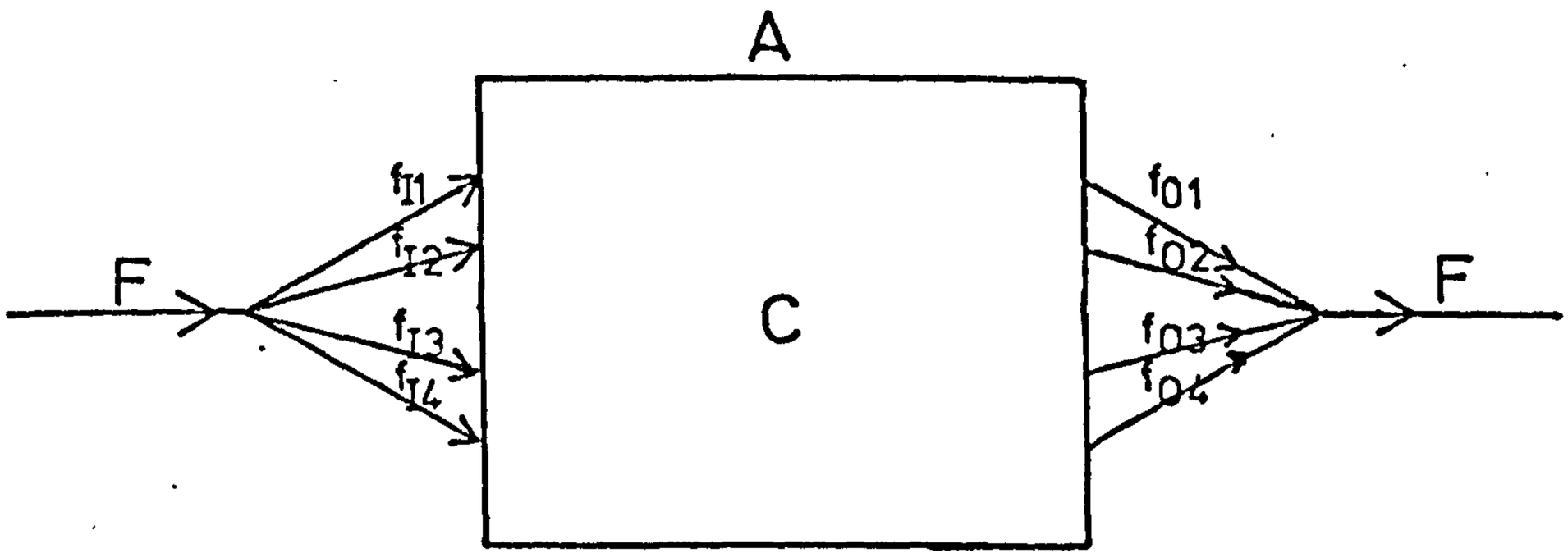

Figure II.2. Time independent tracer dynamics - case of one compartment with net flow.

$$\frac{c}{\bar{\tau}_v} = \left|\vec{f}_O\right| = \left|\vec{f}_I\right| = f,$$

$$\text{or} \quad \bar{\tau}_v = \frac{c}{f} . \qquad \text{Equation II. 2.}$$

<u>One compartment with net flow</u>.

In the case with no net flow through the compartment, molecules were allowed to enter or leave at any point. Consider now the case where the number of such points is restricted, and further, that only exit or entry is allowed at any given point. We now have a set of points (i_1, i_2, ...) as in figure II. 2., where the influx of molecules entering is respectively (f_{I1}, f_{I2}, ...) Similarly, for outflow we have a set of points (o_1, o_2, ...), with respective outflux (f_{O1}, f_{O2}, ...) If the system is in a steady state, i.e., the chemical composition of compartment A is constant, the total <u>flow</u> of molecules through the compartment is:

$$F = \sum_{n=1} f_{In} = \sum_{n=1} f_{On}.$$

In practice, only one entrance and one exit will normally be encountered, but for a real system a problem may arise in defining exactly where these points lie. For example, figure II. 3. shows a compartment with entrance and exit of finite sizes. The obvious definition of the compartment limits in this case would be the plane surfaces I and O formed at the junction between the main body of the compartment and the inflow and outflow tubes. If the compartment A and the inflow and outflow tubes were of irregular shape, this definition might not be so readily applicable, apart from the fact that for the case illustrated in figure II. 3., diffusion will occur across the defined boundary in both directions. This last mentioned problem is simply dealt with, since the probability of movement in one direction must be exactly equalled by that in the opposite direction if the system is in equilibrium, and we are concerned only with the mean behaviour of molecules in the system. On the basis of this argument, we may define the limits of the compartment by surfaces, arbitrarily chosen, through which all molecules of the flow must pass. The only further restriction is of a practical

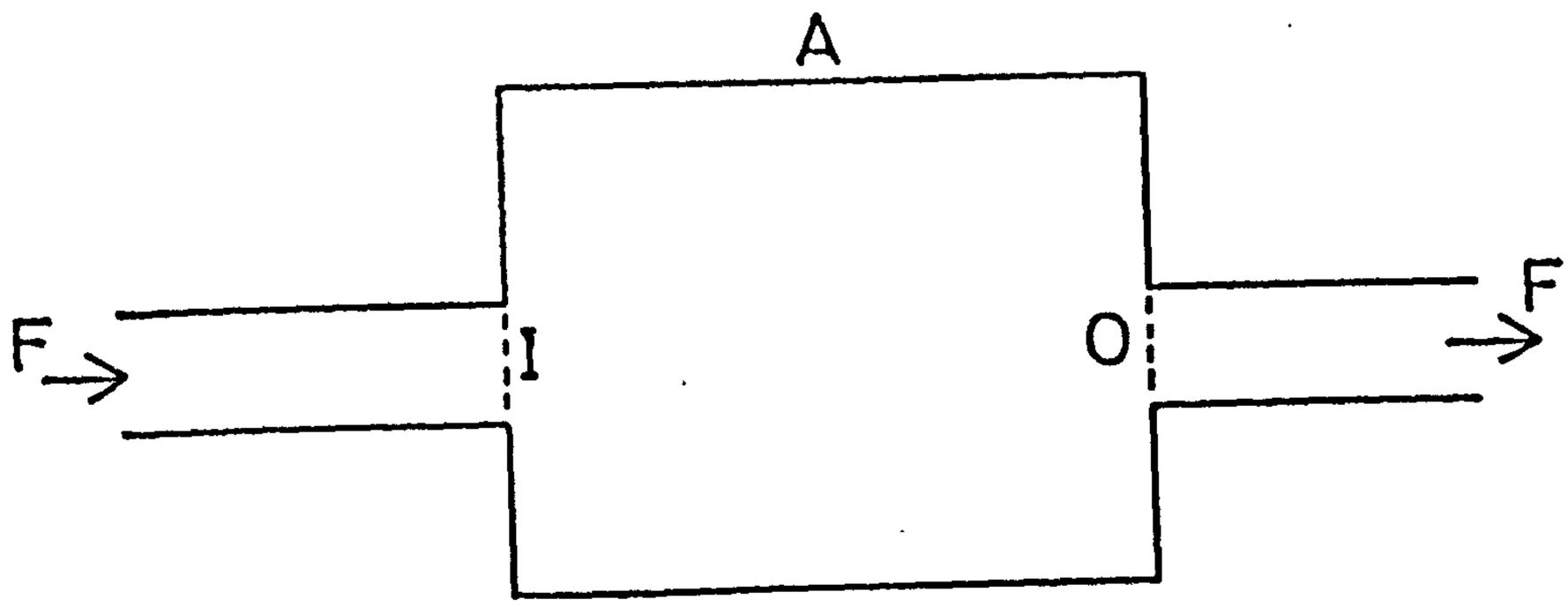

Figure II.3. Time independent tracer dynamics - flow through a compartment having entrance and exit of finite size.

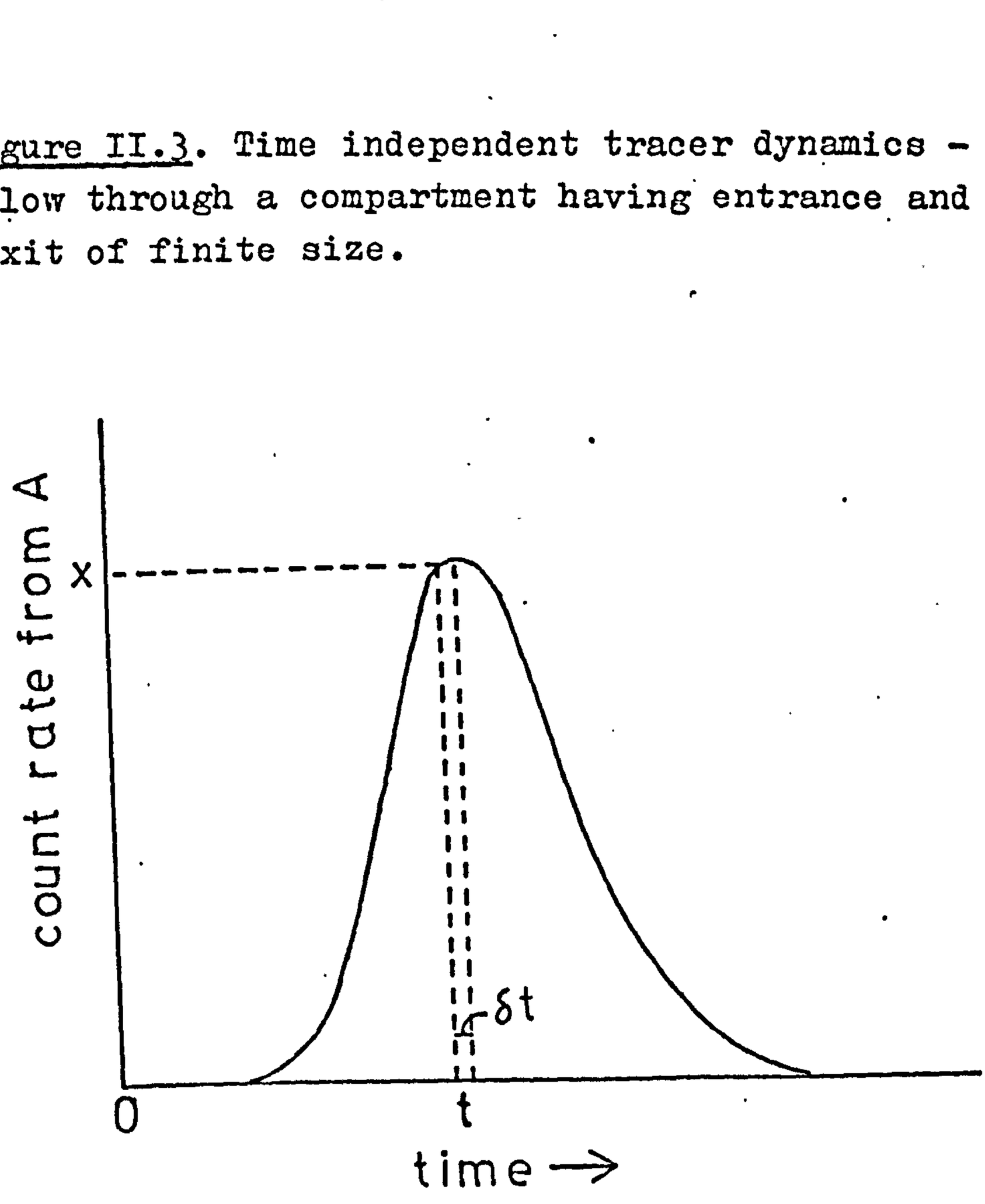

Figure II.4. Expected count rate versus time plot from a homogeneous compartment with constant flow, through which is passed a radiotracer pulse.

nature - the ability to measure the total amount of tracer present in the compartment so defined.

Let us now consider the mean lifetime, or <u>Occupancy</u> of a molecule in A, $\bar{\tau}_A$. The probability that a particular molecule will leave A in unit time will therefore be $1/\bar{\tau}_A$. Since C molecules are present in A at any given time, $C/\bar{\tau}_A$ molecules leave A and the same number enter in unit time, i.e:

$$F = \frac{C}{\bar{\tau}_A} . \qquad \text{Equation II. 3.}$$

Consider a pulse of radiotracer "mother substance" which is added to the flow through A, prior to I , over a short period of time, in comparison with the total length of the experiment, and sufficiently small that it will not substantially affect the chemical composition of the system. If the amount of radiotracer in A is monitored with time, the type of activity versus time curve shown in figure II. 4. would be expected. Ideally, to obtain all the counts from A arising from the tracer pulse, the count rate should be monitored to infinite time. In practice, the experiment might be terminated when the count rate falls below that of the background level.

If we take a time segment, δt, at time t and count rate x, as in figure II. 4., the number of counts observed over δt will be: $\delta N = x\ \delta t$, where N is the number of counts obtained up to time t.

$$\text{As } \delta t \longrightarrow 0, \quad \frac{\delta N}{\delta t} \longrightarrow \frac{dN}{dt} = x$$

$$\text{i.e. } dN = xdt.$$

Integrating over infinite time gives:

$$N_\infty = \int_0^\infty x dt. \qquad \text{Equation II. 4.,}$$

where N_∞ is the total number of counts obtained after infinite time.

If the tracer pulse contains M molecules, and has a total activity of Ds^{-1}, the specific activity of the pulse is D/Ms^{-1} $molecule^{-1}$. As the mean time over which each tracer molecule is monitored is $\bar{\tau}_A$, the mean number of counts obtained from A per molecule is ($\bar{\tau}_A$ D/M),

and the total counts obtained due to M molecules is ($D\ \bar{\tau}_A$), i.e:

$$N_\infty = D\ \bar{\tau}_A, \text{ or } \bar{\tau}_A = \frac{N_\infty}{D} . \qquad \text{Equation II. 5.}$$

Substituting into equation II. 3. gives:

$\frac{N_\infty}{D} = \frac{C}{F}$, or from equation II. 4:

$$\left(\frac{\int_o^\infty x dt}{D}\right) = \frac{1}{F} . \qquad \text{Equation II. 6.}$$

This is the standard form of the Occupancy Principle as used by Orr et al. (122).

The above result is of obvious utility in flow systems where the compartment is of a homogeneous nature, e.g., a gas flow through a "dead volume", but is not of immediate application to the more complex catalytic flow system.

Two interacting compartments.

Figure II. 5. illustrates a case of two compartments, one contained entirely within the other, having individual capacities C' and C" as in the diagram, and total capacity C. The outer compartment interacts directly with the environment via I and O, but the inner interacts only via the outer. A net flow, F molecule s^{-1}, passes through the outer compartment, and the inner compartment interacts with the outer with a flux of f molecule s^{-1}. To make this case more meaningful, we may consider the inner compartment to represent the adsorbed phase on a catalyst surface, and the outer compartment the ambient gas in a catalytic flow system.

Let the mean lifetime of a molecule in the outer compartment (i.e. gas phase) be $\bar{\tau}_g$, the mean lifetime per visitation to the surface be $\bar{\tau}_v$, and the total mean lifetime of a molecule in both compartments be $\bar{\tau}$. In unit time, F molecules pass through the chamber completely, and f molecules visit the adsorbed phase. Hence the mean number of times a molecule will visit the surface while passing through the vessel will be (f/F). Depending on the reaction system studied, this expression may have a wide range of values, both greater and less than unity. We may now write an expression for the total mean lifetime, $\bar{\tau}$ of a molecule in this system:

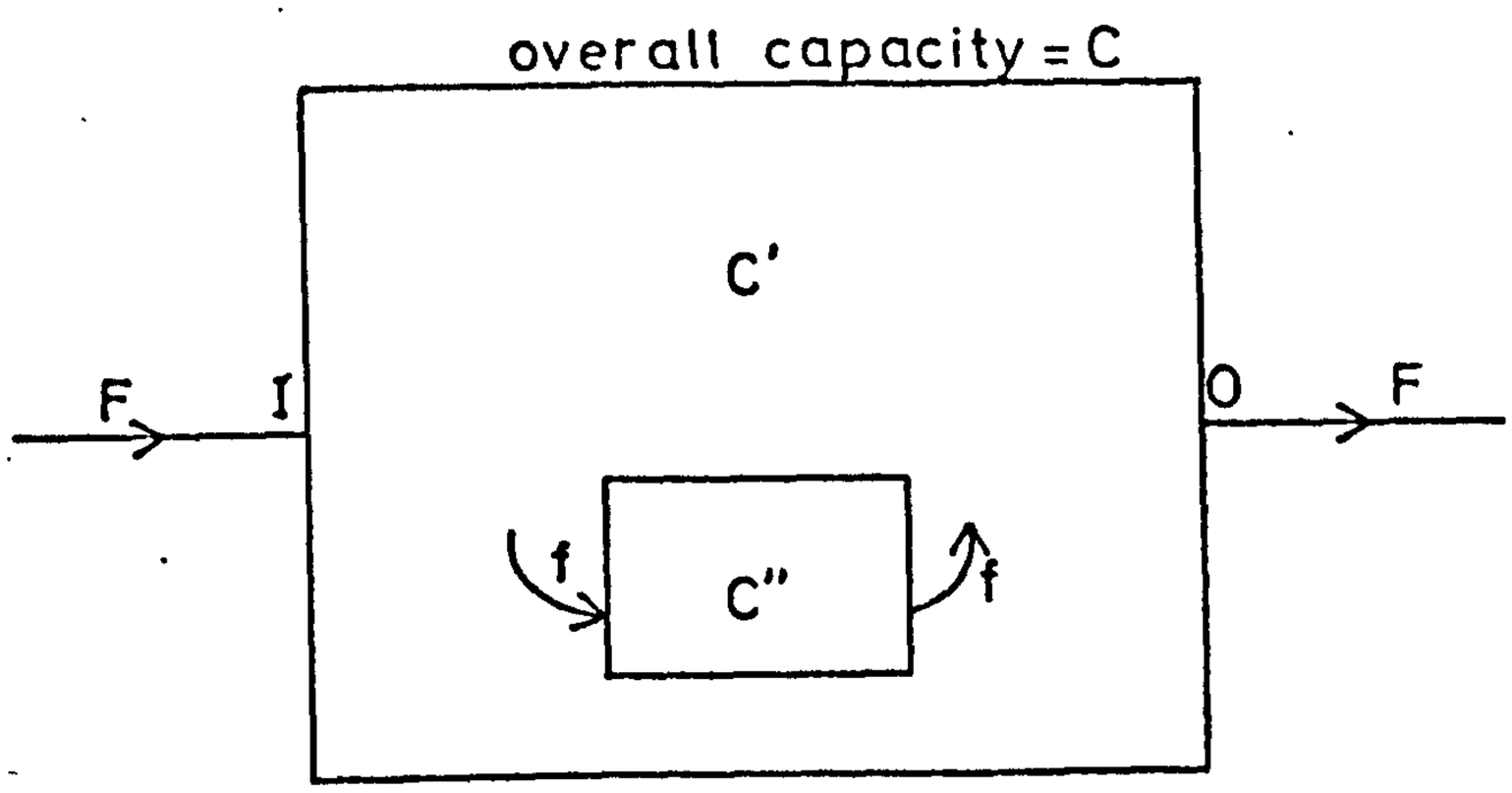

Figure II.5. Time independent tracer dynamics - case of two interacting compartments.

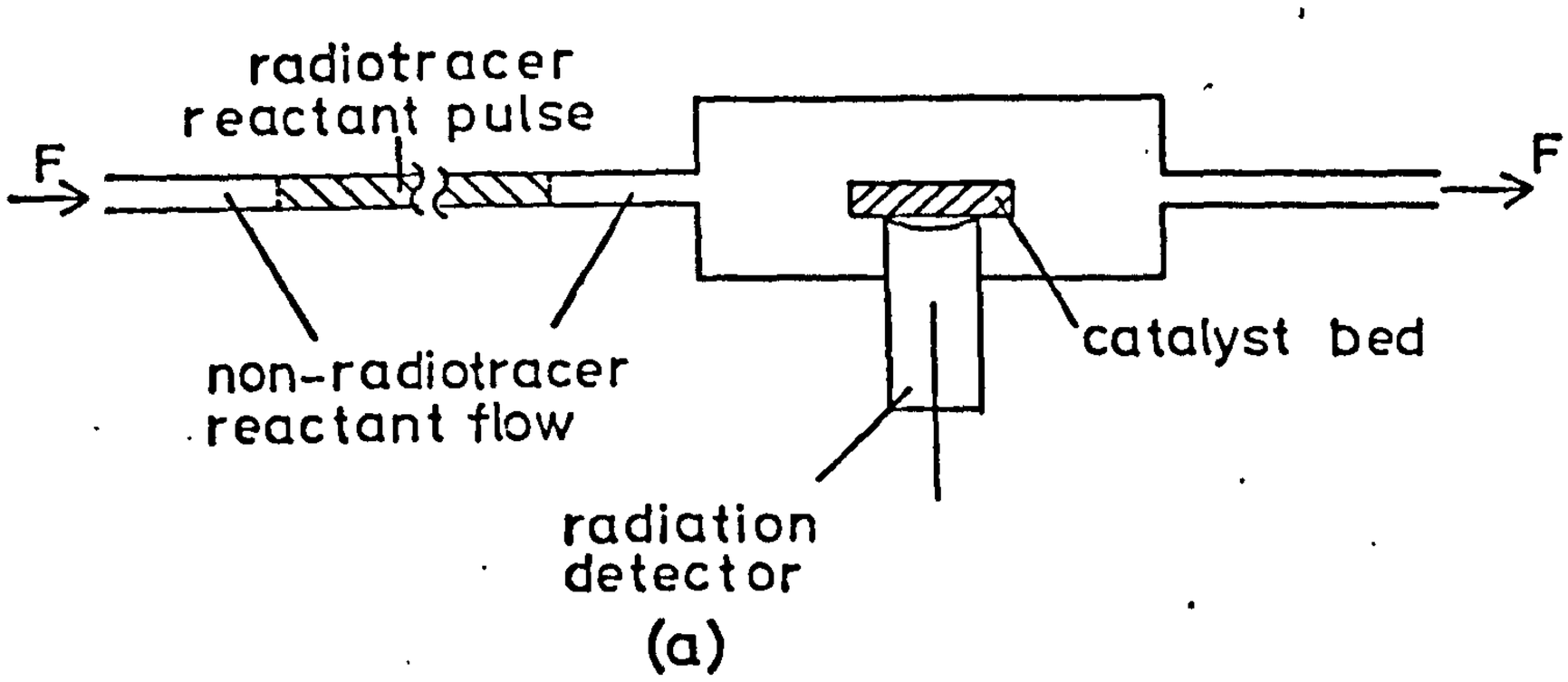

Figure II.6. Time dependent tracer dynamics - passage of a rectangular pulse of radiotracer over a catalyst in a constant reactant flow. (a) The experimental arrangement. (b) Expected count rate versus time plot. (c) Analysis of the radiotracer desorption.

$$\bar{\tau} = \bar{\tau}_g + (f/F)\,\bar{\tau}_v. \qquad \text{Equation II. 7.}$$

Substituting for $\bar{\tau}_g$ and $\bar{\tau}_v$, using equations II. 3. and II. 2. respectively (note: Equation II. 2. applies to a static system here represented by the catalyst in an equilibrium state):

$$\bar{\tau} = \frac{C'}{F} + \frac{f}{F}\cdot\frac{C''}{f} = \frac{C'}{F} + \frac{C''}{F} = \frac{1}{F}(C' + C'').$$

$$\text{i.e. } \bar{\tau} = \frac{C}{F}. \qquad \text{Equation II. 8.}$$

This equation is of fundamental significance in problems relating to flows through heterogeneous systems. It implies that the mean lifetime of a molecule in the system as a whole is independent of the time spent in each part of the system, varying only with the total capacity and flow rate of the system. For a given value of activity of a radiotracer pulse passing through the system in a flow of constant chemical composition, the number of counts obtained in the system will be constant unless the conditions are varied to alter the value of the capacity of any part. Variations in the lifetime of the adsorbed species will be compensated by a change in the adsorption/desorption rate of molecules from the gas phase.

For practical applications, the situation may be envisaged where the only count rate information available is from one part of the system, or where it is merely more convenient to treat that part of the system without reference to the total number of disintegrations occurring in the system as a whole. Let us assume that count rates are available only from the adsorbed phase of a catalytic flow system, once again represented by the inner compartment of figure II. 5.

Assume that a molecule passing through the system visits the adsorbed phase v times on average. With a total tracer pulse of activity D, s^{-1} passed through the system, the effective activity seen by the adsorbed phase with respect to the flux, f, through the adsorbed phase would be $vD\ s^{-1}$. Similarly, f may be equated to vF.

From equations II. 2. and II. 6., we may write for the capacity of the adsorbed phase:

$$C'' = f\,\bar{\tau}_v = vF\,\frac{I''}{vD}$$

$$\text{i.e.}\quad C'' = F\,\frac{I''}{D}\,. \qquad \text{Equation II. 9.,}$$

where I'' is the total number of disintegrations occurring in the adsorbed phase during the experiment.

From this relationship, it is possible to calculate the capacity of a particular part of the system using values of flow rate and tracer activity applying to the system as a whole, but using only the counts observed from that part of the system, assuming that these may be separated from those originating in other parts of the system.

II. 2. Time dependent tracer dynamics.

In the previous section we were concerned with the mean behaviour of a group of molecules in a flow system, averaged over infinite time. We now wish to consider the behaviour of such a group of molecules with time. To this end, we must impose stricter limitations on the shape of the radiotracer pulse passing through the system which we wish to analyse. Given any regular pulse shape, it should be possible to analyse the consequent variation of count rate with time obtained in any part of the system, but the simplest form of pulse to consider, (and to try to achieve experimentally), is rectangular, i.e. a pulse of constant composition over its duration, starting and stopping over a short period of time in comparison with the rates of the processes studied and the length of the pulse.

Consider the diagram shown in figure II. 6(a). Here a "rectangular" pulse of radiotracer gas has been inserted into the reactant flow over a catalyst bed, monitored by a radiation detector. If no adsorption occurs on the catalyst, or if adsorption is of an extremely short duration compared with the length of the tracer pulse, a count rate versus time plot such as that shown by the broken line in figure II. 6(b) would be expected. This assumes that no deterioration of the pulse shape occurs due to its passage through the reaction chamber. Here the radioactivity observed originates solely from the gas phase, and no modification of the pulse shape occurs. If significant adsorption occurs, the expected count rate versus time plot would be similar to that shown by the full line in figure II. 6(b).

At t_o, when the pulse first reaches the catalyst, the count rate rises due to the displacement of non-radioactive reactant molecules adsorbed on the catalyst by radioactive species. The count rate tends exponentially towards a maximum, x_{max}, when all exchangeable molecules are of the labelled group. When the pulse ends, at t', the reverse process proceeds. If the counting efficiency of the system is known, and allowance can be made for the observed count rate due to gas phase species, a value of the number of exchangeable molecules adsorbed may be calculated from the specific activity of the labelled gas. The conditions which have been outlined for this experiment are also suitable for the application of the Occupancy Principle, but here our main interest lies in the exchange kinetics. Let us first consider the radiotracer desorption.

Figure II. 6(c) shows the expected curve type for this desorption, taking t' of (6) as our time zero, and the maximum count rate of (b) (x_{max}) as our initial counting rate (x_o). Let us assume that all exchangeable adsorbed molecules are equivalent on the time scale of the proposed experiment. Since our tracer molecules are chemically indistinguishable from the non-tracer fraction, and the system is under constant flow, steady state conditions, we may assign a mean surface lifetime to all molecules in the system, $\bar{\tau}_s$, regardless of the extent of tracer coverage of the catalyst, and a corresponding probability of desorption in unit time $1/\bar{\tau}_s$.

In a time interval δt at time t during the desorption, the probability of desorption will be $(\delta t/\bar{\tau}_s)$. If, during this time, the surface count rate falls by δx, since the count rate is proportional to the surface coverage by radiotracer molecules, we may write:

$$-\delta x = x\,\frac{\delta t}{\bar{\tau}}\ , \text{ where x is the count rate at time t.}$$

Let $\delta x \longrightarrow^{s} 0$, then $\frac{\delta x}{\delta t} \longrightarrow \frac{dx}{dt}$.

i.e. $$-dx = \frac{x}{\bar{\tau}_s}\,dt\ .$$

Integrating this equation between t = o and t gives:

$$\ln x = -\frac{t}{\bar{\tau}_s} - \ln x_o\ . \qquad \text{Equation II. 9.}$$

i.e. the tracer desorption should be first order, and the value of $\bar{\tau}_s$ readily obtainable from the lnx versus time plot.

The probability of desorption, $1/\bar{\tau}_s$, may be equated to the turnover number for the reaction per active site, assuming that every molecule adsorbed undergoes reaction. If the number of exchangeable molecules is A (i.e. the size of the active pool of molecules), then the rate of reaction, r molecule s^{-1}, is given by:

$$r = \frac{A}{\bar{\tau}_s} . \qquad \text{Equation II. 10.}$$

If the reaction rate is known, and a value of $\bar{\tau}_s$ calculated from equation II. 9, then A may be calculated using equation II. 10.

For the radiotracer adsorption process, between t_o and t' on figure II. 6(b), by similar arguments to those for the desorption, one can write:

$$-\frac{d\,(x_{max} - x)}{dt} = \frac{1}{\bar{\tau}_s}\,(x_{max} - x). \qquad \text{Equation II. 11.}$$

By analysis of the adsorption kinetics, a value of $\bar{\tau}_s$ should be available, but for practical reasons this will generally be a less accurate process than analysis of the desorption curve. During adsorption, values of $(x_{max} - x)$ must be taken, generating a relatively large combination of errors from the values of x_{max} and x. For desorption, the count rate at time infinity is expected to be relatively small, so that the values of x used in the analysis are inherently more accurate.

One of the assumptions made in the foregoing treatment was that the adsorbed species are effectively equivalent, i.e., that they are either identical, or several unlike species equilibrate at a much faster rate than that of reaction. If dissimilar species are held immobile by the adsorption/reaction sites until reaction occurs, it would then be necessary to assign independent desorption probabilities to each species. As an illustration of the assignment of individual desorption probabilities, let us examine the radiotracer desorption kinetics expected from a heterogeneous surface having two distinct types of adsorption site, *firstly* when the adsorbed species are immobile, and secondly when they equilibrate rapidly.

At time zero for the desorption, let the count rates observed due to the two types of adsorbed species be y_o and z_o, and the count rates at time t be y and z respectively. If the adsorbed species are immobile we may treat each species separately, and using the exponential form of equation II. 9:

$$y = y_o \exp\left\{-\frac{t}{\bar{\tau}_y}\right\} \text{ and } z = z_o \exp\left\{-\frac{t}{\bar{\tau}_z}\right\}, \text{ Equation II. 12.,}$$

where $\bar{\tau}_y$ and $\bar{\tau}_z$ are the mean adsorbed lifetimes respectively of the two species. If x is the total adsorbed activity, then:

$$x = y + z = y_o \exp\left\{-\frac{t}{\bar{\tau}_y}\right\} + z_o \exp\left\{-\frac{t}{\bar{\tau}_z}\right\}. \text{ Equation II. 13.}$$

If the values of $\bar{\tau}_y$ and $\bar{\tau}_z$ differ substantially, the lnx versus time plot would be of the type shown in figure II. 7. In this situation, it is possible to analyse a curve of this type in terms of the two broken straight lines shown in the diagram (c.f. the radioactive decay of two isotopes having different half-lives).

If equilibration occurs between the two surface species observed, at any time t, the ratio y/z will be constant and equal to the original value y_o/z_o. Hence, for the two regions of the surface we may formulate desorption rates:

$$-\frac{dy}{dt} = x\,\frac{y_o}{x_o}\,\frac{1}{\bar{\tau}_y} \quad \text{and} \quad -\frac{dz}{dt} = x\,\frac{z_o}{x_o}\,\frac{1}{\bar{\tau}_z}\,.$$

The total desorption rate will be:

$$-\frac{dx}{dt} = \left(-\frac{dy}{dt} - \frac{dz}{dt}\right) = \frac{x}{x_o}\left(\frac{y_o}{\bar{\tau}_y} + \frac{z_o}{\bar{\tau}_z}\right)$$

Integrating this equation:

$$\ln x = -\frac{1}{x_o}\left(\frac{y_o}{\bar{\tau}_y} + \frac{z_o}{\bar{\tau}_z}\right)t + \ln x_o\,. \qquad \text{Equation II. 14.}$$

Analysis of the curve obtained from a system of this type would be deceptively simple. The overall mean lifetime is:

$$\bar{\tau}_x = \frac{x_o\ \bar{\tau}_y\ \bar{\tau}_z}{\left(\bar{\tau}_z\ y_o + \bar{\tau}_y\ z_o\right)}$$

This treatment for the case of two types of adsorption site may of course be extended to any number of types, and the observed lifetimes will effectively be an "averaging" of the behaviour of individual types.

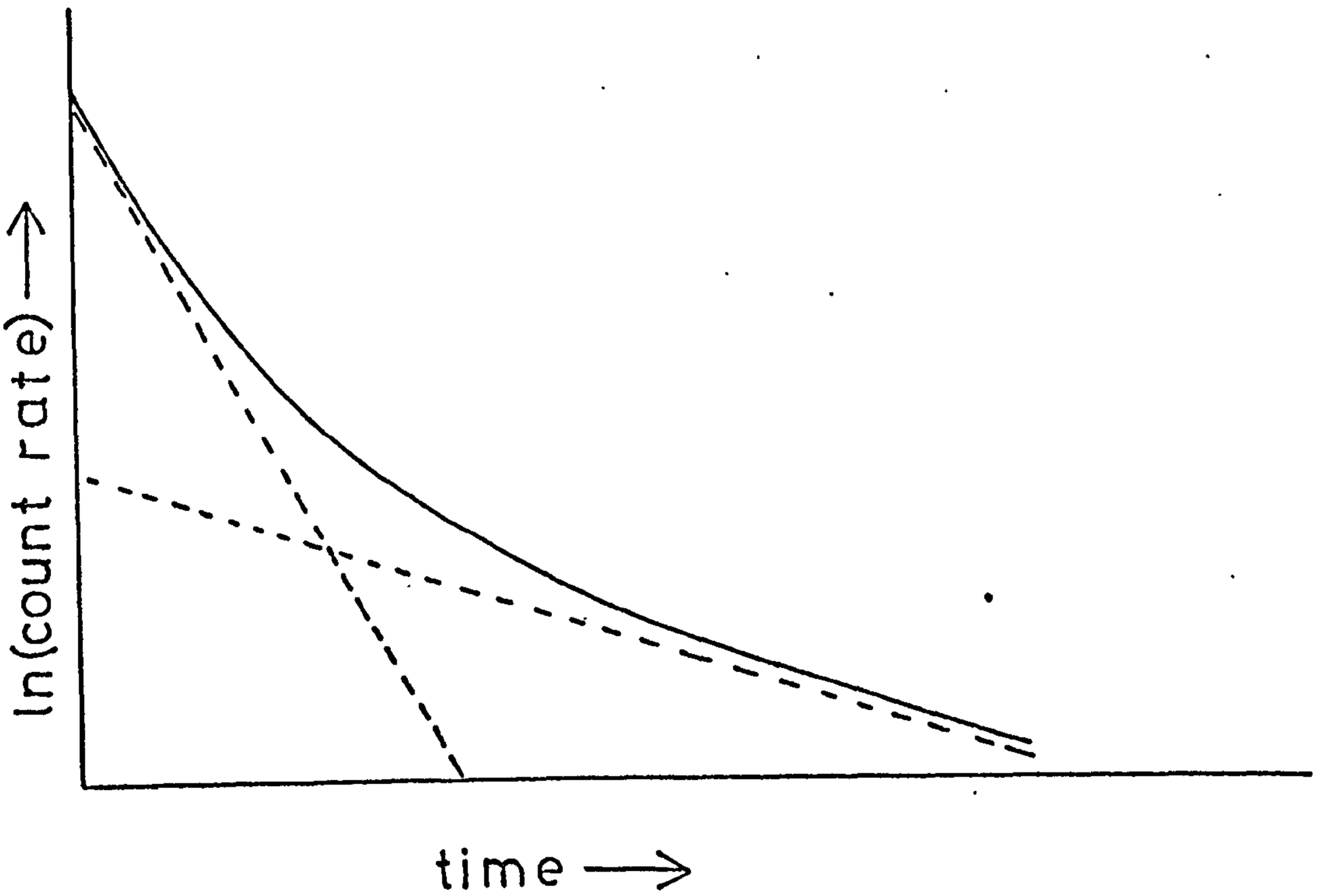

Figure II.7. Radiotracer desorption from a catalyst in a constant flow system, with two types of adsorption site and no interchange between sites. Observed desorption curve (——). Desorption curves for molecules adsorbed on each type of site (- - -).

II. 3. Tracer dynamics with non-continuous flow (pulsed flow).

In the constant flow systems so far considered, the analyses were based on a "chemically" steady state of the system, the only variable being the substitution of radioactively labelled molecules for a fraction of the total molecular population. The generality of first order radiotracer adsorption/desorption processes for each type of surface adsorption site was based on this point. If we now consider, for example, a desorption process from a catalyst where the reactant is no longer present in the gas phase, the chemical nature of the system will change with surface coverage. In such a system surface heterogeneity would play a much more important role, e.g., molecules may be rapidly desorbed from more active sites initially, followed by a slower desorption from stronger, less catalytically active sites. Obviously, the results obtained from such an experiment would be dependent to a much greater extent on the entire system, rather than the most active part. Although more information might be obtained, the analysis of the observed kinetics would be correspondingly more complex.

Problems of a more serious nature might be envisaged in applying the time independent, integral approach to a pulsed flow system. The Occupancy Principle, as formulated in section II. 1., would, for the reasons outlined above, not be directly applicable. The method consists of a single "averaging" of all the processes occurring during an experiment, a process which, while yielding valuable information under the conditions of constant flow, may give misleading information when the nature of the system varies with time. It therefore seems probable that a critical application of a time dependent analysis to a non-constant flow system will yield results of greater interest and reliability.

Appendix III. Kinetic analysis programs.

III.1. ØCl PLOT

```
Ø: PRT "ØCL PLOT"⊢
1: SPC 2;Ø → A → B → C → X → R11⊢
2: ENT "K",R6,"K2",R2,"K5",R5⊢
3: ENT "M",R3,"ZØ",R4⊢
4: R5/R6 → R7;R2/R6 → R8;R4-R3 → R9⊢
5: 1 → R15 → R17Ø⊢
6: C+1 → C;CR15 → R15 → R(17Ø+C)⊢
7: IF 69>C;JMP -1⊢
8: X → B⊢
9: (-R8R9)↑A/(A+1-R7)R(17Ø+A)+B → X⊢
1Ø: IF B≠X; A+1 → A;JMP -2⊢
11: XR8R9+EXP (-R8R9) → X⊢
12: XR3R9↑(-R7) → R1Ø⊢
13: Ø → A → B⊢
14: IF A>2Ø;JMP 11⊢
15: Ø → B → Y⊢
16: R9EXP (-2ØØAR6) → X⊢
17: (-XR8)↑B/(B+1-R7)R(17Ø+B)+Y → Y⊢
18: B+1 → B⊢
19: IF R11≠Y;Y → R11;JMP -2⊢
2Ø: (-R8R3*X↑(1-R7))Y → Y⊢
21:  EXP (XR8)*X↑R7(Y+R1Ø) → Y⊢
22: X+Y → R(1ØØ+A);2ØØA → R(25Ø+A)⊢
23: FXD 3;PRT "T=",R(25Ø+A)⊢
24: PRT "Z=",R(1ØØ+A);A+1 → A;FLT 9;JMP -1Ø⊢
25: SPC 2;PRT "T IN SEC";SPC 2;FLT 3⊢
26: PRT "K=",R6,"K2=",R2,"K5=",R5⊢
27:PRT "M=",R3,"ZØ",R4;SPC 9;END⊢
```

III.2. ØCL FIT.

```
Ø: PRT "ØCL FIT";SPC 2⊢
1: Ø → A → B → C → X⊢
2: ENT "K1",R1,"K2",R2,"K5",R5⊢
3: ENT "M",R3,"ZØ",R4,"Z6ØØ",R151⊢
4: ENT " Z14ØØ",R152,"Z3ØØØ",R153⊢
5: 1 → R15 → R17Ø⊢
6: C+1 → C;CR15 → R15 → R(17Ø+C)⊢
7: IF 69>C;JMP -1⊢
8: R1+R2R3 → R6;R5/R6 → R7;R2/R6 → R8⊢
9: R4-R3 → R9;Ø → R11 → X → A⊢
1Ø: X → B;(-R8R9)↑A/(A+1-R7)R(17Ø+A)+B → X⊢
11: IF B≠X;A+1 → A;JMP -1⊢
12: XR8R9+EXP (-R8R9) → X⊢
13: XR3R9↑(-R7) - R1Ø⊢
14: Ø → A → B → C → Y⊢
15: C+1 → C;IF C>3;JMP 11⊢
16: IF C=1;3 → A⊢
17: IF C=2;7 → A⊢
18: IF C=3;15 → A⊢
19: Ø → B → Y;R9EXP (-2ØØAR6) → X⊢
2Ø: (-XR8)↑B/(B+1-R7)R(17Ø+B)+Y → Y⊢
21: B+1 → B;IF R11≠Y;Y → R11;JMP -1⊢
22: (-R8R3X↑(1-R7))Y → Y⊢
23: EXP (XR8)X↑R7(Y+R1Ø → Y⊢
24: X+Y → R(25Ø+A)⊢
25: JMP -1Ø⊢
26: R2(R253/R151)↑.5 → R2;PRT R2⊢
27: IF ((R253-R151)/R151)↑2>.00001;JMP -19⊢
28: R3R152/R257 → R13;R2R3/R13 → R2;R13 →R2;R13 → R3;
    PRT R3⊢
29: IF ((R257-R152)/R152)↑2>.00001;JMP -21⊢
3Ø: R5R265/R153 → R5;PRT R5⊢
31: IF ((R265-R153)/R153)↑2>.00001;JMP -23⊢
32: SPC 2;FLT 3;PRT "K1=",R1,"K2=",R2⊢
33: PRT "K5=",R5,"M=",R3,"ZØ=",R4⊢
34: PRT "Z6ØØ=",R151,"Z14ØØ=",R152⊢
35: PRT "Z3ØØØ=",R153;SPC 9;END⊢
```

REFERENCES

References

1. H. S. Taylor, Proc. Roy. Soc., A 108, 105 (1925)
2. S. Brunauer, P. H. Emmett and E. Teller, J. Am. Chem. Soc., 60, 309 (1938)
3. M. Boudart, Adv. Catalysis, 20, 153 (1969)
4. G. C. A. Schuit and L. L. van Reijen, ibid., 10, 242 (1958)
5. J. C. Schlatter and M. Boudart, J. Catalysis, 24, 482 (1972)
6. S. Brunauer and P. H. Emmett, J. Am. Chem. Soc., 62, 1732 (1940)
7. O. Beeck, A. E. Smith and A. Wheeler, Proc. Roy. Soc., A 177, 62 (1940)
8. M. A. H. Lanyon and B. M. W. Trapnell, ibid, A 227, 387 (1955)
9. R. P. Eischens, S. A. Francis and W. A. Pliskin, J. Phys. Chem., 60, 194 (1956)
10. R. P. Eischens and W. A. Pliskin, Adv. Catalysis, 10, 1 (1958)
11. A. C. Yang and C. W. Garland, J. Phys. Chem., 61, 1504 (1957)
12. P. C. Aben, J. Catalysis, 10, 224 (1968)
13. R. R. Ford, Adv. Catalysis, 21, 51 (1970)
14. H. L. Gruber, J. Phys. Chem., 66, 48 (1962)
15. T. R. Hughes, R. J. Houston and R. P. Sieg, Ind. Eng. Chem. Process Design Develop., 1, 96 (1962)
16. J. H. Sinfelt and D. J. C. Yates, J. Catalysis, 10, 362 (1968)
17. T. A. Dorling and R. L. Moss, ibid, 7, 378 (1967)
18. P. Wentrcek, K. Kimoto and H. Wise, ibid, 33, 279 (1973)
19. H. Charcosset, D. Barthomeuf, R. Nicolova, A. Revillon, L. Tournayan and L. Trambouze, Bull. Soc. Chim. France, p. 4555 (1967)
20. H. Chon, R. A. Fischer, E. Tomesko and J. C. Acton, Actes 2e Congr. Intern. Catalyse, Paris, 1960, Vol. 1, p. 217, editions Technip, Paris (1961)
21. G. Weidenbach and H. Fuerst, Chem. Tech. (Berlin), 15, 589 (1963)
22. H. L. Gruber, J. Phys. Chem., 66, 48 (1962)
23. J. E. Benson and M. Boudart, J. Catalysis, 4, 704 (1965)
24. L. Spenadel and M. Boudart, J. Phys. Chem., 64, 204 (1960)
25. B. Lang, R. W. Joyner and G. A. Somorjai, Surface Sci., 30, 454 (1972)

26. Z. Paal and S. J. Thomson, J. Catalysis, 30, 96 (1973)
27. E. B. Prestridge and D. J. C. Yates, Nature, 234, 345 (1971)
28. C. R. Adams, H. A. Benesi, R. M. Curtis and R. G. Meisenheimer, J. Catalysis, 1, 336 (1962)
29. L. Spendel and M. J. Boudart, J. Phys. Chem., 64, 204 (1960)
30. H. P. Klug and L. E. Alexander, "X-ray Diffraction Procedures", Wiley, New York (1954)
31. D. Cormack and R. L. Moss, J. Catalysis, 13, 1 (1969)
32. D. Pope, W. L. Smith, M. J. Eastlake and R. L. Moss, ibid., 22, 72 (1971)
33. L. Weil, J. Chim. Phys., 51, 715 (1954)
34. P. W. Selwood, Adv. Catalysis, 9, 93 (1957)
35. P. W. Selwood, S. Adler and T. R. Phillips, J. Am. Chem. Soc., 77, 1462 (1955)
36. C. Herbo, J. Chim. Phys., 47, 454 (1950)
37. G. M. Schwab, J. Block and D. Schutze, Angew. Chem., 71, 101 (1959)
38. G. M. Schwab, Disc. Faraday Soc., 41, 252 (1966)
39. J. E. Germain, Bull. Soc. Chim. France, p. 23 (1966)
40. G. C. Bond, "Catalysis by Metals", ch. 19, Academic Press, London (1962)
41. P. A. Sermon and G. C. Bond, Catalysis Rev., 8, 211 (1974)
42. S. J. Khoobiar, J. Phys. Chem., 68, 411 (1964)
43. J. H. Sinfelt and P. J. Lucchesi, J. Am. Chem. Soc., 85, 3365 (1963)
44. G. E. E. Gardes, G. M. Pajonk and S. J. Teicher, J. Catalysis, 33, 145 (1974)
45. G. F. Taylor, S. J. Thomson and G. Webb, ibid., 12, 150,191 (1968)
46. G. Webb and J. I. Macnab, ibid.,26, 226 (1972)
47. A. D. O. Cinneide and J. K. A. Clarke, Catalysis Rev., 7, 213 (1972)
48. N. Sheppard, N. R. Avery, B. A. Morrow and R. P. Young, "Chemisorption and Catalysis", Ed. P. Hepple, p. 135, Inst. Petroleum (1970)
49. D. Cormack, S. J. Thomson and G. Webb, J. Catalysis, 5, 224 (1966)
50. P. Tetenyi, L. Babernics, L. Guczi and K. Schachter, Proc. 3rd Int. Congr. Catal. 1964, Vol. 1, p. 547 (1965)

51. R. W. Maatman, J. Catalysis, 19, 64 (1970)

52. idem, Catalysis Ret., 8, 1 (1974)

53. M. Boudart, A. Aldag, J. E. Benson, N. A. Dougharty and G. C. Harkins, J. Catalysis, 6, 92 (1966)

54. M. Boudart, "Kinetics of Chemical Processes", p. 206, Prentice - Hall, Englewood Cliffs, New Jersey (1968)

55. F. M. Dautzenberg and J. C. Platteeuw, J. Catalysis 19, 41 (1970)

56. P. C. Aben, J. C. Platteeuwand B. Stouthammer, Rec. Trans. Chim. Pays-Bas, 89, 449 (1970)

57. P. Ratnasamay, J. Catalysis, 31, 466 (1973)

58. A. A. Balandin, Adv. Catalysis, 19, 1 (1969)

59. M. Boudart, A. W. Aldag, L. D. Ptak and J. E. Benson, J. Catalysis, 11, 35 (1968)

60. J. R. Anderson and N. R. Avery, ibid., 5, 446 (1966)

61. D. D. Eley and M. A. Zammitt, ibid,, 21, 366 (1971)

62. G. J. K. Acres, D. D. Eley and J. M. Trillo, ibid., 4, 12 (1965)

63. R. L. Burwell, G. L. Haller, K. C. Taylor and J. F. Read, Adv. Catalysis, 20, 1 (1969)

64. K. M. Sancier, T. Dozono and H. Wise, J. Catalysis, 23, 270 (1971)

65. E. J. Arlman, ibid., 3, 89 (1964)

66. M. Boudart, American Scientist, 57, 97 (1969)

67. P. B. Weisz, Annu. Rev. Phys. Chem., 21, 175 (1970)

68. J. A. Rabo, C. L. Angell, P. H. Kasai and V. Schomaker, Disc. Faraday Soc., 41, 328 (1966)

69. J. T. Richardson, J. Catalysis, 9, 182 (1967)

70. W. N. Delgass, R. L. Garten and M. Boudart, J. Phys. Chem., 73, 2970 (1969)

71. D. R. Ashmead, D. D. Eley and R. Rudham, Trans. Faraday Soc., 59, 207(1963)

72. S. Glasstone, K. Laidler and H. Eyring, "The Theory of Rate Processes", ch. 7, McGraw - Hill, New York (1941)

73. D. N. Misra, J. Catalysis, 14, 34 (1969)

74. R. W. Maatman, P. Mahaffy, P. Heckstra and C. Addink, J. Catalysis, 23, 105 (1971)

75. R. W. Maatman, W. Ribbens and B. Vonk, ibid., 31, 384 (1973)

76. Y. I. Yermakov and V. A. Zakharov, Proc.4th. Int. Congr. Catalysis, 1968, Vol. 1, 276 (1969)

77. S. J. Thomson and G. Webb, "Heterogeneous Catalysis", ch. 8, Oliver and Boyd, Edinburgh (1968)
78. P. H. Emmett, Adv. Catalysis, 9, 645 (1957)
79. J. T. Kummer, T. W. De Witt and P. H. Emmett, J. Am. Chem. Soc., 70, 3632 (1948)
80. W. K. Hall, R. J. Kokes and P. H. Emmett, ibid.,82, 1027 (1960)
81. idem, ibid.,79, 2983, 2987 (1957)
82. J. T. Kummer, H. H. Podgurski, W. B. Spencer and P. H. Emmett, ibid.,73, 564 (1951)
83. G. Blyholder and P. H. Emmett, J. Phys. Chem., 63, 962 (1959), ibid.,64, 470 (1960)
84. J. T. Kummer and P. H. Emmett, J. Am. Chem. Soc., 75, 5177 (1953)
85. J.A.Altham and G. Webb, J. Catalysis, 18, 133 (1970)
86. G.F.Taylor, S. J. Thomson and G. Webb, ibid, 12, 191 (1968)
87. K. C. Campbell and S. J. Thomson, Trans. Faraday Soc., 55, 306 (1959)
88. idem, ibid.,55, 985 (1959)
89. idem, ibid.,57, 279 (1961)
90. S. J. Thomson and J.L.Wishlade, ibid, 58, 1170 (1962)
91. G.K.L.Cranstoun and S. J. Thomson, ibid.,59, 2403 (1963)
92. S. J. Thomson and J. L. Wishlade, J. Chem. Soc. p. 4278 (1963)
93. D. Cormack, S. J. Thomson and G. Webb, J. Catalysis, 5, 224 (1966)
94. J. J. McCarroll and S. J. Thomson, ibid.,19, 144 (1970)
95. J. U. Reid, S. J. Thomson and G. Webb, ibid.,29, 421, 433 (1973)
96. idem, ibid.,30, 372, 378 (1973)
97. K. Tamaru, Bull. Chem. Soc. Japan, 31, 666 (1958)
98. idem, Adv. Catalysis, 15, 65 (1964)
99. P. Mars, J.J.F.Scholten and P. Zwietering, "The Mechanism of Heterogeneous Catalysis", Ed. J. H. de Boer, p. 66, Elsevier, Amsterdam (1960)
100. F. E. Massoth and D. A. Scarpiello, J. Catalysis, 21, 294 (1971)
101. S. M. Hsu and H. L. Kabel, ibid.,33, 74 (1974)
102. K. Tamaru, Trans. Faraday Soc., 55, 824 (1959)
103. idem, ibid.,57, 1410 (1961)
104. K. Fukuda, T. Onishi and K. Tamaru, Bull. Chem. Soc. Japan 42, 1192 (1969)

105. E. R. Kaering and A. Syverson, J. Catalysis, 32, 396 (1974)

106. G. Schay and G. Szekely, Acta. Chim. Acad. Sci. Hung., 5, 167 (1954)

107. K. Tamaru, Nature, 183, 319 (1959)

108. J. Nakanishi and K Tamaru, Trans. Faraday, Soc., 59, 1470 (1963)

109. D. W. Bassett and H. W. Habgood, J. Phys. Chem., 64, 769 (1960)

110. P. J. Owens and C. H. Amberg, Canad. J. Chem., 40, 941 (1962)

111. C. S. G. Phillips, A. J. Hart-Davis, R. G. L. Saul and J. Wormald, J. Gas. Chromatogr., 5, 424 (1967)

112. R. M. Lane, B. C. Lane and C. S. G. Phillips, J. Catalysis, 18, 281 (1970)

113. C. S. G. Phillips and C. R. McIlwrick Anal. Chem., 45, 782 (1973)

114. A Lawson, J. Catalysis, 11, 283, 295 (1968)

115. J. Fahrenfort, L. L. van Reijen and W. M. H. Sachtler, "The Mechanism of Heterogenous Catalysis", Ed. J. H. de Boer, p. 23, Elsevier, Amsterdam (1960)

116. N. Sheppard, N. R. Avery, B. A. Morrow and R. P. Young, "Chemisorption and Catalysis", Ed. P. Hepple, p. 135, Inst. of Petroleum, (1970)

117. K. Tamaru and M. Boudart, Adv. Catalysis, 9, 699 (1957)

118. L. O. Apel'baum and M.I.Temkin,Zh. Fiz. Khim., 35, 2060 (1961)

119. P-E.E. Bergner; J. Theoret. Biol., 1, 120 (1961)

120. P-E.E. Bergner, ibid, 1, 359 (1961)

121. P-E.E. Bergner, Acta. Radiol. Suppl., 210, 1 (1962)

122. J. S. Orr and F. C. Gillespie, Science, 162, 138 (1968)

123. P-E.E. Bergner, J. Theoret. Biol., 6, 137 (1964)

124. K. Riviere, D. Comar, C. Kelleshohne, J. S. Orr, F. C. Gillespie, Lancet, and J. M. A. Lenihan, 1, 389 (1969)

125. F. C. Gillespie and J. S. Orr, Phys. Med. Biol., 14, 639 (1969)

126. J. S. Orr, J. Shimmins and C. F. Spiers, Lancet, ii, 771 (1969)

127. W. A. Harland and J. S. Orr, J. Physiol., 200, 297 (1969)

128. I. Hasbrouck, Previously unpublished observations reported by P. N. Rylander, in "Catalytic Hydrogenation over Platinum Metals", p. 406, Academic Press, New York and London (1967)

129. F. F. Blicke and F. J. McCarty, J. Org. Chem., 24, 1061 (1959)

130. R. J. Harper and C. Kemball, Trans. Faraday Soc., 65, 2224 (1969)

131. M. Kraus and V. Bazant, "Catalysis", Ed. J. W. Hightower, Proc. 5th Int. Congr. Catalysis (1972), Vol. 2. p. 1073, North Holland, Amsterdam, London (1973)

132. L. P. Hammett, J. Am. Chem. Soc., 59. 96 (1937)

133. J. Horiuti and T. Toya, "Solid State Surface Science", Ed. M. Green, Vol. I, p. 1, Marcel Dekker, New York (1969)

134. G. Parravano, J. Catalysis, 22, 96 (1971)

135. Z. Bastl, Coll. Czech. Chem. Commun., 38, 477 (1973)

136. F. A. Matsen, A. C. Makrides and N. Hackermann, J. Chem. Phys., 22, 1800 (1954)

137. J. L. Garnett and W. A. Sollich-Baumgartner, Adv. Catalysis, 16, 95 (1966)

138. S. J. Thomson, private communication.

139. P. Sabatier and J. B. Sanderens, Compt. Rend., 124, 1368 (1897)

140. S. Koestenblatt and E. N. Ziegler, A. I. Ch. E. J., 17, 391 (1971)

141. K. J. Laidler and R. E. Townshend, Trans. Faraday. Soc. 57, 1590 (1961)

142. I. Langmuir, ibid.,17, 621 (1922)

143. C. N. Hinshelwood, "Kinetics of Chemical Change", Clarendon Press, Oxford (1926)

144. E. K. Rideal, Proc. Camb. Phil. Soc., 35, 130 (1939)

145. R. N. Pease, J. Am. Chem. Soc., 45, 1196, 2235, 2296 (1923), ibid.,49, 2503 (1927)

146. A Farkas and L. Farkas, ibid.,60, 22 (1938)

147. O. Toyama, Rev. Phys. Chem. Japan, 11, 153 (1937), ibid.,12, 115 (1938)

148. H. zur Strassen, Z. Physik. Chem., A 169, 81 (1934)

149. G. H. Twigg and E. K. Rideal, Proc. Roy. Soc., A 171, 55 (1939)

150. idem, Trans. Faraday. Soc., 36, 533 (1940)

151. O. Beeck, Rev. Mod. Phys., 20, 127 (1948), Disc. Faraday Soc., 8, 118 (1950)

152. G. I. Jenkins and E. K. Rideal, J. Chem Soc., 2490, 2496 (1955)

153. C. J. Kemball, ibid.,735 (1956)

154. R. Wynkoop and R. H. Wilhelm, Chem. Eng. Progr., 46, 300 (1950)

155. M. V. Sussman and C. Potter, Ind. Eng. Chem., 46, 457 (1954)

156. O. A. Hougen and K. M. Watson, ibid, 35, 529 (1943)

157. A. C. Pauls, E. W. Comings and J. H. Smith, A. I. Ch. E. J., 5, 453 (1959)

158. Ho-Peng Koh and R. Hughes, J. Catalysis, 33, 7 (1974)

159. G. H. Twigg, Disc. Faraday Soc., 8, 152 (1950)

160. E. K. Rideal, J. Chem. Soc., 121, 309 (1922)

161. K. Kato, N. Takeuchi and K. Ku Bota, J. Chem. Eng. Japan, 2, 204 (1969)

162. W. A. Pliskin and R. P. Eischens, J. Chem. Phys., 24, 48 (1956)

163. R. P. Eischens, S. A. Francis and W. A. Pliskin, ibid., 22, 1786 (1954)

164. L. H. Little, N. Sheppard and D. J. C. Yates, Proc. Roy. Soc., A 259, 242 (1960)

165. B. A. Morrow and N. Sheppard, ibid., A 311, 391 (1969)

166. J. Erkelens and Th. J. Liefkens, J. Catalysis, 8, 36 (1967)

167. I. Horiuti and M. Polanyi, Trans. Faraday. Soc., 30, 1164 (1934)

168. JJ.Rooney and G. Webb, J. Catalysis, 3, 488 (1964)

169. N. Sheppard, private communication

170. R. M. Atkins, R. Mackenzie, P. L. Timms and T. W. Turney, J. C. S. Chem. Commun., 764 (1975)

171. T. I. Taylor in "Catalysis", Ed. P. H. Emmett, Vol. 5, p. 257, Reinhold, New York (1957)

172. C. Kemball, Adv. Catalysis, 11, 223 (1959)

173. G. C. Bond and P. B. Wells, ibid., 15, 91 (1964)

174. R. L. Burwell Jr., Acc. Chem. Res., 2, 289 (1969)

175. C. Kemball, Catalysis Rev., 5, 33 (1971)

176. idem, J. Chem. Soc., 735 (1956)

177. J. H. Sinfelt and P. J. Lucchesi, J. Am. Chem. Soc., 85, 3365 (1963)

178. C. H. J. Van den Brekel, J. Phys. E. Scientific Instruments, 3, 878 (1970)

179. G. Friedlander, J. W. Kennedy and J. M. Miller, "Nuclear and Radiochemistry", 2nd edition, p. 411, Wiley and Sons Inc., New York (1964)

180. G. Webb, private communication

181. G. Friedlander, J. W. Kennedy and J. M. Miller, "Nuclear and Radiochemistry", 2nd. edition, Wiley and Sons Inc., New York (1964)

182. D. O. Hayward and B. M. W. Trapnell, "Chemisorption", 2nd edition, ch. 4, Butterworths, London (1964)

183. N. E. Johnson and F. L. Kickemeister, "Calculus with Analytical Geometry", 4th edition, p. 779, Allyn and Bacon, Boston (1969)

184. G. C. Bond, "Catalysis by Metals", ch. 13, Academic Press, London (1962)

185. P. Tetenyi and Z. Paal, Z. Physik. Chem. Neue Folge, 80, 63 (1972)

186. N. C. Pitkethly and A. G. Goble, A Paris (1960), Vol. 2, p. 1851, Editions Technip. Paris (1961)

187. P. A. Sermon, J. Catalysis, 24, 460 (1972)

188. S. Ross and J. P. Oliver, "On Physical Adsorption", p. 245, Interscience, New York (1964)

189. J. H. de Boer, "The Dynamical Character of Adsorption", p. 47, Oxford University Press, London (1953).

190. J. H. Sinfelt and D. J. C. Yates, J. Catalysis, 8, 82 (1967)

191. R. B. Moyes, P. B. Wells, K. Baron, K. Compson, J. Grant and R. Heselden, ibid.,18, 224 (1970)

192. J. H. de Boer, "The Dynamical Character of Adsorption", ch. 3, Oxford University Press, London (1953)

193. G. C. Bond, J. J. Phillipson, P. B. Wells and J. M. Winterbottom, Trans. Faraday Soc., 62, 443 (1966), ibid.,60, 1847 (1964)

194. G. C. Bond, G. Webb and P. B. Wells, Trans. Faraday Soc., 61, 999 (1965)

195. J. P. Candy, P. Fouilloux and P. Bussiere, Radiochem. Radioanal. Letters, 14, 145 (1973).